

A Review and Analysis of Automatic Optical Inspection and Quality Monitoring Methods in Electronics Industry

ABD AL RAHMAN M. ABU EBAYYEH  **AND ALIREZA MOUSAVI, (Senior Member, IEEE)**

Department of Electronic and Computer Engineering, Brunel University London, Uxbridge UB8 3PH, U.K.

Corresponding author: Abd Al Rahman M. Abu Ebyayeh (abdalrahman.abuebayyeh@brunel.ac.uk)


This work has been carried out in the framework of the IQONIC Project, which received funding from the European Union's Horizon 2020 Research and Innovation Program under Grant agreement No. 820677.

ABSTRACT Electronics industry is one of the fastest evolving, innovative, and most competitive industries. In order to meet the high consumption demands on electronics components, quality standards of the products must be well-maintained. Automatic optical inspection (AOI) is one of the non-destructive techniques used in quality inspection of various products. This technique is considered robust and can replace human inspectors who are subjected to dull and fatigue in performing inspection tasks. A fully automated optical inspection system consists of hardware and software setups. Hardware setup include image sensor and illumination settings and is responsible to acquire the digital image, while the software part implements an inspection algorithm to extract the features of the acquired images and classify them into defected and non-defected based on the user requirements. A sorting mechanism can be used to separate the defective products from the good ones. This article provides a comprehensive review of the various AOI systems used in electronics, micro-electronics, and opto-electronics industries. In this review the defects of the commonly inspected electronic components, such as semiconductor wafers, flat panel displays, printed circuit boards and light emitting diodes, are first explained. Hardware setups used in acquiring images are then discussed in terms of the camera and lighting source selection and configuration. The inspection algorithms used for detecting the defects in the electronic components are discussed in terms of the preprocessing, feature extraction and classification tools used for this purpose. Recent articles that used deep learning algorithms are also reviewed. The article concludes by highlighting the current trends and possible future research directions.

INDEX TERMS Automatic optical inspection, classification algorithms, electronics industry, feature extraction, image processing, image sensor, machine learning, machine vision.

I. INTRODUCTION

Defective products increase costs and deteriorates manufacturing processes [1]. Timely and accurate detection of defects helps industries to apply quality control and stabilization strategies to maintain competitive edge over competition [2]. Several quality monitoring approaches such as ultrasonic inspection, Eddy current, dye penetrant testing, thermography, circuit probe, X-ray and optical inspection are currently being used to assess products' quality in order to achieve 100% qualified products. Most of these approaches are considered non-destructive, where each one of them has its own advantages and disadvantages as shown in table 1.

The associate editor coordinating the review of this manuscript and approving it for publication was Mehul S. Raval .

Among these techniques, optical inspection approach for defect detection is one of the most common procedures used in industry [3]. Optical inspection techniques can be subdivided into manual optical inspection (performed by a human inspector) and automatic optical inspection (AOI) which is performed by using an image sensor and processor.

The rapid development and effective fusion of image capturing and processing technologies in recent years has caused tectonic shifts in the success of AOI techniques over manual optical inspection for quality monitoring and non-destructive testing in various industries [3]. The automation of quality monitoring and control process will lead to major productivity gains in the future. Noteworthy, manual optical inspection increases inspection time and reduces accuracy. Authors in [12], [13] have also showed that human vision

TABLE 1. Summary of quality monitoring approaches used in industrial inspection.

Quality Monitoring Approach	Description	Advantages	Limitations
Ultrasonic Testing	A typical ultrasonic-based inspection system consists of several functional units such as pulser, receiver, transmitter, and display device. Ultrasonic inspection uses the electrical voltage generated by the pulser to activate the transmitter. Transmitter generates sound signals at frequencies beyond human hearing (more than 20 kHz), to estimate some properties of the irradiated inspected component by analyzing either the transmitted or received signals detected by the receiver [4].	Speed of scan. Good resolution and flaw detecting capabilities. Suitable of use in the field and assembly line where the same part design must test repeatedly [5].	It is necessary to align signals that relate to materials of different thicknesses. High skill is needed to scan a part accurately. Need of test sample to insure accurate testing [4], [5].
Eddy Current	A typical Eddy current inspection system consists of magnetic coil that induce magnetic field and electromagnetic sensors. The interaction between the subjected magnetic field and the component under inspection induces eddy current which can be measured using electromagnetic sensors [6], [7].	Highly sensitive to material conductivity. Very simple and easy to implement. Inspection can be implemented without any direct physical contact between the sensor and the inspected component.	Electric signal obtained is low; thus, a high-performance measurement technique is required to improve signal-to-noise ratio. Scanning speed has to be improved when considering PCB testing. Inspection is limited to conductive materials (ferromagnetic or non-ferromagnetic) [6], [8].
Dye Penetrant Testing	Colored fluid penetrant is applied to the surface being inspected to detect any discontinuities. Light source is usually used by inspector to highlight the defective features on the surface being inspected.	Suitable to reveal surface defects such as cracks. Considered simple and low-cost method.	This method was a subject of research till the 90's but no further significant developments have been published there after. The capillarity and the viscosity of the fluid used for inspection can affect the accuracy of this method [9]. Requires human inspector interference.
Thermography	Thermal sensor is used to measure the infrared radiation from the inspected component and convert the radiation flux to temperature. The temperature distribution can be then illustrated in a form of thermal images.	Suitable for surface and inner inspections. Suitable for detecting large voids and crack defects.	Thermal noise can affect the accuracy of results. The ability of detecting inner defects is limited to certain inspection range. Overheating problems may occur [10].
X-ray	A typical X-ray inspection system consists of three components: X-ray source (tube), X-ray detector and a fixture to hold and control the position of the inspected component. Transmission of X-ray by a source through an object and a receiver receives the transmitted energy. From the transmitted energy, the internal condition of the inspected component can be assessed.	Suitable for surface and inner inspections. Suitable for detecting large voids and crack defects.	Conventional X-ray methods can be destructive. Relatively low resolution in micro level inspection. Long processing time (in the order of hours) [10].
Circuit Probe testing	Widely used for semiconductor wafers inspection by establishing a temporary electrical contact between test equipment and each individual die on a wafer to determine the state of a die (defected or non-defected). The major components of a circuit probe testing system include probes, probe cards, probe stations, and test equipment.	Circuit probe testing procedures are the simplest and most direct method of testing unencapsulated bad dies in semiconductor wafers.	Considered destructive testing. Probing errors may arise which cause good dies in the semiconductor wafer to be faulty [11].
Optical Inspection	Detects surface flaws and defects according human's visual perception. Optical inspection is performed using human inspector (manual inspection) or image sensor and processor (automatic inspection). A typical automatic optical inspection system is shown in Figure 16.	Most basic, low-cost and frequently used type among all quality monitoring approaches. Considered non-contact and non-destructive. Can detect surface defects and flaws. Automatic inspection can save time and enhances detection's accuracy.	Not efficient for inner defects. Manual optical inspection considered costly and can cause fatigue for human inspector.

inspection capabilities declines with dull and endlessly routine jobs (i.e. fatigue). On the other hand, modern capturing devices are capable of detecting tiny defective features and features with low intensity and contrast that even the most experienced inspectors cannot detect them using their naked eye. Recent studies have also revealed that humans cannot handle identifying color defects as color is psychological perception even though it is triggered by physical radiation [14], [15]. Automated machine vision data capture system have paved a way for large scale observations helping to gather statistically viable information for quality analysis and assurance methods [16], [17]. Chen and Harlow in [13] gave six productivity and efficiency reasons for using AOI instead of manual inspection. Freeing humans from the dull and routine, saving human labour costs, performing inspection in unfavorable environment, reducing demand for highly skilled human inspectors, analyzing statistics on test information and keeping records for management and decisions, and matching high speed production with high speed inspection. To add to these, one can include the expansion in scale, scope, application, and techniques that provide depth, breadth and multiple perspectives.

Recently, AOI algorithms were further enhanced by integrating them with machine learning techniques and deep learning, which at occasions could improve the result and speed of the detection process remarkably [18], [19]. Timm and Barth in [20] suggested that an AOI algorithm must satisfy two major requirements; 100% detection rate and minimum false alarm rate. Convolutional Neural Networks (CNN) was one of the common used deep learning algorithms recently for inspection purposes [21]. The reason behind this is because CNNs are specialized in dealing with image data. Furthermore, it does not need feature extraction or preprocessing for the images. Hence, preprocessing and feature extraction processes are embedded within the hidden layers of the CNN.

AOI technologies are currently used in many fields for inspection such as food [22], textile [23], construction [21], metals [24], and medical applications [25]. The aim for this study is to review and critique research articles that conducted AOI systems and algorithms for detecting defects in electronics industry during the last two decades. It is worth mentioning that this review paper is intended to highlight the current AOI trends in electronic industry, and may help researches to have a helicopter view of the recent developments in this area. The research questions studied in this review are summarized in Table 2. In this review paper, we will begin by highlighting the applications for AOI systems in electronics industry (section II). The defects investigated using AOI in the electronics industry are then mentioned and explained (section III). Section IV will discuss about the hardware setup of AOI system. Section V will explain the inspection algorithms used. Section VI will discuss about the sorting mechanism used in industrial inspection system. Finally, section VII will discuss about possible limitations and future directions of AOI systems. Mindmap in

TABLE 2. Research questions.

Question Code	Research Question
RQ1	What are the common inspected electronics components in the electronics industry using AOI?
RQ2	What are the defects investigated in each electronic component?
RQ3	What are the current hardware requirements for AOI system in electronics industry?
RQ4	What are the advantages and shortcoming in various hardware inspection setups?
RQ5	What are the current studied inspection algorithms applied in electronics industry for feature extraction and classification?
RQ6	What are the advantages and shortcoming of the currently used inspection algorithms?
RQ7	How the reviewed studies are distributed according to the country of research?
RQ8	How can optical inspection evolve in the future and what are the current challenges?

Figure 1 shows an overview for the structure of the review.

II. AOI APPLICATIONS IN ELECTRONICS INDUSTRY

Electronics is one of the fastest evolving, most innovative, and most competitive industries [26]. The past five years, have been characterized by growth in emerging markets and introduction of new products, leading more people to buy consumer electronics. The global consumer electronics industry was valued at \$1 trillion in 2020 [27]. Production of electronics involves many manufacturing processes from automated assembly lines to testing and final manual assembly [28]. The electronics product sizes are getting larger for home display devices such as the LCD TV sets. Or, the product sizes are dramatically reduced for handheld or wearable devices such as smart phones and smart watches, as a result the need for an AOI system to the various sizes of electronics products were not an exception from any other industry [29]. In fact, the challenges facing the electronics industry is much severe compared to others, as the electronics products and manufacturing plans evolve rapidly and the electronics products tend to have short life cycles [30]. These challenges require to change the process parameters accordingly. All of these changes (whether they are sudden or long-term) cause defective products, and therefore quality assurance and process improvement is very essential in electronics industry. According to Xie et al in [31], in electronic manufacturing industry, a defect is a condition that may be insufficient to ensure the form, fit or function of the end product.

The keywords used in the searching process for the reviewed articles are explained in Appendix. The results for the conducted search are found in the map of Figure 2. We found that AOI in electronics industry was widely used in four major applications: light emitting diodes (LED) inspection, semiconductor wafer inspection, printed circuit board (PCB) inspection and flat panel display (FPD) inspection (e.g. LCD and OLED). We also found that some literature considered AOI for some miscellaneous

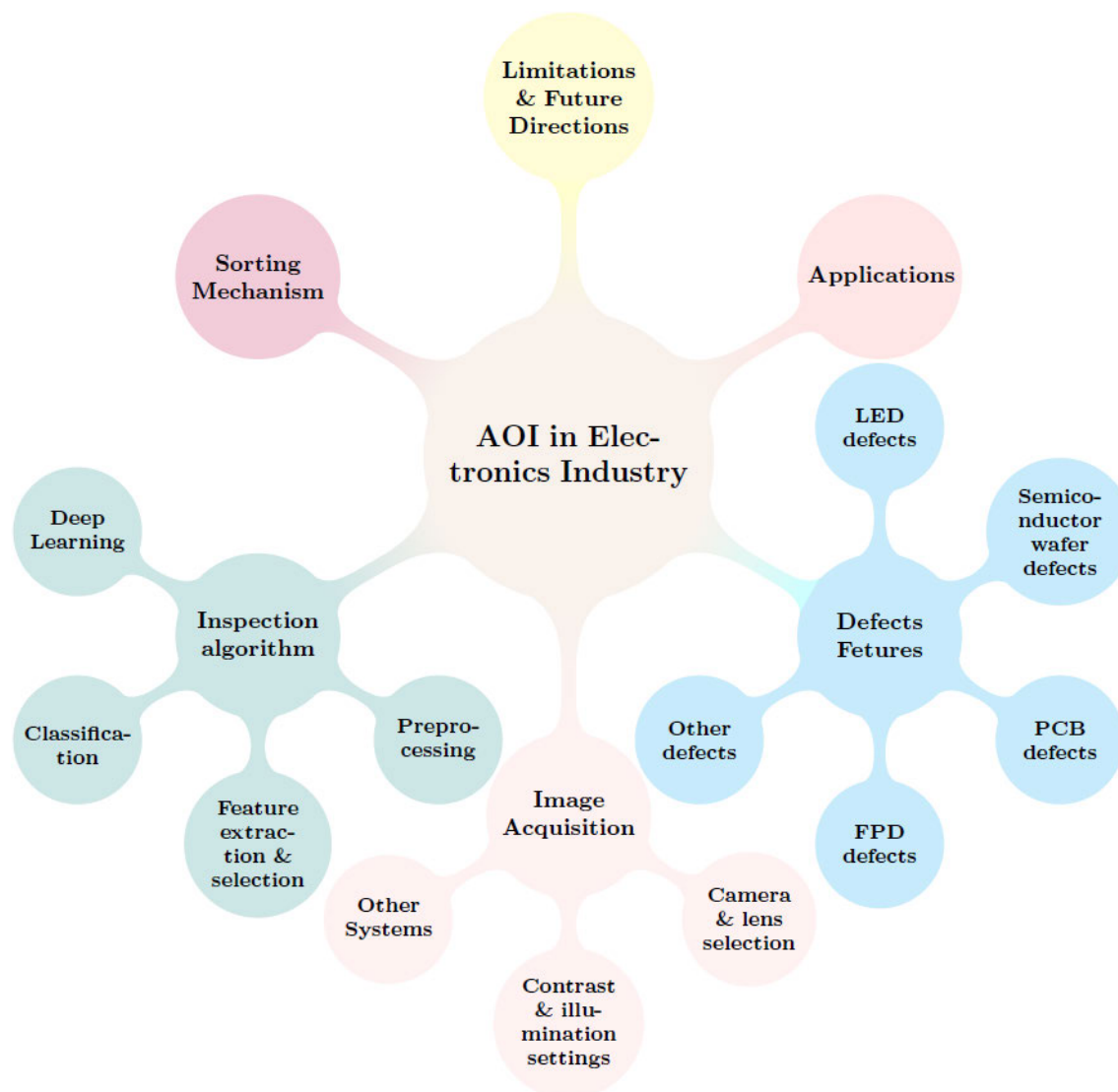


FIGURE 1. A mindmap that shows the structure of the review article.

applications such as detecting defects in camera modules, fuses, and passive electronic components. Figure 2 shows that 93 of the reviewed articles used AOI techniques for semiconductor wafer defects detection, 83 for FPDs, 75 for PCBs, 19 for LEDs and 12 for miscellaneous electronic component defects. We also observed that the highest concentration for the research articles reviewed in this paper are conducted in Taiwan with a percentage of 41.84%, followed by china mainland with 22.7%, then South Korea with 12.8%. This comes with no surprise as according to the report in [32], most of the world’s supply of electronic components and products are produced in Asia. Furthermore, Asia is now the major end market for many of these goods too. In 2018, for example, 40% of all personal computers sold worldwide, were sold in China alone. According to the same report, electronic exports in Taiwan alone accounts 45% of the country’s total exports, while China and South Korea account 35% each. The average for Asia total electronics exports is 30%.

III. DEFECT FEATURES

In this section we report and appraise the historical evolution of the process of transition and translation of visible defect features detected by sensors, into data for automatic feature extraction, classification and evaluation of components by vision systems.

A. LED DEFECTS

Due to their proliferation and importance, LED have been the focus for many researchers and industrialists [33], [34]. LEDs are used in various applications that include mobile phones, lighting equipment, vehicle accessories and panels of various sizes [35]. According to the application there are various types of LEDs such as dual-in-line package (DIP) LED, surface-mounted device (SMD) LEDs and High Power (HP) LEDs (also called chip-on-board COB LEDs) as shown in Figure 3. To meet consumer and industry needs, LED products are being made in smaller sizes, which increases

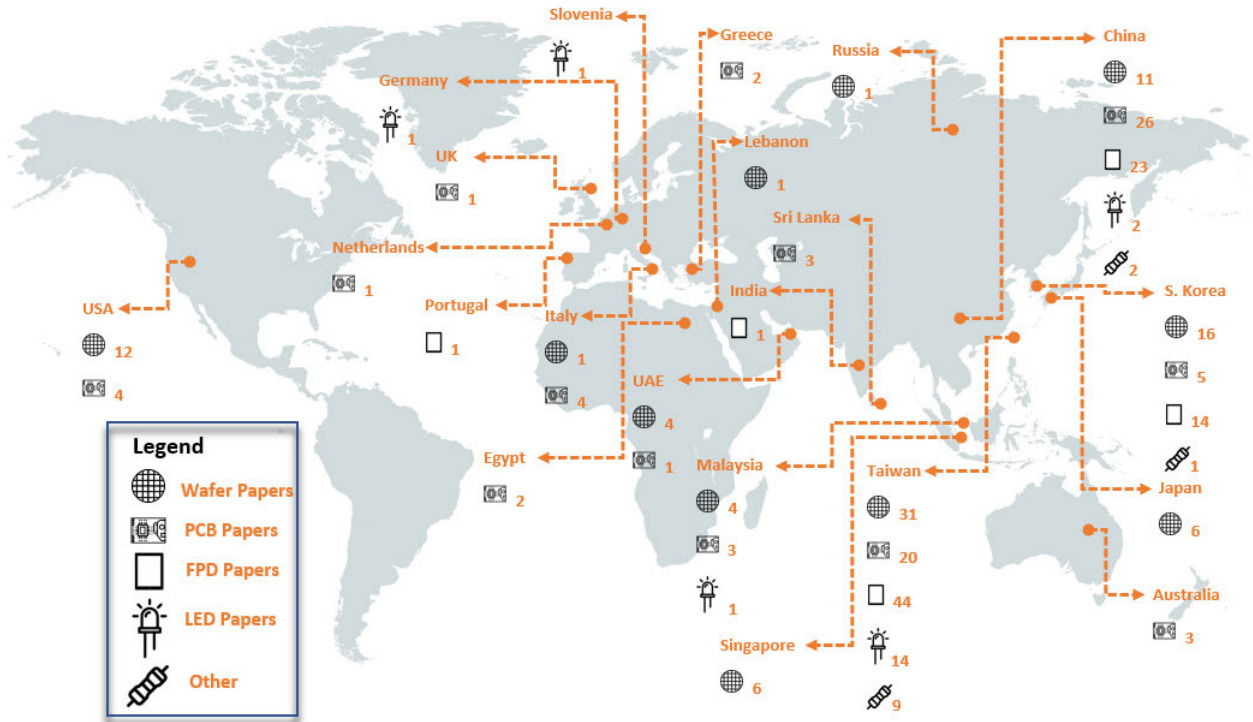


FIGURE 2. A map that shows the literature found for reviewing according to the country and the defect type considered.

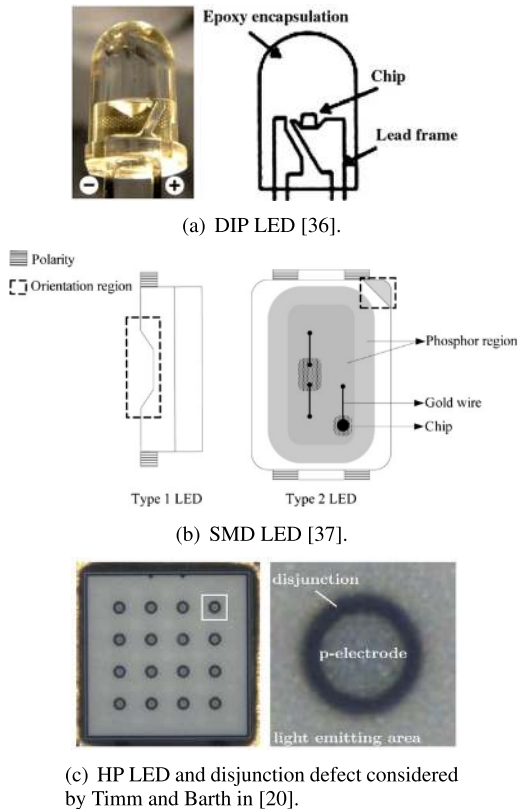


FIGURE 3. Different LED types.

the difficulties of product inspection [38]. Mainly there are two types of inspection, electrical and optical inspection.

The electrical inspection ensures correct functionality, but since an extensive stress test cannot be applied for all LEDs, defects that might cause malfunction after a period of time cannot be detected accurately [20]. Therefore, many researchers have conducted studies to detect different defects of LED types using AOI techniques. Ahmed Fadzil and Weng in [39] were one of the earliest researchers to consider LED defects using AOI. Their study inspected cosmetic flaws on the epoxy dome of DIP LEDs such as contamination, scratches, blister/blemish and fuzzy defects as these kind of defects impair the appearance of LED chips as well as their functionality and security [36]. They showed that each type of defect has special features in order to be detected efficiently by the image sensor. For example, contamination defects (which are caused by contaminated mould cups or dust) appears to be flat black region on or inside the epoxy and is easily discerned from the uniform background. On the other hand, bubble defects (which are results of improper curing process control) appears as small black circle and may look like a small ring if the bubble is big enough to reflect the light from the bubble region. Other type of defect such as blister/blemish and fuzzy (which are caused by different manufacturing process deviations) appears as group of scratches. Lin and Chiu in [38], [40] considered similar kinds of these external defects. Yang *et al.* in [41] considered different types of external defects (aperture defects) in LED bulbs, which affects rivet installation process as shown in Figure 4. Defected apertures can be recognized by their circular area and contour lines appearance. Therefore, an optical inspection algorithm was used in this study to extract the maximum

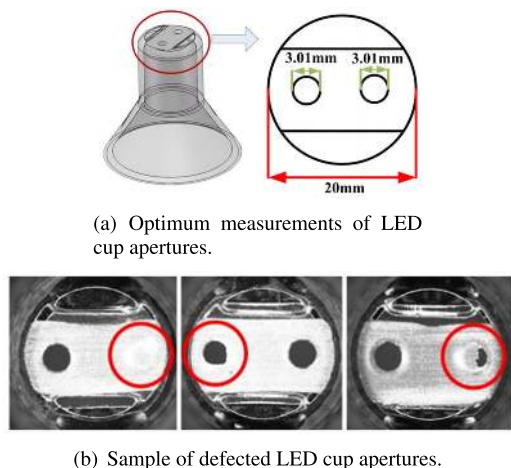


FIGURE 4. LED cup aperture defects studied in [41].

inscribed circles of the apertures and calculate the diameters for evaluation.

Perng *et al.* in [37] considered investigating Type 1 and Type 2 SMD LEDs shown in Figure 3(b). An orientation region was labelled in both types to distinguish their polarities. In Type 2 LED, there are three gold wires and a chip in the phosphor region. The quality of the phosphor region influences the LED illuminating efficiency. Defects of lighting phosphor region can be inspected visually in Type 2; however, the lighting phosphor region of Type 1 cannot be seen due to its physical placement when it is packaged. Therefore, in this study, only external defects are considered in Type 1 LED. Generally speaking, the defects in both types take place during fabrication and taping processes. Examples of these defects are mouse bites, missing gold wires, surface flaws, missing component, wrong orientation and inverse polarity. These defects can be identified visually by converting the acquired image of a sample LED into a binary image and examine the number of pixels of the segmented areas that represent the regions of interest. Perng *et al.* in [33] considered the same types in their study. However, they subdivided Type 1 LED into 2 sub-types, namely, small polarity and big polarity for better defect classification. A similar approach proposed by Kuo *et al.* in [42] to detect missing component, no chip, wire shift and foreign material defects in SMD LEDs.

Some researchers considered evaluating the light intensity and other physical properties of LEDs using AOI system. Bürmen *et al.* in [43] analysed the optical properties of LEDs by projecting the LED light on screen and analyzing the image of the resulted projection. The optical properties studied in this paper were intensity, mean color, color variation, viewing angle and divergence of the optical axis. In order for them to conduct the study, they connected in series two LEDs; one of them were a reference LED (non-defected) and the other were the LED for testing purposes, to pass the same electrical current for both. The reflected light for both LEDs from a screen were captured by image sensors for further analysis. The optical properties of the reference LED were

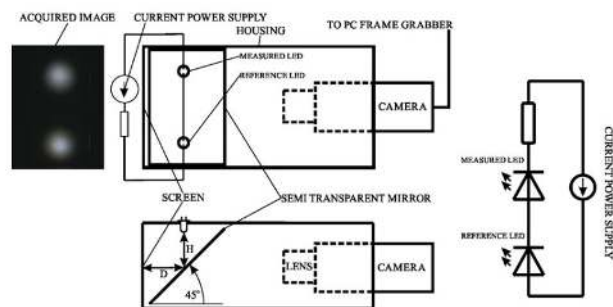


FIGURE 5. Image acquiring technique considered in [43].

compared to the one for testing. One drawback in this method that through the testing process the properties of the reference LED may change by time, and therefore the testing may not be reliable.

Other researchers considered internal LED defects that take place in the LED die regions, where such defects are considered hard to detect and need special arrangement such as scanning electron microscope (SEM). Chang *et al.* in [44] proposed an AOI system to detect defective dies in a four-element wafer, such that each wafer consists of more than 8000 dies and the physical area of each die is about $200 \mu\text{m} \times 200 \mu\text{m}$. The die first were divided into three regions: light-emitting area, p-electrode, and background. The inspection of the die regions was performed geometrically and heuristically. In geometric inspection the die size, width, height, the electrode radius, and the center of the electrode are evaluated according to pixel intensities. In heuristic inspection, abnormal regions in the image are evaluated such as empty pixels in light-emitting region. Timm and Barth in [20] followed the same path in investigating die defects in HP LEDs. They have focused their attention to the p-electrode of the die and its surrounding area, where discontinuity and erosion defects could occur (as shown in Figure 3(c)). Erosion and discontinuity defects cause the p-electrode gets directly connected to the light emitting area and thus can lead to critical malfunction of the LED. Since p-electrodes are circular regions, radially encoded features were examined to look for pixels intensities that could indicate a presence of a discontinuity defect. Besides the complexity of the defects, low contrast and strong image noise of these defects make this problem very challenging. Lin in [36] investigated water-drop defects that cause surface blemishes which fall across two different background textures in DIP LED chip (shown in Figure 6). This defect occurs due to the steam generated during the production process. As the case in epoxy packaging defects, these kinds of defects impair the appearance of LEDs as well as their functionality and security. The detection process of water-drop defect is not straight forward as the blemish has a semi-opaque appearance and a low intensity contrast with the rough exterior of the LED chip. Moreover, the blemish may fall across two different background textures, which further increases the difficulties of defect detection. Therefore, the images acquired images

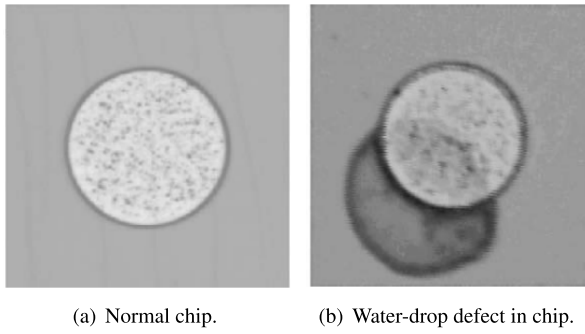
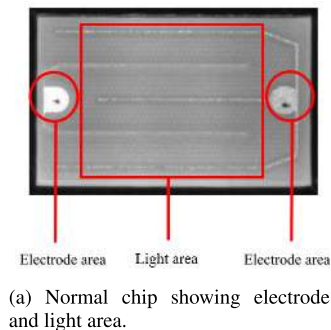
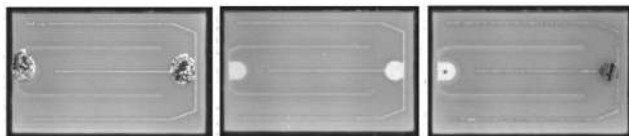


FIGURE 6. Water-drop defects considered in [36].

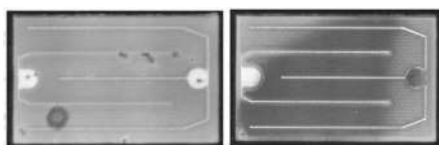
for these defects were converted to the frequency domain for extracting the defect features as discussed in section V-B1. Kuo *et al.* in [45] considered multiple LED chip defects such as fragment chips, scratch marks and remained gold on the pad area, scratch marks on the luminous zone and missing luminous zone. These defects were analysed geometrically by evaluating area and perimetric measures of the segmented areas of interest acquired from images. Kuo *et al.* in [46] investigated LED chip defects in two areas of the chip; electrode area and light area, which directly affect the luminous efficiency (shown in Figure 7(a)). The investigated defects in electrode area in this study are contamination, non-probe and scrape as shown in Figure 7(b). While light area defects include breakdown and color aberration defects as shown in Figure 7(c).



(a) Normal chip showing electrode and light area.



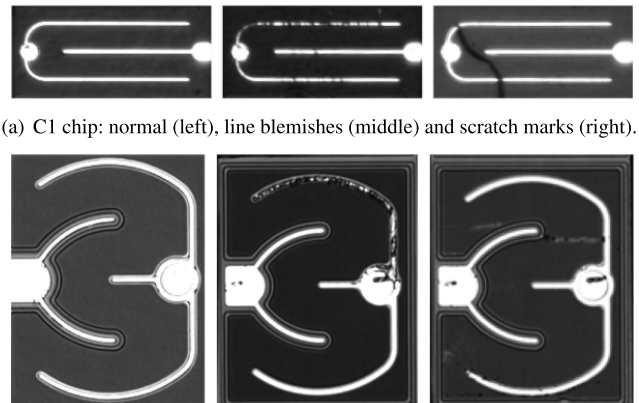
(b) Electrode area defects: contamination (left), non-probe (middle) and scrape (right).



(c) Light area defects: breakdown (left) and color aberration (right).

FIGURE 7. LED chip defects considered in [45].

In similar study, Lin *et al.* in [47] investigated line blemishes and scratch marks of two different types of LED chips, namely, C1 and C2 as shown in Figure 8. Zhong *et al.* in [48] investigated polycrystalline and fragmentary defects in LED chips. Polycrystalline defects are referred to the LED chips that contain a part of another chip and is therefore bigger than a normal one. It is referred also to the chips that has a tiny distance difference between them. Fragmentary defects are referred to the chips that lack a part and are smaller than normal chips. Polycrystalline and fragmentary chips are mainly caused by improper cutting. The acquired images of these defects were segmented into blobs that represent the regions of interest. The pixels intensities and geometrical features are analysed based on the pose of the minimum enclosing rectangle of each blob to extract the defected features.



(a) C1 chip: normal (left), line blemishes (middle) and scratch marks (right).

(b) C2 chip: normal (left), line blemishes (middle) and scratch marks (right).

FIGURE 8. LED chip defects considered in [47].

Table 3 summarizes the LED defects studied in literature according to the part being investigated.

B. SEMICONDUCTOR WAFER DEFECTS

Advances in semiconductor technology and design have been the driving forces behind the successful progress of electronics industry [53]. The majority of integrated circuits (ICs) that are used in microelectronic and optoelectronic devices are manufactured using semiconductor wafers on their surface [54]. Semiconductor wafers consist of repeated dies which have the same structure and results in large numbers of ICs and devices. Therefore, the process of fabrication is a complex, long and costly which involves hundreds of chemical steps that must take place in a clean room environment such as oxidation, photolithography, etching, ion implementation, and metallization and requires monitoring a large number of key process parameters [55], [56]. After the fabrication process, wafer testing on each fabricated die is performed using test equipment called “wafer probe” (also “circuit probe”) to verify whether all dies meet the product specifications and ensure that only good dies are sent to the next manufacturing process [55]. To visualize the defective dies in a wafer, a Wafer Map (WM) is created. WM allows

TABLE 3. Summary of articles that used AOI system to investigate LED defects.

LED Part	Reference	Inspected Defects
Exterior parts	[39]	Defects occur on the epoxy dome of the DIP LED such as contamination, scratches and blister/blenish and fuzzy defects.
	[40]	Tiny surface flaws (flaws that occupies 0.0015 – 0.0229% of the total surface area) on the transparent epoxy dome-shape encapsulation of DIP LEDs
	[38]	Blemish defects in curved LED lenses that occur on the external surface of the lens
	[41]	Aperture defects in LED bulb cups
SMD LED	[37] [33]	Two types of LEDs were studied, and the defects investigated are: missing component, wrong orientation, inverse polarity, mouse bites and surface defects
	[42]	Missing component, no chip, wire shift/defect and foreign material presence
LED optical properties	[43]	Intensity, mean color, color variation, viewing angle and divergence of the optical axis.
	[49]	Luminance and forward voltage inspection
LED chips	[44] [50]	Inspection of LED die defects geometrically (in terms of die size, electrode size) and heuristically in terms of other defect types in light-emitting regions and electrode region such as empty points in light-emitting region
	[36] [51]	Water-drop defects that causes blemishes on LED chip surface
	[52]	Overall inspection of LED dies in a wafer in terms of the quality of light-emitted area, N-electrode, P-electrode and probe marks
	[52]	Overall inspection of LED dies in a wafer in terms of the quality of light-emitted area, N-electrode, P-electrode and probe marks
	[20]	Discontinuity and erosion defects located at the area of p-electrodes and disjunction region of LED die.
	[45]	LED chip defects that include: fragment chips, scratch marks and remained gold on the pad area, scratch marks on the luminous zone and missing luminous zone
	[35]	LED wafer luminance test
	[48]	Polycrystalline and fragmentary defects
	[46]	Electrode area defects such as contamination, scrap, and non-probe defects. Light area defects such as breakdown and color aberration defects
	[47]	Line blemishes and scratch marks in two types of chips

to compare neighbor dies with each other and locate how many dies are defected visually using a map image [57]. Wafer maps are also called Wafer Bin Map (WBM) when the dies are represented in binary form such as the defective dies has logic '1' and the non-defected has logic '0'. Normally three types of wafer defects occur, which are random defects, systematic defects and mixed defects. Random defects (Figure 9(h)) result from random manufacturing environmental factors, such as particles in the clean room; these can become randomly scattered all over the wafer. Such defects are long-term and expensive to correct. On the other hand, systematic defects are normally generated by an assignable cause such as a human mistake, particles from equipment, or chemical staining [58]–[60]. Systematic defects usually

follow a specific pattern, for instance, a center pattern (also known as bull's eye) concentrated in the center of a wafer typically occurs when there are uniformity variations caused by a chemical mechanical process (CMP), the distance between the wafer center and the center of the region is less than four dies (shown in Figure 9(a)). A ring pattern (shown in Figure 9(b)) appears along the wafer edge when there is a layer-to-layer misalignment in the storage-node process, which results in a write recovery time failure that is due to the decreased size of the contact holes, most of the failed dies occur along the wafer edge and encompass more than four-fifths of the wafer perimeter. A scratch pattern as shown in Figure 9(d) (also known as line pattern) is caused by agglomerated particles and the hardening of the pad during the CMP, where most of the failed dies on the wafer form a line, and the length of the line is five or more dies. A shot pattern (shown in Figure 9(e)) is caused by a probe-card problem when multiple dies are simultaneously tested to reduce the test cost. A zone pattern (also known as blob, spot, or cluster) at a specific location on the wafer is caused by non-uniformity or uneven cleaning, where most of the failed dies on the wafer occur as an arbitrary shape, and the distance between the wafer center and the center of the region is more than four dies as shown in Figure 9(g). A checkerboard pattern as shown in Figure 9(f) is generated because of the mask misalignment during the lithographic process. Mixed defect consists of a random defect and a systematic defect in one map. Most WMs are of this type. Hence, it is important to separate random and systematic defects in

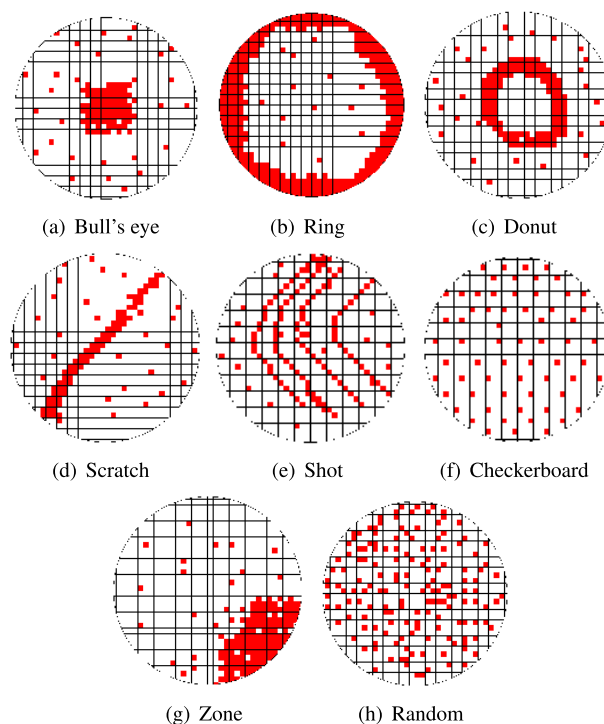


FIGURE 9. Different WM patterns (red squares indicate defective dies).

the WBM since the systematic defect’s signature can reveal the process problem. Therefore, it is important to detect and classify these defects, in order to identify the root causes of failure and to take appropriate actions for quality and yield enhancement [55], [58], [59], [61]. Although after generating the WM, the defective dies can be detected by an experienced human inspector; however, as this process can be costly and time consuming, many researchers evaluated the dies’ quality using AOI techniques [62]. Most of the AOI techniques used in semiconductor wafers can be considered semi-optical for the purposes of this review since most of them does not require establishing an image acquisition system (e.g. camera and illumination setup). Hence, the WM image is constructed from the circuit probe scanning. However, some articles still considered conducting an image acquisition system (usually with the aid of SEM) for the inspection purposes of semiconductor wafers. In order to distinguish between both methods used, research articles that used circuit probe to produce the WM are labelled as “semi-optical” in Table 4. On the other hand, research articles that used optical inspection setup are labelled as “optical” in Table 5.

C. PCB DEFECTS

In recent years, demands for the placement of electronic components on PCBs at a higher density have increased [136]. These components are assembled through electronic assembly lines which are applied in the manufacturing of all electronic products such as TV, digital cameras, etc. The main steps in the manufacturing of PCB are the following: applying solder paste to PCB, placing IC on the board at correct positions and placing the board in an oven to solder components to pads. [137]. During the manufacturing of PCBs, various defects may occur at each stage, most of them occur at soldering and component placement stages as shown in the pie chart of Figure 11. For example, at the IC placing stage, defect cases of missing, wrong or doubled components may occur. In terms of possible soldering defects, most of them happen after the reflowing stage, such as the defects at the IC package components (pseudo joint, excess solder, insufficient solder, shifting Solder and bridge defects) and the defects at the non-IC components (side termination, tombstoned components, raised components, pseudo joint, excess solder, insufficient solder, shifting, solder bridge) [138]. These defects can severely affect the functionality of the PCB. For instance, a missing solder joint or insufficient solder joint can cause an open circuit of the PCB and thus the overall functionality of the circuit will be affected. Excess solder joint can cause bridging with other PCB solder joints which can lead to a short circuit. Pseudo solder (also known as cold solder) is considered a complex defect for detection [139]; this defect occurs when the solder joint terminals are seemed to be connected with the electronic component; however, there is no physical connection occurring which may lead to open circuit contact. A pseudo joint is formed when insufficient heat is applied to completely melt the solder [140]. Figure 10 shows commonly investigated defects in PCB industry.

TABLE 4. Summary of articles that used semi-optical system (circuit probe) to produce WM for inspection.

Inspection Type	Reference	Defect / Pattern Type considered
Semi-optical	[63]	Ring, scratch, zone and repeating types
	[64]	Ring, scratch, random and new patterns
	[65]	Systematic and random patterns
	[66]	Circle, cluster, scratch and spots
	[67] [68]	Bull’s Eye, Edge ring, scratch, random, multiple zones, multiple scratches, ring-zone mixed pattern and ring-scratch mixed pattern
	[69] [70]	Multiple zones, multiple scratches, ring-zone mixed pattern and ring-scratch mixed pattern
	[71] [72]	Cluster defects such as scratch, strains and localized failures
	[58]	Checkerboard, ring, right-down edge, composite and random patterns
	[73]	Spatially homogeneous Bernoulli process, cluster, circle, spot, repetitive and mixed pattern
	[74]	Scratch, center and edge
	[75]	Quarter ring, up and left, Quarter ring, up and right, Edge effects, Ring effects, Semi-ring, up, Semi-ring, up Edge effects, up and bottom Cluster
	[76]	Annulus, half-annulus, band and half-ring
	[77]–[81]	Curvilinear, amorphous, and ring
	[82]	Linear and circular patterns
	[83] [84]	Bull’s eye, Bottom, Crescent moon, edge and random
	[85]	Random, ring, curvilinear and ellipsoid
	[59]	Line, edge, ring, blob and bull’s eye
	[61] [53]	Bull’s eye, blob, line, edge, hat and ring
	[86]	Multiple patterns including ring, checkerboard and five radial zones
	[87]	Random, systematic and mixed patterns
	[88] [57]	Circle, cluster, repetitive and spot
	[56], [60], [62], [89]–[94]	Center, donut, edge-local, edge-ring, local, random, scratch, near-full and non-pattern
	[95]	Center, edge, repeated scratch, C-shape and donut, center+edge and mask+local
	[96]	Rings, semicircles, clusters, and scratches
	[97]	One-side, center, and edge
	[98]	Random patterns
	[99]	DRAM wafer failures
	[100]	Random, cluster, circle, and repetitive
	[101]	
	[102]	General patterns
[103]		
[55]	Circle, ring, scratch, shot and zone	
[104]		
[105]	Systematic patterns	
[106]	Random, edge ring, line scratch, curved scratch, non-random cluster, gross defect at entire wafer and each half.	
[107]		
[108]	Circle, spot, cluster, scratch, circle-spot, cluster-scratch and circle-scratch	
[109]	Donut, moon, reticle, scratch, center, and edge	

Electric tests and manual vision inspection test are still used; however, introducing surface mount technology (SMT) to the PCB assembly process made the PCB circuits much finer and more complex, which make the previously mentioned defects more likely to occur and highlight the necessity of an AOI system [142]. In fact, it was proven that around 80% of the optically recognizable defects could not

TABLE 5. Summary of articles that used image acquisition optical system to inspect semiconductor wafers.

Inspection Type	Reference	Defect / Pattern Type considered
Optical	[110]–[118]	Overall quality inspection of wafer
	[119]	IC wafer contamination
	[120]	Micropipes defects
	[121]–[123]	Chip-out, bridging, metal lifting, glassivation and peel off
	[124]	Wafer topside scratch, foreign material, ink residue, pad damage, passivation/metal damage, ink smeary, and passivation covering
	[125]	Pinhole defects
	[126]	Protrusion, dent, flat and bumpy defects
	[127]	Hole, Protruding and flat patterns
	[128]	Particles, contamination and scratches
	[129]	Defects between line edges
	[130]	Hole, flaw and scratch defects
	[131]	Alignment, probe marks and bump defects for in-tray semiconductor chip
	[132]	Spots, scratches, and bruises
	[133]	Bond pad discoloration
	[54]	Die edge, die street and determination of chipping size and shape
[134]	Spot, rock-shaped particle, ring-shaped particle, misalignment and scratch	
[135]	Defects are classified as small, medium and large	

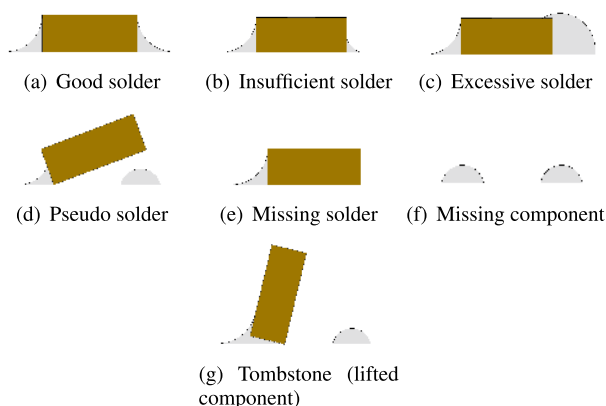


FIGURE 10. Commonly investigated PCB defects.

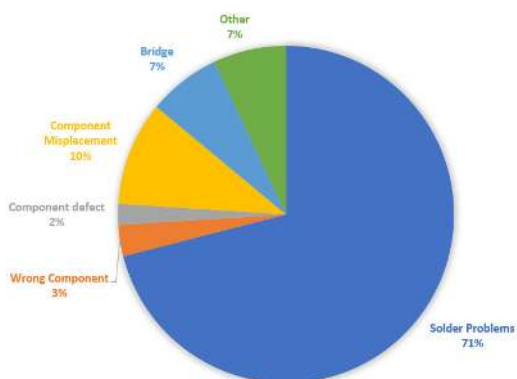


FIGURE 11. The frequency of PCB-related defects [141].

be recognized electrically [143]. Therefore, many researchers have investigated different types of PCB defects using AOI techniques. Hence, AOI for PCB boards was one of the

oldest subjects among other aspects in electronics industry. Chin *et al.* in [144] can be considered one of the earliest researchers to use AOI in PCBs. Most of the research articles that investigated PCB defects using AOI considered solder joint defects and IC component placement using SMT as shown in Table 6. Few studies considered IC marking inspection. In IC marking inspection, incorrect direction or marking will lead to incorrect placement of an IC on a PCB [145]. The inspection has to identify print errors such as illegible characters, missing characters and upside down printing which frequently occur due to the malfunction of the machinery [146], [147]. A typical industrial version of an inspection system has to check about 7,300 – 7,500 IC chips per hour, which justify the need for an AOI system to handle the inspection task [146].

Where most of the researcher focused on inspecting SMT solder joints, Fonseka *et al* in [148] inspected through hole technology (THT) solder joints. In contrast to SMT, the bulkier packages of THT components have a higher positioning tolerance and are soldered from the other side of the PCB. Solder joints of THT connections have highly reflective metallic surfaces and thus are a very challenging object for typical light based profilometric measurement systems [149]. Fonseka *et al.* conducted 4 studies to investigate THT solder joint defects. Three of these studies [150]–[152] were focusing on extracting the features and creating color models for pad and solder joint detection. While the fourth study [148] was a continuation approach that focused on automatic solder quality classification for solder bridging, voids in drill-hole region, voids on pad region, and excess solder on solder joint. According to them, THT solder joint inspection must be carried out within 6 seconds to meet the manufacturing requirements. However, their inspection system needs 8 seconds, which may affect its ability to be implemented in inline inspection task.

Golden fingers of PCBs were also one of the visually inspected components in literature; golden fingers are connecting terminals found on the edge of PCBs to enable connections between multiple boards. They can be made from gold combined with nickel or copper materials. Like all other parts of PCBs, gold fingers are prone to many kinds of defects. Jiang *et al.* in [153] considered 4 types of golden fingers defects: scuffing, blotting tin, exposed nickel, and un-plating defects. Jiang *et al* in [154] considered bulged, coarse, and wet-tinned golden fingers for inspection. Tsai *et al.* in [155] considered defects such as pinholes, copper exposure, and nicks and roughness on gold-plated surfaces. Similarly, many articles found in literature considered PCB traces’ defects. Traces refer to the copper wiring in PCB that is responsible for passing the electric current. Ibrahim and Al-Attas in [156] was one of the studies which considered these types of defects. In their investigation, they have divided the defects that occur in this area into two categories namely functional and optical defects. Functional defects seriously cause damage to the PCB, meaning that the PCB does not function as needed. Visual defects do not affect

TABLE 6. Summary of articles that used AOI system to investigate PCB defects.

PCB Part	Defect Type	Reference
Solder Joint	Missing Solder	[139], [158]–[163]
	Insufficient or open solder	[143], [158]–[172]
	Excess or bridged solder	[139], [143], [148], [158]–[170]
	Pseudo Solder (cold solder)	[139], [159], [160], [163], [171], [172]
	Solder Joint Overall Quality	[173]–[176]
	Solder Paste Inspection	[142], [177], [178]
Electronic Components	Missing Component	[137], [139], [163], [179]–[181]
	Wrong Component	[139], [171], [172], [180]
	Shifted or rotated component	[139], [159], [160], [163], [171], [172], [179], [180]
	Component lifted (tombstone)	[139], [159], [163], [171], [172], [180]
	Component misplacement	[182]–[186]
	IC molding surface	[187]
	Electronic Component Overall Quality	[29], [137], [188]
PCB Holes	Via holes	[148], [189]
	Microdrill bits	[190], [191]
Other	Golden fingers	[153]–[155]
	Traces & Inner layers	[156], [192]–[194]
	Marking inspection	[145]–[147], [181]
	Cosmetic & small defects	[31], [194]
	Scratches and improper etching	[195]
	Glue quality	[196]
	Flux Cutting	[181]
	Alignment and position inspection of PCB	[29], [197]
	PCB Overall quality	[188], [198]–[200]
	Ball Grid Array (BGA)	[136], [157], [188], [201]–[209]

the functionality of the PCB in short term. But in long period, the PCB will not perform well since the improper shape of the PCB traces could contribute to potential defects. Fourteen types of functional and visual defects were considered in this study: breakout, short-contact, pin hole, wrong size hole, open circuit, conductor too close, under-etch, spurious copper, mouse-bite, excessive short, missing conductor, missing hole, spur and over-etch.

Similar to PCB, Ball Grid Arrays (BGA) is a kind of a SMT package which is used in electronic products to mount electronic components such as ICs and microprocessors. The pins used for connection are called solder balls which are arranged in grid-like pattern. BGA packages are normally placed on a similar grid pattern of copper pads on the required PCB. Unlike conventional mounting method, the BGA takes advantage of the bottom surface, instead of the perimeter of the IC for connection. Hence, BGA provides an opportunity to increase the number of pins, shorten the average lead lengths, and improve the high-speed performance. However,

as the size of the solder balls becomes smaller and the pitch between solder balls shortens, there is a higher demand on the optical measurement system of component placement machines [157]. Therefore, many researchers considered inspecting the resulting defects that can occur during the BGA fabrication and placement process. Table 6 summarizes research articles that used AOI system for defect detection according to the PCB part and defect type.

D. FPD DEFECTS

Since the existence of the father of all displays, the cathode ray tube, electronics displays became an important aspect of human’s modern life [210]. Currently, Liquid Crystal Display (LCDs) are the dominant technologies in the field of electronics visual displays due to the variety of their applications ranging from smartphones, tablets, computer monitors, televisions (TVs), to data projectors. LCDs as the name states are made from liquid crystals, which are considered non-emissive materials and therefore does not emit light. Therefore, a backlight is usually needed to light the LCD display panels. Owing to the advances in material research, thin-film transistor (TFT) LCD technology has gradually matured in all aspects; some key hurdles, such as the viewing angle, response time and color gamut, have been overcome [211]. Thus, manufacturers have been devoting considerable efforts toward increasing production of TFT-LCD. In general, TFT-LCD manufacturing process can be divided into three stages: TFT array process, cell process and module process [212]–[214]. TFT array process alone consists of five successive operation: gate electrode (GE), semiconductor electrode (SE), source and drain (SD), contact hole (CH), and pixel electrode (PE). Therefore, the complex manufacturing processes of these displays make the TFT-LCD subject to many kinds of defects. Many factors contribute to these defects such as the nonuniform color of color filter substrate, the anisotropy of polarizer, the non-uniformly distributed liquid crystal material, the open or shorted scanning lines, the defective TFTs, the unevenness of TFT-array substrate, and the foreign particles within liquid crystal [215]. According to [216], [217], FPD defects can be approximately classified into three types: area defects, line defects and point defects. While Nam *et al.* in [15] classified them into achromatic and chromatic. Mura (derived from Japanese which means blemish) defect is one of the achromatic defects and is widely investigated among researchers using AOI techniques. Mura defect is a local lightness variation on a surface without clear contours and causes an unpleasant sensation to the human vision [215]. Figure 12 shows different types of Mura defects investigated in literature. According to Wu *et al.* in [218], that classified TFT-LCD defects into macro and micro defects, Mura defects are considered one of the macro defects that are relatively large and can be recognized by naked eye. Despite of that, some Mura defects are relatively hard to inspect and often appears as low contrast and blurry contours. And the global intensity inhomogeneity of defect-free region makes the inspection

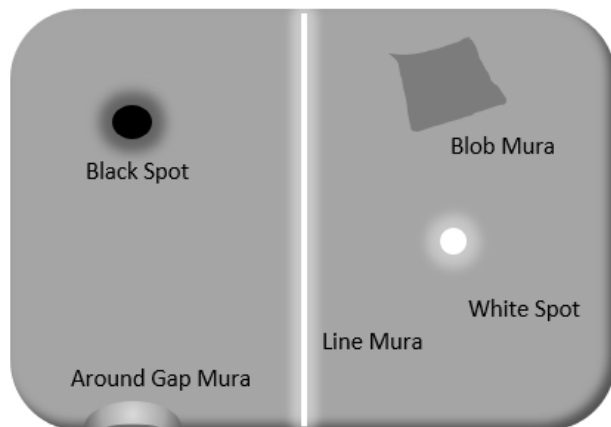


FIGURE 12. Different types of Mura defects.

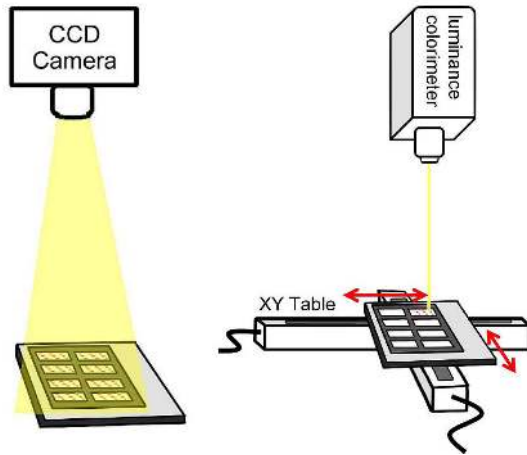
even harder. As these Mura defect always has no distinct difference from background region in both intensity and gradient, simple image processing methods for detection are infeasible [219]. In general, Mura assessment is performed by observing any imperfections present on the scale of a few pixels to usually less than 20% of the screen diagonal and not on a large area [220]. Researchers in [221], [222] investigated one of the assembly processes that may produce gap Mura defect in TFT-LCD. In this process, the assembly of the two glass substrates with sealant around the four sides takes place. The sealant is dispensed from syringes, leaving a very narrow space called the cell gap between the two substrates, which is later filled with the liquid crystal material. However, in some cases during the attachment process, the glass substrates may not be aligned with each other. Moreover, the distance between them may not be the same at every point. When this occur, the assembled TFT-LCD can be observed with blurred interference patterns. The three main causes that may contribute to such situation are: are nonuniformity of the sealant (bubbles inside the sealant or excess sealant) around the panel, foreign materials in the panel, and a fibre cluster at the edge of the panel. The main advantage in the inspection of this method, the testing procedure takes place before injecting the liquid crystal material which can prevent the waste of material in case a defect has been detected.

Authors in [223]–[229] considered inspecting polarising film defects, according to the fact that polarising film is a key component in LCDs. Special aesthetic defects in polymeric film polarizers have nearly identical reflectivity and transmissivity as normal regions. Such defects, in the industry known as “convex or concave points”, have extremely low contrast and are difficult to image under normal illumination. Authors in [224]–[227], [229] defined them as “transparent defects”, such as dents, bulges and transparent impurities. Because of their extremely low contrast, these transparent points are the main obstacle to detecting defects in polymeric polarizers with existing detection technology. According to Deng *et al.* in [225] machine vision is the only feasible way for detecting the aesthetic defects of polymeric film polarizer, where they simulated the defects using lens optical arrangement.

Wijesinghe *et al.* in [230] investigated defects that occur in liquid resins. Liquid resins are gel substances that located between the window glass layer, optical thin film, and LCD panels. Several defects can occur in these resins such as fine dirt (dust particles) and impurities, which may lead to change the refractive index of the LCD panel. These kinds of defects require high resolution capabilities for the optical inspections system, therefore optical coherence tomography (OCT) was proposed to aid the image acquisition system. Ferreira *et al.* in [217] investigated a type of point defects that evaluates sub-pixel functional defects in the pixel of the display. They have also considered a special type of point defect that is called joint defects which are the defects that occurs on small number of adjacent pixels. For a colored LCD, subpixel elements (also called dots) are referred to the red, green, and blue subpixels that create each colored pixel. In this study they have constructed an AOI such that the resolution of the image sensor (e.g. camera) can be less than the resolution of the inspected display, by addressing the display with sparse periodic pixel patterns, while analyzing the aperiodicities in the display response to those patterns. Additionally, a color transformation between the sensor color space and the display color space compensates the crosstalk between sensor and display RGB channels, disambiguating intra-pixel dot intensities.

Lin *et al.* in [231] were one of the early researchers to inspect light guide plate used in LCD backlight module. The purpose was to detect the degree of non-uniformity of these plates by analyzing the intensity of light reflected by the tiny holes of the plates. The non-uniform regions will appear as bright spots which have larger intensity than the other regions. Lin and Jhuo in [232] also inspected backlight module defects in LCDs such as nonuniform luminance. Usually in inspecting such defects a luminance colorimeter is used to examine the luminance emitted from selected areas called check points within the backlight module as shown in Figure 13(b). However, since backlight module consists of many check points, this study proposed fast luminance inspector that uses a CCD camera to inspect multiple backlight modules simultaneously as shown in Figure 13(a). This can enhance the inspection speed remarkably and make their system suitable for online production inspection compared with other similar studies such as in [231].

More recently, the market for Organic LED (OLED) has grown rapidly and a challenge between both LCD and OLED technologies has risen to the surface for their applications, especially in the small-sized display market. Compared with OLEDs, LCDs have advantages in lifetime, cost, resolution density and peak brightness. While, OLEDs are emissive; their inherent advantages are obvious, such as true black state, fast response time and an ultra-thin profile, which enables flexible displays [211]. As the case in LCD panels, OLED panels are subjected to many types of defects. Kwak *et al.* in [233] considered a special type of defects in OLED called salt-and-pepper defects, which appear as dispersion of black and white pixels across the display.



(a) CCD camera cap- (b) XY table repeatedly moves the fixture so that colorimeter can inspect backlight modules in a sequential shot.

FIGURE 13. LCD backlight module inspection [232].

This type of defects is caused by a malfunction in the chemical process and is considered difficult to detect using conventional automatic fault detection methods that specialize in recognizing certain shapes, such as line or Mura defects. Park and Kweon in [234] considered ambiguous surface defects that are difficult to detect in active-matrix organic light-emitting diode (AMOLED) touch displays. Different types of ambiguous defects were considered in this study such as scratch, long dust, circle dust, pit and stain. This paper highlighted some problems in inspecting such defects, such as confusing critical and non-critical defects. For instance, dust defect which is considered non-critical defects because it can be removed easily can be confused with scratch which is considered a critical defect. Authors in [235], [236] proposed AOI system that can detect defect in directional surface defects in general. To validate the efficiency of their system, they conducted experimental trials on defective and non-defective samples of polymer light-emitting diode (PLED) and OLED.

Table 7 summarizes the defects investigated in literature using AOI system for different FPD types.

E. OTHER DEFECTS

In the previous sections (III-A-III-D) we discussed about the most common inspected components in literature in a categorized manner. However, other researchers have studied certain electronic component defects that are not widely investigated. For instance, Ko *et al.* in [289] inspected four types of defects in complementary metal-oxide-semiconductor (CMOS) camera module named black and white defect, dim defect, color defect, and line defects. Their method achieved an overall of 99.6% inspection accuracy. However, they chose different inspection algorithms for each type of defect inspected, which reduce the efficiency of their method to deal with new defect

TABLE 7. Summary of articles that used AOI system to investigate FPD defects.

FPD Type	Reference	Inspected Defects
LCD	[215], [219], [237]–[250]	Mura defects
	[251]–[256]	TFT-LCD panel defects
	[218], [257], [258]	TFT-LCD panel micro-defects such as pinholes, scratches, particles and fingerprints
	[29], [223], [259], [260]	Polarising film defects
	[261]–[263]	Glass substrates defects in TFT-LCD
	[264]	Defects during photolithography process
	[231], [232], [265]–[267]	Backlight defects
	[212], [213], [268], [269]	GE operation defects during TFT array process
	[270], [271]	SD operation defects during TFT array process
	[272], [273]	Color filter defects
	[214]	TFT array defects such as fibre defect, particle defect, pattern damage, pattern residual and pattern scratch
	[274]–[277]	Anisotropic Conductive Film defects
	[278]	Optical thin film defects
	[279]	TFT-LCD pad area defects
	[280]	LCD surface deformation for smartphones
OLED	[224], [225], [225]–[227]	Polarizer transparent microdefect
	[230]	Liquid resin defects
	[217]	Subpixel (dots) functional defects
	[235], [236]	Directional textured surface defects in OLED and PLED
	[234]	Ambiguous surface defects of AMLOED such as scratch, long dust, circle dust, pit and stain
	[281]	Macro defects such as film tear and pit and micro defects such as scratch and spot
Mobile and Touch Panels	[233]	Salt-and-pepper defects
	[282]–[286]	Mobile screen defects
All Types	[287], [288]	Touch panel defects
	[15]	Chromatic (color) defects
	[243]	Mura defects

types and increase the complexity and time consumption. Furthermore, particles in the range of 2 – 3 pixels were not accurately detected. Infrared Cut-off (IR-CUT) filter in CMOS and charge-coupled device (CCD) cameras is also one of the investigated components in literature. IR-CUT filter is designed to reflect or block mid-infrared wavelengths while passing visible light. It is applied in all kinds of color cameras and video devices to prevent infrared light radiation from reaching imaging sensor, in an attempt to capture images as close to those perceived by the human eye as possible. Defects in this part can affect quality of the image, through chromatic aberration phenomenon and redundant objects in the image. Therefore, Liu and Yu in [290] proposed an AOI system to investigate three types of common surface defects in IR-CUT filter: stain, scratch, and edge crack. Stain is caused by the dirt in the air or dirty objects in contact with

it. The cleaning and testing process of optical IR-CUT filter may bring scratches on the surface by contact with sharp things such as tweezers. Crack is generated in the process of segmentation after coating.

Lin *et al.* in [291], [292] considered inspecting ripple defects in the surface barrier layer chips of ceramic capacitors. Difficulties exist in automatically inspecting ripple defects because of their semi-opaque and unstructured appearances, the gradual changes of their intensity levels, and the low intensity contrast between their surfaces and the rough exterior of a the chip as shown in Figure 14. To overcome these difficulties the sample image has to be converted to the frequency domain in order to capture the defect features as will be explained in section V-B1. Sun *et al.* in [293] considered inspecting four types of thermal fuses defects. A thermal fuse, also known as a thermal cut-off, is an important component in both electrical and electronic devices. Thermal fuses prevent circuits from overheating or becoming overloaded. While fuses generally allow the passage of current, they can short circuit to cut power to appliances as a safety feature. The four inspected defects in this study are located on the head of the thermal fuse which are bur, black dot, small-head, and flake defects. Bur defect (Figure 15(a)) appears as a deckle edge in the outer ring area of the fuse case, it is mainly caused by using incorrect material for the lead or worn out punch. This defect is very difficult to be detected by human inspector even with the help of magnifier. Black dot defect (Figure 15(b)) is mainly caused by the existence of foreign materials (e.g. dirt or dust) during the assembly of the case and lead. Small-head defects (Figure 15(c)) occurs when insufficient force is provided during the punching process of the lead, this will cause smaller dimension of the head diameter. Flake defects (Figure 15(d)) is caused by the chip-off of the case wall during the electroplating process.

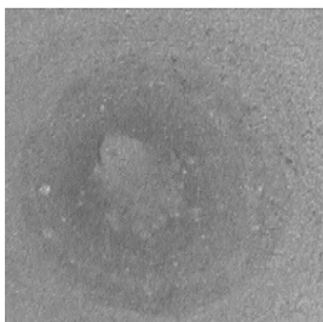


FIGURE 14. Example of ripple defect investigated in [291], [292].

Table 8 summarizes miscellaneous defects that were investigated using AOI techniques.

IV. IMAGE ACQUISITION TECHNOLOGIES - HARDWARE SYSTEMS

An effective imagery system should ensure minimum escape rates and false alarms [300]. Image quality is an essential

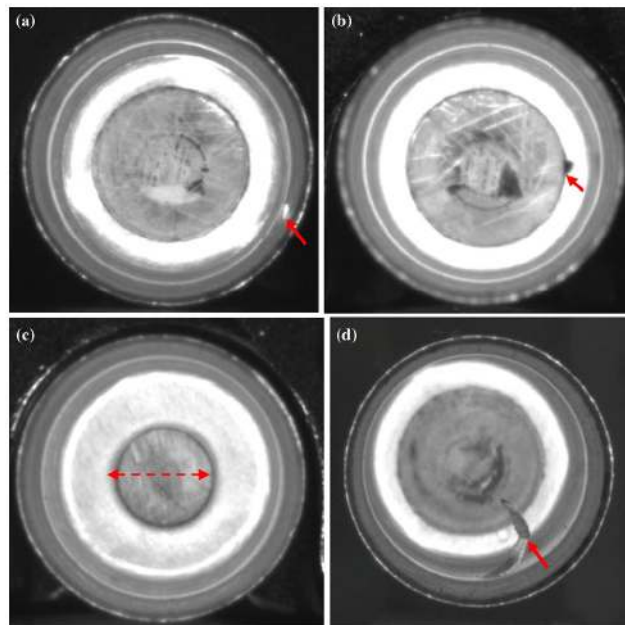


FIGURE 15. Defects of thermal fuse. a Bur, b black-dot, c small-head, d flake [293].

TABLE 8. Summary of articles that used AOI system to investigate miscellaneous electronic components defects.

Inspected Component	Reference	Inspected Defects
Camera Modules	[289]	Black and white defect, dim defect, color defect, and line defects in manufacturing process of CMOS compact camera module
	[294], [295]	Six major defects: solid white dot, gray dots, black spots halo, strip defect, bubble defect, and solid black spots. Minor defects were also included in separate category.
	[290]	IR-CUT filter defects such as stain, scratch, and edge crack
	[296]	Surface defects in micro multi-layer non-spherical lens module of CMOS such as bright spot, dark spot, scratch, foreign material and hole
	[297]	Compact camera lens and spacer ring defects such as stain, bright dot, scratch, pit, and scar
Passive Components	[291], [292]	Ripple defects in the surface barrier Layer chips of ceramic capacitors
	[298]	Tiny surface defects in the surface barrier Layer chips of passive electronic components
	[299]	Surface defects of film capacitors
Thermal Fuse	[293]	Bur, black dot, small-head, and flake defects

prerequisite for data acquisition and processing. Therefore, a careful consideration should be made for the selection of appropriate image acquisition system. According to Chin and Harlow in [13], a standard AOI system consists of camera and lightning setup, computer (processor), conveyor and sorting mechanism as shown in Figure 16. The illumination is responsible for providing constant/customized lightning conditions. The camera that includes an image sensor is responsible in acquiring the image. The conveyor is responsible

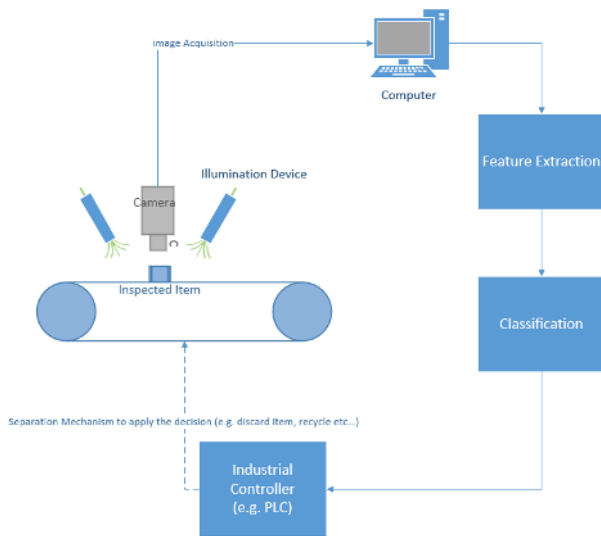


FIGURE 16. AOI system.

in moving the object across different inspection stages. The computer is responsible for applying the inspection algorithm in terms of preprocessing, feature extraction and selection and classification. Finally, the sorting mechanism with the of industrial controller (e.g. PLC) is responsible for separating the products for further consideration (e.g. scrap, recycle etc.) according to the decision made by the inspection algorithm.

A. CONTRAST AND ILLUMINATION SETTINGS

Contrast is an important factor that contribute to image quality, it defines the differences in intensity values between the inspected object and the background [22]. Therefore, it is very important to select background that has different intensity levels than the inspected items, so that the inspected components can be distinguished when applying image processing techniques and feature extraction. Contrast and other factors that contribute to image quality can be also affected by illumination and lightning settings, since the camera does not see the object; it sees the light reflected by the object. Good illumination can reduce shadow, noise, and reflection and increase image contrast, thereby shortening the image processing time and increasing their accuracy [301]. In machine vision applications, the environment light is avoided since it changes with the change of environmental conditions and this can affect the image quality and thus the detection algorithm. Therefore, non-varying illumination sources are used in such applications [302]. Inspected component size, color, surface feature, geometry, material, inspection environment and system needs are all important factors to be considered in selecting the right illumination source. LED, fluorescent lights and quartz halogen light with fibre optics are commonly used as illumination sources for machine vision applications. Moreover, positioning of the illumination source plays important role as well especially when inspecting polished and shiny objects (e.g. metal parts and solder joints) that reflects

light with specular reflections. On the other hand, dull surfaces such as plastic diffuse light in several directions [303]. Therefore, the positioning of the illumination source highly depends on the applications as well [301]. Bartlet *et al.* in [304] used four overhead fluorescent lamps and one fluorescent ring lamp to effectively inspect solder joints and avoid shadows in the captured image. Capson *et al.* in [140] proposed multilayer tiered-color illumination approach to inspect solder joint defects. The illumination setup that they proposed consisted of circular red and blue fluorescent lights designed in a hemispherical configuration and subjected to the solder joint with different angles, in which blue and red light are reflected by the surface that each light is subjected to. The reflected light will have special contour geometry according to the quality of the solder joint. This technique will capture the 3D behaviour of the solder joint in to 2D image. Many recently published articles about solder joint defects used the same techniques with some or no modifications as shown in Table 3. Wu *et al.* in [171] used 3 colors (red, green, and blue) shaped in hemispherical array of LEDs as shown in Figure 17. The red, green, and blue lights irradiate to the flat, the slow slant, and the rapid slant of the solder joint surfaces, which are reflected to the camera, respectively such that each solder joint quality condition will have unique color distribution based on the light reflection. Zeng *et al.* in [305], [306] used tiered-color ring-shaped LEDs to highlight PCB components such as markings, and via-holes. The color distribution direction of each solder joint is also evaluated in order to aid in specifying the type of defect. However, these studies were considered a foundation for an inspection system and did not apply defect classification approach. Despite of multi-layer tiered-color illumination ability's to highlight the defective features of solder joints efficiently, this system requires three images of each solder joint to be scanned and processed, this can increase the computational time significantly. Chiu and Perng in [168] proposed a single tiered-color illumination setting by choosing an optimal incident angle (φ) that can do the inspection with processing a single image only as shown in Figure 18. φ must be carefully selected in order to mimic the efficiency of three layers tiered-color lights. Shadow on inspected components should be avoided, therefore the incident angle should be as small as possible.

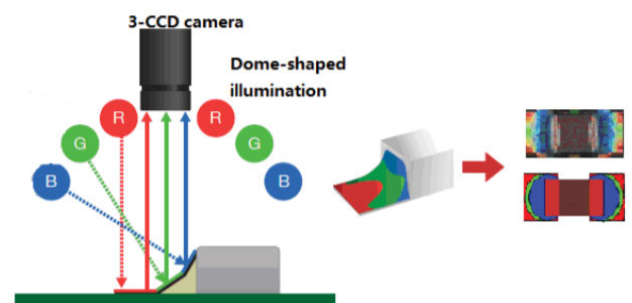


FIGURE 17. Illumination setup considered by Wu *et al.* in [171].

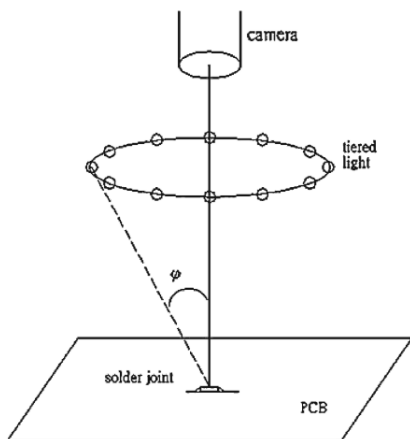


FIGURE 18. Illumination setup considered by Chiu *et al.* in [168].

Ideally ϕ must be equal to zero; however, in this case the light must be placed either in front of the camera or at an infinite distance from the camera which are both unrealistic. Therefore, by trial and error the study tested a small angle range between 20° and 30° to acquire high quality inspection images. Liu and Yu in [290] proposed special mechanical configuration and illumination settings to inspect IR-CUT filter surface defects. Because there is no refracted infrared light into the optical IR-CUT filter, another side of it cannot be captured in a single photo. The researchers thus constructed a flipping mechanism to flip the samples to both sides. Multi-layer infrared LED light were considered as an illumination system for this study (shown in Figure 19) because infrared beam cannot pass through the IR-CUT filter and therefore the nature of the reflected light will be an indication for a defect detected. The angle for the infrared beams were carefully chosen, such that two layers of infrared lights were used. The first layer omits a beam with an angle of 30° , which is intended to reflect a perpendicular beam from major surface defects detected. The 60° tilted beam is intended to reflect the light from the minor surface defects perpendicularly to the camera. In case of no defect has been detected, the light will be scattered such that it will not be detected by the camera. Tsai and Tsai in [249] used unconventional illumination and image acquisition techniques in

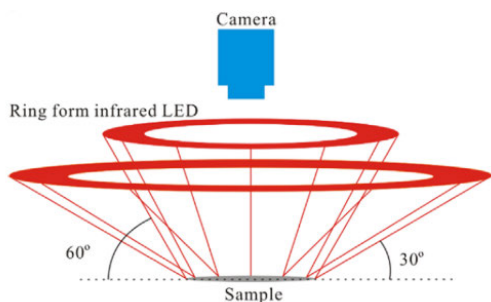
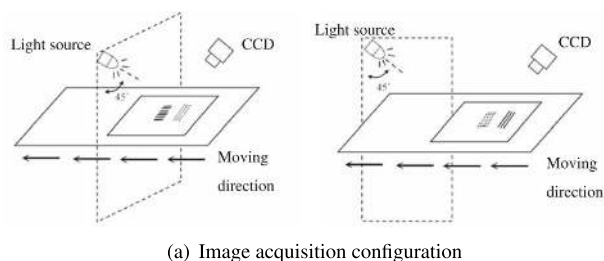


FIGURE 19. Illumination setup considered by Liu *et al.* in [290].

inspecting Mura defects in LCDs. The LCD panel is assumed to move along a track. While the panel passes through a fixed camera, the light reflection from different angles can effectively enhance the Mura defect in the low-contrast images. The Mura detection problem is therefore treated as a motion analysis in image sequences using optical flow techniques. Figure 20(a) shows the configuration for the image acquisition system. Figure 20(b) shows the difference between using conventional illumination and camera settings and the proposed method in highlighting the Mura defect. Based on these spatial arrangements, they used optical flow algorithm to highlight Mura defects in LCDs, where this algorithm calculates the displacement of brightness from one frame to another. There are two types of optical flow algorithms. The first type calculates the displacement of brightness for the entire pixels of the image (called dense optical flow algorithm). The second type calculates the displacement for specific pixels of the image (called sparse optical flow algorithm) [307]. Due to its efficiency and accuracy, a sparse optical flow algorithm called Lucas-Kanade were used for on-line defect inspection in manufacturing. Here three types of feature values were calculated using Lucas-Kanade algorithm to highlight Mura defects. These feature values are flow magnitude, mean flow magnitude and flow density in the optical flow field. A certain threshold for each feature value were decided such that if the value exceeds the threshold the sample image is considered to have a Mura defect and the opposite otherwise.



(a) Image acquisition configuration



(b) Difference in highlighting two types of defects A and B (left) between conventional setup (middle) and proposed system (right)

FIGURE 20. Imaging setup proposed by Tsai and Tsai in [249].

Authors in [221], [222] took advantage of a phenomenon called optical interference pattern to investigate certain type of Mura defects in TFT-LCD. This phenomenon is due to interference caused by light reflecting and refracting from two different transparent surfaces. This will cause optical fringes, which are light and dark bands that are in phase or out of phase with each other as shown in Figure 21. The patterns

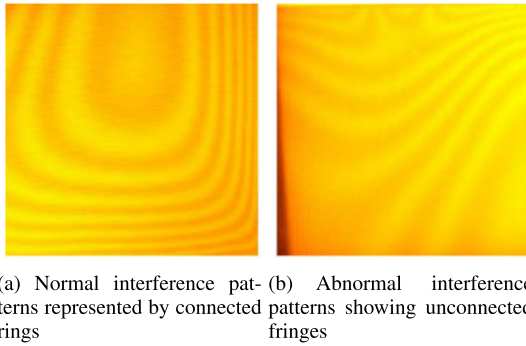


FIGURE 21. Illumination setup proposed in [221], [222].

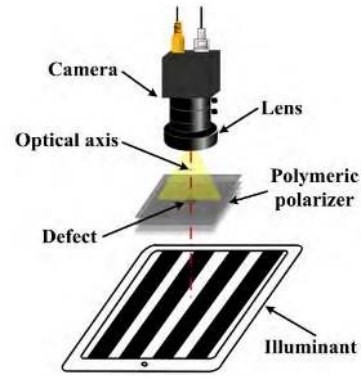
of these fringes are indicators of Mura defects. Sodium light were used to highlight the fringes as monochromatic light highlights the fringes into dark and light bands. When a regular light source used instead (e.g. fluorescent lamp), the interference pattern will appear as color fringes of different wavelengths. However, if one uses a monochromatic light source, such as a sodium lamp, an alternating bright and dark interference pattern appears. Deng *et al.* in [227] proposed binary structural illumination source to enhance the image contrast of the aesthetic defects in polymeric polarizer of TFT-LCD as shown in Figure 22(a). The illumination is provided by binary black and white stripes displayed on a display, such that the width of the stripes can be controlled, and the defect sample is placed between the camera and the striped light. A conventional light source with uniform brightness was used to ensure the image is clear. Compared with using a conventional illumination settings, binary structured lighting improves the contrast of the defects by a range between 36 – 84.7% depending on the nature of the defect [225]. Figure 22(a) shows the difference in detecting the defects using conventional light source and striped light source.

Chang *et al.* in [288] offered an AOI system to filter and classify touch panel glass defects. Their illumination setting consisted of two LED lights with fan-shaped light transmission. For a perfectly smooth surface the camera will record a mostly dark image since the majority of the light reflected is specular. This will indicate that no defect has been detected as shown in Figure 23(a). The presence of defect will cause the light to scatter in the direction of the camera, appearing as a bright area in a dark background as shown in Figure 23(b). To reduce false alarm rates, the carrier of the inspected plates were coated with high reflective substance so that the subject appears darker.

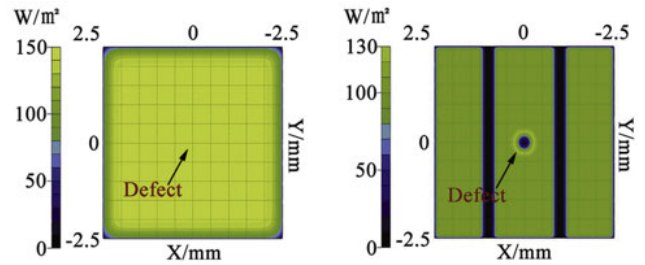
Table 9 summarizes advantages and limitations for the various illumination setups used for inspection.

B. CAMERA/LENS SELECTION AND POSITIONING

According to National Instruments in [309], to set up an AOI system using imagery modus operandi, a number of factors need to be considered. These factors are: the working distance (WD) (distance from the camera lens to the object under inspection), resolution (smallest feature to be inspected),



(a) Structural light configuration using black and white stripes



(b) Conventional light configuration in highlighting defect (left), proposed structural light configuration in highlighting defect (right)

FIGURE 22. Illumination setup proposed by Deng *et al.* in [227].

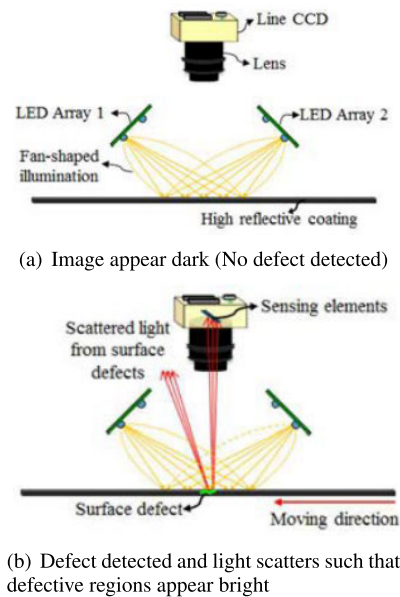


FIGURE 23. Illumination setup proposed by Chang *et al.* in [288].

pixel resolution (PR) (the minimum number of pixels needed to represent the object under inspection), depth of field (maximum object depth that remains in focus), image sensor size (SZ), the size of sensor active area, field of view (FOV) (the area of the object under inspection that the camera can acquire), and frame rate (FR) as shown in Figure 24. The common image sensors used in inspection cameras are CCD, and

TABLE 9. Summary for illumination systems used in AOI applications.

Illumination Setup	Reference	Description	Advantages	Limitations
Three-layer tiered light	[139], [159], [160], [163], [164], [171]–[176], [182], [305], [306], [308]	This setup was used for solder joints inspection in PCBs. The setup consisted of 3 (red, green and blue) circular ring-shaped lamps at 3 levels constructed on hemispherical way with different light reflection angles that can be fixed or controlled by host computer.	The 3D nature of the inspected component is converted into 2D image. Each kind of defect is related to unique arrangement of multi-colored image and intensities, which make it easy to classify the defect. Suitable for solder joint inspection	System Configuration is very complex [143] The processing of color images require higher computation time and complex processing [169]. Precise geometric calibration of the light source position is required to yield accurate results [169]
Single-layer tiered light	[168]	This setup was used for solder joints inspection in PCBs. The setup consisted of tiered LED light at one level instead of three as in the previous settings.	The 3D nature of the inspected component is converted into 2D image. Each kind of defect is related to unique arrangement of gray-scale image and intensities, which make it easy to classify the defect. Low computational time and more convenient system configuration compared with the multi-layer adjustment Suitable for solder joint inspection	Angle φ must be carefully selected and maintained for good results.
Two lights	[169]	This setup was used for solder joints inspection in PCBs. The setup consisted of two different light sources, namely, direct-top and diffuse-wide were used. Direct-top is the light source coming directly from the distant top, whereas in diffuse-wide, the light source is diffused evenly before being directed to the solder joint.	The computational time required to process the images is low compared with the tiered illumination sources.	The system is susceptible to error in lighting condition variations.
Blue coaxial light	[280]	This setup was used to detect surface deformation in LCD of smartphones with the aid of precision plate. By the illumination from the blue coaxial light, the images of the standard circle holes on the precision plate are reflected on the surface of the measured LCD, and then the images are further reflected onto the surface of the CCD camera by the semi-reflecting mirror, thus the circle hole images from the measured reflected LCD	Provide high reflection rate of the measured LCD surface	Limited in application
Sodium light	[221], [222]	This setup was used to detect gap Mura transparent defect in TFT-LCD, where a sodium point light source is projected onto the panel	Light band appears as dark and light instead of colored for easier defect identification	Applicable for transparent defects only.
Two LED lights	[249]	This setup was used to detect Mura transparent defects in LCD. Two LED movable, lights one parallel to flow direction of the flow and the other is perpendicular. Both are tilted with an angle of 45° .	Highlighting low contrast Mura defects in LCDs	Require special configuration and limited in application
Structured light	[224]–[227], [229]	This setup was used to detect aesthetic defects in LCD. The setup consisted of white and black stripes that is positioned under the inspected polymeric polarizer.	Enhance the image contrast of the aesthetic defects. Black and white stripes sizes can be adjusted.	Detecting tiny defects in illuminated stripes is difficult [226]
Two fan-shaped LED lights	[288]	This setup was used to detect touch panel glass defects. The setup consisted of white and black stripes that is positioned under the inspected polymeric polarizer.	Defects can be easily distinguished such as dark images correspond with no defects and bright regions in the image represent the defect	Carrier of the inspected items must be maintained coated with high reflective substance to avoid false alarm errors

CMOS which mimics human's perception in vision [310]. In addition to the previous factors several criteria are considered in determining the suitable image sensor and its size such as responsivity, dynamic range, uniformity, speed of operation and reliability. Using the field of view (FOV),

the pixel resolution can be obtained by equation 1

$$PR = 2 \cdot \left(\frac{FOV}{Resolution} \right) \quad (1)$$

And the focal length, which is used to determine the lens specifications, can be obtained using equation 2

$$FL = \frac{SZ \cdot WD}{FOV} \tag{2}$$

Focal length is important for selecting the right lens for application, as can be seen from equation 2, the three factors that affect selection of right focal length are sensor size, working distance and field of view. Frame rate is also important factor to consider when selecting a camera especially in batch inspection in industries that have high production rate [303].

Spatial calibration techniques are commonly used in order to set the camera in optimal position for the application. In most optical inspection applications, the position of the camera is fixed [300] and positioned in 90° with the plane of inspected components to avoid image distortion and reduce perspective errors as shown in Figure 24 [309]. However, in some cases the camera can be aligned in different angles. In the following discussion, we will highlight the research articles that used unconventional camera setups.

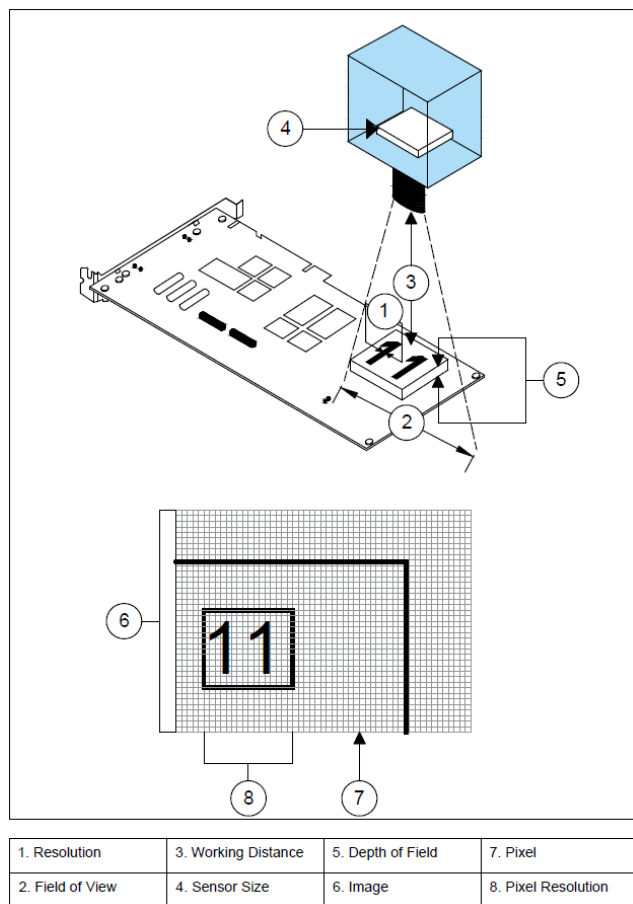


FIGURE 24. Factors considered in selecting camera and lens [309].

For inspecting glass substrate defects in TFT-LCD, cameras are aligned in two different positions: transmission and reflection. In transmission position the camera captures the projected images with light transmitting through the glass

whereas in the reflection position it captures the reflected images with light reflecting off the substrates as shown in Figure 25 [263]. Hence, Yousefian-Jazi *et al.* in [263] used the transmission method for inspecting TFT-LCD glass substrates. Similar techniques are considered when inspecting highly reflective surfaces, in which certain geometrical laws must be applied to measure the optimum lengths and angles of the camera and illumination settings [311]. Ong *et al.* in [169] proposed dual viewing angle to acquire solder joint images for defects inspection. Their approach consisted of conventional orthogonal and oblique camera setups as shown in Figure 26. The oblique setup was adjusted with inclined viewing direction of 40° by using pyramid mirror. The setting seems to provide better geometrical information of the solder joint and can save feature extractions step by sending the acquired images directly for classification. However, the setup procedure is laborious and prone to human error. Li *et al.* in [206] proposed a setup for detecting the height of solder balls in BGA. They used stereo vision system to capture the 3D nature of the solder ball using two CCD cameras at two opposing angles and two ring lights around each camera lens that captures two 2D images in parallel as shown in Figure 27. Because of the reflective nature of solder balls, the lighting provides the means to generate features on the balls which are then used to determine height. These features will appear as bright regions in the captured images. This method of acquiring image can reduce the time for the feature extraction process such as simple segmentation and thresholding approaches are enough to determine the features of the component. Zhao *et al.* in [312] proposed a similar stereo vision system using two cameras to inspect the pins on multi-type electrical connectors of the components.

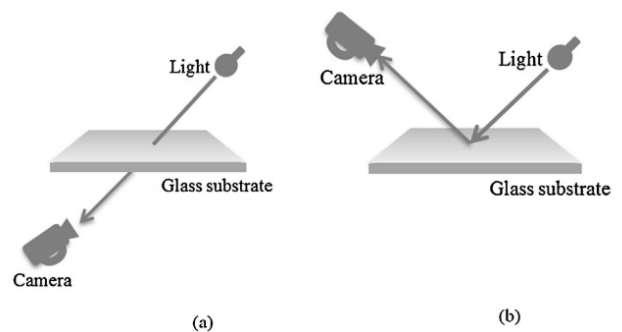


FIGURE 25. (a) transmission and (b) reflection imaging system [263].

Because each film capacitor has six surfaces to be detected, Yang *et al.* in [299] used four image acquisition systems that are adjusted to detect the surface defects of capacitors. Each camera gets the image information of two surfaces from side angle, as shown in Figure 28. When the capacitor reaches the specified position, a laser tube will number the capacitor and produce trigger signal. Industrial camera captures the surface image of this capacitor and optical inspection algorithms are applied to detect the surface defects in real time. Park and Kweon in [234] proposed four image acquisition systems as

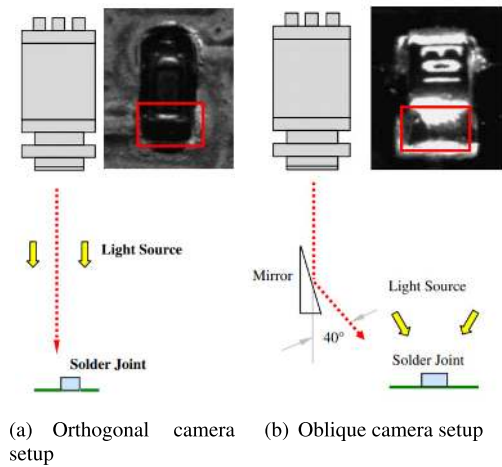


FIGURE 26. Camera setups considered by Ong *et al.* in [169].

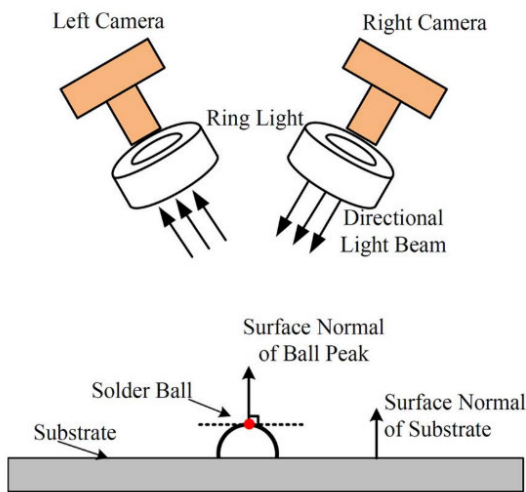


FIGURE 27. Imaging system setup considered by Li *et al.* in [206].

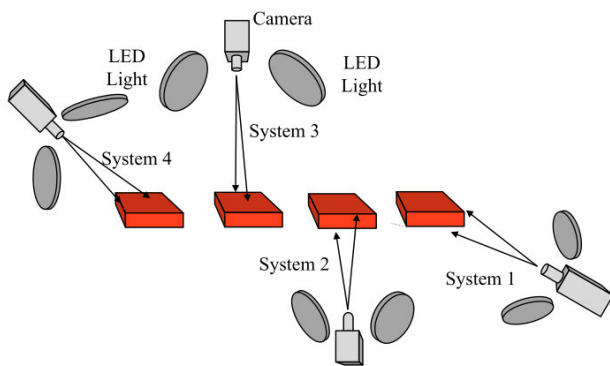


FIGURE 28. Imaging system setup considered by Yang *et al.* in [299].

well that consisted of four different combinations of camera and LED sources with different orientation angles for inspecting AMOLED defects as shown in Figure 29. The multiple imaging systems with different orientation angles are used for acquiring images for the same component multiple times

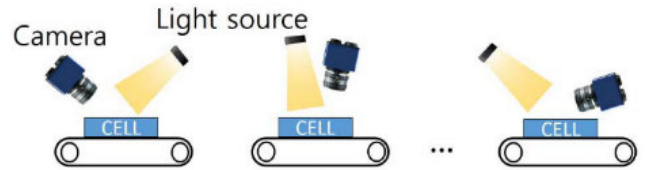


FIGURE 29. Imaging system setup considered by Park *et al.* in [234].

such that the defective features are detected from at least one of the four images. The four images is then compared with each other using image filtering to choose the best image that describe the defective features such that feature extraction and classification algorithms can be applied on it.

C. AUXILIARY SYSTEMS AND OTHER IMAGE ACQUISITION TECHNIQUES

Scanning Electron Microscope SEM and Optical Coherence Technology OCT are two examples of auxiliary systems that still need visible light sensor devices to capture the image. OCT is a non-invasive and non-destructive optical imaging technique that uses a low-coherence Michelson interferometer to generate high-resolution cross-sectional imaging of samples. The OCT technique shows the structure of a material by measuring small changes in back-scattered light at various depths. The OCT- scanning depth is a function of absorption and scattering with a resolution on the order of microns and a depth range of 3 – 4mm [230], [313]. The interference signal from the interferometer can be acquired using CMOS or CCD line scan camera. The OCT technique has been successfully applied to the early diagnosis of many diseases originating under superficial areas, including cancers [314]. For the scope of this article, many researchers used OCT to inspect various FPD defects such as optical thin film, industrial resin, and minute defects in LCDs as shown in Figure 30. SEM is usually used to detect micro defects in semiconductor wafer (shown in Figure 31(b)) and LED chips with the aid of image sensing device, it can be used also to detect small defects in FPD as in [315].

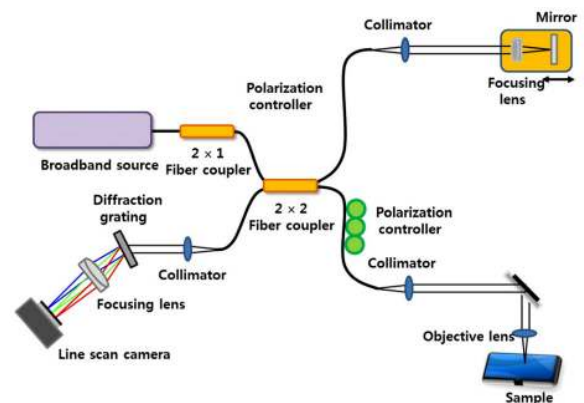
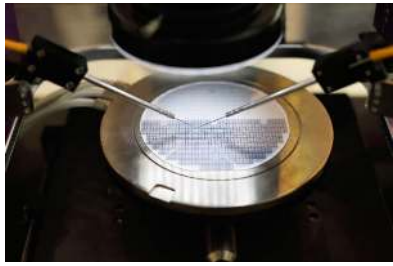
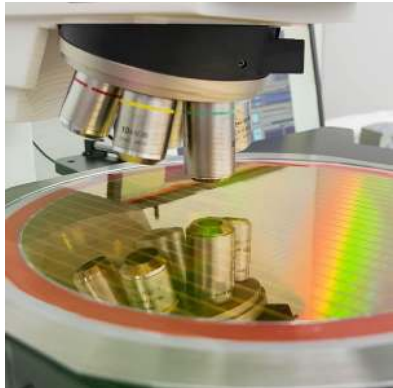


FIGURE 30. OCT setup used in [313].



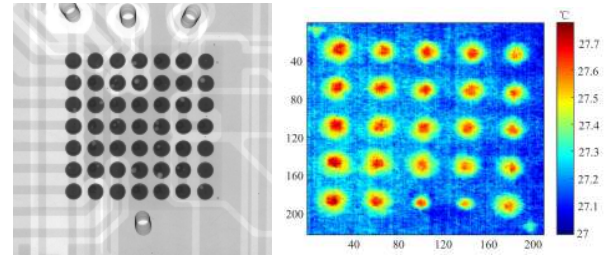
(a) Semiconductor wafer testing using circuit probe [316]



(b) Semiconductor wafer testing with the aid of SEM [317]

FIGURE 31. Various semiconductor wafer testing techniques.

The use of alternative methods of imagery alongside the traditional surface optical systems such as thermography and X-ray are also gaining momentum. For example, X-ray scanning for alignment and defect inspection of IC components and inner layers of PCBs as shown in Figure 32(a). However, X-ray technology is not efficient in detecting fine cracks and open solder joints, as the small air gap in the defects do not attenuate the X-rays. Although 3D X-ray system (e.g. CT) can solve some of these problems, but data processing and image resolutions could reduce their deployment in embedded in process production systems [209]. In thermography, a camera with a thermal sensor is used to measure the infrared radiation from the sample and convert the radiation flux to temperature. The temperature distribution can be then illustrated in a form of thermal images. For inspection applications, some defects such as solder ball defects will change the heat flow resulting in abnormal thermal behaviours, which is dependent on the defect size, location, and thermal physical properties of the material as shown in Figure 32(b) [209]. In such cases thermography inspection is considered an efficient tool to highlight these defects for further analysis and classification. Unlike previously mentioned technologies, circuit probe does not need image sensor to operate as the defect map (WM) is generated according to the data provided by circuit probe. As mentioned in section III-B, this technology is widely used for semiconductor wafer inspection as shown in Figure 31(a). Table 10 summarizes the other image acquisition techniques and auxiliary systems used for AOI in literature.



(a) Solder ball inspection using X-ray [208] (b) Solder ball inspection using thermography [209]

FIGURE 32. Various technologies used for solder ball inspection.

TABLE 10. Summary of articles that other image acquisition techniques and auxiliary systems.

Technology	Reference	Defects considered			
		LED Defects	Wafer Defects	PCB Defects	FPD Defects
Circuit Probe	Articles in Table 4		✓		
SEM	[111], [113], [117], [126], [127], [134], [135], [318]		✓		
	[44], [315]	✓			✓
OCT	[230], [278], [313], [314]				✓
Thermography	[209], [319]			✓	
X-ray	[197], [204], [205], [208], [319]–[321]			✓	

V. INSPECTION ALGORITHM

Most of traditional inspection systems use subtraction or template matching technique to compare the inspected component with the reference template image as will be shown in section V-B3. Choosing a suitable inspection algorithm can enhance the classification process and avoid escape and false alarms rates. Usually in AOI application, the collected images have to undergo some enhancement (preprocessing) before the application of inspection algorithms. Feature extraction and selection techniques are then used to segment the defective regions and to discover the important defect features. The final stage is to provide the processed information to the classifier algorithm as shown in Figure 16.

A. PREPROCESSING

The purpose of this stage is to preprocess the raw image for the next stage of feature extraction and selection [310].

This stage involves many operations such as image masking, spatial filtering and geometric transformations. Masking operations can be applied to the acquired image in order to define the region of interest (ROI). This step is very important in reducing the inspection time such that the feature extraction is only applied into certain region instead of the entire image. After specifying the ROI, the resulting image can be subjected to geometric transformation or/and filtering for further enhancement before applying the inspection algorithm. Geometric transformation involves calculating the projection of each pixel in the ROI onto another space. This method can help in image restoration and correction in case of any presence of geometric distortion. The geometric transformation includes scaling, rotating and translation of the image [189].

Image denoising and filtering are common practices in preprocessing acquired images before using feature extraction algorithms. The process of image data filtering and denoising reduces noise and enhances the data for highlighting the important features. They can smooth, sharpen, transform, and remove noise from the image, so that the inspection algorithm can do the feature extraction task easily. For instance, image filtering and denoising techniques are very useful in removing random defects from mixed patterns WM so that classification algorithms can specify the type of defect according to the systematic pattern [109]. The mathematical application of filters can be in form of linear or non-linear. In the case of linear filters, a convolution kernel is specified, it can be square (e.g. 3×3), or a rectangle (e.g. 3×5). Examples of linear filters are Laplacian, and Gaussian filters. Non-linear filters use non-linear functions for the parameters of the kernel, the process of recalculating the pixel is similar as in the linear filters. Some examples of nonlinear filters are median filters and Prewitt filter. Median filters are popular preprocessing method for abnormality detection in electronic device inspection applications [71]. More advanced denoising techniques such as deep learning models [322], low rank approximation [323], and weighted nuclear norm minimization [324] are also used in literature. Park and Kweon in [234] proposed novel filtering technique called neighboring difference filter (NDF) from the background of AMOLED sample images. NDF is used to compare the intensity of neighboring pixel regions with a strategically placed gap space to differentiate similar patterns from other (i.e. abnormality detection).

B. FEATURE EXTRACTION AND SELECTION

Feature extraction process involves applying one or more of image processing techniques (e.g. frequency analysis and segmentation) in order to describe the characteristics of the studied regions (e.g. defects and abnormalities). These characteristics are usually described using a set of values called *Feature Values* that can be represented in vector or matrix form. The purpose of feature selection step is to consider the important feature values only that can contribute to the classification process and discard the redundant ones. This step is very essential in reducing the computational time for the inspection algorithm. Principle Component Analysis is very

popular technique used in feature selection. Other algorithms such as along Genetic Algorithm (GA), Particle Swarm Optimization (PSO), Ant Colony Optimization (ACO), Adaboost and Neural Networks are also used for this purpose.

1) FREQUENCY DOMAIN ANALYSIS

Frequency domain analysis can be used to convert pictures from the spatial domain to the frequency domain. This is very useful for capturing the global structure of the image and minimising reconstruction errors. In frequency analysis, high pass and low pass frequency filters can be used to attenuate the unnecessary noise in the image. After attenuation, the picture can be transformed back to the spatial domain for further processing. Frequency analysis is preferably used in investigating defects that have low contrast and high illumination noise such that spatial domain cannot capture the features of the defect. Examples of defects that have these features are Mura defects shown in Figure 12, and ripple defects in ceramic capacitors shown in Figure 14. The frequency representation can be obtained by various transform functions such as Fast Fourier Transform (FFT), Discrete Wavelet Transform (DWT), and Discrete Cosine Transform (DCT). Transform functions allows for a noninvertible transformation from the spatial domain to a reduced dimensionality feature space. Thus, facilitating classification with substantially less features and manageable classification error.

DCT is mainly applied to perform image reconstruction and dimension reduction by converting the image to a frequency spectrum and attenuates certain coefficients that lays into two major bands, namely, low frequency, and high frequency [125]. In most AOI applications, since illumination variations mainly lie in the low-frequency band (in upper-left corner of the frequency spectrum), an appropriate number of DCT coefficients in low-frequency band are truncated to minimize variations under different lighting conditions as shown in Figure 33 [161]. Chen and Kuo in [240] applied DCT and background image filtering strategy to detect Mura defects in TFT-LCD. The background of the sample images was first located and reconstructed using the DCT approach with the aid of low-pass filtering to illuminate unwanted noise. DCT coefficients are then selected and

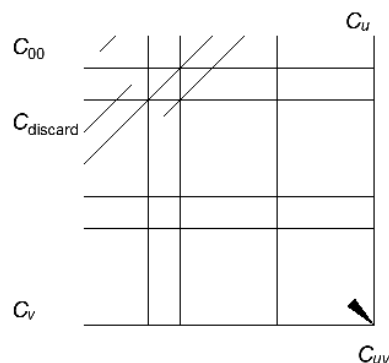


FIGURE 33. Truncating lower frequency coefficient (C_{00}).

the image can be transformed back to the spatial domain using inverse DCT. The Mura defects can be then subtracted from the background using image subtraction method. Despite the slight difference in brightness and non-uniformity between blob-Mura defects and the background, the proposed approach is very efficient in detecting blob-Mura defects as well. However, because of the low-pass filtering step conducted, micro defects can be eliminated with the noise. Therefore, the approach proposed cannot handle detecting micro-defects in TFT-LCD. Even if it was modified to detect micro-defect, the computational time of the process will be lengthy. Perng and Chen in [236] used DCT to highlight the defective features directional textured surfaces in FPD such as PLED and OLED. The sample images were transformed to the frequency domain using DCT so that the dominant directions of the textures are compacted with the lower frequency band coefficients of the frequency image. The linear primitives associated with high energy in the DCT domain are then eliminated by reducing them to zero. After that, the image is transformed back to the spatial domain using inverse DCT, which makes the defective features visible. Thresholding and Statistical Process Control (SPC) chart were then used to classify the defects. Several advantages were observed using this approach such that it is insensitive to horizontal and vertical shifting, changes in illumination, and image rotation. However, this study did not provide any details about the accuracy of the proposed approach nor of the computational time consumed. Similarly, Lin in [298] used DCT to investigate tiny surface defects in Surface Barrier Layer found in passive electronic components, whose random surface texture contains no repetitions of basic texture primitives. Therefore, DCT approach is well suited to be applied in this problem since it does not require any textural feature information. The proposed method achieved a relatively high overall accuracy of 94.74%. However, this method is only suitable to detect defects in the range between two to fourteen pixels. Furthermore, this method is considered time consuming since it takes four seconds only to apply forward and inverse DCT without the classification takes place. Lin and Chiu in [38], [40] used Block discrete cosine transform (BDCT) to highlight the defected features of tiny surface flaws in epoxy domes of LEDs and blemishes of curved LED lenses respectively. BDCT method is similar to DCT; however, in BDCT the image is divided into non-overlapping image blocks of equal sizes which DCT can take place in each block separately instead of applying DCT to the whole image. In both studies it was found that the dark background of the image can affect the BDCT and can be confused with the defect features. Therefore, after specifying the ROI, an image mask is used to delineate the ROI. Since BDCT can only process rectangular regions and the ROI is circular, therefore the dark background that has been removed can be replaced with a background that has duplicated average gray level of the ROI. Uneven self-illumination lighting will result in gradual shades, which will cause high frequency peaks after performing BDCT. Therefore, gray relational analysis is used to attenuate the

high frequency values then transform the image again to the spatial domain after the attenuation. Otsu-thresholding were then used to transform the resulted image into digital image with highlighted flaws being detected. Lin and Ho in [125] found that after transforming the digital image of a chip in a wafer to the DCT domain, the frequencies of the pinhole defects spread around the middle and high frequency regions. Therefore, to highlight pinhole defects features, high pass filtering were used to attenuate the frequency components of the non-defect regions by setting their values to zero. Similar to the approaches that were conducted in [38], [40] to adapt the background for DCT implementing, the proposed method were insensitive to light variations, since the low frequency band has been eliminated. However, this method has some limitations such as defect size, background property and processing time. Defects of large size features can be lost after the attenuation of low frequency band. Moreover, defects embedded in structure textures cannot be detected because this method is suitably applied to identify defects in random textures. Finally, the proposed method takes four seconds to process a forward and an inverse DCT transformation, which could not meet the requirements of an on-line inspections system.

As mentioned earlier that DWT is one of the frequency domain analysis methods for feature extraction. DWT has the advantage of providing an easy way for multi-resolution representation, from which defect texture features can be easily extracted. The merits of using DWT include local image processing, simple calculations, high speed processing and multiple image information. Lin in [36] considered one type of wavelet transform called Haar transform to highlight water-drop defects on LED chip surface. Haar transform is considered the simplest approach among wavelet transforms. The transform is performed to each row of pixel values and then performing another wavelet transform to each column. Four wavelet transforms were used that generate four sub-images; one level of wavelet decomposition generates one smooth sub-image and three detail sub-images that contain fine structures with horizontal, vertical and diagonal orientations. Each sub-image represents certain characteristic that has half the number of columns and rows of the original image. Wu *et al.* in [218] used Fourier transform to highlight the micro-defects of TFT-LCD by removing background textures. Haar-wavelet transform were also used to eliminate the influence of uneven illumination. Ferreira *et al.* in [217] took advantage of the periodicity and used Fourier filtering technique with the aid of thresholding to highlight dots defects in FPDs. The factor that was under scope in this study was the luminous intensity of dots, such that defective dots may be identified by changes in the expected light functional response to their addressing digital value. The main advantage of this study that it was able to construct an AOI system using a camera that can have lower resolution of that in the display inspected. However, there are restrictions in detecting defects using the Fourier transform when the frequency component of a defect may not have a

repeated pattern [260]. Tsai and Hung in [251] proposed a system based on Fourier reconstruction and wavelet transform for inspecting micro-defects such as pinholes, scratches, and particles in TFT-LCD. This study works on the 1D line images instead of the traditional two-dimensional area images. Unwanted frequency components, which represent the periodic structural pattern of the image in the frequency spectrum, can be eliminated. Using inverse Fourier transform, the image can be transformed back to the spatial domain. Finally, wavelet decomposition is further applied to remove uneven illumination in the filtered image so that defects can be easily segmented for the classification process. Control limits were considered for the classification process using certain threshold to distinguish between anomalies and uniform background. In similar study [252], Tsai *et al.* conducted a slightly different approach in which the segmented 1D profile image is divided into small segments, each of the length of the repeated period for a given TFT-LCD panel. The divided 1D segments are then combined as a 2D image. Then the same procedure applies on the 2D image as it was on the 1D image in the previous study. Another difference in this study, that it did not use wavelet transform. The proposed methods have main advantage of not relying on the design of quantitative features to describe various defect types, nor require a template image for comparison. Thus, they alleviate all limitations of the feature extraction and template matching methods. However, several drawbacks were observed in [252] such as the periodic of a faultless scan line cannot be effectively removed since the number of the divided segments is generally small with respect to the length of the period in a scan line. Furthermore, the method proposed is rotation-dependent and computationally intensive [253]. In examining the previous two studies, which were conducted by same first author, a contradictory statement were found. In Tsai and Huang [251], they claimed that they were able to detect micro-defects in high resolution images successfully. However, in Tsai *et al.* [252] they referred to the previous study to be unsuccessful in detecting micro-defects in high resolution images. Another similar approach were proposed by Tsai and Chuang that dealt with 1D profile image to identify TFT-LCD panel micro-defects as well in [253]. This approach integrated Normalized Cross Correlation (NCC) method to identify anomalies by comparing the image segment with its two neighboring segments. This method has reduced the number of segments considered compared with the previous two studies, which in return reduced the computational time. However, as the case in the previous studies, the proposed method could not locate the exact position and shape of the defect.

2) SEGMENTATION

Segmentation is a process of grouping an image into units that are homogeneous with respect to one or more characteristics; it is an important step in image processing and feature extraction [325]. Segmentation can be divided into three classes, thresholding, edge detection, and region

extraction [326]. Morphological operations are used to aid segmentation process by removing the noise or unwanted regions. Morphological operations contain erosion, dilation, opening and closing processes.

a: THRESHOLDING

Thresholding techniques are mainly effective when the contrast between various features are well established. Thresholding is considered one of the segmentation techniques that split the image into two regions; a particle region (e.g. feature or component) and background region with the aid of gray-level threshold value [309]. In this manner, all the gray-level pixel values that belong to the particle region (above threshold value) are set to logic 1 and the rest of pixels that represent background (below threshold-value) are set to 0; in other words the image is converted into binary image. The threshold value can be selected automatically with the aid of a histogram [327]. The x-axis of the histogram represents the gray-scale values of the image (in case of 8-bit image it will be 0-255) and the y-axis represent the number of pixels for each intensity value. Choosing the right thresholding value is considered a key factor in the thresholding process. In general, thresholding techniques can be subdivided into two categories Global and Local. Global thresholding performs the same mentioned in the previous discussion, in which a single threshold value from the histogram of the entire image is selected. However, local thresholding (also called adaptive thresholding) uses localized gray-level information to choose multiple threshold values. Local thresholding methods are superior to the global ones when ununiform illumination settings are applied. On the other hand, global thresholding is considered much simpler and require less computational time. For defect inspection applications, since the illumination settings are well-controlled and uniform, global thresholding is preferable [327], [328]. Otsu-thresholding is considered one of the widely used global thresholding techniques. This method selects threshold value that maximize the between-class variance of the histogram [327], [329]. Otsu-thresholding techniques are preferably used when the feature of the defect has high contrast when compared to the background. Example of these defects are missing component and missing solder defects in PCBs. Perng *et al.* in [33], [37] and Kuo *et al.* in [42] used Otsu-thresholding to extract defect features in SMD LEDs. In [37], they denoted to the resulting number of pixels of the bright regions after applying thresholding by a . A certain threshold k_1 was defined, such that if a is less than k_1 that means there is a missing component and the image is classified as *missing component defect*. Otherwise, if a is greater than k_1 that means the image has be further analysed for other defects (wrong orientation, inverse polarity, mouse bites and surface defects). A similar threshold k_2 were defined to classify images that contain mouse bites defects. Figure 34 shows the bright regions extracted after applying thresholding for different types of SMD LED defects. Similar approaches were also conducted in [33], [42].

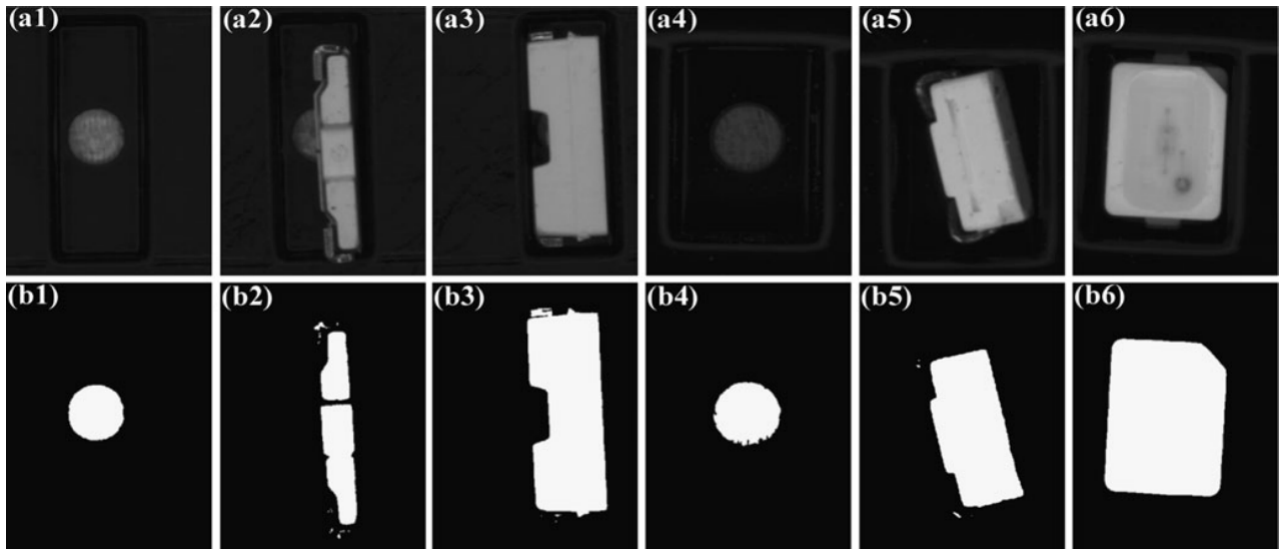


FIGURE 34. a1–a6 are the input images for different defects. The brighter regions in b1–b6 are obtained by applying Otsu's auto-thresholding [37]

However, in [42] template matching with the help of maximum correlation coefficients were also used to define the threshold values along with Otsu-thresholding. Li *et al.* in [221] used thresholding to highlight the fringes features in TFT-LCD, which may indicate a presence of Mura defect. Width, ratio of fringe, curvature of fringe and fringe size were then estimated from the resulting binary image and used as inputs for a Neural Network for classification. Noh *et al.* in [260] used adaptive thresholding technique to investigate six types of polarising film defects in TFT-LCD. The proposed approach determines the defect type through image analysis using various features, such as the geometric characteristics and the shape descriptor with intensity distribution. Various rule-based algorithms were used to classify the defects according to features extracted such as minimum bounding rectangle, actual defect region and region-based descriptor. The proposed approach achieved a very high precision and recall rates in locating the defects. However, the recall and precision rates for classification results were considerably low. Yang *et al.* in [299] combined adaptive thresholding with a frequency filtering technique called Non-subsampled Contourlet Transform (NSCT) to inspect surface defects of film capacitors. The NSCT was developed from the wavelet theory as a multi-scale geometric analysis method and was chosen due to its ability in describing the edge contours of film capacitor defects. Adaptive thresholding with the aid of Gaussian kernel function is first applied to separate the foreground from the background, and therefore highlighting the defected features. The defects are then classified according to the frequency distribution of sample images to defected and non-defected. Their proposed approach achieved an overall accuracy of 98.7% with 0.1s inspection time. The main advantage in this study is the large number of real samples used in the algorithm testing as they

used a total of 10000 capacitors, including 1000 defective ones. This can validate their results remarkably and prove the efficiency of their proposed method. Kwak *et al.* in [233] proposed a simple yet effective algorithm to inspect salt-and-pepper defects in OLED panels. First, the background of the sample images is generated using median filter. Then the generated images are subtracted from the original to highlight the noise that represent the defects. Otsu-thresholding were then used to binarize the image, such that the black pixels of the binarized image represent defective pixels. Finally, feature value was generated according to the number of pixels and certain control limits were established to classify the sample images as defect or non-defect. The proposed method was compared to other algorithms such as DCT and DWT and it was proven that the proposed method outperformed other algorithms remarkably in terms of the computation time. However, in terms of the accuracy, DWT and DCT outperformed the proposed method, especially when the noise level is mid and high. Jiang *et al.* in [154] investigated four types of golden fingers defects in PCBs. Using selected threshold value, the binary image and gray level values for each defected area was obtained. Due to the lack of sample data provided, this study applied Bootstrap sampling technique to generate more sample for the defective features based on their gray level values. Four types of features related to the gray level values were extracted from the generated samples: sample mean, standard deviation, mean absolute difference and skewness. These features were sent to classification algorithm to specify the defect type. However, for using Bootstrap sampling, the illumination environment must be well controlled. If a non-uniform lighting source was used, the gray values obtained from the sample defect images are no longer reliable. This will affect the analysis and classification. Jiang *et al.* in [145] proposed an approach

based on Gray Relational Theory for IC marking inspection. The basic idea of gray relational analysis is a ranking scheme that ranks the order of the gray relationships among several sub-systems. Several image processing techniques were implemented to apply the gray relational theory. Image rotation was first applied to make sure that IC is in correct position for character identification. Morphological opening operations were then applied to remove noise and help in the segmentation process for the characters. Thresholding were finally applied to convert the gray image into binary one in order to reduce the data amount as possible. Six key features were extracted using the previous processes: area, perimeter, ferret elongation, diameter, compactness, and moment were used to identify the type of problem occurred in the marking process such as broken and wrong characters. As compared to traditional methods (i.e. Euclidean distance, Canberra distance, Chi-square, and correlation coefficient), there are three advantages in the proposed approach: 1) no large amount of data is needed; 2) no specific statistical data distribution is required; and 3) there is no requirement for the independency of the factors to be considered. Furthermore, their proposed approach achieved an identification rate of 97.5%. However, their study did not include IC marking recognition for multitype, multidirectional, and various angular settings. Also, they did not include trademarks and punctuations in the IC marking recognition process. Furthermore, their proposed approach did not integrate the software and hardware into a whole automatic inspection system. Nagarajan *et al.* in [146] proposed a similar study for IC marking errors such as illegible characters, missing characters and upside down printing. For character recognition, four feature extraction methods were applied: projection profile, moment, zoning (same as segmentation) and contour profile. After extracting the features using the four methods mentioned, these features are sent to neural network for classification according to the three error types considered. Their approach achieved 100% classification accuracy. However, the proposed approach does not detect marking defects accurately when the IC chips are placed with rotation angles [147]. Furthermore, the feature extraction techniques considered in this study are time consuming that takes 1.844 – 2.093s for single inspection task. Said *et al.* in [204] proposed a study to inspect non-wet solder joints in processor sockets and BGAs. Images in this study were acquired using X-ray optical inspection system. Thresholding and segmentation approaches were done automatically to locate the solder joint regions with minimal effect of illumination noise. This automatic process can be performed with the aid of statistical modelling using a mixture of Gaussian distributions to find the optimal threshold value. The centroids of the solder joints are then located, and a mathematical model were then estimated to check the degree of alignment of each joint's centroid with respect to joints in the same directional cluster. A certain threshold was used to classify the solders as defected and non-defected according to the degree of alignment. The conducted performance evaluation and resulting statistics showed that the proposed

algorithm provides a detection rate of 95.8%. Despite of this method effectiveness to deal with nonuniform illumination conditions; however, disregard issues of nonuniform brightness distributions may lead to over-segmentation and under-segmentation problems [207]. A similar study [205] was also conducted to detect voids in solder balls. Voids are defined as cavities formed inside a solder ball due to the amount of outgassing flux that gets entrapped in the solder ball during reflow. The main challenge that this study encountered is to make their algorithm able to differentiate between voids and vias as both vias and voids have similar features. Another challenge is to avoid considering void-like shapes that are in the solder ball region, which may increase the false alarm rates. As in the previous study the sample images are acquired using X-ray AOI system. Template matching were first applied to choose the perfect template candidate that can be used to identify other solder ball regions. To exclude vias in the detection, a method for segmenting vias and locating them were conducted in this study. The voids are then located and labelled using certain measures and features such gray level value, area, and compactness factor and certain thresholds were estimated from these measures to perform the classification process. Finally, to remove further any detected phantom voids that were not eliminated by the previous operations due to similarities with the actual voids, a circularity constraint is imposed and is quantified using the compactness factor and the principal axes ratio. However, the proposed method did not show a solution if the actual voids in the final check were not of circular shape (e.g. irregular or any complex shape) [330]. Another study conducted by Van Veenhuizen in [208] to inspect voids in solder balls as well; however, deep learning model were used for the defect classification process. Lu *et al.* in [280] constructed an optical inspection system to measure LCD deformations for smartphones and to locate the position with maximum deformation. The system consisted of CCD, mirror adjusted with certain degree and precision plate filled with equally sized holes. If there a deformation exists, the image acquired of the holes via the inclined mirror will look irregular. Otherwise, if there is no deformation the holes will appear intact. Morphological operation with the aid of thresholding were used to remove the holes along the image edge and to repair the shape of the other holes via dilation. A certain threshold was defined, such that if the sizes of the deformed holes are larger than the threshold then the LCD is considered deformed. However, there was no discussion about the accuracy of their proposed algorithm. Jiang *et al.* in [158] proposed simple image processing techniques based on thresholding, segmentation, and morphological operations to detect three types of solder joint defects. First, to reduce the complexity of feature extraction analysis, the background is removed using simple thresholding to separate the solder joints from the background. Segmentation and dilation operations were then performed in order to highlight the solder joint regions. Two sets of features were selected for the determination of normal or defect solder joints: nine binary image-based features and

seven gray value-based features. Pareto chart and box plots for these features were then examined for selecting the best features that could discriminate between the normal defect types. Finally, rule-based classification was applied using certain rule and thresholds to classify the defects according to the type. Many advantages have been observed in their study such as their methodology did not require special lighting or special equipment to capture the PCB image. Furthermore, their approach of background removing reduced the computational time for feature extraction. Nakagaki *et al.* in [127] proposed a system for recognising circuit patterns and defect severity of semiconductor wafers using thresholding and segmentation techniques. The images were collected using SEM and different patterns were observed such as protruding, hole and flat patterns. Hole and flat patterns were identified using thresholding techniques by calculating the average of pixels in the binary image resulted. The algorithm for identifying protruding patterns were selected according to the density of the pattern. Thresholding were used again for identifying dense protruding patterns, while segmentation with the aid of binarization and edge detection were used to identify sparse protruding patterns. The study also classified the defects of the circuits in wafers according to the severity of the defect into killer and non-killer defects. However, the algorithm of the classification was not explained. The accuracy for the pattern recognition in this study was 98.8%, while the accuracy for defect severity evaluation was 95.6%. In a similar study conducted by the same authors in [126], template matching technique were used to analyse the defects. However, this study resulted in minor improvement of accuracy as the accuracy recorded was 98.9%.

b: REGION EXTRACTION

Connected Component algorithm is a commonly used region extraction technique which regard each pixel as a node in a graph. Connected Component Labelling (CCL) can be used after this step in defect inspection tasks to label the regions found (e.g. defective regions) into certain classes. Chang *et al.* in [44] applied CCL algorithm to identify the number of LED dies from the binary image map. The algorithm were applied after segmenting the die region pixels as 1s and non-die region as 0s in a binary image that have the same size as the original image using Hopfield neural network (HNN). The CCL algorithm examine each die region pixel to give it a label and compare this pixel to neighbor pixel so that all neighbor die region pixels are considered as one die. This procedure is repeated until all the dies are recognized. Ooi *et al.* in [61] proposed a comprehensive data-mining process using a Segmentation, Detection, and Cluster-Extraction (SDC) algorithm to extract common defective wafer patterns from the raw production test data. The proposed SDC algorithm has been developed to extract meaningful cluster features from a database of manufacturing test results accurately and automatically. It can be implemented either in an online or offline mode. CCL algorithm were used to simply pairing adjacent 1s (that represent defective dies) and

0s (that represent normal dies) in a binary image. Finally, morphological operations were used to remove the noisy parts. This study has achieved a 90% accuracy rates in detection. Furthermore, SDC algorithm have helped in reducing the false alarm rates by more than 90% when compared to using segmentation algorithm alone. A similar study was also conducted by Xie *et al.* in [96], where four defect patterns of WMs were generated by connecting-components and morphological operation approaches. Wijesinghe *et al.* in [230] considered similar approach; however, in inspecting liquid resin defects in LCDs. The acquired images from the OCT are binarized and pixels were classified as defective and non-defective according to certain threshold related to the intensity. Next, CCL technique were used to define the boundary of the defective regions and non-defective regions by grouping each pixel's class together. This technique is repeated until all regions are classified. Using this approach does not only evaluates the particular defective location; however, it defines the magnitude of each defect, and the number of defects in a unit sample.

Sindagi and Srivastava in [281] used two feature extraction approaches to highlight micro and macro defective features of OLED panels and generate feature vector to be used as an input for the classifier. Due to its important advantages of computational efficiency and good texture discriminative property, a modified version of Local binary patterns (LBP) was considered as one of the approaches for feature extraction. In LBP algorithm, a 3×3 operator is used to compare each central pixel with its eight neighbor pixels to generate a binary code that can be converted to a decimal value. The neighbors which have smaller pixel value than the central pixel are set to logic 0, otherwise they will be set to logic 1. Then the generated binary code resulted from the neighbor pixel value can replace the central pixel value. In the modified version of LBP, a uniformity measure is defined which is the number of transitions between 0's and 1's in the LBP code. Patterns having uniformity measure below a certain threshold are labelled as uniform. During the evaluation of this method, it was observed that it performed well on macro defects like pit and film tear but failed to be effective on micro defects like scratch and spot. Therefore, another feature extraction technique called local Inlier-Outlier Ratios were integrated with LBP to be able to detect micro defects. Lin *et al.* in [231] considered segmentation-based method called wrapping to locate the bright spots defected features in light guide plate of LCD panel. At the beginning, the entire image was scanned to find a bright spot. The system then scans along the upper part to the edge of the spot. The distance between the lower and upper edges is calculated and a center point were estimated by dividing the distance by two. The center point measured represents the center of the bright spot. A circle wrapping method is proposed in this case where the scanning sequence follows a counter-clockwise rotation from one corner to the opposite corner until all of the bright spots have been marked. Certain measurements were then applied to assess the quality of the bright spots. However,

the classification procedure was not explicit. Furthermore, there was no discussion for the computation time required no of the accuracy achieved. Kubota *et al.* in [120] used Region Growing to extract the shape feature of the micropipe wafer defect. Their algorithm procedure starts by extracting points of local minimum within a square region of pixels centred at the pixel of question called neighborhood region. If the local minimum point value is within predefined range, then this point belongs to the specified region. Furthermore, they extracted the surface curvature features of the defected. Then they created a feature vector out of the extracted features and fed it to a neural network for classification. Hsieh and Chen in [63] used multiple feature extraction approaches based on sub-region analysis for defining the possible defective point of semiconductor wafers. Then they applied Minimum Rectangle Area approach to combine the defective points into clusters. However, they did not mention how to specify the number of clusters or and how to use clustering features to separate various types of defect patterns [67]. Hui and Pang in [177] proposed a study to detect solder paste defects by first constructing 3D profile to represent the solder paste block. Segmentation technique were used to divide the block into four edges and surface top area. The overall solder paste block is also considered to be another region. A global classifier was used to assess the quality of the overall block region and declare if there is a defect or not. Two features were used to feed this classifier which are volume and aspect ratio. However, a solder paste block can still be defective if it passes the global classifier. This is because a deformed solder paste block can have the same volume and aspect ratio as the normal one. Therefore, additional five local classifier were established corresponding to the five regions segmented. Same features were considered for the four edges which are contour lines standard deviation and area of the edge, where these features are fed to four classifiers. While top surface height standard deviation and area of the top surface were chosen as features for the top surface region classifier. Finally, AND logic operation was implemented between the output of local classifiers and global classifier, such that if a defect is detected in one of them at least this means that the final result will show a defect is detected. Despite of achieving a 100% detection rate in this study, they did not mention the nature of the classifiers chosen. Furthermore, since a total of six classifiers were chosen in this study, it was important to mention the computational time needed for classification. Liao *et al.* in [95] proposed morphology-based similarity approach to generate simple and complex wafer sample patterns with certain degrees of similarity, as compared to the objective target WMs. Several morphological operations were used in this process including dilation, erosion, opening, closing, position shift, density change and rotation with variations. The generated data were then sent to classifier to specify the type of the patterned defect. Lin and Lue in [201] proposed a fast positioning and inspections system for BGAs. Edge detection and thresholding techniques were first applied to find the boundary regions of the pads and holes, then using

the least-square circle approach the centers of the holes and pads are found. The alignment shift is then tested by using four sample images, where the centers of holes and pads for these sample images are compared together. Certain thresholds were used to decide if the variation resulting from the comparison process are accepted or not. Unfortunately, this study did not provide any information about the efficiency of the proposed method in terms of the recognition accuracy and computational time. Deng *et al.* in [225] investigated transparent aesthetic defects of polymeric polarizers by simulating them using a microscale plano-convex lens. They employed gray morphology (dilation and erosion) approach to identify the investigated defects and extract the features of them. The features extracted were related to location, shape and size of the defects. Despite of having an efficient detection system with relatively low time of detection 1.6s and considering the fact that detection of the simulated defects were consistent with the experimental results. However, this study did not consider an algorithm for defect classification. Furthermore, they mentioned that irregular defects can be simulated by using irregular shaped lenses; however, they did not verify their claim experimentally. Finally, they did not show the necessity of using such a simulated technique. Authors in [226], [229], conducted similar approaches; however, they considered extremely slight transparent aesthetic defects.

c: EDGE DETECTION

One of the used segmentation techniques to extract used in machine vision applications is edge detection. This technique is very useful in applications that requires locating a feature, alignment or for gauge inspection and measurements. As the name says, edge detection is used to find boundaries in the image and sharp edges, this can be performed by locating the discontinuities in pixel intensities in the image using several filters and operators such as Prewitt, Canny, and Sobel. Pixels that are found on the boundary using this technique are called edge pixels. An edge pixel can be described using two parameters; edge strength (also called edge contrast) which defines the minimum difference in the grayscale value between the edge and background, and edge direction, which can be defined by the angle of the edge direction [309]. Chang *et al.* in [288] proposed simple image processing algorithm that relies on thresholding and edge detection to classify touch panel defects. The distance measured between the edges of the defects were considered as the criteria for deciding the defect type. For instance, if the measured width and length of the defect ranges from $7\mu\text{m}$ to $21\mu\text{m}$ and 1 mm to 10 mm respectively, the defect is classified as crack defect. The accuracy of the proposed algorithm ranged from 94-99% depends on the defect type. However, the inspection time of the algorithm was relatively long due to the high-resolution images considered. In the two studies conducted by Chao and Tsai in [262], [266], an improved anisotropic diffusion technique was used to highlight defects in low contrast surface images of glass substrates and back-light module in LCD respectively. Anisotropic diffusion

(also called Perona–Malik diffusion) is an image processing technique that can reduce the noise in the image with maintaining important features of it such as lines and edges [331]. This quality of the technique makes it reliable to deal with low contrast images to highlight the defects. In [262], an adaptive smoothing process were integrated with the original technique to further enhance the detection process of defects in glass substrates based on the variation of gradient in the image and by adjusting certain parameter values. For defect classification, the lower and upper limit for intensity variations were estimated by calculating the mean and standard deviation of the gray values of the image. If the gray level of a pixel falls within the control limits, the pixel is classified as a faultless point. Otherwise, it is classified as a defective one. The computation time of this study were estimated to be 0.3 s; however, in [266] they referred to same study time as 0.16s. Therefore, the real time was not completely clear as there is a contradiction between both information. In [266], the original technique were further improved by integrating PSO to automatically determine the best parameter values of the anisotropic diffusion function instead of manually as in the previous study. This study was conducted to detect low contrast backlight module defects in LCD. The classification criteria of the defects in this study was the same as the previous one. The computation time were improved to be 0.06 s with lower number of iterations compared with the previous study. Despite of the algorithm's ability to highlight low contrast defects, this algorithm only performs well with non-textured surfaces, which means it is not suitable to detect all kind of defects in LCD parts.

d: HOUGH TRANSFORM

Hough transform were also one of the techniques used for feature extraction and defect detection applications, due to the ability to detect various shapes (e.g. linear, circular and elliptic shapes), given a parameterized description of the shape. Edge detection operations are used as preprocessing procedures before applying Hough transform. This technique is very suitable for detecting wafer defects patterns in WBM as they tend to follow a specific pattern. Since WBM are considered binary images, Hough transform transforms the binary image into a parameter space and tries to detect the parameterized pattern through a voting process in which each point votes for all the possible patterns passing through it. Patterns with a higher number of votes indicate a higher probability of the occurrence of this pattern on the map. As long as a parameterized model can be established for the spatial pattern, this method can be adopted [59]. White *et al.* in [74] used Hough transform based on linear parameterization to detect defective dies patters on WBM. The patters detected in this study were of linear shapes such as scratches and edge patterns. The main advantage of this study is its simplicity and the ability of being fully automated. However, the study was not useful in detecting commonly defective WBM patterns such as ring patterns. Zhou *et al.* in [82] presented a control chart technique to detect line and circular patterns through

statistical evaluation using Hough transform. This statistical evaluation calculates the number of votes for the line and circular defect maps. When the number of votes is larger than the control limit, an alarm is raised indicating that a pattern is detected. However, this method cannot distinguish specific definite cluster patterns such as blob, bull's eye, edge, and ring. Chang *et al.* in [59] applied Hough transform to detect WM defect patterns and were able to overcome the limitations in previous studies by detecting all the patters that were missed by them.

Despite of Hough transform's ability of detecting various defect patterns, this technique is considered insensitive to gaps (missing pixels), which make it difficult to detect random or mixed pattern defects in WMs since it may group them as one pattern instead of multiple ones [74]. Hough transforms performs poorly when it comes to low contrast images, this may not be a problem in WMs since they are generated using circuit probe techniques. However, it may become serious problem in other cases that utilize illumination to highlight small defects such as Mura defects in LCDs. Furthermore, Hough transform is considered costly in terms of computational time [248]. Li and Tsai in [248] proposed a revised version of Hough transform to highlight defected Mura features in LCD such as spot, line, and region Mura. This revised version can detect low-contrast defect in 1D gray level image with uneven illumination. Unlike conventional Hough transform that are insensitive to gaps and needs sufficient number of points to detect line defect, this method can accommodate distance tolerance. Any point with the distance to the line falls within the tolerance will be accumulated as a function of the distance to the line sought. This approach allows the nonstationary points contribute to the accumulator in the voting processing. Despite of the proposed method's ability to outperform the conventional one; however, it is only capable of detecting nonstationary straight-line and cannot consider nonstationary curved profiles and nonstationary linear/curved surfaces. Chang *et al.* in [297] used Hough Transform as a preprocessing approach to transform the circular shape of camera lens' into a linear shape before inspecting the defects. After the transformation from the polar coordinate into Cartesian coordinates, segmentation and morphological operations were conducted to segment the defects. Five features were extracted from the previous process which are the area of defective regions, ratio of the width and height of defective regions, mean of the gradient of defective regions and variance of the gradient of defective regions. Where the feature vector containing these five features is sent to classifier algorithm for deciding the defect type. Jin *et al.* in [207] introduced a reference-free path walking method to recognize the BGA component locations and diagnose solder ball defects such as oversize ball, undersize, ball bridging, misshapen ball, missing ball, and ball offset. Solder balls were first segmented using adaptive thresholding and median-based Otsu methods, which determine local thresholds for individual cells, to overcome nonuniform brightness. Then path-walking method

(which is a modified Hough-transform approach) to locate the orientation and position of the balls and extract the defective features. Three features are then extracted using these steps which are solder ball area, center of gravity and compactness. Certain rules were then set according to the extracted features to classify the defects. The main advantage in this method that it does not need a reference image which make it more practical in real inspection application. Similar study was also conducted by the same authors in [157] to inspect solder balls defects using coarse and fine positioning technique. Unlike the previous study, this method is model-based in which edge detection filter and a circle fitting methods are employed to obtain the coarse and fine locations of solder balls, respectively. The approximate location of the component is then estimated using a geometrical method and the fine location is calculated by solving a least-squares problem. Finally, a pair of overlapping ratios were used to classify solder ball defects based on their quality and to inspect the accuracy of alignment. Compared with the previous study, this method consumed less computational time for same amount of BGA inspected. However, the accuracy measures in this study was lower than the previous one. A third similar study was conducted by the same authors again to investigate the same defects in [136]. Segmentation and adaptive thresholding were applied in this study as well to locate the solder balls; however, line-based-clustering approach were added to coarsely determine the BGA orientation and to classify the solder balls according to their row and column locations in the BGA array for the feature extraction process. Four features are then extracted after performing the previous steps which are ball area, ball centroid bias, roundness, and ball arrangement matrix. Finally, certain rules are considered according to the feature values in order to classify the defect types. The performed approach outperformed the previous two methods with 100% detection accuracy. However, the computational time consumption was the worst among them all with 200ms to inspect 500 solder balls. Kuo *et al.* in [259] proposed an optical inspection approach to highlight various kind of defects in polarising films of LCDs such as dust, foreign object, scars of hit, bubble and scratch defects. Various image processing and feature extraction techniques were used for this purpose. First, downsampling compression were performed to reduce the size of the inspected images, then Laplace operator were used to detect the edges of the defects. Thresholding and Hough transform were finally used to differentiate the spot defects, like dust, foreign objects, scars of hit and air bubbles in the production process from the line defects, like scratches. This study was able to speed up the inspection time by using downsampling technique as they were able to reduce the image size by 64 times. Furthermore, they achieved a differentiation rate up to 98% in sorting spot defects from line defects. However, this study did not propose a classification technique to classify each type of the investigated defects

3) TEMPLATE MATCHING

Template matching is considered one of the simplest and earliest pattern recognition techniques [332]. In AOI applications, template matching algorithm works by first identifying a reference template which usually represent the non-defected case (also known as *golden template*) that can be used for comparison. The selected template can be compared to the target samples using various kind of correlation functions. Template matching is preferable in investigating systematic defects that have common patterns. The reason behind that is the defect is always compared with a reference template so if the defect occurs is not systematic, the comparison with the reference template will fail and high false alarm rates will occur. Template matching techniques can be used in most application; however, it is not preferable in inspecting WM defects, since most of these defects are of mixed patterns (systematic and random).

Normalized cross-correlation (NCC) function is one of the most commonly used template matching functions, it involves sliding the sub-image over the larger image pixel by pixel and calculating normalized correlation to estimate the degree of similarity between the sub-image and the large image regions [137]. It has been proven to greatly reduce the data storage and also reduces the sensitivity to acquired images when compared with traditional image subtraction [333]. Zhong *et al.* in [48] proposed blob analysis and template matching approach based on NCC to inspect polycrystalline and fragmentary defects on LED chips. Regional image segmentation was first performed to locate the blob defect features and exclude them. NCC approach were also used to locate LED chips at pixel accuracy. A certain threshold was used to classify the abnormal LEDs from the normal ones. The study showed good accuracy in detecting normal chips with zero false alarm rate. However, a false alarm rate is presented in detecting defective chips because of the NCC threshold value selected. Despite of NCC simplicity, this method is time-consuming since it is based on 2D summation and multiplication operations to compute the correlation, and is often combined with the image pyramid method to compress image size to alleviate the computation load of the correlation coefficient method [45], [179]. Furthermore, this method is very sensitive to illumination variations and image shifts, which can increase false alarm rates [188]. In order to reduce the time complexity of this method, Crispin and Rankov in [179] proposed a modified NCC based template matching approach using the generalized gray- model template for inspecting component placement errors in PCBs such as missing, misaligned or incorrectly rotated components. The gray-model template can extract a vector of all edge positions of the inspected component. By only searching the image at edge locations, the number of NCC calculations that are needed to be performed can be significantly reduced. Genetic algorithm was also proposed to replace the sliding sub-image process involved in NCC operation. Despite their efforts in

reducing the computational time of the NCC approach, this method did not mention the classification criteria for the investigated errors (missing and misaligned component). In a similar study, multi-template matching algorithm proposed by Wu *et al.* in [184] that utilizes NCC for component placement inspection on PCBs. The searching process has been carried out by using the proposed accelerated particle swarm optimization (AS- PSO) method to reduce the computational time needed for detection. AS-PSO method were also compared to GA for its ability to perform the same function. However, experimental results have shown that AS-PSO was able to reduce the computational time required more than GA. The recognition rate achieved in this study reached 100%; however, the testing was performed on resistors only and did not involve other components. Similar approach was also proposed in a similar study conducted by the same authors in [185] with some modification to the PSO searching algorithm. However, the same drawback of the previous study was also found in this one. Furthermore, the processing time in this study was much higher of that in the previous one. Annaby *et al.* in [137] suggested an improved normalized cross-correlation (INCC) algorithm to discover the location of missing ICs. The suggested algorithm work in 1D instead of 2D, which reduce the computation time and robust against noise. Moreover, subtraction of the local mean in the INCC provides better robustness than NCC since INCC tolerates uniform brightness variations. Despite their algorithm's ability of reducing the computational time compared with NCC, their algorithm did not improve the accuracy of the NCC approach. Wang *et al.* in [188] have also proposed a modified version of NCC called partial information correlation coefficient (PICC) to inspect surface defects such as particles, foreign matters, and distorted components in PCBs, BGAs and ICs. The PICC uses the technique of significant points to calculate the correlation coefficient. The PICC algorithm procedure has to set three variables: the size of the inspection window, the gray level threshold, and the correlation threshold. The most important difference between NCC and PICC, is that the PICC firstly uses the gray level threshold to obtain significant points in the inspection window and calculate only the correlation coefficient of the selected significant pixel points. Therefore, the inspection speed as well as the false alarm rates can be significantly reduced. The second PICC threshold is the correlation threshold. This value is used to decide whether the image contains a defect. The selection of the proper correlation threshold is also a key factor to determine the algorithm is stable. Experimental results have shown that this method achieved up to 100% detection rate with only 0.3s, compared with 7s in NCC. However, if there is a gap in the expected results, users must determine a new set of variables for applying PICC procedure.

Pearson's correlation coefficient (PCC) is also one of the correlation functions used in template matching for comparing the reference image to the sample images. Unlike NCC, PCC is considered more robust to variations concerning brightness and noise. This method were used by

Timm and Barth in [20] to detect p-electrode defects in LED dies; the study assumed that the template and sample images have the same height and width and they produced a formula based on that assumption with the aid of the mean and standard deviation of the template and sample image. Ibrahim and Al-attas in [156] proposed a template matching and wavelet-based approach to inspect traces defects in PCBs. Reference image was considered as the perfect template for performing the comparison process. Two-dimensional HAAR wavelet transform was applied on both reference and sample images to perform the comparison on the wavelet domain. To avoid unwanted noise due to misalignment and uneven binarization, the comparison between the reference and sample images in this study is performed using subtraction process. The output of the image subtraction operation can be one of the following three cases: positive (potential defect), negative (potential defect), or zero (non-defective). The generated positive and negative images are binarized and then subjected to a noise elimination procedure. These images are lastly sent to XOR logic operation as a final classification to decide whether the images represent a defect or not. Many limitations were found in this study; first, the accuracy and the time requirement for their inspection system were not discussed. Secondly, despite of mentioning fourteen types of defects that their system can detect, their classification scheme only classified these defects using binary approach (defective and non-defective). Lastly, their proposed system can be applied for small and medium fabrication scale only, and cannot be implemented for mass fabrication systems [334]. Cho and Park in [180] proposed a similar method; however, for inspection of component defects such as missing component, wrong component, rotation, and tombstone. As in the previous study the wavelet transform for the reference and sample images were first performed. For the matching process between the reference template and sample image, the mean absolute difference and the mean square difference (MSE) are used to modify each pixel and the whole image matching is performed. To reduce the calculation time in matching, the area of objects was segmented from the overall area of input image. The segmentation step identifies the object area from the compressed image. Their approach was compared to DCT and results showed that their method outperformed DCT. The main advantage of this study is its ability of reducing the memory size, as they have reported that they used 7% only of the original image for the inspection process. This could be also considered a disadvantage as important features may be lost by reducing the size of the image to this scale. Their inspection accuracy was highest in detecting missing component defects with a 96.7%. However, experimental results have shown that variation of brightness and texture highly affect the accuracy as well as the time consumption of the algorithm. Unfortunately, the proposed method did not offer a solution to mitigate these effects. Tsai and Huang in [200] proposed a method, that can be used to investigate PCB and IC dies defects, based on the comparison of the whole Fourier

transformed image between the template and the sample inspected images. It retains only the suspicious frequency components in the Fourier domain of the test image and discards the common frequency components. After the anomalies are detected and the background has been removed, the inverse Fourier transform is then applied to restore the sample image. A simple statistical control limit is finally used as the adaptive threshold to segment the local defect for classification purposes. Unlike conventional template matching approaches, this method is considered invariant to translation and illumination variations in the sample images. Moreover, the proposed approach can detect subtle defects as small as 1-pixel wide. Liu *et al.* in [114], [115] proposed similar approach to detect IC wafer defects. In their studies they used 2D and 1D DWT respectively to extract a standard template image from three defected images using comparison and subtraction approaches. In [115], they showed that the accuracy of detection does not differ between 1D and 2DWT, while the computational time in 1D DWT is less than 2D. The advantage of this method is its robustness to illumination. However, the accuracy measures for these methods were not mentioned in both studies. Rau and Wu in [192] proposed template matching approach to inspect inner layer defects of PCB board. First, a golden template of PCB board was designed using CAD tools for comparison process. Before the comparison takes place, the sample images were normalized by applying geometric transformations such as rotation, scaling and shifting. Then image subtraction is applied to compare between sample images and the golden template. The result of the subtraction process will result in either missing pixels or excess pixels. Missing pixels corresponds to defects such as pens, mouse bites, pinholes and missing conductors while excess pixels correspond to shorts, spurs, excess copper, and missing holes defects. In order to segment these defects, a 4-connectivity logic operation is used to determine the outer boundary of objects in a binary image. Finally, classification algorithm called boundary state transition were proposed to classify the defects according to the 8 investigated defects. The proposed method is considered simple to implement and computationally inexpensive; however, image subtraction algorithms are sensitive to variations in illumination, lighting, color and complex transformations, which may affect the detection accuracy. To investigate traces and cosmetic defects in PCBs, Liao *et al.* in [194] used template matching approach based on Hausdorff-distance. The sample inspected images are compared with a reference template image, that is generated from the compilation of several good PCBs, for aligning them with each other. The alignment process can also help in locating the defects and extracting their features. Several techniques were used in the alignment such as sobel edge detector and geometric transformation as well as finding the minimal Hausdorff-distance. It has been found that traces defects of PCB follow specific patterns, therefore the features of these types of defects are directly sent to the classifier for performing the classification. However, cosmetic defects possess irregular

appearance, therefore for this type of defects color features are also considered in the classification process. Compared with other comparison approaches that are based on XOR operation and logical rules, the proposed approach required less time for extracting the features. Chang *et al.* in [193] proposed two-phase approach to inspect PCB traces defects. The first stage starts by storing sample images to form concept space. Segmentation and morphological operations to extract the features of the defect. The resulting images are then compared with template image that represent the ideal PCB image using rule-based method and XOR operation. The second phase, which is called case based reasoning, is a system that can be created with a small or limited amount of experience and then developed incrementally by adding more cases to the concept space as they become available. The hybrid approach can avoid the main disadvantage of high time consumption in template matching algorithm. Wu *et al.* in [162] proposed template matching approach to investigate solder bump defects. To do that a reference template image was generated that represents the perfect non-defected case. Using several image processing and feature extraction techniques such as thresholding, morphological operations, segmentation, and geometric calibration, four features were extracted from template and sample images. These four features are area of solder bump, the number of edge pixel, the deviation from center, and the deformation ratio. A comparison process were performed for the features of the template image to that of the sample images. Given a set of lower and upper limits rule, the defects are classified according to the matching score between the template and sample images. The proposed method achieved a high recognition rate of 97.96% with a low false alarm rate of 2.61%. However, in order to achieve these good results large number of samples were required (10600 samples), which will significantly increase the computational time. Hassanin *et al.* in [181] investigated more general faults on PCB boards such as missing letters, missing component and flux cutting. Speeded Up Robust Feature Extraction (SURF), segmentation and template matching approaches were used to highlight the defects. However, their approach is very time consuming with a total time of 6.5211s for single image inspection, which may prevent their study to be implemented in inline optical inspection system. Owing to its robustness and its ability of providing distinctive descriptors to the size and rotation transform, Yuk *et al.* in [195] have also proposed SURF algorithm for extracting PCB surface defects such as scratches and improper etching. The features extracted represent information such as the size, angles, coordinates, and color of the defected region by digitalising the input image into a feature vector that contains the previous information. Hessian matrix is used in the algorithm for detecting interest points, which represent the characteristics of the image and include useful information for identification, including corner points. Haar wavelet transform is also integrated with SURF to further increase the robustness and decrease the computational time. The extracted features are then sent to a classifier to decide

the source of the defect. Lin *et al.* in [274] suggested a modified pattern matching method to inspect and measure the movement of anisotropic conductive particles. The study used pattern setup and analysis to add a matrix of miscellaneous gray scale to an adaptive one and run a miscellaneous algorithm on part of the pattern block to improve the executive efficacy of the system. Adaptive feature weight matrix is also introduced to reduce error match. This research was able to identify defective patterns with relatively short time compared with conventional pattern matching techniques. However, the number of samples used for testing and the fact that no classification algorithm was considered are major drawbacks in the study. Ye *et al.* in [176] inspected the IC solder joint component based on an algorithm they call it "Adaptive template method". The algorithm start working by a constructing a dictionary of qualified IC solder images. Certain coefficient can be calculated using the dictionary scheme. These coefficients can be used to construct adaptive template assuming that an unqualified image is considered as a combination of qualified template and noise. Here the noise is considered to be the defect. Hue channel was used as the feature to be considered in calculating the difference between the sample images and the templates. Since relying on the difference only may result in a misleading data, each pixel has a specific weight that depends on the location of the pixels where most likely a defect will occur. Various experiments using several number of penalization functions were used to evaluate the quality of the inspection. For classification, a threshold R is defined based on the hue channel difference between the template and sample image from the dictionary, to identify whether a pixel in the difference image is a potential solder joint defect pixel or not. However, their approach classified solder joint defects as qualified and unqualified without mentioning the defect type. Cai *et al.* in [173] studied IC solder joints defects by comparing a good solder template models (qualified) to other sample images (qualified and unqualified) in a video frame. The inspection algorithm used in this paper is Visual Background extraction algorithm (ViBe), which is originally developed for moving object detection. This method has the advantage of overcoming the feature extraction and selection process, determining of specific threshold for image analysis and debugging of new products. Six templates were used instead of 20 as in the original algorithm usage in object detection to decrease the complexity. These templates were considered according to the hue-channel values. Despite of achieving a 99% inspection accuracy when using large number of training samples, this method does not explore prior knowledge and considered complex to use. Moreover, their proposed approach assesses the overall quality of the solder joint without specifying the cause of defect. Wang *et al.* in [189] proposed template-matching-based approach to evaluate drilling quality of PCB holes. Their method is capable in detecting three types of PCB defects: missing holes, incorrectly located holes, and excessive holes. After applying preprocessing, rotation, and scaling operations on the sample images to match then with

the reference templates, several features are calculated and extracted such as the centers, radius, roundness, and other diameters of the holes. The ratio and angle of rotation are calculated between the testing and the reference images, then they were modified until they became in the same direction and at the same angle. In this paper, the centers of the holes are in the most upper left and most upper right as two datum points for both testing and standard images. Template matching can be then applied between reference and testing images by using three key performance indicators as thresholds which are average and variance for center holes, center compensation, and unit circle scale. Their approach can be effectively applied for high resolutions of $5\mu\text{m}$ and above. However, many limitations have been observed in this study. First, their approach is considered lengthy and computationally expensive as the total inspection time requires 2.5 seconds. Second, the ratio between reference templates and testing images is manually calculated, which makes their approach not fully automated. Finally, by using the most upper left and right points as datum points, it would cause errors because if one or two of them are missing the result will fail. Hsu and Shen in [147] proposed an approach based on template matching to inspect IC marking. Their proposed method starts by first detecting the angle of the chip and then using the sum of absolute difference similarity measure to match the template image and sample image. To reduce the scanning time in the inspection process, the detection algorithm was implemented on a multi-core embedded processor. In addition to that, the operations of the algorithm were performed in parallel using Single Instruction Multiple Data instructions for Arm processors known as NEON. The time needed for their algorithm to distinguish good from bad ICs reached 31ms. Their proposed approach overcame some limitations that were found in similar previous studies in [145], [146] by detecting marking defects accurately when the IC chips are placed with rotation angles, reduce the computational time and integrating the software and hardware into a whole automatic inspection system. However, their method classified the IC marking as good and bad, without highlighting the cause of the error. Lee *et al.* in [279] used multiple feature extraction methods to highlight TFT-LCD pad area defects. The proposed method utilizes an adaptive discrete Fourier transform (DFT) with the aid of a golden template that is transformed using DFT as well to precisely remove wider range of pattern frequencies. The main advantage of this method that it works well on an image having both impedance matching and fan-out areas as these areas either have a changing pattern period or non-repeating components. In the three studies conducted by Acciani *et al.* in [143], [165], [166], different feature extraction techniques were used to classify five types of solder joint defects. They first used template matching approach to highlight the extract the ROI in sample images, which represent the solder joint and IC area for inspection. Ten geometric and eight wavelet features were extracted from the inspected area and were combined together to construct one feature vector. The obtained feature vector

was then used as an input for a classification algorithm in order to classify the defects according to the five types considered. A similar approach were used in a study conducted by the same authors in [167]; however, in this study less features were considered for the defect detection task. Three instead of ten geometric features that represent area of the solder fillet, mean gray level of the image and barycenter position of the solder area were obtained in this study using thresholding and segmentation techniques. Furthermore, wavelet features were not considered here, which reduce the computational time and allows the feature extraction process to be performed automatically without the need of a human expert.

Template matching is still facing some limitations that makes it difficult to use and increase false alarm rates, these limitations include requirement of the reference and test images to be exactly aligned and high influence of noise and illumination settings. One of the major limitations of template-matching for inspection is that an enormous number of templates must often be used, and this makes the procedure computationally expensive [306]. To overcome these limitations, Kim and Yoo in [117] proposed Feature Point Matching approach to inspect defects in wafer images. This method starts by studying the features that may differ defective image than the reference images such as contour, edges, and corner points. Therefore, a feature point has a special property distinguishable from its neighbor points. In this method the comparison is between features instead of pixel-by-pixel comparison as in conventional template matching approaches. In this study corner points were used as feature points for comparison, as it has been found that wafer images with defects results in additional corner points and different gradient values compared to those in the reference images. It has been proven the proposed method outperformed other template matching methods such as subtraction, NP-subtraction, NCC and Eigenvalue. Furthermore, it is less sensitive to alignment and noise. However, this method was not able to locate defects and the processing time has to be further improved in case online testing is required. Xie *et al.* in [110], [112] proposed self-referencing method, in which the dataset of images used for defect detection are also used to create reference image that is used in template matching method. Their algorithm has a learning ability of refining the reference image in case a better match was found. This ability does not require repeating the comparison steps between the reference and sample images which reduce the computational time of the process. Furthermore, their algorithm is not affected by image alignment and uneven illumination. Despite of all mentioned, their study did not propose a criterion for defect classification. Jian *et al.* in [284] overcame common limitations in template matching techniques such as misalignment, and surrounding illumination variations, by proposing contour-based registration (CR) method to generate the template image. In this technique the contour is considered main feature for alignment such that in the case of rotation and translation, the contour geometry remains unchanged. This algorithm was used to inspect mobile screen

glass defects. A subtraction and grayscale projection were then conducted on acquired images and template to extract defect. Using certain threshold, an internal classification procedure was performed to binary classify the sample images into defected and non-defected samples. Finally, an improved Fuzzy c-means clustering (IFCM) technique were proposed to segment defects with fuzzy boundary contours. Despite of the good sensitivity and specificity results achieved in this study, the approach considered did not include final classification process to classify the defects according to their type. Furthermore, the inspection time of 1.6601s is considered relatively long for on-line inspection environment. Also according to [285], it is insufficient for image distortion rectifying to consider only rotations and shifts, and thus the extraction after subtraction is not accurate. In a similar study conducted by the same authors in [283], an AOI system were proposed to inspect mobile screen glass defects such as scratch, pit, dirt, and edge breakage. In order to avoid the problem of higher dimensionality features that exists in common feature extraction techniques, this study proposed a technique based on multifractal spectrum for feature extraction. Using this technique, only two features can be extracted named multifractal spectral width and spectrum subtraction, which are considered for classifying the defect type using classification algorithm. Liang *et al.* in [287] proposed AOI system to detect touch panel defects. In their approach, they first calculated the gray-values of the images and considered them as feature values. Then they established a dictionary of defect-free features; however, since these features can be redundant, sparsely reconstruction were proposed to choose the optimum set of features. Orthogonal matching pursuit (OMP) were then used to sparsely represent the testing images based on the dictionary. Finally, sparsity ratio of the sparse representation coefficients (between testing image and template) is estimated to determine whether the testing image is defective or not with the aid of certain threshold. Experimental results showed that under various illumination conditions, the proposed approach can efficiently and quickly detect the touch screen defects for low resolution images and different defect types. However, their approach used binary classification (defected, non-defected) for inspection without specifying the defect type. Furthermore, their approach is considered computationally expensive since their method is highly iterative. Tsai and Hsieh in [29] proposed a template-matching-based algorithm that can be used for detecting both PCB and LCD polarizer film defects. To solve the alignment problems encountered in template matching approaches, this study used fast image alignment method called the expectation-maximization (E-M) technique. This technique starts with edge detection to extract edge points in the image. The E-step of the E-M procedure finds mutual edge points in both compared reference template and sample inspected image by assigning weights to individual edge points. The mutual edge points give larger weights, while the foreign edge points in two images have smaller weights. The M-step then calculates the geometric

transformation parameters using the weighted edge points in individual images. Finally, spiral search is carried out by a predetermined lookup table to find the nearest point, where the weight of each edge point is inversely proportional to the neighboring distance. Unlike conventional template matching approaches such as NCC, this method does not require to slide the window pixel by pixel throughout a search region and no computation is involved in the look up table search process, thus, this method is computationally very efficient. Moreover, NCC is highly sensitive to rotation changes, which increases more computation load to find the rotation angle. The proposed E-M positioning method needs only to fix the window of the test object at the same location as the template in the image. However, in order to achieve high accuracy in this approach, the object to be detected can only present a minor geometric deviation with respect to the template [335]. Furthermore, this study only presented defect detection and positioning approaches without considering defect classification. For PCB defect inspection, Tsai and Yang in [198] proposed a similarity measure approach based on the shape of the pair-wise gray-level distribution to compare between a reference image that represents a non-defected PCB and sample image. The gray level distribution between the compared images is represented using 2D map called gray-level correspondence map. In case of identical images were detected, the gray-level distribution will be a diagonal line. On the other hand, if the two compared images are different, the distribution will be a non-linear shape. The shape of gray-level distribution is then measured by the eigenvalues of the covariance matrix of the data points in the gray-level correspondence map. The smaller eigenvalue of the covariance matrix is used as the similarity measure of two compared images. It will be approximately zero if the two compared images are identical, which represent that no defect has been detected. Whereas it will be distinctly large if the two compared images are different to some extent, which represent the case of defected image. Experimental results showed that the discrimination capability of the proposed similarity measure is superior to the traditional NCC approach. However, this method requires a noise-free environment and perfect alignment of the sample images [117]. Gaidhane *et al.* in [199] also proposed a similarity approach to detect PCB surface defects. As in the previous study, a reference template image that represents the ideal PCB state is generated to assess its similarity with the sample inspected images. Symmetric matrix is then calculated using the companion matrices of two compared images. The rank of the symmetric matrix is used as the classifier that can distinguish between defected sample and non-defected one, such that if the rank of the matrix is zero it means the sample image is non-defected, otherwise it means a defect has been detected. Unlike the previous study, this approach does not require feature extraction and calculation of eigenvectors or eigenvalues, which can reduce from the computational time needed for detection. Compared with other similarity approaches such as NCC, this approach achieved better recognition accuracy and lower false alarm

rates. However, this study only verified its effectiveness when small rotations (2° to 6°) and translations (2 to 10 pixels) of the inspected samples are considered.

4) GRAY-LEVEL CO-OCCURRENCE MATRIX

Various statistical features can be extracted from (Gray-level Co-occurrence Matrix) GLCM such as energy, entropy, contrast, variance, correlation, and inverse difference moment. Considering large number of features for extraction will increase the quality of the assessment; however, it will increase the computational time in return [336], [337]. Li and Huang in [75] used GLCM to extract eight features: entropy, energy, contrast, local Homogeneity, mass, centroid, geometric moments, and central moments along with seven moment invariant features (translation, scaling and rotation) for WBMs. These features were fed to classifier algorithm to classify detected patterns. Yoon *et al.* in [223] used GLCM along with segmentation and template matching to detect polarizing film defects in TFT-LCD. Image magnification were first used to inquire the images with the of high-definition CCD sensor since the defects considered were in the micro-scale. Image segmentation were then applied to isolate the defective regions from the sample images. GLCM were then used to extract four features from the defective regions: actual defective region (ADR), center of gravity of ADR, contrast and angular second moment. Finally, template matching was used to compare these features with non-defected samples and certain thresholds were used to identify the defect types accordingly. A high inspection recall and precision were achieved in this study (95% and 96% respectively). However, their method in magnifying the image during the image acquisition approach could result in high inspection process time that may affect the capability of this method for inline inspection. Yang *et al.* in [214] calculated 11 features using GLCM to highlight five defects in the TFT-array process. However, considering that this is a large number of features to be extracted, this may affect the inspection speed. Youesefian-Jazi *et al.* in [263] used multiple feature extraction techniques to extract surface flaws and scratch defects in TFT-LCD glass substrates. To reduce unwanted noise from illumination, DWT were first used on each glass substrate sub-image. After that two GLCMs were calculated, where each one has 22 features to be extracted. Due to the correlation between the extracted features and to avoid redundancy, PCA were used for dimension reduction before sending the extracted features as inputs to the classification procedure. Liu *et al.* in [212] used segmentation and GLCM-based method to extract the defected features (target and non-target defects) of GE process during TFT array fabrication. Eight feature vectors were used for this purpose to represent target and non-target defects. These vectors were sent to a classification algorithm for further consideration. However, during the experiments conducted in this study, one of the defective images were misclassified as a target defect, even though it was non-target defect. This can be due to the few number of feature vectors considered or

the whole feature extraction method needs to be reconsidered. After separating the background textures from the foreground defective features using NDF filter, Park and Kweon in [234] considered extracting feature set that consists of geometrical, intensity, statistical, and textural features to investigate AMLOED defects. GLCM were used for this purpose and 33 total features were extracted in this step. PCA technique were also used in this study during the experimental trials to investigate its performance in reducing the dimensional space of the sample images. Kuo *et al.* in [228] used multiple feature extraction techniques in order to classify dent, foreign material, bright spot and scratch defect of polarising films. They started by transforming the defect image into the frequency domain using Fourier transform combined with a Butterworth high pass filter to highlight the defects details. Then they converted the image back to the spatial domain and segmented the defect regions using edge detection techniques with the aid of Canny edge detector. Finally, homogeneity, contrast, maximum gray level and eccentricity features were obtained from GLCM matrix and used as input for classification process. Hence, each feature of GLCM matrix is specially obtained to highlight each type of the defect investigated. For instance, homogeneity were used to highlight foreign material defects, contrast for dent defects, maximum gray level for bright spot defects and eccentricity for scratch defects. Wang and Chen in [109] noticed that the WM defect pattern features are rotation invariant because of the round shape of the wafer's image. This means that the output of the features is not affected by the rotation of the input image. Therefore, they proposed three rotatable weight masks of the same size of the circular area of WM to extract the defected features. They named these masks polar masks, line masks and arc masks. Rotation invariance is achieved by making several rotated copies of each mask and only the max feature value is retained for each master mask. Polar masks aim to extract features of concentric patterns, while line and arc masks are designed to mainly deal with eccentric patterns such as scratches. For polar mask the area of the mask is divided into several zones using two methods: angle binning and circle binning as show in Figure 35. Angle binning (shown in Figure 35(a)) divides WM circle into equally spaced circular sectors, while circle binning (shown in Figure 35(b)) draws concentric circles of the WM, which separate the circle into annuli. The features are extracted using these zones, for example edge defect pattern appears mostly at interval $[0.8R, R]$, so circle binning at $0.8R$ could help detect "Edge" pattern.

5) COLOR ANALYSIS

To avoid long computational processing, most feature extraction techniques used gray-level analysis to analyse and extract defective features from images. However, some defects require to implement color analysis techniques in order to capture the important features of them. Color analysis techniques are performed with the aid of color channels such as RGB, HSV, YIQ and CLEIUV which provide the color representation of the picture. In general, four methods are

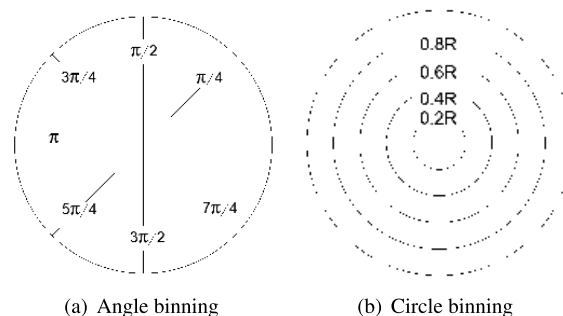


FIGURE 35. Binning of WM circle of radius R .

usually used to perform color analysis for feature extraction purposes [338]:

- 1) Analyzing each color channel individually by applying gray-level methods (e.g. thresholding) on each color channel. In this case each channel is considered independent from the other such that only spatial interaction is considered.
- 2) Transforming the image into different color space (e.g. RGB to YIQ) such that features can be easily extracted from the transformed space. The selection of the color space is usually application dependent.
- 3) Combining spatial and spectral interaction between channels such that gray-level is applied on each channel while the pixel interactions between different channels are also considered.
- 4) Using fully 3D models to analyse color textures. In this case scenario, the spatial and spectral interactions are simultaneously handled. However, some difficulties arise in effectively representing, generalising, and discriminating 3D data.

Chiou *et al.* in [203] considered inspecting BGA defects that occur in gold-plating areas such as stain, scratch, solder-mask, and pinhole. A neural network was first used to locate the gold-plating areas by feeding the network with the RGB information for each pixel. Beside the geometric variations for the defective regions, the study showed that some defects have unique color representation. For example, a scratch on the gold-plating regions that expose the copper or nickel underneath will change its color from golden to copper or silver. Furthermore, a stain or oxidation on the gold-plating regions will also change the color on the defected area. Therefore, color information was used in this study during the feature extraction process. Color segmentation, morphological operation and edge detection techniques were used for extracting six types of features that represent color and geometric information of the defect which are circularity, roughness, longest/shortest distance ratio between each defect, R-mean, and G-mean. These features were fed to another neural network for specifying the defect type from four types of defects considered. Nam *et al.* in [15] evaluated chromatic defects of FPDs using high-dynamic-range (HDR) imaging. First, the images are acquired by HDR imaging system.

An image of flawless FPD was considered as a reference for comparison. Color matching techniques were then used by converting both reference image and test samples into color maps and comparing the color variance for each pixel using Euclidean distance. A certain threshold according to the distance were considered in order to classify defected and non-defected pixels. This study was one of few which considered color defects in FPDs and they achieved an accuracy up to 95.61% in detecting colored defects. Tsai and Lin in [155] developed two entropy measures to detect gold-plated surface defects in PCBs. One entropy measure uses two chromatic features derived from the CIELUV color space to detect color anomalies such as copper exposure, and the other measure uses edge angles to detect structural defects such as roughness on gold-plated surfaces. The entropy is computed by sliding a neighborhood window on a pixel-by-pixel basis throughout the entire gold finger regions in the sensor image. A pixel defined in a small neighborhood window in a homogeneous gold-plated region will have small entropy value, and one in any irregular region will yield a large entropy value. Simple statistical process control principle was applied to set up the threshold for distinguishing defective regions from homogeneous regions in the resulting entropy image. However, the recognition accuracy for the proposed algorithm was not assessed in this study. Chang *et al.* in [113] used color variance measures and GLCM parameters such as contrast, entropy, homogeneity to extract semiconductor wafer defective features. The color information is represented by the average intensity values of the RGB components. The feature vector represented by color information and GLCM components is then sent to classification algorithm. Xie *et al.* in [159] acquired the sample images of solder joint and IC components using tiered-color illumination system, after that the image is divided into twelve sub-regions as shown in Figure 36. Each defect will correspond to different color distributions and patterns in one or more of the sub-regions. To highlight the defective regions, a feature extraction process took place for the three red, green and blue sub-images for each sample image, these features describe the geometrical and color distribution of the selected regions such as area, constant ratio etc. Ten features were selected for each sub-image (thirty in total for the three sub-images). An improved Adaboost algorithm was used in this study to select optimal and minimal number of features that carries as much information as possible. Adaboost is supervised learning algorithm that is usually used for classification; however it can be also used for feature selection as in this study. After selecting the featured using Adaboost, the selected features are sent to classifier to classify them according to the defects considered. Saving computational time by using Adaboost algorithm is considered a main advantage of this study. A similar approach was also considered by Wu and Zhang in [160]. In this study tiered-color illumination source was used to acquire images and the IC solder joint were also divided into several subregions which called shape features as shown in Figure 37. Seven types of defects were considered

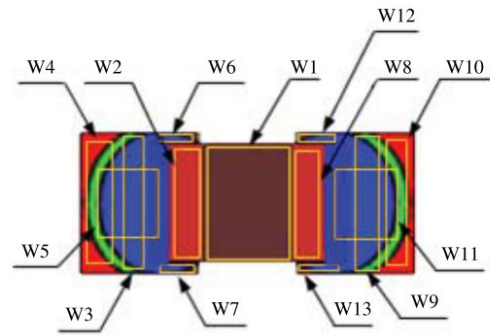


FIGURE 36. Twelve subregions of chip and solder components [159].

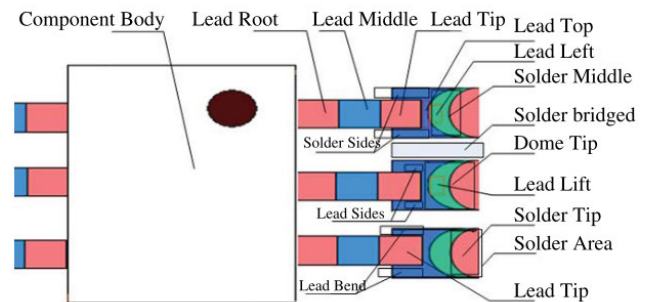


FIGURE 37. Subregions of IC chip and solder components [160].

in this study: surplus solder, lacking solder, lead lift, lead bend, shift, bridge, and pseudo joint. Where each defect type corresponds to different pattern and color distribution. Digital features were then used to evaluate the solder quality of the subregions by analyzing each sub-image component (red, green, and blue). These digital features are expressed by the color, area, mass center, and continuous pixels of each sub-image. Logical features were then considered such that the defective subregions that is associated with certain defect type are marked with logic 1, and the non-defective regions are marked with logic 0. Finally, the defects are classified according to certain rules and thresholds, where an overall recognition rate of 98.6% has been achieved. However, many thresholds should be elaborately determined to achieve a satisfactory classification. This causes the operator to spend much time in selecting the appropriate thresholds [173]. Similar illumination settings were used by Wu *et al.* in [171] to inspect defects in two regions: component body (IC) and solder pad. Seven color features and one template matching feature were extracted from the acquired photo for each region. The color features included the average intensity value and percentage of highlights, while template matching approach utilized a reference template to compare it with sample images acquired using NCC function. It has been found that these features are not independent and as a result considering them all will add on the required computation time for training. Feature selection methods based on information gain were used to ignore the redundant features and retain the important ones. The selected features were then

fed to classification algorithm. The main advantage in this method that only features that can contribute in the quality of the classification process were selected, which can reduce the computational time required. The same exact approach were also considered by Wu *et al.* in [172]; however, in this study genetic algorithm were used for the feature selection process. Song *et al.* in [139] have also used genetic algorithm to select optimized features for solder joint and electronic component defects inspection. In their approach, they have also used tiered-color illumination system to acquire the sample images. The solder pad and component package regions were divided into several subregions to extract the regional features for 10 types of defects. Four types of color features were also considered for each sub-region. The genetic algorithm was used to select the optimal number of regional features. Experimental results in this study showed that selection of nine subregions led to best recognition results. The selected features were then sent to classification algorithm to specify the type of defect detected. Wu and Zhang in [163] proposed a similar approach for inspecting seven types of solder joint and IC component defects in PCB. The same tiered-color illumination system that was used in the previous study was also used in this one to acquire the images. Region, evaluation, and color grads features were extracted from the acquired images. The region features were defined by dividing the acquired images into regions where the defect will mostly occur. Evaluation features can be observed by measuring area, barycenter, and defect distribution in the inspected region. Finally, color grads features describe the color sequence (pattern) from one side to others in a pointed region, it plays an important role in the proposed method to inspect solder joints. According to the values obtained from the evaluation features and the color sequence obtained from the color grads features, simple Boolean rules and conditional statement are used to classify the defects into the seven defect types considered and one more class to represent the good solder class. The proposed method achieved an overall detection rate of 97.7% with detection speed of 11s per PCB. However, since Boolean rules were used for classification, their algorithm needs to be reprogrammed if a new defect type has to be considered. Mar in *et al.* [170] used several image enhancement and feature extraction techniques for detecting solder joint defects such as insufficient and excess solder joint. Hough transform were first used to allocate the PCB in the image so that the PCB does not need to be placed onto a precision X-Y table. In this study DCT was used to normalize the images to appear stable under different lighting conditions, which is performed on the entire image to obtain all the frequency components of the image and remove the coefficients of lower frequency bands. The image is then transformed from the RGB to YIQ color model, due to the advantages of this model such as (1) processing the Y component only will differ from unprocessed image in its appearance of brightness and (2) most high frequency components of a color image are in Y. Finally, segmentation and region filling techniques were used to highlight the solder joint component regions.

Despite the method's efficiency in detecting the defects, this study did not consider a classification algorithm to classify the defects. In the study conducted by the same authors in [161], they continued with the same approach; however, with some enhancement of the feature extraction process and with addition to a classification approach to overcome the previous limitations. After image segmentation, DCT were used again along with other approaches such as Gabor filter and DWT to extract the features of solder joint defects and to construct filter bank form by grouping the detail coefficients together at each level. Mahalanobis Cosine Distance was used as classification approach to compute the similarity measure between two filter banks. In the comparison the study showed that fusion of various feature extraction methods (DCT, DWT and Gabor filter) led to better classification results. However, the computational time of 20-30 s that takes to classify one defect is considered extremely high, which makes it difficult to implement this study in inline process inspection system. Kuo *et al.* in [272] used several feature extraction techniques to highlight black defects (e.g. particle and fibre) and white defects (e.g. gel and resist coating) in color filters of LCD. Since black and white defects have difference appearance in the sample test image as shown in Figure 38, the method of highlighting each defect type is different than the other. Therefore, Otsu thresholding were first used to classify each type of defect into white and black using a certain threshold. Canny edge detection along with segmentation and morphological operation were used to highlight the defected region areas. Four types of feature values were extracted using these feature extraction methods which are area, aspect ratio, squareness ratio and damage rate. Where these feature values were used as an input to a neural network for further classification. In a similar study, Kuo *et al.* in [273] considered investigating color filter defects as well; however, the defect types considered as well as the feature extraction techniques are slightly different. Multiple feature extraction techniques were used to extract five key features: including defect gray value, defect R component, defect G component, defect B component, and aspect ratio. In order to do so, orthogonal projection was first used to locate each pixel on the image. An image comparison was then performed in order to select a reference template based on the quality of the template. Subtraction procedure were then applied between sample and template to obtain new image with highlighted defects.

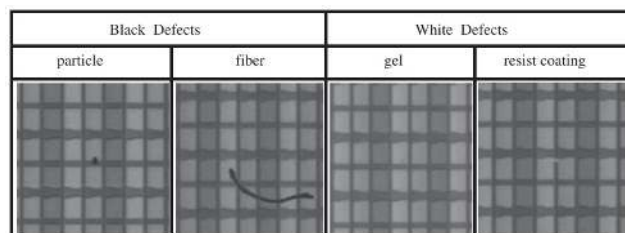


FIGURE 38. Black and white defects of color filters [272].

Control limits were then used to separate the defected regions from the non-defected. Finally, segmentation and morphological operations were implemented to extract the five key features that will be used as an input to classifier for defect classification process.

6) MODEL-BASED FEATURE EXTRACTION

Model-based feature extraction methods are based on the construction of an image model that can be used to describe a feature and synthesize it. The model parameters capture the essential perceived qualities of feature [339]. Chen *et al.* in [76] proposed an algorithm based on a growing wavelet hidden Markov tree (gHMT) statistical model to extract WM defect patterns. The hierarchical tree-based model, gHMT, utilizes the growing and learning procedure to increase successively the size of the wavelet tree for better feature extraction performance. Maximum likelihood classifier were then used to classify the patterns detected into four classes: annulus, half-annulus, band and half-ring. Jiang *et al.* in [178] proposed a model approach to classify solder paste defects based on learning the color biological feature sub-manifold. The biologically inspired color feature (BICF) is applied to represent the solder paste images by generating feature maps and introduce a new sub-manifold learning method to extract the intrinsic low-dimensional BICF manifold embedded in an extrinsic high-dimensional ambient space. This approach can simulate the optical inspection task performed by human inspector by identifying poor from good quality solders. The output for the BICF approach in then fed to classifier for the classification process. However, this method cannot analyse the details of the defects effectively [139]. Xie *et al.* in [31] proposed a model-based approach to detect defective pixels in PCB sample images, the model conducted in this study is called localized defects image model (LDIM). In manual inspection task, workers focus on the local defects rather than global defects by considering both regional color deviation from the local dominant color and regional color rapidly changing as possible defects. This model can mimic the manual inspection process by considering two main factors: color deviation and color fluctuation. An ROI of size 100 - 1000 pixels is extracted from the original image so that the LDIM model can be applied by identifying local differences in color between potential defects in the foreground and the background. A specific threshold was used then to classify each pixel as defective and non-defective. Second, labelling and blob analysis are performed to characterize the shape and size of the defects. In this step, the labelling of eight connected components was calculated and a particular area threshold value was applied to each of these images. Their proposed method achieved 100% detection rate with zero false alarm. It is also worth mentioning that their approach outperformed template matching approaches by analyzing color variations and color-related defects. Furthermore, it can detect tiny defect embedded in a pad image that may differ only slightly from the surrounding region. However, their approach cannot classify the PCB defect by type and

therefore it cannot be considered fully automated for inspection purposes. Lu *et al.* in [209] used model-based approach and thermography to inspect solder ball defects such as missing balls in BGAs. Thermography can help in detecting the heat changes as a result of the defect in the thermal images, such that each defect has its own heat signature. Furthermore, location and size of the defect can be easily determined using this technique. The details of constructing the thermography detection system for this study was already discussed in earlier study conducted by the same authors in [319]. In order to improve the signal-to-noise ratio, mathematical model based on polynomial fit and differential absolute contrast techniques were utilized to reconstruct the thermal images. Three statistical feature vectors were then extracted from the reconstructed images that represent the area of the solder ball, the variance of the hot spots and temperature. The three vectors are then sent for classification algorithm to classify the defects. Despite the effectiveness of thermography to detect certain types of defects, this method has relatively low spatial resolution (typically 640×480 pixels), which makes it not suitable for small defects detection that requires high resolution [340]. Jiang *et al.* in [238] proposed statistical models to identify Mura defects in TFT-LCD in addition to their sizes and locations. This study used luminance meter (light sensitive device) instead of a CCD device to measure panel surface brightness in a darkroom environment with the panel switched to white background. LCD panel is divided into 144 areas. Five points are measured to obtain the luminance data. Using the acquired data, Analysis of Variance (ANOVA) were implemented to identify areas significantly different from other areas in a panel. A certain threshold was defined according to the luminance, such that if the value exceeds the threshold, the sample is considered non-defective. Otherwise, the sample is considered to have Mura defect and a further step is required to identify the location and size of the defect. Exponentially Weighted Moving Average (EWMA) control chart concepts were used to detect the non-uniformity areas in a panel and to identify the location of Mura defects along with their sizes. Despite the capability and simplicity of their method to identify the defect type, location, and size, several limitations have been observed in their study. Their proposed procedure was limited to 15-inch LCD panels as produced by a local manufacturer. Furthermore, the method used for acquiring data limited their ability to identify a defective area partially overlapping two or more of the testing samples. Finally, certain parameter that was important to calculate EWMA, was estimated by trial and error, which make their method not fully automated. Another statistical approach that were used to accelerate defect detection process called multivariate Hotelling T-squared statistics. Hong-Dar Lin used this method extensively in his research articles to highlight defects in LEDs [36], [38], LCDs [245], and ceramic capacitor chips [291], [292]. After dividing the image into several sub-images using image masks, feature vectors can be obtained using wavelet analysis as in [36], [291], [292], energy features as in [38] or color models as in [245].

These feature vectors are used to construct what so called T^2 distance or T^2 value. T^2 value can be regarded as a distance value of a multivariate processing unit. The larger the T^2 statistic value, the more distinctive the region is from the normal area. Thus, the more easily the region can be judged as defective. Owing to the blurriness and low contrast nature of Mura defects in LCDs, Gan and Zhao in [219] proposed a modified local binary fitting model (LBF) to highlight the defected regions. LBF models are considered one of the segmentation techniques that can solve the problem caused by intensity inhomogeneity [341]. The proposed modified LBF model made robust to initial contour and competent for the extraction of defect boundaries. Furthermore, in order to detect multiple defects with different brightness levels, the study introduced a simple processing scheme to narrow the brightness range of defects based on statistical thresholding. Their method achieved a very high recognition rate along with low false alarm rate compared with other method. However, this method is considered computational expensive and less efficient compared with similar methods such as Markov concurrent vision (MCV) and independent component analysis (ICA). Bi *et al.* in [242] proposed a level set based method for segmenting Mura defects with a new region-based active contour model, which is an improvement on the Chan-Vese model. Chan-Vese model is an active contour model which uses region based information rather than the gradient of the image. Thus, the objects whose boundaries are not defined by gradients or have very smooth boundaries can be detected and the position of the initial curve can be anywhere in the image even not surrounding the objects [342]. In this study, Gabor filter were first used to remove the background then the proposed model was used for defect identification. The defect detecting rate of this study was relatively high (up to 96%). However, some drawbacks were observed on this study. For instance, the proposed model is based on the assumption that image intensities are statistically homogeneous in each region and thus is not suitable for small Mura defects with uneven backlight and cannot be applied in online display inspection due to its very large search space and excessive time consumption [219], [243]. Also, how to choose the parameters of model was still not a standard of theoretical knowledge as a guide [284]. Furthermore, the proposed study did not include a classification algorithm to automatically classify the defects. Yang *et al.* in [243] proposed similar approach to investigate Mura defects in FPDs. The method proposed consisted of two parts: an outlier-prejudging-based image background construction (OPBC) algorithm which is intended to quickly reduce the influence of image backgrounds with even brightness and to coarsely estimate the candidate regions of Mura defects. Then, region-gradient-based level set (RGLS) algorithm is applied only to these candidate regions to segment the contours of the Mura defects. The algorithms used in this study were compared to similar algorithm such as the one used in [242] and it showed better performance in terms of accuracy and false alarm values. Moreover, the model proposed in [242] requires almost 500s

of computational time which is more than 40 times slower compared with the algorithm used in this study. Lee and Yoo in [237] proposed a complicated data fitting approach based on regression to detect region-Mura defects with uneven brightness in TFT-LCD. The study estimated the background region of the sample image modified regression diagnostics, then the background region was approximated by a low order polynomial to generate a background surface. The reason behind this procedure is to perform subtraction process for the background from the original image. This subtraction can remove the influence of non-uniform background and transform the segmentation problem into a simple thresholding one. The resulting image is then post-processed by median filtering, morphological closing, and morphological opening to remove noise and refine the segmentation result. Finally, a certain threshold was used according to the gray-level intensity, which can be adjusted according to the panel quality to classify the defective samples. The experimental results showed that the proposed method succeeded in detecting the region-Mura defects. However, it is very computationally intensive because the background surface must be estimated recursively by eliminating one pixel at a time throughout the entire inspection image [265]. Chen and Chang in [239] used the same approach as the previous study; however, the order of the polynomials used in the regression process was specified. The detection rate of Mura defects achieved in this study was over 90.9% and the number of defects and the achieved rate of defects on each panel may reach 100%. In another similar study, Fan and Chuang in [247] proposed Mura defect detection algorithm based on regression diagnostics. The sample images were converted to gray-level data, this process was accelerated by dividing the image into several sub-images. Gray-level data are then modelled using the linear regression model. Prediction error sum of squares were then estimated to filter out the Mura defects. Image morphological dilation techniques were used to identify defected neighbor pixels. Finally, the differences of all the gray-level values (including Mura and non-Mura pixels) between original and estimated images are filtered by using a threshold and SPC method to classify the defects. If the difference is greater than the threshold, then the pixel is classified as Mura pixel. This method has the advantage of performing the inspection in relatively low processing time with low false alarm rates. Despite of these advantages this method cannot detect defects with sub-pixel accuracy [315]. Ngo *et al.* in [220] performed background reconstruction to extract the features of different mura defects in TFT-LCD. Several algorithms were used for this purpose such as DCT, polynomial surface fitting and segmentation. The usage of polynomial surface fitting and DCT was according to the size of mura defect such that if the size of the mura defect is small (according to predefined threshold) compared with the image, then polynomial surface fitting is used for background reconstruction. Otherwise, DCT is used for background reconstruction. Based on the sensitivity of the human eye to Mura defect, the level for each Mura candidate is quantified using the concept of just-noticeable

difference, which is used to identify real Mura defects by grading as either pass or fail. The proposed method can be used to extract low-contrast Mura defects from nonuniform background images. However, image background approaches utilize all image data to reconstruct the image background, without considering the influence of Mura defects. Hence, the reconstruction quality of the image background is never sufficiently accurate. Therefore, these methods can effectively detect certain types of medium-sized Mura defects, but cannot address small Mura defects [243]. Authors in [276], [277] constructed AOI system to inspect the deformation of the conductive micro-spherical particles in anisotropic conductive films that contribute to the resistivity of the interconnection between substrate and chip. Handcrafted feature models were created and used for this purpose with the aid of limited number of collected samples. However, since micro-spherical may vary in shape and size, the handcrafted feature models may not be accurate method in detecting the deformations [343]. Bai *et al.* in [186] proposed corner point-based algorithm for SMT component placement and positioning. Their approach used properties of the components movement on the pick-up head to introduce two types of model key points that indicate the shape of a model component and extracted approximate corner points by using the Harris corner detection algorithm and subpixel corner points. Distance and shape feature matching methods to compute the correspondences between the generated models and the corners detected using Harris algorithm. After the corresponding point pairs have been obtained, the coarse and fine positioning problems are formulated as least squares error problems. The time needed to execute the proposed algorithm took between 13.7 – 16.8ms, depending on the component type considered. Compared with other algorithms such as HALCON and SM482, the proposed method did great job in reducing the computational time. However, the variety of SMT components and packages in the market makes the proposed method, which used two components only in their experiments, limited in application [344]. Chiu and Perng in [168] proposed area features descriptive to classify the solder joint defects (insufficient and excess solder), based on the distinctive shapes acquired for defect type as shown in Figure 39(a). In Figure 39(a) the defective features are presented by the bright pixels. Using mathematical modelling, the sample images are partitioned into four regions as shown in Figure 39(b). Rule-based classification is then applied using certain if-else statement according to the width and length of the regions. For instance, if width of region III is larger than width of region I, then insufficient solder defect is detected. The proposed method achieved a recognition rate of 95% with less computational time compared to studies that used three tiered-color illumination settings. However, only two types of solder joint defects were considered in this study.

7) PRINCIPLE COMPONENT ANALYSIS

Principle component analysis PCA is a statistical technique that is used for extracting information from multi-variety

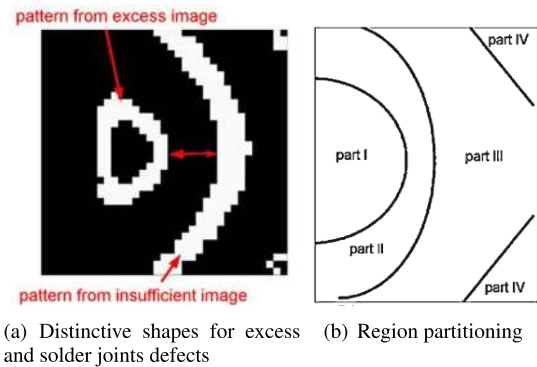


FIGURE 39. Method proposed in [168] to highlight defect features of solder joints.

dataset [345]. It was first proposed in 1933 by Hotelling to solve the problem of decorrelating the statistical dependency between variables in multivariate statistical data derived from exam scores. PCA reduces the dimensionality of the original data by defining a set of new variables, the principal components (PCs), which explain the maximum amount of variability in the data [346]. There are multiple methods to achieve the ideal number of PCs such as, broken-stick model, Velicier's partial correlation procedure, cross-validation, Bartlett's test for equality of Eigenvalues, Kaiser's criterion, Cattell's screen-test, and cumulative percentage of variance. In terms of image data, PCA is used to find useful image representation by finding a "better" set of basis images so that in this new basis, the image coordinates (PCs) are uncorrelated, i.e., they cannot be linearly predicted from each other [347]. This is very useful in feature selection process and for reducing the computational time of the algorithm. However, due to the linear nature of PCA, the performance is sometimes limited [269]. Therefore, most researchers have used modified versions of PCA algorithm. Li *et al.* in [282] used PCA with the aid of thresholding and morphological operations to highlight five types of defects in mobile cover glass. The morphological operations using thresholding and blob analysis is important step for detection of connected components which represent defective regions. Where each blob is assigned a unique label to separate it from other blobs. In this study PCA were used for dimensionality reduction and to aid in classification process. In a process similar to template matching, template set of labelled defective and non-defective images were considered and the eigenvectors of those templates were compared to the eigenvectors of sample images for inspecting. According to this comparison the defects is classified to the certain defect type (class). The proposed method achieved a considerably low false alarm rate of 6%. However, the extracted features are too primitive and the measured accuracy cannot satisfy the requirement of practical applications [285]. Chen and Perng in [235] investigated textured surface defects of OLEDs and PLEDs using PCA analysis. The gray-level image in this study is divided into an ensemble of horizontal scan lines (row vectors). The input

spatial domain image is then transformed into principal component space so that the directional textures are well approximated by first major components and their corresponding weight vectors (named truncated component solution (TCS)). TCS are determined by first normalising eigenvalues of each image and then retain only those components whose normalized eigenvalue are greater than one. Subtraction process were then applied between TCS and original image to reveal the defective features and blur all directional textures. Finally, thresholding with the aid of SPC chart were applied to classify the defects. The proposed has major advantages of being insensitive to horizontal and vertical shifting, changes in illumination, and image rotation. However, the method proposed in this study is not suitable to deal with high resolution image because the inherent complexity of PCA [348]. Furthermore, it is not suitable for detecting relatively large defects since large defects seriously destroy the regularity of texture. Tsai *et al.* in [267] proposed PCA-based method called *Integral Image* for defect detection in non-textured and homogeneously textured images such as LCD panel backlight and solar wafers. Compared to conventional PCA, this method can increase the computation speed of eigenvalues. The method consists of a small neighborhood window that slides over the inspected image and for each window the regularity measure is then derived from the PCA. Two main parameters were used in the algorithm that plays vital role in the detection performance; control constant K which defines threshold value for detection, and sliding window size for the sample image. Since this paper deals with many surface defects (e.g. solar wafers and backlight), the value of optimal K may vary according to the application; however, a value of 3 has been demonstrated to perform well in most applications. A proper value of the window size has major role in determining how accurate and efficient the algorithm is. A small window size such as 25×25 or less detects only partial defects or defect edges. Conversely, an excessively large window size with respect to the defect size may smooth the detected region and omit subtle defects or small-sized defects. Therefore, in this study window sizes between 31×31 and 61×61 can well detect the presence of defects for most of the defects considered. Compared with other method such as Fourier transform, this method is considered relatively fast as it needs only 0.032 s to process sample image compared with 0.172 s in Fourier transform. Zervakis *et al.* in [182] performed post-placement inspection of SMD on PCBs. The developed approach involves the indirect measurement of each lead displacement with respect to its ideal position, centralized on its pad region. This displacement is inferred from area measurements on the image data of the lead region through a classification process. Sample images of the proposed approach were a mixture of acquired images via hardware optical inspection setup (CCD and illumination devices) and Monte-Carlo simulated images. After defining the ROIs and performing geometrical transformation, a four-level Otsu thresholding is applied on each ROI, to segment the lead images that are included in the examined ROI image.

This process will aid to extract twelve features for the lead region that represent area and geometrical measurements of the regions. To reduce the dimension of the feature vector that contains the twelve features, Karhunen-Loeve transformation (similar to PCA) is used for this purpose. The reduced features were finally sent to classification algorithm. Goumas *et al.* in [183] proposed a similar approach that further improves the positioning measurements of individual leads by means of information fusion and multiple classification. In this study, three sets of features are extracted from each segmented lead image, which represent different characteristics. The first set represents optical characteristics by means of simple area measures that sustain the most desirable image attributes. The second set reflects only the edge information, whereas the third set pertains to features derived from the one-dimensional projection profile of the lead image in one direction. Liu *et al.* in [269] proposed a nonlinear version of PCA, called kernel PCA (KPCA) to investigate defects during GE stage in TFT-LCD manufacturing. KPCA can capture the nonlinear relationships between pixels, extract more discriminating features, and reduce the dimensionality of the input image. KPCA has shown to have better performance than PCA in terms of feature extraction in other applications such as in face recognition [349]. In this study, segmentation and KPCA were used to highlight the defective areas in the pixel region of GE pattern. The feature vector was then sent to an input to a classifier to further identify the category of the highlighted defect. Despite of overcoming the PCA main disadvantage due to linear behaviour, KPCA is considered computationally expensive since the kernel matrix needs to be stored after the training, and as a test datum arrives, a large number of dot-product calculations is needed to obtain the projection of the test datum [268]. Liu *et al.* in [268] proposed a powerful non-linearity dimensionality reduction technique called locally linear embedding (LLE) to deal with the large-input-dimensionality in the image dataset of GE defects in TFT-LCD. After performing the segmentation process to locate the defective regions in the image samples, LLE can map the high-dimensional input data into a single low-dimensional embedding coordinate system by manifold learning. By LLE, the input dimensionality of the classifier can be reduced substantially, therefore reducing the complexity of the classifier. This method overcomes similar non-linear dimensionality methods such as KPCA in terms of the reduced computational time. Cai *et al.* in [174] proposed a modified PCA technique to inspect IC solder joint defects called Robust Principle Component Analysis (RPCA). Their procedure starts by decomposing a set of qualified IC joints images and tested samples of IC solder joints images into low-rank component and an error component using RPCA. Hence, the data used for RPCA is acquired from hue channel of the image, since hue channel contains major information for color. Then, a defect score (threshold) is defined based on the appearance model and used to evaluate the quality of IC solder joints. Location prior knowledge is also used to enhance the defect score selection. Their proposed

method showed similar results to ViBE algorithm (proposed by the same authors in [173]) in the case of inspecting qualified ICs. However, in the case of unqualified IC inspection the proposed method outperformed ViBE algorithm. Despite of the previous observations, the proposed study faced some limitations such high computational time which can be partially solved by employing hardware acceleration and parallel computing. Moreover, their approach classified solder joints defects as qualified and unqualified without using classification approach to specify the type of defect. Lai *et al.* in [224] used RPCA algorithm as well for detecting aesthetic polarizer defects with the aid of structured illumination. Their algorithm achieved up to 99% detection rate. The algorithm was also capable of detecting other type of defect that were not intended to be detected such as dust, stains, and scratches. Despite of RPCA's robust behaviour to outliers [350], RPCA is considered a very complicated mathematical model. According to Cai *et al.* in [175], there is no report of using RPCA in real industrial applications.

Cen *et al.* in [254] used low-rank matrix reconstruction technique, which is considered a similar method to RPCA, along with segmentation to highlight surface defect features in TFT-LCD panel. In this algorithm, the textured background of the sample image is considered the low-rank matrix, while the foreground image with defect can be treated as sparse matrix. The defective region in this study is considered tiny compared with the whole image. However, if the defected region is relatively large, this may be reflected to the background features and will affect the background reconstruction method [351]. Furthermore, this method can only solve LCD images with simple background [352].

Similar to PCA, Singular Value Decomposition (SVD) is another linear method used to extract the significant feature components of the image, which can be also used to calculate PCs. This applies by considering the image as a matrix so that eigenvectors of an image matrix (eigen-images) can be obtained. Eigen-images are then used to calculate singular values (which represent feature data of the image). Only the relevant parts of the singular values need to be retained as the compressed data for reconstructing the original images. The local, detailed information can be truncated to eliminate the redundancy of image compression [258]. Lu and Tsai in [257], [258] investigated micro-defects such as pin-hole, scratches, particles and fingerprints in TFT-LCD using SVD. The singular values which represent the background were selected. The image was then reconstructed without the selected singular values in order to eliminate the effect of the background and highlight the defective regions (anomalies) in the foreground. SPC were used to set up the control limits for distinguishing defects from the uniform region. This method is suitable for detecting defects of highly periodic textured surfaces; however, the variety of LCD manufacturing processes and the higher image resolutions of LCD products often lead to less periodical, more complicated textural structures in sensed images [245]. Furthermore, the proposed method is highly sensitive to texture direction and face

difficulties in separating faint and large defects such as Mura from the texture background [242], [286]. Kim *et al.* in [99] used Regularized Singular Value Decomposition (RSVD) method, which is based on SVD, as a feature extraction approach to extract failure patterns of DRAM WBM. The benefit of the proposed RSVD is to obtain binary eigen-images from a binary matrix of WBM. Each resulted eigen-image represents different defect pattern of the failed chips of WBM, thus the matrix norm of the eigen-image is equivalent to the contribution that the failure patterns of each eigen-image make to WBM. Finally, the detected patterns are classified using K-means clustering to specify the defect type.

Another technique which is considered a generalization of PCA called Independent Component Analysis (ICA) is considered in literature. ICA is a method of extraction of statistically independent signals (called sources) from observed linear mixtures, to generate simultaneously observed sequences of data (de-mixing matrix) without any prior knowledge of the mixing mechanisms. This method is widely used in dealing with medical signals and telecommunication [246], [353]. Tsai *et al.* in [265] investigated backlight module and glass substrate small defects in low-contrast uniform surface images. For this purpose, they proposed a constrained ICA model with the aid of PSO algorithm to design an optimal filter with the objective that the convolution filter will generate the most representative source intensity of the background surface without noise. Therefore, by sliding the filter in the inspection image, all pixels in non-defected regions will have approximately the same impulse responses, while the pixels in defective regions have distinct responses in the filtered image. Certain control limits were used to classify the defective regions from the non-defected ones. Experimental results from the backlight panels and LCD glass substrates have shown that the proposed ICA-based filtering scheme can effectively detect various small defects in low-contrast surface images. However, the convolution filtering scheme cannot work effectively for the detection of large-sized defects such as gravity-Mura since the defective region is too large to be confined in a limited filter window, and sliding a very large filter window pixel by pixel in the image is computationally expensive [246]. Tsai and Lai in [354] used ICA to highlight defected features in periodic complex patterns such as TFT-LCD panels and color filter. In this study, the sample images were scanned top-down direction by horizontal scanning and was transformed into 1D image. The resulting 1D image was then divided into two segments of equal length. ICA were then applied and de-mixing matrix of size 2×2 were obtained with the aid of probability density function (PDF) and PSO algorithm to recover the translation between the two divided segments. Finally, NCC template matching were applied to compare between the divided segments and detect defects incase an abnormality was detected. Due to the small size of the de-mixing matrix used, this method is considered computationally efficient, which makes on-line, real-time implementation of the proposed method for

defect detection in a manufacturing process become possible. A similar study were conducted by Lu and Tsai in [355] to detect micro-defects in periodic surfaces such as TFT-LCD panel and can also be implemented on the color filter defects as in the previous study. An enhanced ICA algorithm was also used in this study which was called *FastICA*. As in the previous study, each 1D image segment that has no defects is trained by the *FastICA* algorithm to obtain a de-mixing matrix and independent components. The independent components which show spiky profiles represent an edge of a pattern. These components are sorted and preserved because they are regarded as representing global pattern structures. The de-mixing matrix is regenerated according to the corresponding independent components and applied to a new test image to determine any anomalies in the background pattern. This method has the advantage of being able to detect defects by training one segmented image and it does not use template matching techniques as in the previous study which saves computational time. However, both studies have two common drawbacks which are the loss of the size and shape information, and sensitivity to the vertical shift [234]. Tseng and Tsai in [246] used a modified version ICA to highlight low-contrast Mura defects in LCDs. In this study the image to be inspected is assumed to be a linear mixture of the representative basis images. The basis images which have the full size of the LCD image are given by the product of a transformation matrix and a training data matrix that contains defect-free images as the row vectors. PSO is then applied to find the transformation matrix under the objective that the basis images are both statistically independent and spatially exclusive. To classify defected and non-defected samples, a control limit where established according to distance measurement such that if the measurements exceeds this limit the sample is considered defective. Experimental results have shown that the proposed method can effectively detect both small-sized, low-contrast defects such as spot-Mura and line-Mura, and large-sized defects without clear edges such as the hardly detectable gravity-Mura. However, the proposed method can only detect the presence of Mura defects in an image. It cannot be directly used to identify the actual location and shape of a Mura defect.

C. CLASSIFICATION

Classification is considered the last stage of the inspection algorithm. In this stage the inspection algorithm uses the extracted features as an input in order to produce a an output of categorized classes. In terms of the nature of the output, classification can be subdivided into binary classification and multi-class classification. In binary classification, the outputs are categorized into two groups (e.g. pass/fail, defect/non-defect). In multi-class classification, the outputs are categorized into more than two groups. Classification can be also subdivided according to the algorithm used in this process into rule-based classification and learning-based classification (machine learning).

1) RULE-BASED CLASSIFICATION

As a simple and easy way to classify defective and non-defective products, a lot of researchers used simple logic classifiers such as conditional statement (if-else) and Boolean rules. Hence, these statements are considered pre-programmed and has no ability to learn as the case in machine learning tools that are discussed in section V-C2. These classifiers are usually used after implementing a relevant image processing technique to highlight the features for analysis, therefore the accuracy of them is highly dependent on the image processing tool for feature extraction. A certain threshold is then used for the assessment process. For instance, in template matching this threshold is called the matching score. On the other hand, if thresholding and segmentation techniques were used, then the threshold could be the number of bright pixels. Human assessor can define a threshold value for the previous thresholds such that if the obtained value exceeds threshold value, an action must be made (e.g. consider the sample defective).

Shankar and Zhong in [122] set up a series of five logic rules based on the energy features of the sample images to classify the wafer defects. Such that, if the energy features of error image exceeds $1\mu\text{m}$, this means the sample image suggests a defect (rule 1). Further on, if the energy features of the chip-out region is greater than energy features of scratch, bridging, and metal lifting then the defect is caused by chip-out (rule 2) and so until all the investigated defects are classified. The previous study suggested a simple and less computational time consuming algorithm. However, there was no discussion about the accuracy rate of the classification. Yeh *et al.* in [128] classified semiconductor wafer dies defects such as particle contamination and scratch based on conditional logic algorithm. The features are extracted using a recent approach called wavelet transform modulus sum (WTMS). A golden sub-image (which represent a defect free sample) were also used for comparison with sample images. The WTMS approach is modified in this paper to detect abnormalities in each pixel of the sample image that may indicate a possible defect. Various coefficients are investigated (e.g. vertical wavelet coefficient and horizontal wavelet coefficient), were these coefficients are called "wavelet energy". The investigated object (wafer) preserve more energy than background does. Furthermore, pixels on corners clustering noisy spots or irregular edges maintain much more wavelet energy than pixels on small portions of an object do. A ratio between a pixel and its neighbor can describe the status of this pixel. The ratio is treated as threshold, such that if it is more than or equal to zero, the pixel is considered as a defect otherwise the sample goes to another check which compares the sample pixel with the golden sample pixel to see if they belong to the same coordinate. If the comparison failed to show that they belong to the same coordinate, the pixel is considered a defect, otherwise it will be considered as defect-free. Lim and Jeong in [261] proposed a rule-based inspection algorithm to classify fatal and non-fatal glass substrate defects in TFT-LCD. The rules and thresholds considered

are based on the information of defect position, size, and gray-level. Despite of the low false alarm rate achieved in this study; the overall accuracy is relatively low compared with other studies. In Ye *et al.* [176], after using the adaptive template method, they used a conditional statement using a threshold to identify whether a pixel in the difference image is a potential solder joint defect pixel or not. The threshold R is defined based on the hue channel difference between the template and sample image from the dictionary. Where R is an empirical threshold in the context, which is not sensitive to the inspection performance. Cai *et al.* in [173] classified the hue channel value of an input pixel (sample) into qualified or unqualified one by comparing it with the templates. If the pixels of the samples are in the range of hue channel in any of the defined templates, the sample is considered qualified and vice versa. The threshold that is used for classifying the defects is called defect degree.

Fuzzy Logic which is a form of multi-valued logic was also one of the classification techniques used in literature. Fuzzy logic is capable in handling the problem of blurred uncertainty phenomenon that cannot be described by binary logic (0s and 1s). Therefore, an appropriate value is taken between 0 and 1 to represent the degree of one element belonging to a set (called fuzzy set). A set of rules is used to represent the fuzzy values based on if-then statements, the process of converting an input value to a fuzzy value is called fuzzification and is used in fuzzy logic controllers. Lin in [83] noticed the fuzziness of WBM patterns classification, as not all maps should belong to one pattern only. Therefore, the study proposed new fuzzy variable of clustering pattern (FVCP) by using fuzzy logic control. Where FVCP represents a numerical value ranges from 0 to 5 according to the five patterns considered in this study. Hence, the FVCP can be a decimal number, for instance if the value of 4 represents bottom pattern and a value of 5 represents crescent moon pattern, then an FVCP of 4.7 implies that the recognized clustering pattern has 70% degree belonging to crescent moon pattern and 30% degree belonging to bottom pattern. Acciani *et al.* in [167] proposed two-level fuzzy-based classifier to classify solder joint defects. The first level contains three fuzzy blocks that take each feature of the three extracted features as an input and gives a human-friendly classes which describe the defect. For the first two blocks that have area of the solder fillet and mean gray level features as inputs, the possible defects that can be detected from these features were described in five classes as poor (insufficient solder), acceptable poor, good, acceptable excessive and excessive. While the output of third block, which has barycenter feature as an input, results in three classes: badly-centred, medium centred and centred. The second level performs the final inspection task and the outcomes of this level are similar to the first two blocks outcomes considered in level one. Compared with a previous study conducted by the same authors in [166] (that used neuro-fuzzy classifier), this method reduces computational time as well as human intervention in the feature extraction process. Furthermore, the recognition

accuracy in this study was improved compared with the previous one.

Statistical process control (SPC) charts were used as a mean to visualize features extracted statistically and to perform rule-based classification as well. The x-axis on the control chart can correspond to the location on the image and the y-axis to the frequency of analysed feature value at that location (e.g. number of pixels, intensity level etc.) [356]. Upper control limits (UCL) and lower control limits (LCL) are established on the y-axis to aid the classification process, such that if the feature value exceeds the limit an action must be taken (e.g. consider a defect is detected). Many factors contribute to the quality of this method such as the window size considered on the x-axis and the range between UCL and LCL [357]. Despite of this method simplicity, it is necessary to manually determine if there is any abnormality in the control charts and what kind of abnormality occurs. Furthermore, it is easy to detect abnormalities beyond the control limit, but difficult to do so within the control limit, which is easily affected by the experience level of quality control personnel [358].

2) MACHINE LEARNING CLASSIFIERS

Unlike rule-based classification approaches mentioned in the previous section, machine learning provides the ability of the algorithm to learn the correlation between inputs and outputs which can be used to perform certain classification and regression tasks. In manufacturing and optical inspection applications, supervised machine learning techniques are mostly applied among the other categories [359]. Multi-layer perceptron (MLP), convolutional neural network (CNN), support vector machines (SVM), decision trees and k -nearest neighbor (k -NN) are all examples of supervised learning algorithms. Unsupervised learning involves the process of developing a model or function without predefining the outputs. This method is typically used for finding meaningful patterns (e.g. WBM defect patterns) or classifications within a large data set [360]. Clustering, adaptive resonance theory network (ART), Hopfield neural network (HNN), Cellular Neural Network, and self-organizing map (SOM) are all examples of unsupervised learning algorithms.

Machine learning is considered very powerful tool in classifying the defects detected by the image data. However, there are two major problems that must be considered before applying machine learning algorithms to avoid classification errors. These two problems are overfitting and data imbalance. Unfortunately, these problems are very common in defect inspection using machine learning techniques. Overfitting occurs when the classification performance is highly dependent on the training data. Overfitting problems appear when few samples are used for the training process, and it could be a challenge for industries that do not have enough image samples for the defects so they can train their machine learning algorithm. The lack of training data problem can be solved by generating more datasets using several techniques such as bootstrapping and Generative Adversarial

Network (GAN). Furthermore, regularization techniques such as L2 regularization and dropout are widely used among neural networks and deep learning models to avoid overfitting. On the other hand, data imbalance occurs when the training data for certain classes are more than others. This is very common in optical inspection problems when certain defects occur more than others in the data provided. Data imbalance problem will make the classifier more biased by the data of the dominant class, which in return affect the quality of the classification. One way to solve the data imbalance problem is to create or modify the algorithm to include a cost-sensitive method. The other way is using data preprocessing techniques such as sampling, in which either new samples are added, or existing samples are removed from the original data. The process of removing samples is known as under-sampling and the process of adding new samples is known as over-sampling [263]. Hence, GAN and Bootstrapping can be used to solve the data imbalance problem as well.

a: NEAREST NEIGHBOR CLASSIFIER

Nearest neighbor algorithm also known as k -nearest neighbor (k -NN) is a supervised machine learning algorithm, which can be used for both classification and regression. In this algorithm a k value must be selected, which represent the k nearest data points (whose classes are already known) in the feature space that are closest to the target point to be classified. For instance, if we want to classify an unknown point (?) according to the two classes \triangle and \square as illustrated in the feature space of Figure 40. If k is selected to be 1, the output of the unknown data sample will be simply assigned to the class of its nearest neighbor (in this case \triangle). While if k is selected to be 3 the data sample will be labelled according to the dominant class in the range of 3 nearest neighbors (in this example it will be \square). Generally speaking, the output value for the predicted data sample is usually determined by estimating the mean value of its k nearest neighbors [361]. Several advantages can be observed in using this classifier of such as the ability to train large dataset with relatively short time and the fact that information present in the training instances is never lost (because the instances themselves are stored explicitly). However, many disadvantages can be found in this classifier as well, such as the cost of classifying new targets can be high. This is because nearly all the computation takes place at classification time rather than when the training process. A second disadvantage is that all the training set are considered in the attempt of the classification process instead of considering the relevant ones only, which require large memory capabilities. Finally, this classifier is highly biased by the value of k selected [362], [363]. k -NN algorithm was not widely used in the research articles reviewed in this paper. However, some articles such as in [12], [73], [91], [116], [143], [153], [154], [171], [297] used k -NN to compare its performance with the main classification algorithms they used in their studies. Furthermore, [178] used nearest neighbor algorithm mainly to classify solder paste defects in PCBs based on the data provided by the BICF model.

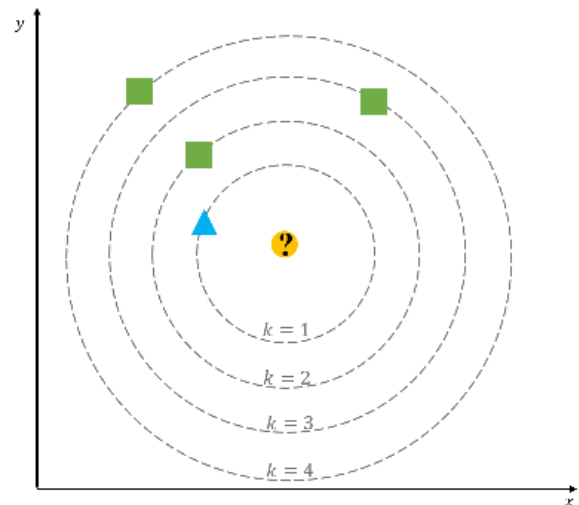


FIGURE 40. Illustration of k -NN algorithm.

The proposed approach has achieved a recognition rate of 97.5%. However, this method cannot analyse the details of the defects effectively and considered computationally expensive [139].

b: BAYESIAN CLASSIFIER

Naïve-Bayes classifier (simplified as Bayes or Bayesian classifier) is one of the simple machine learning algorithms that is based on Naïve-Bayes theory as in equation 3

$$P(A|B) = \frac{P(B|A) \cdot P(A)}{P(B)} \quad (3)$$

where the probability of A can be obtained given that B has occurred. In machine learning terms, B is the evidence and A is the hypothesis. The assumption made for the algorithm is that features are independent, in which the presence of one feature does not affect the other. As the case in k -NN, Bayesian classifier has limited usage among the reviewed articles in this paper. Studies such as in [53], [101], [153], [175], [196] compared Bayesian classifier to the main algorithms they used in classification. Wu *et al.* in [171] used Bayes classifier as binary first-stage classification approach to filter the defected and non-defected PCB samples before sending the non-defected results to an SVM multi-class classifier to specify the type of defect. Yuan *et al.* in [80] used Bayes classifier as second stage classification after using Support Vector Clustering (SVC) to locate random and systematic defects in WMs. Zervakis *et al.* in [182] performed post-placement inspection of SMD on PCBs. After receiving the reduced feature vector using PCA approach, the feature vector is fed to Bayesian classifier which produces a classification of the lead shift to several classes. The performance of the Bayesian classifier was compared with LVQ network and experimental results have shown that Bayes classifier without PCA derive the best estimates, in terms of their proximity to the actual values. However, in terms of time

requirements, LVQ classifier performed less time compared with the Bayesian one. Unfortunately, the accuracy rates for the classifiers were not mentioned in this study.

c: DECISION TREE CLASSIFIER

As its name indicates, a decision tree is a decision support tool that uses a tree-like graph or model to describe relationships among different variables and makes decisions [361]. Decision trees are considered one of the supervised learning classifiers. They share some similarities with rule-based classification; however, they have the ability to learn by setting cost-function-like measures such as information gain and Gini impurity. Jiang *et al.* in [154] used decision tree classifier to classify four types of golden finger defects in PCB. The samples used in this study were generated using bootstrap sampling techniques to overcome the lack of samples problem and minimize overfitting. The features extracted from these samples were then fed to the decision tree classifier for classification. Experimental results have shown that decision tree classifier was capable of classifying bootstrapped sampling accurately with a recognition accuracy of 97.87%. Moreover, it outperformed other classifiers such as minimum distance and nearest neighbor classifiers. However, it has been observed that decision tree classifier has a difficulty in selecting the range for each defect type for each feature. Thus, the tree classifier cannot be easily extended to different cases in manufacturing. A preliminary analysis must be made for the determination of each class range. In a similar study, Jiang *et al.* in [153] combined decision tree with logistic regression to classify four gold fingers defects in PCBs. Color features of each defective region are represented by the RGB values of all pixels and used as inputs for the logistic regression tree classifier. Compared with other classifiers such as k -NN, Bayesian and minimum distance classifiers, the proposed regression tree classifier outperformed them all with an accuracy of 89.33%. However, once the number of defect types become large with many overlapped data points, where to start and where to continue becomes an issue. Furthermore, this study did not consider the seriousness of the defects and multiple defects on one golden finger. Wang *et al.* in [67] proposed hybrid algorithms that integrates fuzzy c -means clustering scheme with hierarchical linkage to cluster defect patterns and produce a feature vector that contain convexity and eigenvalue ratio as feature values. The feature vector was fed to a decision tree classifier that is used to classify the detected patterns. However, the proposed scheme was not robust to some dataset [70]. A similar approach was also conducted by Wang in [68]. Xie *et al.* in [159] used the optimal feature data set, that is selected using Adaboost algorithm, as an input to classification and regression tree (CART) classifier to classify the solder joint and IC chip defects in PCB. The classifier was used on each sub-region of the thirteen sub-regions selected. The two-class classification problem can be converted into multi-classification by increasing the number of nodes in the tree such that all the defects are classified to the correct class. This study achieved a total

recognition rate of 97.2%. The main advantage of this method is the ability of reducing the feature selected using Adaboost algorithm and choosing simple classification criteria using CART. Chen *et al.* in [294] also used CART to investigate six major defects in color filter and micro-lens of CMOS. Several features extraction techniques such as thresholding and Canny edge detection were used to extract ten color, shape, and statistical features. In order to generalize their study to detect different defect types, the minor defects were filtered out using similarity matching approach, such that if an image cannot meet the similarity criteria for each feature, this study classified it to another category. CART classifier was then used to deal with the six major defects after excluding other defects. Despite of achieving an overall accuracy of 94% and relatively low false alarm rate of 5%; however, some defects such as black spots halo were detected with low accuracy. Furthermore, the false alarm rates for black spots halo, bubble and other defects were very high. A similar study was conducted by the same authors in order to investigate similar CMOS defects as well in [295]. This study was intended to reduce the false alarm rates and increase accuracy using data from a CMOS manufacturer in Taiwan. The classifier of this study was chosen to be SVM classifier without noticeable modifications to the feature extraction techniques. Compared with the previous study this study showed remarkable improvement in increasing the accuracy and reducing the false alarm rates of classification.

C4.5 (which is one of the modified decision tree algorithm) has achieved best accuracy classification results compared to others for actual manufacturing data sets of WM pattern defects in the study conducted by Chang *et al.* in [59]. In this study the training process for the classifiers used artificially generated defect data along with actual manufacturing data. In this study, circular Hough transforms, linear Hough transforms and zone ratio were used to identify bull's eye, line, and ring patterns respectively. Logitboost has achieved the best classification accuracy in terms to the artificial manufacturing data. Even though that this study achieved a considerably accurate classification results; however, if two or more defect clusters partially overlap, the proposed method was unable to classify them accurately.

Ooi *et al.* in [53] investigated WM pattern defects using a modified decision tree called "alternating decision tree" (ADTree) to overcome the main disadvantage of conventional decision tree algorithm which is empty or null-leaf phenomena. This phenomena occurs when there is a valid path with no corresponding learning example, which results in an unclassified instance. ADTree is considered a combination of boosting algorithm and decision tree which generates classification rule that are relatively simpler and easier [364]. The boosting process combined with decision tree involves training the weak classifiers of the decision tree, which are reweighted according to the mistakes occurred in the classifier. In their approach, they have considered that the dies in the wafer tend to have circular shape rather than square, therefore they have used rotational moment invariants (RMI)

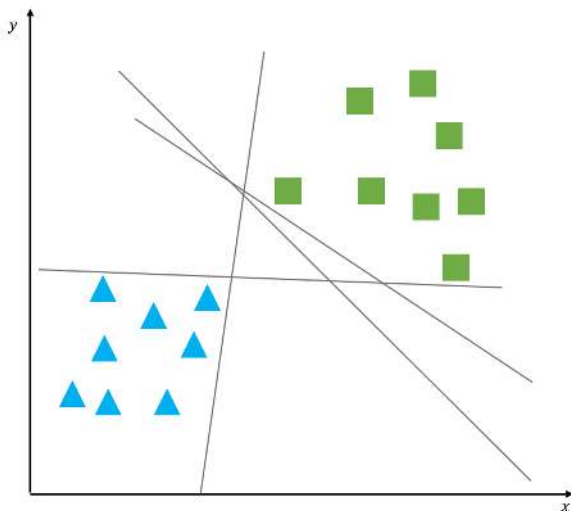
method for feature extraction to feed the ADTree. They have achieved classification accuracy of 95%. Even though that their system was trained to recognize a limited set of defects including bull's eye, blob, line, edge, ring and hat. However, the system could be trained to recognize new defect types by specifying their geometry and simulating it. Piao *et al.* in [90] proposed a decision tree ensemble-based WM failure pattern recognition method based on the radon transform features. The radon transform is the projection of image angle and were used for feature extraction. Four features were extracted; max, min, average and standard deviation of projections from the radon transform and used to build the decision tree ensemble. The classifier has the ability to classify the defect according to eight failure patterns. Even though the accuracy of the classifier achieved relatively good results for all the selected patterns (90.5%); however, the proposed method failed to efficiently recognize several pattern types, which may indicate that using the four previously mentioned features of projections are not enough to present the geometric and spatial information of defects in WM. Kim *et al.* in [101] proposed a generalized decision tree classifier to classify dynamic-random access memory (DRAM) semiconductor wafer based on WM. The WM they used shows the severity of defected chips on the wafer according to color code, then the WM is binarized to form WBM. The uncertain features of the WBM is then classified according to the generalized decision tree approach according to shape patterns and location of defects. Based on their proposed algorithm, they achieved an average accuracy of 95.6%. Despite of the good results, their study considered only four patterns, rather than considering all possible patterns. Furthermore, the defect size of the pattern was not an important factor in this study.

Another classification technique that is based on decision tree called *Random Forest* is also used in literature for defects classification tasks. A random forest is a set of the multiple decision trees generated by bootstrap sampling, which can be trained by bootstrap aggregation (bagging) and feature bagging processes. The bagging causes each tree to be trained with a part of the dataset randomly selected from the whole training dataset. The bagging process has the effect of allowing the system to avoid redundant tree training by decreasing the correlation between the trained trees. The feature bagging process is used to randomly select some parts among the input features in every tree node split to avoid the repeated effects and correlation that come from features having strong influence on the response variable during the training. A random forest shows different performances along the way according to how the features are quantified [234]. Park and Kweon in [234] utilized RF algorithm to classify different defect types of AMOLED. The input for the proposed classifier were acquired from the features set obtained from GLCM and NDF filtering processes. The classification accuracy for this method ranged from 87% to 98% depending on the defect type. However, their inspection speed could be affected since four optical inspection systems were considered to acquire the images instead of one. In the study conducted

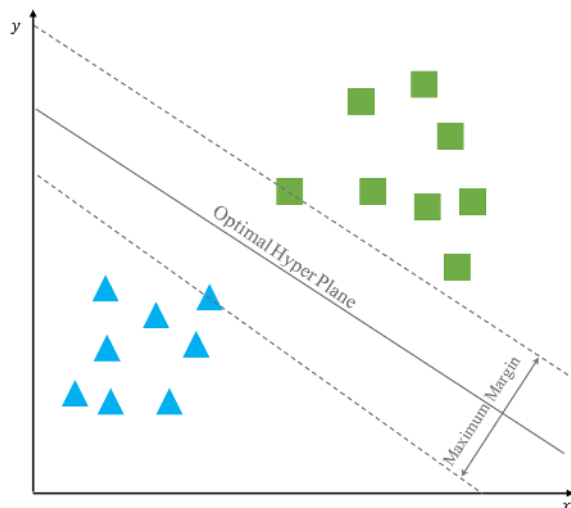
by Kang *et al.* in [97], random forest was used for wafer dies' defect prediction before the assembly process takes place. Four feature variables were studied to make the predictions which are: distance of the die from the wafer center, previous final yield at the die position, wafer test fail rate for the adjacent dies, and abnormalities of the WM pattern. Their approach is promising in that accurate prediction of die fails in the final test enables the yield to be managed more effectively. The final test can be skipped for dies that will almost certainly pass or fail, which leads to significant saving in time and cost. However, some limitations were found in this study such that some variables from the four considered showed low importance in the prediction process, which makes the algorithm to spend extra time cost without effective results. Furthermore, the wafer fabrication data were not available in this study in spite of their importance. Random forest's performance can be severely affected when imbalanced dataset are being used, therefore, in the study conducted by Yuk *et al.* in [195] to classify PCB defects, random forest was used as intermediate classification process to predict the probability for the input features to be classified as a defect rather than giving the final decision for classification. Weighted kernel density estimation (WKDE) map was used to aid the random forest after calculating the probability. KDE is a probability density estimation method using a kernel function. In addition, it is a nonparametric method that is even applicable to high-dimensional data. A binary classification was applied based on a single continuous WKDE value to examine whether a feature is a fault. The features were classified by comparing the WKDE value with a threshold (called the cut-off value). A feature was classified as a fault if the WKDE function exceeds the cut-off value and was classified as normal otherwise. Despite of achieving relatively good classification accuracy ($\approx 91\%$), ten samples were only used for the training process which may lead to overfitting. Moreover, further work needs to be conducted to redefine the fault type when it is not specified, and an appropriate detection method for each type of defect should be studied.

d: SUPPORT VECTOR MACHINE

Support Vector Machines (SVMs) are a family of supervised machine learning algorithms used for binary classification problems [365]; however, it can be modified for multi-class classification [366]. Its objective to find a hyperplane (also known as kernel function) in two or higher dimensional problems to separate the two classes as shown in Figure 41(a). If the two classes are non-separable, we can still look for the hyperplane that maximize the margin between the classes such that the misclassification error can be minimized as shown in Figure 41(b) [367]. SVMs have been found to be an excellent tool in terms of the computational time requirement, high classification accuracy and stability. A key feature of SVMs classification method is its ability to use high-dimensional data without the need of feature selection step to reduce the dimensionality of the data [368]. However,



(a) Hyperplanes that separate the two classes



(b) Region partitioning

FIGURE 41. Optimal hyperplane that separates the two classes.

SVM classifier is not very effective against data imbalance problem because the error penalties for positive and negative classes are the same. This will make the optimal separating hyperplane move toward the smaller class. In other words, if the positive class is smaller than the negative class, then the hyperplane will move toward the positive class, which will further result in numerous false negative errors [269]. Kuo *et al.* in [46] investigated two types of defects in the light area and three types of defects in the electrode area of LED chip using several SVM-based algorithms. Since SVM is optimized for binary classification, a standalone SVM algorithm were used to classify light area defects into two defect classes: breakdown and color aberration. However, to investigate the three defects in electrode area, a multi-class classification scheme must be applied. Therefore, a combination of decision tree and SVM algorithms called DTSVM were used for the multi-classification task. Baly and Hajj in [116]

suggested SVM classifier due to its ability for efficient classification of multi-modal, multivariate, and inseparable wafer data points. Their proposed model applied multidimensional hyperplanes for separating and classifying wafer data into high-yield and low-yield classes. They evaluated the accuracy of their model along with other models such as partial least squares (PLS), General Regression Network (GRN), C4.5 and k -NN. The results of their experiments illustrate that the SVM model outperforms all other models in term of classification accuracy. However, their classification approach classified wafer defects as good or bad without specifying the cause of defect. After generating WMs using morphological operation (based real defective wafers data), Liao *et al.* in [95] used SVM classifier to specify the type of the defect according to the pattern generated. The experimental results showed that the proposed method achieved an overall catching rate of 95% with only 5% false-alarm rate. However, this study faced difficulties in detecting some patterns such as donut and repeated scratches, such that low catching rates of 72% and 73% were achieved respectively for detecting these patterns. Kuo *et al.* in [296] used an algorithm called Retinex for brightness correction and to identify the small-scale features in micro multi-layer non-spherical lens module of CMOS. This algorithm has color constancy as it has good treatment effect on the influence of illumination. For this particular application, Retinex can correct the halo formation resulted from the light into multilayer lens module. Thresholding and segmentation techniques were then used to extract four features values which are area, aspect ratio, average gray level and gray level difference. These feature values were then used an input to multi-class SVM classifier to decide the defect type. Despite of achieving a relatively high inspection accuracy of 95.83%, their proposed method took 15s to inspect single image, which is considered a very long computational time. Chang *et al.* in [297] have also used SVM classifier to classify defects in camera lens module after acquiring a feature vector containing five features that represent the defects. The feature vector was used as an input to the SVM classifier to detect six types of defects. Despite of achieving high accuracy rate of 93.44%, some defects could not be detected because of their narrow area and low-intensity contrast. Chao and Tong in [84] used multi-class SVM to classify five wafer defect patterns. The intensity of the defects was extracted using four feature vectors that were called cluster index, angle variation, distance variation and average number of defects per unit area. These parameters were used as input for the multi-class SVM algorithm. The classification results for wafer defect pattern recognition showed that the proposed multi-class SVM achieved a more accurate recognition rate than the radial-basis function (RBF) model. Xie *et al.* in [96] proposed an SVM approach as well to detect four wafer defect patterns. They showed that their proposed method is rotation invariant and can work correctly in noisy images with the variations of defect locations and angle. However, this method directly generated the probability of failure according to physical locations and did not explicitly separate clustered

defects and random defects [369]. Li and Huang in [75] proposed a hybrid approach combining the supervised SVM classifier with the unsupervised SOM clustering for binary bin defect pattern classification. The feature extracted from the GLCM and moment invariant steps were used as inputs of the SOM model. Seven and fourteen classes were tested to be the output for the SOM model respectively, which represent the defect patterns of the WBM. The fourteen-classes model has the advantage of providing more detailed information to the process engineer for specific consideration. One-against-all approach (which allow to reduce the multiclass problem to a set of binary problems, enabling the basic SVM approach to be used) were then integrated with the SOM model for multi-class SVM classification. Their hybrid SOM-SVM approach achieved an overall accuracy of over then 90%, it also showed an outperformance when compared to other hybrid methods such as SOM-BP. Furthermore, the study showed that using hybrid SOM-SVM can reduce the computational time of using standalone SVM classifier. Wu *et al.* in [171] used two-stage classifier approach to classify five type of defects that occur in the component body and solder pad regions in PCB. Before sending the extracted features to the classifiers, the features went through feature selection process to select only the important ones for classification. Bayesian binary classifier were considered as first stage of classification to classify the sample images as defected and non-defected. For second stage classification, the non-defective results from the Bayesian classifier were fed to modified SVM model that uses one-against-one for multi-class classification. This approach achieved a 100% recognition rate, and outperformed other classifiers such as decision tree and k -NN. However, decision tree and k -NN achieved less computational time than the proposed method. Vafeiadis *et al.* in [196] considered SVM classifier in classifying glue defects in electronic components attachment process in PCBs. The pixels of ROI were used as the feature vector and PCA technique were applied for the feature reduction and selection process. The reduced features were then used as an input for the SVM classifier for detecting the defect type. Different kernels were used for the SVM classifier and were compared together such as POLY and RBF kernels. Experimental results showed that both kernels achieved similar accuracy levels. Furthermore, the performance of SVM were compared to that of decision tree naive-Bayes, logistic regression, MLP and gradient boosting (GB) classifiers, where results showed an outperformance to SVM. However, the best achieved accuracy of 81.39% is still considered low compared to other studies. Wu *et al.* in [218] integrated PSO with one class SVM classifier PSO-OCSVM to classify mirco-defects of TFT-LCD. The input of the classifier is fed by the extracted features from the Fourier, Haar and PCA approaches. The accuracy of their classification achieved were 91.7%. Song *et al.* in [139] compared between three types of algorithms SVM, MLP, and decision tree to classify ten types of solder joint and component package defects. The features to feed these algorithms were selected using genetic algorithm.

Experimental results have shown that SVM outperformed all other algorithms with 94.9% classification accuracy, followed by MLP with 94.6% and finally decision tree with 43.6% according to nine featural regions selected by the genetic algorithm. Their method has achieved a relatively short inspection time of 1.54ms. However, some limitations were observed in this study. First, the components used for defect type classification are limited to capacitor and resistor. Second, only component images obtained using RGB illumination are applicable to the defect type classification. Yousefian-Jazi *et al.* in [263] used SVM to classify surface flaws and scratches defects in TFT-LCD glass substrates. The sample data were first balanced using a technique called Synthetic Minority Over-sampling Technique (SMOTE), where in this technique the minority classes are over-sampled by creating “synthetic” instances in feature space rather than by over-sampling with a replacement. The results of the SVM classifier achieved an accuracy of 89.5% and outperformed other classifiers such as MLP and CART that were compared to. However, in the case of imbalanced data were used, MLP outperformed all the other algorithms. Despite of the good results achieved, this study only considered surface flaws and scratches defects and did not consider other common glass substrate defects such as air bubbles and particles, surface roughness, surface wrapping and surface waviness. Given the information that the constructed AOI system is capable of detecting surface waviness defects. Furthermore, SMOTE technique cannot solve the problem of the increasing number of unimportant training dataset [370]. Jian *et al.* [283] have also encountered data imbalance problem in inspecting mobile screen glass defects. For example, scratches and dirt defects appear frequently, whereas pit and edge breakage defects appear occasionally. The different probabilities cause an imbalance in the numbers of defect examples, in which scratches and dirt defects are viewed as the majority class and pit and edge breakage defects are the minority class. To tackle this problem, this study proposed a method called example contribution (ECS) to re-sample the imbalanced defect data and improve the prediction accuracy of the minority defect examples. After extracting the two features and performing ECS to resample the data, SVM classifier were used for the classification process. Since multiple defect types were considered, the binary SVM classifier were converted to a multi-classification SVM using a one-against-one strategy. The method achieved a high overall accuracy rate of 96.61%. However, the computational inspection time cannot meet the requirement of online inspection system with a total time of 4.4268 s. Furthermore, the proposed method is incapable of detecting the defect’s size [285]. Liu *et al.* in [269] encountered data imbalance problem during their study since target defects during the GE stage in TFT-LCD fabrication occurs more frequently than non-target defects. Therefore, they have proposed an algorithm called the imbalanced SVM (ISVM) that can overcome this problem, in addition to its ability of multi-class classification (using one-against-one strategy) since four type of defects were investigated in this study.

The proposed classification algorithm achieved 96% accuracy of classification. However, the proposed study only covered pixel region areas during the GE stage and did not consider other regions.

Another classification algorithm that share a lot of similarities with SVM called Support Vector Clustering (SVC). SVC acts the same as SVM classifier; however in the final step of this algorithm, the classifier tries to search for an enclosed hypersphere instead of hyperplane in the feature space to cover all data samples as tightly as possible [70]. Wang *et al.* in [70] used SVC classifier to identify and classify multiple zones, multiple scratches, multiple rings and ring-zone mixed type pattern defects in WBM. To further categorize the unclassified defect patterns from the SVC classifier, a decision tree approach where used for this purpose. SVC were also used in the study conducted by Yuan *et al.* in [80] to separate random defects from systematic defects in WMs, which improve both classification accuracy and computational accuracy for further classification of defect patterns using Bayesian classifier. Despite the good results that were achieved, the speed of the clustering significantly depends on the number of defects and the number of clusters. If a lot of clusters exist on the wafer, efficiency of the proposed algorithm may be suffered from computationally intensive simulation.

Some researchers considered one class classification technique based on Support Vector Data Description (SVDD) for classifying FPD defects. Given a target set, SVDD is to find an optimal hypersphere that can enclose all or most of the target data. The obtained hypersphere boundary is the decision boundary used to distinguish outliers from the target data [271]. A main advantage of this techniques that it can deal with the data imbalance problem as only the positive data are needed for the training process. Liu *et al.* in [268] used SVDD algorithm as a classifier for the previous advantage to deal with imbalanced image dataset of GE defects in TFT-LCD. The input for the classifier were acquired after performing data reduction using LLE algorithm. Their resulted in overall detection rate of 98%. However, when faced with some data types, SVDD would suffer from two critical problems: the overfitting problem due to outliers, and the multi-cluster distribution problem. Both problems would result in high false alarm rates [212]. Furthermore, SVDD algorithm requires long computational time, which could not meet the requirements of inline inspection system. Therefore, most similar studies that dealt with SVDD algorithm used a modified version of it to overcome the previous problems. Liu *et al.* in [212] used modified SVDD algorithm called Fuzzy-SVDD to detect GE defects during TFT-array process in LCD manufacturing. Features vectors that were extracted in the feature extraction step were sent to the proposed algorithm for generating labels for the defects. The proposed Fuzzy-SVDD has three main advantages that makes it preferable than using conventional SVDD. First, it is less sensitive to outliers and therefore the overfitting problem can be solved. Secondly, the membership values of

the target data can be assigned in a higher-dimensional feature space automatically. Lastly, the proposed method partitions the whole target set into disjoint subsets by using a partition-entropy-based kernel fuzzy c-means (KFCM) algorithm, and then one Fuzzy-SVDD member is responsible for learning a hypersphere to enclose one target subset. Thus, a Fuzzy-SVDD ensemble containing several Fuzzy-SVDD members is formed. By doing so, the multi-cluster distribution problem can be solved. Rule-based classification was then used as a final decision-making step for the labelled defects from Fuzzy-SVDD algorithm. A certain threshold were used according to the number of defective pixels detected in the labelling process to generate three classes: target defect, non-target defect and misclassification. The proposed target defect identification system reached high identification rate (up to 98.9%). The mean time between two defective images capturing is around 8s with 3s time to inspect one defective image, which in total considered a relatively long time compared with similar studies. Moreover, without the prior knowledge of the training data, it is difficult to define the fuzzy membership function [371]. Liu *et al.* in [271] proposed a modified version of SVDD called fast SVDD (F-SVDD) to detect SD operation defects during TFT array stage. Compared with traditional SVDD, F-SVDD can provide a much faster classification speed with close accuracy because its testing complexity is independent of the number of training patterns. This method achieved a detection accuracy of over 95% with a detection time of 7.8s compared with 30.17mins in traditional SVDD. Despite their remarkable achievement in reducing the detection speed, their classification algorithm was binary (defected/non-defected). They justified considering binary classification to avoid data imbalance, as some of defects occur more frequent than others and considering a multi classification scheme will affect the accuracy of the classifier because of the data imbalance. One more drawback that this study considered defects in the pixel region of SD pattern, despite of the existing of two more regions (source electrode and drain electrode). Liu *et al.* in [270] used the exact same inspection approach in the previous study as an experimental procedure to demonstrate the capability of F-SVDD. In their study they claimed that full inspection of LCDs can only be achieved using F-SVDD. Furthermore, they have verified that conventional SVDD cannot be used at all for LCD inspection purposes due to the long computational time of the method. In a similar study, Liu and Chen in [213] used another modified SVDD algorithm called quasiconformal kernel SVDD (QK-SVDD) to classify GE operation defects during TFT array stage. The QK-SVDD can significantly improve generalization performance of the traditional SVDD by introducing the quasiconformal transformation into a predefined kernel. In this study they obtained a detection accuracy of 96% with 60ms detection time. They have also showed that their algorithm's accuracy outperformed the conventional SVDD by 30%. However, the same drawbacks of the previous studies apply in this one. Sindagi *et al.* in [281] proposed

adaptive-SVDD (A-SVDD) algorithm based on SVDD to classify OLED panel defects. A-SVDD classifier aims to learn an incremental classifier based on the existing classifier using an objective function similar to SVDD and can tackle distributional change in OLED panel datasets. The feature vector obtained from modified-LBP and Local Inlier–Outlier Ratios feature extraction steps were used as an input for the classifier. The algorithm were compared to other similar techniques and showed an outperformance in terms of recognition, true positive and false alarm rates. However, compared with similar studies, the computation time of the proposed method is relatively long.

For LCD defects, Deng *et al.* in [227] used Support Vector Regression (SVR) to develop 3D measurement system for detecting and measuring polarizer transparent microdefect. SVR used the same principle of SVM; however, it is considered a regression model and not a classifier, therefore the output of this model is a continuous value. A set of tolerance (epsilon) is used around the separating hyperplane in the case of regression. The inputs for their SVR model are the image gray value and the physical depth of the defect and output is the defect geometric size. The reason that a regression model was used in this study that they are building a 3D model of the defect which will result in a continuous parameter (defect geometric size). Defects below a certain size can disappear in the production process, and defects above a certain size cannot automatically disappear. Therefore, this size should be an interval range rather than an accurate value. The 3D shape of the defect can be measured indirectly by using the functional relationship between the depth scale of the defect and the grayscale of image. Lin and Jhuo in [232] used a modified SVR algorithm called Multiple Kernel Support Vector Regression (MKSVR) to investigate backlight module defects in LCDs. As the name suggests this algorithm uses multiple kernel functions instead of one as in conventional support vector algorithms. In this study, the images of several backlight modules are converted into luminance value and examined all at once using the MKSVR algorithm. The number of kernel functions and the parameters of the kernel functions are automatically determined in this algorithm according to the data distribution characteristics of the training samples. Unlike other learning algorithms such as the neural network and the SVR (which treat all training samples equally), this system is considered more robust and provides more flexibility.

e: CLUSTERING

Clustering is considered one of the unsupervised machine learning algorithms. Hence, it does not require training set for performing classification problems. Hierarchical and K-means clustering are one of the commonly used clustering algorithms [372]. In optical inspection applications hierarchical clustering is suitable with small datasets. It creates a hierarchy of clusters that can be represented in a tree structure where the root of the tree consists of single cluster that contains all the dataset and the leaves correspond to

individual dataset. Hierarchical clustering methods are either agglomerative, in which the algorithm starts with the leaves and merge the clusters together, or divisive, in which the algorithm starts with the root and gradually split the clusters. The linkage criterion is the deciding factor of which hierarchical clustering method should be used, which is a function of the pairwise distances between observations. K-means clustering defines a K number of points (also known as centroids) that indicates the number of groups which is established a priori by expert. These centroids are initialized randomly within the dataset, in which the algorithm tries to assign the K centroid to the nearest neighbor of datasets in order to group the near datasets into one cluster. To calculate the degree of homogeneity and heterogeneity, the K-means clustering method employs the Euclidean distance as a measure of the similarity between observations and groups. The heart of this algorithm is the for-loop which keep updating the centroids' positions until an optimal position of the centroid is reached [373]. K-means clustering were used in the study conducted by Kuo *et al.* in [45] to classify the LED chip regions into; pad area, luminous zone and background. The average gray level of LED appearance structures serves as the cluster center of the K-means clustering method, where the number of clusters K is set to three (which corresponds to the number of regions). Beside using Gaussian EM algorithm to classify both linear patterns and elliptic patterns, and spherical shell algorithm to classify ring patterns in WMs, Wang *et al.* in [69] combined K-means and hierarchical clustering techniques to identify the different defect patterns when both convex and non-convex clusters simultaneously occur on the wafer. The combination of the two clustering techniques can overcome the problem of specifying the number of clusters to execute the algorithm.

Clustering algorithms can be also developed based on probability models. The term model is often used to represent the type of restrictions and geometric properties of the covariance matrices. Unlike previously mentioned clustering techniques, model-based clustering algorithms tries to optimize the fit between the data and models used for clusters, where data are viewed as generated by a mixture of probability distributions in which each component represents a different cluster [374]. Model-based clustering has many advantages in classifying wafer defects over other clustering approaches (that cluster aggregated local defects), such as identifying defect clusters simultaneously and obtaining spatial pattern information in the ICs yield model [81]. Hwang and Kuo in [77] used model-based clustering along with a spatial nonhomogeneous Poisson process, the bivariate normal distribution and the principal curve to classify WM defects according to their defect generation mechanisms. Their proposed algorithm was able to identify complicated defect patterns with fewer parameters. Yuan *et al.* in [78], [79] investigated amorphous/linear and curvilinear WM defect patterns simultaneously, and modelled them using multivariate normal distributions and PCs, respectively, extending the traditional model-based clustering approach by considering

the mixture of two different probability densities. However, their approach is mainly based on simulated results and lacks the capability to detect closed-ring shaped patterns that have been widely observed in WM defects. Furthermore, their approach is computationally intensive when the number of defect clusters is relatively large [81]. Yuan *et al.* in [81] used clustering for multi-stage classification of spatial defect patterns in WMs. First, they used k -NN to classify the local defect from the global defects and for noise removal. The local defects filtered from the previous step is then grouped into different clusters using similarity-based clustering method, which is well-structured procedure based on a simple total similarity objective function and is considered a robust method in terms of its initialization, outliers and the ability of detecting clusters with different shapes. Finally, pattern identification along with fine tuning were then used for each of the local defect clusters (e.g. linear, curvilinear) via various model-based techniques. The proposed method for classification were compared to the model-based clustering approach used in [78] and it has been found that they were able to detect more clusters for three chosen WM samples. However, in [78] they were able to detect more clusters for one of the samples. Despite of the good results achieved, their proposed approach faced some limitation such as it uses location information only to analyse defect clusters. Furthermore, if two or more clusters are close to each other or polarity overlap, the proposed algorithm will not be able to accurately distinguish between them. Finally, the k -NN noise removal approach may not perform well in some situation, as when multiple local defect clusters on the same wafer have different defect densities. Nakata *et al.* in [102] have also used multi-stage approach to identify failure in WM patterns, identify the causes of the failure, and monitor the failure recurrence. To identify failure in WM patterns, they used K-means++, which is proven to be faster by conventional K-means algorithm for clustering wafer patterns. A pattern mining approach called FPGrowth were then used to identify responsible devices of the failure patterns. FPGrowth is an efficient algorithm for association rule mining. It uses a data structure called frequent pattern tree (FP-tree) to store compressed information about frequent patterns [375]. Finally, a CNN were used to monitor recurrences of failures. This study has used various methods to reduce the computation time so that it can be applicable for practical application.

A less commonly used clustering algorithm called Dynamic Time Wrapping (DTW). DTW is frequently used in speech recognition applications but can be also used for different classification problems. DTW is able to find optimal global alignment between sequences based on the Levenshtein distance (also called edit distance), it also provides an overall real number that quantifies similarity. Furthermore, DTW is able to correctly re-align one sequence with the other, a process which highlights similarities that Euclidean distance is unable to capture [376]. Jeong *et al.* in [73] used DTW algorithm to detect anomaly defect patterns of WBM

and compared it with nearest neighbor classifier that is based on Euclidean distance. First, they presented the spatial pattern on the WBM using a spatial correlogram, where a spatial correlogram represents the correlation between values of the same variable at different locations. Spatial correlogram gives more useful information for the monitoring of defect patterns that appear on WMs because this can describe spatial dependence, a phenomenon known as spatial autocorrelation. Then they calculated the distance using DTW approach to identify the different defect patterns. However, the proposed approach did not show robustness to some defect patterns such the rotation-variant defect patterns [96]. Furthermore, it could not identify the geometric shape of the defect pattern [377].

Another clustering techniques used to classify defect patterns in WMs called density-based spatial clustering of applications with noise (DBSCAN). In this algorithm, the density associated with certain data point is obtained by measuring the number of neighbor points along predefined radius, where neighbor points with a density above a specific threshold are considered as clusters. DBSCAN have several advantages such as detecting clusters of arbitrary shapes and patterns and the ability of detecting clusters without specifying the number of clusters in advance [378]. Jin *et al.* in [56] used this algorithm to classify wafer defects, where the Cartesian and polar coordinates of all defective regions and edge die were extracted to be used for calculating DBSCAN parameters. These parameters are the radius of the neighborhood points and the minimum number of points in the neighborhood. In this procedure, the outlier detection and defect pattern detection can be done simultaneously. Taha *et al.* in [103] proposed a clustering-based algorithm called Dominant Defective Patterns Finder (DDPfinder) that clusters the patterns of defective chips on wafers based on their spatial dependence across WMs. The algorithm begins by selecting a number of chips randomly across a WM, where the intensity of these chips is greatest at the edges and lowest at the center. This is due to two reasons: (1) the yield in the near-edge region is usually as much as 50% less than the yield in the center region, and (2) the high yield loss in the near-edge region can have a significant impact on the overall wafer yield and fab profit. The chips selected are then used to construct Voronoi regions with the chips selected are the centroids of these regions. The region is considered defected or non-defected based on how dependent are the spatial patterns of their centroid points on the dominant defective centroid points across WMs. By using this technique, the overall time complexity for classifying defects can be reduced significantly, because the centroid point of each Voronoi region will be used as a representative of all chips within the region. This will cause the size of the processed data to be significantly reduced. This technique was compared to other algorithms such as RGRN, MLP, and RBF. It was found that DDPfinder outperformed all the other mentioned algorithms in terms of reducing computation time only.

f: SUPERVISED NEURAL NETWORKS

Artificial Neural Networks (ANNs) can be classified according to the data processing criteria as feed forward and recurrent networks. Furthermore, ANNs can be classified according to the necessity of a training set as supervised and unsupervised networks [379].

One of the most commonly used supervised ANNs are Multilayer perceptron (MLP) networks (also known as back-propagation neural network BPNN), they are also considered as feed-forward networks. The development of back-propagation learning algorithm for determining weights and biases was the main reason behind the popularity of these networks among researchers. The basic building block of this type of networks is called *Perceptron*. The perceptron takes one or more inputs that go through specific activation function in a neuron to produce an output, for example the perceptron in Figure 42 has n inputs that goes inside a neuron and produces an output y .¹ Rosenblatt proposed simple yet effective rules to compute the output by introducing weights; weights are real numbers the describe the importance of each input to the system, in which the input with less importance will be penalized by multiplying it with low or in some cases zero weight, on the other hand the inputs that have high influence on the system will be rewarded by multiplying them with relatively high weights. Activation function (e.g. sigmoid function, tanh, or ReLU) is used to add non-linearity to the process and help in decision making, applying the activation function takes place after multiplying the weights with the inputs. As the name suggests, MLP is consisted of multi-perceptron in order to deal with complex problem, the general topology of this network is shown in Figure 43 which represent a 2-layer MLP (hence: the input layer is not counted as a layer). The outputs of each layer from the perceptron are fed to the next layer as inputs and so on until final layer is reached, this process is called feedforward process. In order for the MLP to work efficiently it has to be trained, this can be performed by relying on the historical data (training data) for the inputs and corresponding outputs. Ideally, if the inputs from the historical data were fed to the MLP, the same corresponding outputs from the historical data have to be obtained. Therefore, a sort of comparison process has to be established between the actual outputs of the network and real outputs from the historical data to have a sense of the error. This comparison can be made by using cost function (e.g. MSE). After the cost function is defined, the weights and biases of the MLP has to be updated until to the cost function reaches a minimal value. In order to do so, partial derivative is used to track the change of cost function with respect to the weights and biases. The process of getting the optimum weight that corresponds to minimal error is called Gradient Descent. This step begins from the output layer until the error is investigated at the input layer which

¹When sigmoid activation function is used, the perceptron structure shown in Figure 42 can be also used in Logistic Regression classifier which is the simplest form of ANN

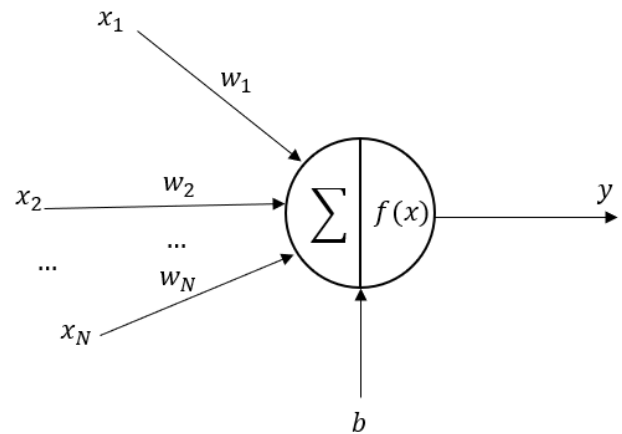


FIGURE 42. Perceptron structure.

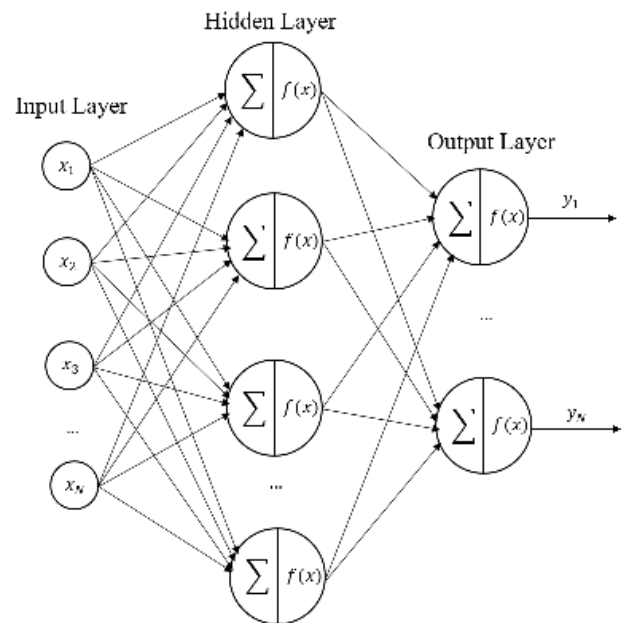


FIGURE 43. MLP structure.

justify the name *backpropagation* for this process. MLPs are usually described according to the number of neurons and layers used. For example, a 3-5-4 MLP means that this is a two-layer network that consists of three layers; input layer with three inputs, hidden layer with five neurons and output layer with four outputs. Another type of supervised neural networks that is widely used among reviewed articles in this paper called Learning Vector Quantization (LVQ). LVQ are also formed using input, hidden and output layers; however, the hidden layers of these networks are not fully connected to the outputs, which can reduce the computation time. A modified versions of LVQ, namely, LVQ1 and LVQ2 were also proposed by Kohonen in [380], which further reduce the computation time and increase the stability of the learning process. Kuo *et al.* in [45] used two MLPs to investigate five defect types in LED chip. K-means clustering with the

aid of NCC was first used to divide the area of the chip into three regions: pad area, luminous zone, and background. The reason behind this step is to classify the defected features according to the region. Otsu auto-thresholding method were then used to highlight four features for each selected region and the overall chip; these features are area, perimeter, tightness, and defect rate. The extracted features were then fed to the first MLP that is responsible to decide whether the sample contain fragment chip defect are not. Another 15-10-5 MLP were used to classify the samples according to the remaining four defect types considered. The total percentage of defect recognition according to this method was 97.83%. Chiou *et al.* in [203] used two MLPs as well in their study to investigate the defect occur in the gold-plated regions of BGAs. The first MLP (3-5-2) was used before the feature extraction process take place to identify the gold-plated pixels from other pixels. Three inputs were used to feed this MLP which are R, G and B information for each pixel. The output layer has two output units, i.e., gold-plating pixel and non-gold-plating pixel. The second MLP (6-7-5-7-4) was used after the features are extracted. Six inputs were used in this network that represent the number of features extracted, and four outputs that represent the number of defect types considered. The proposed study achieved good classification accuracy results of 96%. However, it fails to distinguish a defect that is connected to the non-gold-plating regions, because the pixels that make up the defect have been classified as non-gold-plating pixels. Furthermore, the regions inspected, and the number of defects considered in this study are limited. Lin in [36] used two approaches to classify water-drop defects on LED chip surfaces: wavelet-based multivariate statistical (WMS) and MLP network called wavelet-based neural-network (WNN). In WMS, wavelet features were used to obtain the Hotelling T^2 value such that the distance between defective features can be estimated. The T^2 value is then classified according to upper and lower limits, such that if not in the range this means a defect has been detected. WNN approach uses four wavelet characteristics as the input values of MLP neural network which has two neuron outputs that represent two classes: in-control and out-of-control. The detection rates using WMS and WNN approaches were 92% and 95% with false alarm rates of 5.8% and 7.5% respectively. However, these results were contradicted by another study conducted by the same author in [51] that used the same exact approach with different results obtained. The detection rates for this study using WMS and WNN approaches were 92.4% and 90.8% with false alarm rates of 6.1% and 4.4% respectively. The reason for this contradiction is not explicit; however, since the major difference was in the WNN results, it could be due to different sample images used in both studies for the training process. In a similar approach, Chiu and Lin in [245] investigated blemish defects in LCD panels using T^2 hotelling approach with the aid of ACO and BPNN. The T^2 hotelling value were obtained using four color models, so that the distance represents the color variations (dark and bright variations

in the grayscale). ACO algorithm is applied to detect the abnormal spot blemishes in the distance diagram. Finally, the BPNN were applied to classify the regions of slight color variation blemishes based on the T^2 distance values. Su *et al.* in [111] used three types of ANNs to inspect semiconductor wafer post-sawing quality, which are BPNN, RBF and LVQ. Where the RBF network can be considered similar to BPNN; however, it only consists of one hidden layer and it lack of connection weights between input layer and hidden layer. They achieved optimum results in their study upon using 360 image mask size and 224 input nodes for all the neural network used. The number of hidden layer nodes in the three ANNs to achieve optimum results were; 20 in BPNN with accuracy of 100%, 15 in RBF with accuracy of 90% and 18 in LVQ with accuracy of 100%. It is clear in this study that BPNN and LVQ showed an outperformance in the inspection when compared to RBF. However, the proposed study is not suitable for high variety of defects. In the study conducted by Aghaeizadeh Zoroofi *et al.* in [119], BPNN have also showed an outperformance in classifying IC wafer contamination defects when compared to maximum likelihood and maximum distance classifiers. However, these algorithms were used as binary classifiers and did not give many details about the defect. Chen *et al.* in [264] used multiple ANNs to classify TFT-LCD defects during the lithography process. RBF, BPNN, LVQ1 and LVQ2 ANNs have been used and comparison between their results were investigated. Due to the difficulty in collecting sufficient defect data, this study simulated various defect data to fit enough numbers for modelling. Special considerations regarding using masks for the sample images have been made, such that the ROI does not take many inputs from the neural network and in the same time make it big enough so that the accuracy is not affected. Experimental results showed that LVQ2 had the best accuracy results with an accuracy of 97%, while RBF performed the worst with an accuracy of 87%. Despite the good results they have achieved, the proposed approach is inferior in terms of system setup lead-time and flexibility to product complexity. Sun *et al.* in [293] have also compared between the performance of MLP and LVQ networks to classify four types of thermal fuses defects. Four features were first extracted using thresholding, segmentation, and morphological operations, which are mean grayscale value, variance, rang and entropy. These features were used as inputs for both networks. Experimental results have shown an outperformance of MLP over LVQ in terms of accuracy. However, LVQ consumed less computational time compared with MLP. Acciani *et al.* in [143] proposed two neural networks: LVQ and MLP to classify five types of solder joint defects. They have also conducted experiments on k -NN classifier and compared the performance between the three classifiers considered. The input for these classifiers was the feature vector that contain the geometric and wavelet features of the inspected area, and the output consisted of five neurons in the ANN classifiers. The results have proved that MLP classifier that fed with the combined geometric and wavelet feature vector performed

the best compared with LVQ and k -NN classifiers with a recognition accuracy of 98.8%. However, many limitations have been noted in this study, such as the number of images used to train the classifiers is not the same for all the defect types (e.g. 32 images for defect type 5 and 76 images for defect type 3), this can cause imbalanced data and can affect the validity of the recognition accuracy obtained. Furthermore, the defect types considered in this study was limited compared with other similar studies. Another note that the results obtained in this study were partially contradicted with another study conducted by the same author in [165], which obtained 99.5% accuracy for the same approach. However, this contradiction is due to the fact that only a small number of samples have been tested in the later study. A similar approach was also proposed by the same authors in [166] in terms of the defects considered and feature extraction technique; however, in this study a neuro-fuzzy classifier was used instead. Their hybrid classifier consisted of three MLP networks and two modules based on fuzzy rules. Several advantages were observed by using fuzzy-based classifier such as low computational costs of the fuzzy systems that could satisfy urgent time constraints in the in-line detection. Kuo *et al.* in [228] used GLCM matrix as inputs to two ANNs: BPNN and RBFNN to classify polarized film defects into four types of defects. The accuracy of the classification procedure is 98.9% for RBFNN and 97.3% for BPNN and the processing time of one single image is 2.57 seconds. Huang in [71] used four self-supervised MLP networks that operate simultaneously with one hidden layer to detect clustered chip defects of wafers and classify them to bad and good wafers. The input of the network is fed from the output generated at the end of preceding training cycle. The feedback connection between the output and input layers were used to elucidate the structure in the input data without a priori teaching. Backpropagation with gradient descent concept were used for the training purposes of the network. Lin in [83] proposed BPNN integrated with ACO algorithm to predict the wafer yield. ACO can be integrated with BPNN to look for the optimal set of parameters (weights and biases), which can reduce the time of training process. This will result in ACO-BPNN. The input for this network is obtained from the defect count, cluster index and FVCP. Yang *et al.* in [214] proposed a BPNN to classify the five defects considered in the TFT array process. The input for this network were the eleven features extracted using the GLCM process, and the output were the five classes considered according to the number of defects. Thirty hidden layers were considered along with bipolar sigmoid activation function. The defect recognition rate of proposed system was estimated to be 83.3%. However, it is noted that when the defect type changes or type of TFT array samples change, the proposed defect classifier must be retrained in order to adapt to new defects or sample, which is considered a limitation for the system. Kuo *et al.* in [272] proposed a Taguchi based BPNN to classify four types of color filter defects in LCD panels. The combination of Taguchi and BPNN were utilized to

avoid a possible disadvantage of using BPNN alone such that the global minimum cannot be obtained if learning cycles are insufficient. Four feature values were used as an input to the BPNN. The output consists of four neurons according to the defect classes considered (fibre, particle, gel and resisting coating). This study achieved an overall recognition rate of 94%. In a similar study, Kuo *et al.* in [273] used BPNN classifier to classify six types of color filter defects and the results were compared to another classifier type called minimum distance classifier (MDC). MDC classifier calculates the distance between the unknown graphic type and all training types and selects the shortest distance for decision making. The five key features obtained from the feature extraction step were used as inputs to both classifiers, and the output was the six defect types considered. In this study BPNN achieved an accuracy of 93.7%, while MDC achieved 96.8%. Despite of the good results achieved; the proposed method could not recognize defects in the case of overlapping of different defects in the same position. Li *et al.* [221] proposed an MLP with four inputs: width, ratio of fringe, curvature of fringe and fringe size to classify the Mura defects into three types. The number of outputs of the MLP were four including the three defect types considered and the normal (non-defected) case. Ko and Cho in [164] proposed a combined approach of LVQ networks and fuzzy rules to inspect solder joint defects in PCBs. Each inspected image is divided into three sub-images and an LVQ network is used for each sub-image. The objective of this approach is to reduce the burden of the LVQ classifier when classifying the complex solder joint patterns. The input data of each classifier are the color intensities of each pattern as shown in the form of three-color patterns obtained under the three-color circular illumination. To avoid any misclassification, fuzzy logic scheme was integrated with the LVQ classifier. The classification rule is described in a linguistic way like a human's, rather than represented by precisely numerical quantities and the classification task is performed by predefined rules. Several advantages have been observed by using the proposed techniques: one is that the combination of three discriminant boundary functions makes more complex boundaries than the original LVQ algorithms. The other is that expert knowledge can be reflected in the pre-defined fuzzy classification rule. Therefore, the classification boundaries can be easily readjusted, by changing the fuzzy rule tables and membership functions. However, since the proposed approach uses multiple algorithms and deals with three sub-images for each image, this can increase the computational time making this method not suitable for rapid inspection applications. Ong *et al.* in [169] proposed LVQ network to classify solder joint defects. The input for the classifier were directly obtained from the grayscale acquired images without feature extraction or preprocessing steps since special camera setups were established to avoid these steps as shown in Figure 26. They compared the recognition rate for the classifier according to the images acquired from different setups. They have shown that their classifier performed the best

when a combination of oblique and orthogonal setups was used to acquire the images compared with only orthogonal setup was used. However, when the sample images increase to about 130 images for training, both setups performed the same. Their classifier achieved a high recognition rate (up to 100%) with no false alarm. However, their method has faced various drawbacks. First, their system is very sensitive to lightning variations, therefore the success of a vision inspection system is very much dependent on the good design and robustness of the light source system. Furthermore, despite that feeding the LVQ without preprocessing or feature extraction can reduce a lot from the computational time required; however, these steps are still necessary to alleviate the effects of error arising from different sources of variation. Adly *et al.* in [57] proposed a novel algorithm that combines a general regression network-based (GRN) consensus learning model with randomization technique to detect defective patterns in semiconductor wafers, where the combination results in randomized general regression network (RGRN). GRN are single-pass associative memory feed-forward type ANNs which use normalized Gaussian kernels in the hidden layer as activation functions [381]. The randomization technique was applied by implementing randomized bootstrap to the original data. Randomized bootstrap technique creates random new subset of data by sampling from the original dataset (with replacement). This method of applying RGRN with randomization technique were compared to other techniques such as MLP and it showed an outperformance compared to them with an average accuracy of 99.8%. Adly *et al.* in [88] conducted the same previous approach; however, they proposed a data reduction technique based on data partitioning and clustering to simplify the overall algorithm. Voronoi Diagram were used for the portioning of data, where it clusters the whole vector space into smaller Voronoi regions. k -means clustering is used to fetch the centroid of each Voronoi region to be used as representative of all original vectors. By using the centroids, the size of the data is reduced and therefore the computation time of the algorithm is also reduced. Their overall accuracy using this technique were slightly improved compared with the previous method, as they have achieved an accuracy of 99.884%. RGRN algorithm were used again in the study conducted by Tello *et al.* in [108]; however, they added a CNN model in order to identify and classify both single and mixed defect patterns. This study suggested using a *splitter* based on information gain concept to classify single and mixed patterns separately. The proposed approach achieved overall accuracy of 86.17%. Even though the accuracy achieved were lower than the one conducted by Adly *et al.* in [57], [88] that used similar methods; however, these two studies considered single defect patterns only and did not consider mixed defect patterns as in this study.

g: UNSUPERVISED NEURAL NETWORKS

For the scope of this review, unsupervised neural networks are mostly used for identifying defect patterns in WMs. Recurrent networks are example of unsupervised learning

networks. They are called recurrent because inputs to the neurons of these networks come from external input, as well as from the internal neurons, consisting of both feed-forward and feedback connections between layers and neurons. Hopfield neural network (HNN), Self-organising map (SOM) and adaptive resonance theory network (ART) are all examples of recurrent neural networks [382]. HNN can be used as an associative memory and can also help in optimization problems. Chang *et al.* in [44] used two HNNs to investigate LED die defects. The first one was called Contextual HNN and was used to locate the dies in the sample sub-images. The number of the input neurons for this network were equal to the number of pixels for the sample sub-image. The network detecting criteria must satisfy the fact that intensity distribution of pixels in die region in the sample sub-image must be similar to that of template image. Since the network is used to identify the die locations, the output neurons of this network form a die map of individual dies. Each neuron node represents the state of the pixel digitally, such as if the pixel is located within a die region the neuron state is 1 otherwise it will be 0. Therefore, the die map represent a binary image that has the same dimension as sample sub-images. The regions that represent a die location are considered 1's, and the ones that are not considered regions are considered 0's. The die region are then identified using CCL algorithm. The second HNN is called competitive HNN were used to classify the die image into three classes; light emitting region, p-electrode and background in an unsupervised approach. The number of neurons of this network depends on the gray intensity values and the number of classes. In competitive HNN, winner take all (WTA) approach were applied. The WTA ensure that no two neurons are categorized with two different classes and also guarantees that all gray scales are classified. The die defect inspection algorithm were then applied to compare geometrical and heuristical defects against the selected template. 10% threshold margin were used to compare the sample sub-images with the template image. The method achieved an accuracy of 95% in detecting defective dies. Chen and Liu in [64] used a modified ART called ART1 to recognize pattern wafer defects. Unlike other types of ANNs that are less likely to learn new information without damaging what was previously learnt, ART network has the advantage of not forgetting after learning [379]. ART1 is considered an unsupervised binary network that accepts binary inputs. In this study, an unsupervised technique were selected as they found it difficult to decide how many clusters of defect spatial pattern to be selected, therefore the learning was accomplished using input data alone. They also gave detailed explanation behind the reason of choosing this algorithm as:

- If the characteristic of a new pattern is quite similar to a previously stored pattern (vigilance test passed), only a slight modification of the knowledge contained in the old patterns will be executed. The characteristics of the old and new patterns can be satisfied and the old knowledge can be properly retained. Stability of the system can be maintained.

- If the characteristics of a new pattern are not similar to all of the previously stored patterns (vigilance test failed), new knowledge for the new pattern will be created. This implies quick learning of a new pattern, or the so-called plasticity.

The network was able to recognize both ring and scratch defects using matching values. They compared the performance of ART1 to SOM. They showed that ART1 outperformed SOM in the comparison. Even though, they did not achieve high matching scores for the detected pattern; however, this study over comes others in predicting the possible defect patterns rather than assuming a pre-defined scenario. Unlike the outcomes achieved in the previous study, Di Palma *et al.* in [66] showed that ART1 is not adequate due to AND logic usage, whereas SOM provide completely satisfactory results including visually effective representation of spatial failure probability of the pattern classes. However, their method cannot separate ring patterns from the other types of defect clusters [86]. Liu *et al.* in [65] implemented the same approach in [64], in which they used ART1 to detect the defect patterns in WBM. They were able to detect more patterns than the previous study such as bull's eye pattern and they reached a recognition rate of 95%. However, the low number of WBM provided to them limited their ability to identify further patterns. Choi *et al.* in [85] conducted a study similar to what have been done in [64], [65]. However, they proposed an advanced ART1 algorithm called "multi-step ART1", where it sequentially uses the modules to classify each pattern separately, instead of training all patterns at once. This algorithm has a specific learning procedure according to the characteristics of each pattern by changing and re-learning the preprocessing of the input data, the threshold decision method, the type of similarity and the vigilance parameter during module generation. Their proposed algorithm was able to detect more type of defect pattern including mixed pattern compared to the similar studies. Hsu and Chien in [58] developed a hybrid data mining approach which combined ART1 and spatial statistics to quickly extract systematic and random patterns from WBM. Furthermore, a decision tree algorithm was constructed for identifying the root causes of specific patterns. However, due to the vigilance parameter settings used in ART1, some systematic patterns were misclassified as random patterns in this study. Hence, the lower the vigilance threshold value, the more patterns are extracted from the maps. On the other hand, a low vigilance threshold value may also cause dissimilar maps to group in the same cluster. Huang *et al.* in [72] conducted similar study to what have been investigated in [71]. However, cellular neural networks combined with genetic algorithm were used to classify wafer patterns instead. A cellular neural network (not to be confused with convolutional neural network) is an unsupervised neural network that is composed of a massive aggregate of analog circuit components called cells. Setting up a cellular neural network needs a proper selection of circuit parameters of cells. The dynamics of a cellular neural network is determined

by the set of circuit parameters, which are collectively called the cloning template. A genetic algorithm was used to settle the cloning template for the cellular neural network owing to its success in the applications of optimization. This study outperformed the previous study in [71] remarkably as it achieved an accuracy of 99.2%. However, the false alarm rate of this study was relatively high. Furthermore, no explanation was provided for the different accuracy results for using MLP algorithm, despite of using same approaches in both studies. Liu and Chien in [87] used different type of ANNs for different purposes to analyse and classify WBM defects. Cellular neural network was used first to eliminate WBM defect noise and enhance the patterns against random errors. Moment invariant and ART1 were then used for pattern clustering and classification respectively, where moment invariant can make the same shape in one cluster, whether the shape's size or position are changed. ART1 can self-learn by characteristic of each WBM. These algorithms were integrated with a user interface system that allows users to execute the following system operations including: loading the analysed dataset, adding or retracting the decision knowledge, controlling the parameters in WBM patterns clustering system, and monitoring the clustering results. Chien *et al.* in [86] used ART1 classifier as a final classification step to deal with the wafer being classified as having spatial random defects with higher failure percentage and to find new defect patterns for further classification. The filtered wafer defects that feed ART1 algorithm came from predefined conditions using SPC charts that cannot detect all types of defects (e.g. sparse defects). In SPC chart a set of thresholds were used upper control limit (UCL) and lower control limit (LCL) such that if the failure percentage of the WBM exceeds the UCL the wafer will be classified as a defect, otherwise if it fall below the LCL will be checked for further defects using various filters and ART1 classifier as mentioned before. Chang *et al.* in [113] proposed an automatic inspection approach for classifying wafer defects into four classes based on a SOM. The feature vector containing GLCM parameter and color information were used as an input to the network. The inspection results achieved a sensitivity value of 0.967 and a specificity value of 1.

Unfortunately, unsupervised neural networks involving SOM, ART, and Cellular Neural Networks cannot identify two shift-variant or two rotation-variant defect patterns that in fact belong to the same failure cause (i.e. distinguishing between two parallel scratches or between a top zone and a bottom zone) [70].

D. DEEP LEARNING

Deep learning has recently become the most influential technology in machine vision and pattern recognition problems [383]. Deep learning concept involves the usage of Deep Neural Networks (DNN), which can handle feature extraction and classification methods in machine vision problems. DNN is considered a class of ANN; however, the main difference that make any ANN considered a DNN is DNN consists of

three hidden layers or more. Moreover, DNN requires little preprocessing and feature extraction as these processes are embedded inside the network itself. DNN also uses large number of layers compared to the number of nodes to realize highly nonlinear functions. DNNs learn new useful representations from available features that capture essential statistical regularities present from data itself, then the representation features can be formulated for classification, regression and specific problem in information retrieval. The independence from prior knowledge and human effort in feature design is a major advantage for deep learning in general and DNNs [384]. For AOI applications reviewed in this paper DNNs are implemented using the following methods: Autoencoders and Convolutional Neural Networks (CNNs).

In DNN, set of models is used to learn high-level abstractions representation in data such as autoencoder (AE), denoising autoencoder (DAE) and stacked denoising autoencoder (SDAE) [93]. AE is a three-layer network including encoder and decoder. The encoder maps the input data from a high-dimensional space into codes in a low-dimensional space, and the decoder reconstructs the inputs from the corresponding codes. AE can learn features in unsupervised manner by minimising reconstructed errors between input data and output. However, the intrinsic problems of AE, such as simply copying input layer to hidden layer, make it not effective to extract meaningful features even though its output can be a perfect recovery of the input data [385]. On the other hand, DAE takes a corrupted version of data as input and is trained to reconstruct or denoise the original inputs from a corrupted one, which can prevent the AE from just simply learning an identity mapping between the input and the reconstructed output, and captures more informative hidden patterns and obtains robust and powerful representations from the noisy features. DAE also consists of an encoder process and a decoder process. Several DAEs can be stacked together to form a deep network and learn high-level representations which can be called SDAE. Therefore, SDAE is considered a special class of DAE where stochastic noise is added to the input layer of the AE and then trains it to output the same input without noise. In general, the training process of SDAE includes an unsupervised pre-training step and a supervised fine-tune step. Another popular type of AE family is Sparse Autoencoder (SAE) which is considered is a variation of Autoencoders, where it offers reduction in the neurons used in the hidden layer and therefore these neurons are considered inactive and do not fire. This can improve the performance of traditional autoencoder and exhibits more practical application values [384], [386]. Hence, autoencoders in general do not have the ability to classify on their own and are usually integrated with other deep learning layers such as CNN to fulfill the purpose of classification [387]. Yu in [93] proposed detection and recognition system for detecting WM defects based on a modified version of SDAE called enhanced stacked denoising autoencoder (ESDAE). They have also integrated manifold regularization in the learning procedure which improve the algorithm's performance effectively due

to the preservation of intrinsic information in the data. The overall detection accuracy of the proposed method reached 89.6% which overcame other methods used for comparison such that SDAE, DBN, BPN and LR. However, due to the large number of parameters used, deep autoencoders in general are easy to suffer from overfitting with small size sample, which limits the generalization ability of the deep autoencoders to learn effective features [388]. A similar approach was also proposed by Lee *et al.* in [389] to assess wafer's quality. However, sensor data were used instead of WM, which is beyond the scope of this review. In a similar study that proposed detection and recognition system for detecting WM defects, Yu *et al.* in [91] integrated SDAE and CNN to form a new deep learning model called stacked convolutional sparse denoising auto-encoder SCSDAE. The new model proposed can learn effective features and accumulate the robustness layer by layer, which adopts SDAE as the feature extractor and stacks well- designed fully connected SDAE in a convolutional way to obtain much robust feature representations. The challenges faced this study and others that use same dataset is the imbalance of data, in order to handle this problem under-sampling and over-sampling methods are generally used to against highly imbalanced datasets. Under-sampling randomly eliminates majority class examples, while over-sampling increases the number of instances in the minority class. Both of them aim to obtain approximately the same number of instances of the classes. The detection accuracy rate in this study was 95.13% in the simulation case and 94.75% in the industrial case. The results were compared to other classification algorithms such SDAE, AlexNet, DBN, SVM, BPN, k -NN and C4.5 and outperformed all of them in the simulation and industrial cases. However, the problem of limited training data will lead to overfitting of SCSDAE. Moreover, due to labeled data scarcity for some patterns in WMs, it is a challenging issue for SCSDAE to implement pattern recognition on imbalanced dataset.

Data imbalance and the lack of training data are major problems as mentioned earlier in our discussion. Traditional image augmentation techniques such as rotation, mirroring and scaling can overcome these problems in some cases. However, as these techniques only manipulate the real dataset without providing new insight for the data, inaccuracy and overfitting in classification results may occur. Goodfellow *et al.* in [390] proposed GAN that can be used for data augmentation to generate more data for training. The original proposed model consisted of two networks, namely, generator and a discriminator. The two networks are trained at the same time and compete against each other in a minimax game. The generator is trained to deceive the discriminator by synthesizing realistic samples, whereas the discriminator is trained to be equipped with high discriminative capability for the synthetic samples. These networks complement each other and can help to understand the original data distribution, providing a new perspective for the forthcoming classification algorithm. However, the training of the two networks

can be quite unstable and may suffer mode collapse problem [391], [392]. Wang *et al.* in [94] proposed an improved GAN model integrated with CNN and other deep learning models called adaptive balancing generative adversarial network (AdaBalGAN) for identification of defective patterns in WMs. This algorithm was specially proposed to enhance the classification results against imbalanced datasets. Moreover, the study proposed a conditional categorical generative adversarial network to rebalance the WM dataset by generating simulated instances for minority class of defective patterns. Three parts are involved in the previous process; the first part is a pattern recognition model which consists of CNN that classifies the real WM samples, the second part is a generative model which also consists of CNN that generates simulated WMs according to the real samples from first part. Finally, in the last part, a classical CNN (Le-net5) is used to compare between the real wafer and simulated WMs and guarantee the similarity between them. The proposed method resulted in high classification accuracy for some patterns (up to 100%) and also outperformed other algorithms that were compared to it such as SVM, Adaboost, CNN and GAN. Kim *et al.* in [255] proposed an algorithm based on CNN with stacking ensemble model and MLP, to classify four types of TFT-LCD defects. In their investigation, they have noticed that the size of defects is very small compared to the patterned panel in the background. Therefore, they proposed a feature extraction scheme to eliminate the patterns in the background for better classification results by applying three steps: find the pitch of each panel image, calculate the pitchwise difference score for each pixel and apply thresholding. An algorithm was proposed in this study to check the efficiency of using the pattern elimination technique by using several MLP and CNN models. They have achieved an overall accuracy in their classification of 86.13%. However, they did not mention the time needed for the algorithm as they used too many models which may affect the computational time. Mei *et al.* in [215] proposed a method that combined handcrafted features and unsupervised deep learning-based features to detect Mura defects in TFT-LCD. The method was named joint-feature-representation-based defect recognition framework (JFR-DRF). Various unsupervised algorithms were compatible for the unsupervised deep learning-based feature extraction part; however, SAE algorithm was used to demonstrate its ability. The handcrafted features were extracted with methods similar to GLCM technique that requires coefficients such as entropy and anisotropy coefficients based on the grayscale histogram. Then, the features extracted by these parts will be merged into a single feature vector, which acts as the representation for the Mura defect image. After subsequent processing, it will be classified using one-against-all SVM classifier. In this study, it was proven from statistical results that combining handcrafted and unsupervised feature extraction outperformed the performance of using only one of them. However, fused feature representations may also have the risk of being affected by poor representations from modalities which are not appropriate for

the tasks. Moreover, deep learning-based methods can require considerable computational resources and time to perform training and inferencing [244]. Mei *et al.* in [250] proposed an algorithm to detect texture surface defects in general such as LCD panels, ceramic tiles, and textiles. Where Mura defects is one of the LCD panel defects investigated in this paper. The algorithm is carried out by reconstructing image patches with multiscale convolutional DAE (MSCDAE). The MSCDAE method employs a three-layer pyramid to perform multiscale defect inspection. This study used only defective-free samples for model training, since collecting and labelling large number of defective samples is cumbersome. However, their approach requires a separate model to be trained and tested for each layer; therefore, it is time-consuming and leads to excessive memory consumption. Their approach achieved a reasonable recall but relatively low precision [256]. Yang *et al.* in [256] overcame the limitation in the previous study and proposed an algorithm based on fully convolutional autoencoder approach (MS-FCAE) to inspect texture surface defects including TFT-LCD defects. This algorithm can accurately segment various types of product surface defects based on a small number of defect-free product samples (50 defect-free sample). The data sample for the TFT-LCD defects includes spot defects, line defects, and region defects. Their inspection results showed that the proposed algorithm both simultaneously and accurately inspects all types of TFT-LCD defects as it achieved a 98.1% recall and 92.1% precision, whereas the other defect inspection methods compared with the proposed are suitable only for certain types of defects. Furthermore, compared with MSCDAE used in [250], MS-FCAE requires no redundant computation at all. Jo and Kim in [286] proposed a regularized auto-encoder algorithm as a features extraction approach to separate the background of images from the defective regions for inspecting displays of mobile devices. This study focused on comparing their approach to similar feature extraction and dimension reduction approaches low-rank-approximation-based separation methods (specifically SVD) and the segmentation-based method. They have shown that their proposed method was able to detect defects ranging from high visibility such as faint dot type defects to not clearly visible because of the small intensity difference from the background such as Mura defects. On the other hand, the previously mentioned approaches failed to detect these defects. Despite that SVD outperformed the proposed method in terms of the computation time with an average 183ms compared with 313ms in the proposed method. Many drawbacks were also observed in this study, such as in the simulated defect images, overlapping defects were not considered. Furthermore, the method needs to repeat inspection several parts of an image of mobile device because it only processes 700×990 size image due to the limitation of computing resources.

A special case of DNNs is when the matrix multiplications include convolutional filter operations, which is common in DNNs that are designed for image and video analysis. Such models are known as convolutional neural

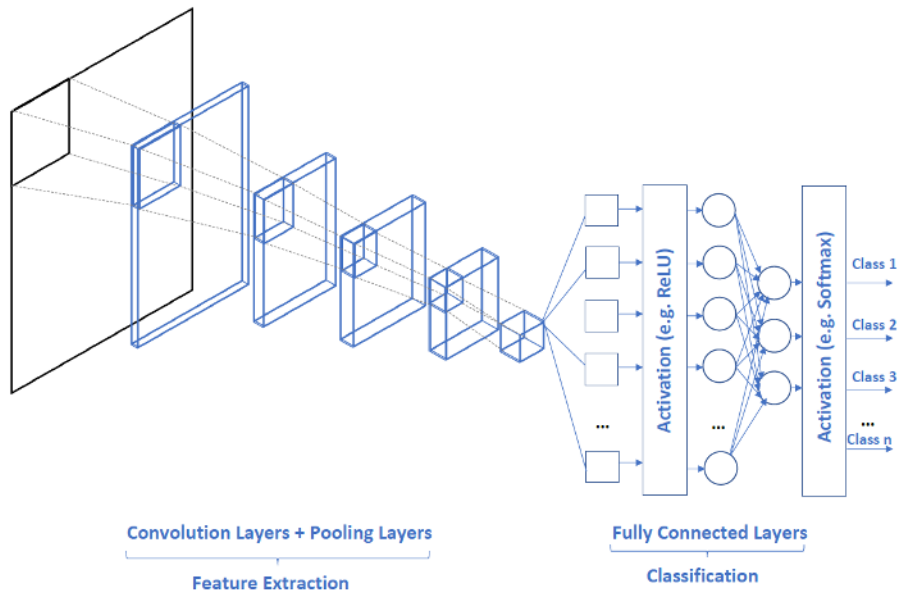


FIGURE 44. CNN structure.

networks (CNNs) [18]. CNNs have been widely known for their high image recognition capabilities in recent years [21], [25]. Usually, the methods based on CNN are preferable in imaging applications and can obtain more precise results compared to traditional methods due to many factors such as; capturing grid-like topology of images effectively, decrease the computation time due to pooling and convolutional layers usage, capability of differentiating large number of classes, and learning image features automatically without using image processing tools for feature extraction [393]. Remarkable achievements in feature extraction and image classification have been produced by CNNs such as AlexNet [394], VGG [395], ResNet [396], and DenseNet [397], which have outperformed conventional classification models such as SVM. As a result, CNN was applied to optical defect detection problems after AlexNet was proposed [383]. A typical CNN consists of input layer, convolutional layers, pooling layers, fully connected layers, and output layer as shown in Figure 44. Convolutional and pooling layers (which performs convolutional and pooling operations respectively) are the main elements that distinguish CNN from other types of NNs. In CNN, pooling layers lay between two successive convolutional layer and output layer follows the last fully connected layer which connects all hidden units in previous layers. The convolution layers play an essential role in extracting features from the input images by performing three operations throughout an input array. First, it performs element by element multiplication (also known as dot product) between a sub-image array (that is equal in size of a kernel) of an input image and kernel with random weights. Secondly, the output of this operation will be added to bias and result in what so called feature map. The initial weights of the kernels are randomly generated, while

the bias can be set based on the networks' configuration. A suitable stride can be defined that identify how many of pixels the kernel can slide across the input image. A careful consideration must be made in selecting the stride size, as a larger slide can reduce computation time, but it may also lose important features from the input image. On the other hand, pooling layers are important in improving image classification. It minimizes computation time by reducing the spatial size of the input image array [398]. This process is often called down sampling. There are two widely used pooling functions used for this purpose which are max-pooling and average-pooling (also known as mean-pooling). Lin *et al.* in [47] used CNN (called LEDNet) for inspecting LED chips defects. They considered two defects in their analysis, line blemishes and scratch marks. The LEDNet they used consisted of six convolutional layers, three max-pooling layers, an average pooling layer and a fully connected layer. Average pooling were used to highlight the importance of each feature and relate them to the correct class (line blemishes or scratch) with the aid of associated weights and class activation mapping in following fully connected layer. Due to the lack of real defected LED chip sample images and since CNN needs large amount of data to be effective, the dataset provided to train the CNN were generated using *geometric transformation technology* that simulates the defects with adjusted images. Rotation, flipping, shift, noising and blurring effects were carried out randomly on the adjusted images to mimic the real situation. The inaccuracy rate of classifying the defects for chip 1 and chip 2 were 5.04% and 5.51% respectively. Their proposed approach were compared to the algorithm used in [45], they got 14.53% and 11.97% inaccuracy rates for chip1 and chip2 respectively which more than twice the inaccuracies used in LEDNet. Even though this study got

considerably low inaccuracy results; however, their algorithm were limited to classify only two kind of defects. Furthermore, there was no evidence that their adjusted images for the training set can simulate the real case for defected chips. Yang *et al.* in [41] used CNN for the purpose of assessing the diameter of the LED cup aperture. Since no feature extraction needed to feed the CNN, the images were directly used as the input neurons of the network. The network consisted of five convolution layers and two fully connected layers. Training samples for the network were used from the captured images, each sample of the image were rotated 90° four times and horizontal flip were applied to each image to further increase the training samples for the network. The detection rate for unqualified cups was 100% with false alarm rate of 8%. However, the need for a large labelled dataset may limit its application [399]. For semiconductor wafer inspection, Kyeong and Kim in [104] used CNN in their classification, in which they considered the WBM as an input binary matrix of 0s and 1s that have a size of 56×53 . In their study three convolutional layers, three pooling layers and a fully connected layer with ReLU and softmax activation functions have been used. The CNN model that they have proposed for classification was designed to detect multiple defects on same wafer. In order to do so, they proposed four individual CNN classifiers for each defect class, in such a way that each classifier determines whether the corresponding pattern exists when several defect patterns are mixed over a wafer. The main drawback of this approach is that to detect a mixed pattern defect, the output of each individual classifier has to be obtained [400]. A similar approach was proposed by Cheon *et al.* in [134]. The proposed CNN model in this study can extract features from the real wafer images that are acquired using SEM and accurately classify the input data into five different wafer defect classes. Their model can also classify the unknown defect classes by combining the CNN model with k -NN classifier. However, the data used in this study were highly imbalanced and no solution were proposed to mitigate the outcomes of this issue [401]. Nakazawa and Kulkarni in [106] also used CNN with three convolutional layers, three pooling layers and two fully connected layers for wafer inspection. The input wafer image size was 286×400 . To evaluate the CNN performance 28,600 WBM images were generated in addition to 1191 real wafers for 22 defect classes which improved the test accuracy up to 98.2%. However, there was high reliance on simulated data for training and validation of the CNN model because real data was highly imbalanced. Furthermore, this study does not provide any information about the defect cluster, size and its location. In a later study conducted by the same authors in [107], Nakazawa and Kulkarni overcame the lack of information problem using different type of CNN models such as Fully Convolutional Network (FCN) [402], SegNet [403] and U-Net [404]. These models were compared to each other with regards to their classification performance and training time. The main concept of FCN is to replace the fully connected layers of typical classification neural networks with convolutional layers so that a network output

can be a two-dimensional heat map, rather than multiple set of classes. In FCN, shallow layer's outputs are merged to deeper layers so that the network can maintain both local and coarse information. SegNet were designed to be an efficient architecture for pixel wise semantic segmentation, where it consists of an encoder network, a corresponding decoder network followed by a pixel-wise classification layer. Each of the encoder and decoder networks consist of 13 convolutional layers. The decoder uses pooling indices computed in a max pooling step of the corresponding encoder to perform non-linear up-sampling. Since positional or boundary information are lost during the max pooling operations in the encoder network, maintaining positional information for each up-sampling operation in the decoder network is critical for accurate pixel-wise segmentation [403]. U-Net is similar to SegNet in terms of having encoder-decoder architecture; however, instead of using the pooling indices in the max pooling step, U-net copies and crops a feature map in each encoder layer to the corresponding decoder layer to maintain local positional information. For the segmentation problem, maintaining local information is the key so that each architecture has its own way to transfer local details from shallower layers to deeper layers. SegNet and U-Net models outperformed FCN in classify WMs with predefined classes and unseen defects. However, they took much longer training time than FCN. Yu *et al.* in [92] constructed an algorithm based on CNN to recognize and classify WM defects. The proposed method was divided into two parallel approaches: offline modelling and online processing. In the offline modelling stage, a wafer defect pattern recognition model that consisted of two sub-models was constructed. These two sub-models were basically two CNNs, one of them was responsible for wafer defect pattern detection and the other for wafer defect pattern classification. Both CNNs consisted of three convolutional layers and three pooling layers, while the detection CNN consisted of two FC layers and the classification CNN consisted of three FC layers. Dropout method were used in both CNNs to avoid overfitting. Furthermore, PCA method were used in the classification CNN after the second FC layer to reduce the feature dimension and then features were normalized. In the online processing stage, the WM is pre-processed and used as an input to both CNN models. It was noticed in their study that the detection CNN has a simple structure and a fast computing speed compared with the classification CNN due to low probability of process faults in the actual manufacturing process. Their proposed method achieved an average detection accuracy of 93.13%, which outperformed the accuracy of other algorithm that were used for comparison. However, using PCA for feature reduction is redundant since CNN has the ability of considering the important features and discarding the unnecessary ones.

Most of the researchers that investigated WM defects using CNN are using simulated data to solve the problem of noisy and imbalanced data for WM pattern defect identification. In this way, they can improve the classification accuracy, but it becomes costly and time-consuming. Also, denoising the

actual data can destroy the actual defect patterns on the wafer images [60].

Cai *et al.* in [175] inspected the SMT solder joint defects in PCBs by using three types of CNNs. The entire sample images were fed to the first CNN (called CNN-1). Sub-regions which represent the ROI were selected from the entire images manually and fed to the second CNN (called CNN-2). The output for CNN-2 were used as an input for a third CNN (called CNN-3). The outputs for both CNN-1 and CNN-3 were used for classification of the SMT solder joint (Good or bad). The concept of the classification depends of the weighted some of both CNNs and the probability of each. The results of the inspection using this method was compared to other methods such as Bayes, SVM, G-MLP, GMM and ViBe. It was proved by experimental results that the proposed method overcame the others by remarkable percentage. However, their approach classified the solder joints as good or bad and did not consider classifying the defect type, which does not justify this study to use such a complex algorithm that is optimized for multi-class classification. Yuan *et al.* in [285] proposed a CNN-based approach to classify IR hole defects in mobile screen glass. In order to overcome the lack of training data, they proposed a data generation algorithm that consists of two steps, defect superposition, and data augmentation. The superposition step overlays defects on a chosen non-defected image in randomly selected locations with stochastic sizes, shapes, and severities. The defect images generated from single one template would naturally have the same scale, shape, and background color, making them not accord with the actual situation. Therefore, the augmentation step is applied followed the superposition step to augment the variety of the generated defect images. Finally, considerable manual labelled real images were collected and used to verify the proposed detection method.

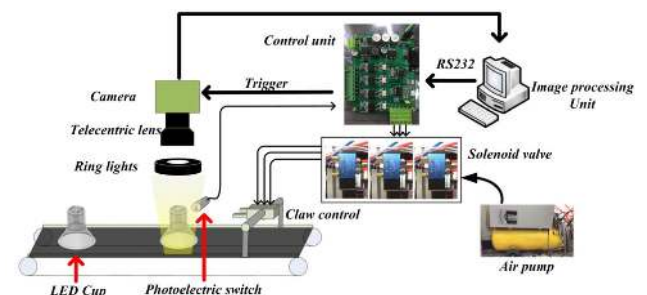
Due to complex and deep structure, CNN requires comparatively large-scale image data, a lot of hyper parameters tuning, high computational power (such as parallel GPUs), and long training time because of the large amount of labelled data used [60]. To overcome these problems, Yang *et al.* in [244] proposed transfer-learning-based approach called online sequential classifier and transfer learning (OSC-TL) to investigate Mura defects in FPDs. Unlike conventional CNN, which assumes that training data and future data must be in the same feature space and must have the same distribution, transfer-learning algorithm reuses the feature extractor portion of a previously trained network using existing large datasets and re-trains only the classification functionality using specific datasets appropriate for different classification tasks. The proposed OSC-TL uses a pretrained CNN using ImageNet LSVRC-2012 dataset for feature extraction step. Then two more modules are used for training and classification of the defects. The proposed algorithm was compared to other deep learning approaches and showed remarkable overperformance in terms of the computational time, while maintaining similar accuracy levels.

Tables 11,12,13,14, and 15 summarize the inspection algorithm details for selected research articles.

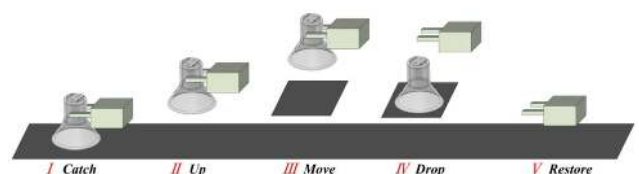
VI. SORTING MECHANISM

To complete the cycle of fully AOI system, some researchers considered establishing a sorting mechanism to separate products into different categories (e.g. good, recycle, scrap etc.) as shown in Figure 16. In order to do so, an industrial controller such as PLC is usually used to send a command (according to the decision received by the inspection algorithm) to the sorting system that consists of motors, cylinders and conveyor belt.

Yang *et al.* in [41] designed a control unit to perform the separation command by removing the defective LED cups from the production line for further considerations. A photoelectric sensor is used to send signal for the control unit indicating that an LED cup has entered the inspection region. Based on the inspection algorithm results, the control unit send a command to series of pneumatic system components such as air pump, air claws, solenoid valves and pneumatic cylinders to perform the task required as shown in Figure 45(a). The separation action is divided into five steps as shown in Figure 45(b). The cylinder is used for moving LED cup to the recovery area. Air claws are used for gripping the LED cup, while the cylinder is used for raising the LED cup up. Both the air claw and the cylinder are driven by solenoid valves and the air pressure is supplied by an air pump. Similar configuration was also considered by Sun *et al.* in [293] to inspect thermal fuse defects as shown in Figure 46. When a thermal fuse was first sorted and fed into the system, a proximity sensor is triggered and a transistor–transistor logic signal is sent to activate the CCD camera to acquire a digital image. The inspection algorithm was then initiated to detect defects in the fuses. If any defect



(a) Overview on the interaction between the separating mechanism with the other inspection modules



(b) Separation procedure

FIGURE 45. Separating mechanism proposed in [41].

TABLE 11. Optical inspection algorithm details for research articles that investigated semiconductor wafer defects.

Ref.	Feature Extraction & Selection Method	Main classification algorithm	Results		Inspection Time	Other algorithms (or studies) compared with main algorithm
			Detection Accuracy	Overall False Alarm Rate		
[64]	ART1	ART1	Up to 98.73%	-	3s/35samples	SOM
[119]	Thresholding & gray-level values	BPNN & MDC & MLC	95.8%(BPNN) 87.5%(MDC) 87.5%(MLC)	-	-	-
[65]	ART1	ART1	Up to 95%	-	3s/20samples	-
[111]	Thresholding	BPNN & RBF & LVQ	100%(BPNN) RBF(90%) 100%(LVQ)	-	<1s/die	-
[120]	Region growing & surface extraction	MLP	96.5%	2.5%	-	-
[58]	ART1	ART1 & Decision Tree	Up to 100%	-	<1min/pattern	-
[73]	Spatial correlogram	DTW clustering	90 - 100%	-	-	-
[78]	Spatial non-homogeneous Poisson process	Model-based clustering	96.6%	-	75s/wafer	[77]
[79]	Spatial non-homogeneous Poisson process	BCSF & BCNHPP	86.5-95.8% (BCSF) 86-95.5% (BCNHPP)	-	28.6-36.6s (BCSF) 276.8-375.3s (BCNHPP)	-
[84]	Angle & distance variations	Multi-class SVM	91.3725%	-	-	RBF
[76]	gHMT & DWT	MLC	Up to 100%	-	-	WT & HMT
[75]	GLCM (moment invariant)	SOM-SVM	>90%	-	-	SOM-BP
[126]	Template matching	Rule-based	98.9%	-	-	-
[127]	Segmentation	Rule-based	98.9% (Pattern recognition) 95.6% (Defect criticality)	-	-	-
[114]	Template matching & 2D DWT	Rule-based	-	-	0.91s/chip	-
[115]	Template matching & 1D FFT	Rule-based	-	-	0.62s/chip	2D FFT
[81]	nearest-neighbor clutter	Clustering	96.4%	-	15.73%	[78], [79]
[61]	SDC	Rule-based	Up to 90%	1 - 3%	<3s/wafer	-
[85]	Zooming strategy & ART1	Multi-step ART1	84 - 100%	-	≈6s (total)	ART1 without zooming
[59]	Hough transform	C4.5 & Logitboost	92%	-	-	NBC & bagging
[116]	-	SVM	95.6%	-	-	PLS, GRN, C4.5 & k-NN
[53]	Polar Fourier transform & RMI	ADTree	Up to 95%	-	10mins (Training time)	Bayesian and other modified decision tree classifiers
[95]	Morphological Operations	SVM	95%	5%	173s (Total)	Anomaly correlation
[117]	Feature point matching	Rule-based	94%	-	0.26s/24feature points	Subtration, NP subtraction, NCC & eigenvalue
[97]	Distance & statistical features	Random forest	>99%	-	-	-
[132]	Edge detection & template matching	Rule-based	97.4%	-	-	-
[106]	CNN	CNN	98.2%	-	0.13s/WM	-
[104]	CNN	CNN	97.4% (Moderate noise) 91% (severe noise)	-	-	SVM & MLP
[90]	Randon transform	Decision tree	90.5%	-	-	C4.5, ANN, Logistic & SVM
[108]	Splitter	RGRN & CNN	86.17%	-	-	RGRN, DSCN, RF, MLP, SVM & RBF
[103]	Voronoi regions	K-means & DDPFinder	>92%	-	≈10s (total)	SSRN, RGRN, GRN, SMO, PNN, MLP, SVN & RBF
[101]	Thresholding	Decision tree	95.6%	-	-	Bayes classifiers
[134]	CNN	k-NN & CNN	96.2%	-	1.813s (testing)	SAE, MLP & SVM
[93]	DNN	DNN (ESDN)	89.6%	0.05%	0.0294/WM	SDAE, DBN, BPN, & LR
[91]	CNN	Hybrid CNN (SCSDAE)	94.75% (Industrial) 95.13% (simulation)	-	-	SDAE, AlexNet, DBN, SVM, BPN, k-NN, & C4.5
[94]	AdaBalGAN	AdaBalGAN	96 - 100%	-	0.07s/piece	Adaboost, SVM, CNN & GAN
[92]	PCA	CNN	93.25%	-	2.1-5.7s/sample	SVM, C4.5 & [62]
[109]	Rotation invariant	MLP	92.3%	-	-	Boosting, RF, k-NN, & SVM

TABLE 12. Optical inspection algorithm details for selected articles that investigated PCB defects.

Ref.	Feature Extraction & Selection Method	Main classification algorithm	Results		Inspection Time	Other algorithms (or studies) compared with main algorithm
			Detection Accuracy	Overall False Alarm Rate		
[164]	Color intensities	Fuzzy set & LVQ	95.83%	-	-	SOM
[154]	Thresholding & bootstarp	Decision tree	97.87%	-	-	MDC & <i>k</i> -NN
[145]	Gray relational theory	Rule-based	97.5%	-	-	Distance measures
[155]	Entropy measures	Rule-based	-	-	1s/image	-
[153]	Thresholding & color features	Logistic regression tree	89.33%	-	-	MDC, <i>k</i> -NN, & Bayesian
[192]	Template matching	Rule-based	-	-	0.2s/3defects	Region merge & projection
[143]	Geometric & wavelet	MLP & LVQ	98.8%(MLP) 95.4%(LVQ)	-	-	<i>k</i> -NN
[165]	Geometric & wavelet	MLP	99.5%	-	1.3s (total)	LVQ
[146]	Projection profile, moment, zoning & contour profile	MLP	100%	0%	1.844 - 2.093s (feature extraction)	-
[168]	Reflection-area-based	Rule-based	95%	-	-	[405]
[158]	Segmentation	Rule-based	97.3%	2.7%	-	-
[202]	Otsu & entropy	Rule-based	96.43%	-	0.7s/image	-
[203]	Edge detection, Color information & MLP	MLP	96%	-	1.05s/image	-
[169]	-	LVQ	Up to 100%	0%	-	-
[193]	Template matching	Rule-based	Up to 100%	-	125s (total)	-
[166]	Geometric & wavelet	Neuro-fuzzy	97.8%	-	-	MLP & LVQ
[184]	Template matching & PSO	Rule-based	Up to 100%	-	≈1min/image	GA
[180]	DWT & Template matching	Rule-based	76.2 - 96.7%	-	8 - 183ms/image	DCT
[159]	Geometrical & color features / Advanced adaboost	CART	97.2%	≈0.6%	8.6ms/IC chip	Conventional adaboost
[160]	Shape, digital & logical	Rule-based	98.6%	≈1.45%	-	[143], [164], [406]
[167]	Geometric features	Fuzzy rules	97.83%	-	-	[166]
[194]	Template matching & edge detection	SVM	93.5%	-	124ms/image	[193]
[178]	BICF	Nearest neighbor	97.5%	-	-	LLSTA, LPP, NPE, LDA, DLA & PNDA
[185]	Template matching (NCC) & PSO	Rule-based	Up to 100%	-	3.19 - 28.41s/3 resistor-network	-
[188]	PICC	Rule-based	Up to 100%	0%	0.3s/image	NCC
[171]	NCC & color features	Bayes & SVM	100%	-	0.53s (SVM)	Decision tree, <i>k</i> -NN & BPNN
[162]	Segmentation & template matching	Rule-based	97.96%	2.61%	-	[158], [161], [168], [405], [406]
[172]	NCC & color features	BPNN	98.46%	0%	-	Decision tree & SVM
[163]	Region, evaluation, & color grads features	Rule-based (Boolean rules)	97.7%	-	11s/PCB	[160], [161], [167], [168]
[31]	LDIM	Rule-based	100%	0%	-	-
[173]	ViBe	Rule-based	Up to 100%	0.9%	0.52s inspection	SDL, SAM & G-MLP
[174]	RPCA	Rule-based	Up to 100%	0.72%	-	ViBe, SAM & SDL
[207]	Modified Hough transform	Rule-based	97.89%	-	160ms/BGA	Ground truth, Samsung SMT482 & HALCON
[136]	Line-based clustering	Rule-based	100%	-	<200ms/BGA	Samsung SMT482
[186]	Model-based	Rule-based	97.73 - 99.46%	0.54-2.27%	13.7-16.8ms	HALCON & SM482
[176]	Adaptive template	Rule-based	100%	0%	-	ViBe, SDL, SAM& RPCA
[199]	Systematic matrix	Rule-based	Up to 100%	0.05%	1.64s (total)	[52], [198], [407], [408]
[196]	Textural features & PCA	SVM	81.39%	-	-	Bayes, MLP, decision tree, logistic regression & gradient boost
[195]	SURF	Random forest & WKDE	≈91%	-	-	-
[209]	Model-based	K-means	100%	-	-	-
[137]	INCC	Rule-based	>96%	-	-	NCC
[139]	Regional and color features & GA	SVM, MLP & decision tree	94.9%(SVM) 94.6%(MLP) 43.6%Decision tree	-	3.7ms/component	-
[148]	Same in [150]–[152]	K-means, FCM, & Mean-shift	98 - 100%	2.2 - 12%	-	-
[147]	Template matching	Rule-based	-	-	31ms/image	[409], [410]
[200]	Template matching & FFT	Rule-based	100%	0%	0.038s/16subimage	-

TABLE 13. Optical inspection algorithm details for selected articles that investigated FPD defects.

Ref.	Feature Extraction & Selection Method	Main classification algorithm	Results		Inspection Time	Other algorithms (or studies) compared with main algorithm
			Detection Accuracy	Overall False Alarm Rate		
[237]	Regression fitting	Rule-based	-	-	0.49s/ image	-
[257]	SVD	Rule-based	-	-	0.2 - 1.51s/image	-
[258]	SVD	Rule-based	-	≈6%	-	-
[252]	FFT	Rule-based	-	-	2ms/line image	-
[261]	Thresholding	Rule-based	>70%	0.02%	-	-
[268]	Segmentation & LLE	SVDD	98%	2.41%	4s/image	PCA & SOM
[240]	DCT	Rule-based	-	-	<75ms/image	-
[253]	NCC	Rule-based	-	-	18μs/line image	-
[269]	KPCA	ISVM	96%	-	<1s (total)	k-NN
[245]	T ² Hotelling & ACO	BPNN	Up to 100%	-	-	Otsu & without ACO
[354]	NCC & ICA	Rule-based	-	0.17%	2ms/image	Fourier analysis
[264]	Thresholding	RBF, BPNN, LVQ1 & LVQ2	87%(RBF) 93%(BPNN) 93%(LVQ1) 97%(LVQ2)	-	<0.5s/defect image	-
[212]	GLCM	Fuzzy-SVDD	Up to 98.9%	2.23-5.29%	11s (total)	SVDD
[247]	Regression diagnostics	Rule-based	-	0%	0.8s/image	[237]
[260]	Adaptive thresholding	Rule-based	78% (precision)	-	>0.203s/image	-
[246]	ICA	Rule-based	-	-	8.1ms/image	-
[249]	Optical flow	Rule-based	-	-	0.054s/image	-
[248]	Modified Hough transform	Rule-based	-	0%	0.696s/image	Hough transform
[271]	Segmentation	F-SVDD	95%	-	7.8s/panel	SVDD
[271]	Segmentation	QK-SVDD	96%	7.54%	60ms/panel	SVDD
[267]	PCA	Rule-based	-	-	0.032s/image	FFT
[219]	LBF	Rule-based	>99% (precision & recall)	0.63%	6.61s (total CPU time)	PF, ICA & MCV
[221]	Thresholding	MLP	-	-	<1s/panel image	-
[272]	Segmentation	Tagushi-BPNN	94%	-	-	-
[282]	Segmentation & PCA	Rule-based	90%	6%	<0.53s/image	-
[214]	GLCM	BPNN	83.3%	-	-	-
[263]	DWT, GLCM & PCA	SVM	89.5%	-	-	MLP & CART
[273]	Template matching & segmentation	BPNN & MDC	93.7%(BPNN) 96.8%(MDC)	-	-	-
[287]	Gray-value & OMP	Rule-based	91.5%	12%	1.15s/image	-
[288]	Segmentation	Rule-based	94 - 99%	-	5.1s/defect	-
[218]	Haar WT & Thresholding	OCSVM	91.7%	-	-	GA & PCO
[15]	Color matching	Rule-based	71.10 - 96.91%	-	2.07s/image	[219], [247]
[234]	NDF & GLCM	Random forest	87 - 98%	-	0.07-0.11ms/defect	DCT, RPCA & Otsu
[284]	CR & IFCM	Rule-based	-	-	1.6601s (total)	Kittler, Niblack & Otsu
[283]	Multifractal features	SVM & ECS	96.61%	1 - 2%	4.4268s (testing)	SVM, B-SVM, US, ROS, SMOTE, GMM, k-NN & Adaboost
[281]	local inlier-outlier ratios augmented with modified LBP	A-SVDD	>96%	≈0.5%	11.3-20.2s training/dataset	[241], [257], [411]-[413]
[215]	JFR-DRF	SVM	Up to 95%	-	-	Handcraft & K-means
[250]	MSCDAE	MSCDAE	≤92.04%(Precision)	-	-	-
[228]	FFT & GLCM	BPNN & RBFNN	98.9%(BPNN) 97.3%(RBFNN)	-	2.57s/image	-
[243]	OPBC & RGLS	Rule-based	Up to 100%	-	8.12s (total)	[242]
[244]	OSC-TL	OSC-TL	≈92%	-	1.5ms/image	DNN+ELM, DNN+SVM & DNN+MLP
[285]	CNN	CNN	98.26%	0.588%	-	-
[286]	Regularized Autoencoder	Regularized Autoencoder	-	-	313ms/image	Segmentation & SVD
[233]	Thresholding	Rule-based	94.2%	-	0.068 - 11.163s /image	DWT, DCT & linear regression
[256]	MS-FCAE	MS-FCAE	98.1%(precision) 92.1%(recall)	-	19321ms/dataset	LCA, PHOT, TEXEMS, ACAE, RCAE & MSCDAE
[227]	Segmentation	SVR	≈80%	-	<10ms/defect	-
[255]	Thresholding	MLP & CNN	86.13%	-	-	-

TABLE 14. Optical inspection algorithm details for research articles that investigated LED defects.

Ref.	Feature Extraction & Selection Method	Main classification algorithm	Results		Inspection Time	Other algorithms (or studies) compared with main algorithm
			Detection Overall Accuracy	False Alarm Rate		
[39]	Segmentation	Rule-based	90%	-	200ms	-
[36]	Wavelet transform & T^2 Hotelling	WNN & WMS	95%(WNN) 92%(WMS)	7.5%(WNN) 5.8%(WMS)	-	Otsu-thresholding
[44]	CCL	HNN	95%	-	22ms/die	BPNN, LVQ, RBF, K-means, FCM
[40]	BDCT	Rule-based	95.8%	4.2%	0.82s/image	WNN and Otsu method
[37]	Otsu-thresholding	Rule-based	95%	7.1%(Type1) 14.7%(Type2)	<0.3s/image	-
[50]	Segmentation	RBFNN	92.5%	-	8.87ms/die	LVQ and K-means
[52]	Optical flow	Rule-based	100%	0%	12ms/image	NCC and Lucas-Kanade
[20]	PCC	One-class SVM	100%	0.13%	1 - 10ms	-
[38]	BDCT	Rule-based	99.67%	0.13%	0.32s/image	Otsu method
[45]	NCC and Thresholding	K-means & MLP	97.83%	-	-	-
[33]	Otsu-thresholding	Rule-based	94.34%(LED _{1S}) 95.17%(LED _{1B}) 96.02%(LED ₂)	-	-	-
[48]	NCC and Segmentation	Rule-based	Up to 99%	Up to 2%	0.9ms/chip	-
[41]	CNN	CNN	100%	8%	<1s/cup	-
[47]	CNN	CNN	94.96%	-	-	[45]
[46]	Correlation coefficient & PCA	SVM & DTSVM	96%	-	1s(SVM) 1s(DTSVM)	-
[42]	Thresholding	Rule-based	98.25%	-	-	-

TABLE 15. Optical inspection algorithm details for research articles that investigated miscellaneous defects.

Ref.	Feature Extraction & Selection Method	Main classification algorithm	Results		Inspection Time	Other algorithms (or studies) compared with main algorithm
			Detection Overall Accuracy	False Alarm Rate		
[292]	T^2 Hotelling & DWT	Rule-based	93.75%	6.4%	≈3s(total)	-
[291]	T^2 Hotelling & DWT	Rule-based	95%	3.2%	0.8s/image	-
[298]	DCT	Rule-based	94.74%	15%	4s/DCT	-
[289]	Segmentation	MLP & Rule-based	99.6%	-	5s/defect	-
[294]	Segmentation	CART	94%	5%	-	-
[290]	Template matching & DWT	Rule-based	96.44%	-	1.05s/sample	-
[295]	Segmentation & similarity matching	SVM	Up to 100%	4.2%	-	-
[299]	NSCT & adaptive thresholding	Rule-based	98.7%	-	0.1s/capacitor	-
[293]	Segmentation	MLP & LVQ	98.5%(MLP) 91.27%(LVQ)	-	0.318s(MLP) 0.297s(LVQ)	-
[296]	Segmentation	SVM	95.83%	-	15s/image	-
[297]	Hough Transform	SVM	93.44%	7.69%	0.051s (testing)/image	k-NN & ANN

was found, a signal is sent to the controller to screen out the defective fuse by a designed mechanism. Authors in [49], [299] have also proposed sorting mechanisms for inspecting LEDs and ceramic capacitors respectively.

VII. LIMITATIONS OF AOI SYSTEMS & FUTURE DIRECTIONS

Despite of the AOI systems' advantages mentioned in sections I and II of this article, many limitations are still facing these systems. One of the major limitations is the precise calibration and configuration needed for the system to provide adequate results. This limitation can narrow the

system's ability to be adaptable for various products and makes it more specific for certain product measurements and features. Illumination variations is also one of the major concerns for these systems, such as the illumination settings must remain constant and/or controlled to avoid unwanted shadows or light noises that may confused with defects. Therefore, research must be directed towards the development of real-time devices that do not get affected by operating or environmental conditions [414].

The viewing angles of image acquisition systems are most of the time limited to certain predefined 2D plane of the inspected component. Yang *et al.* in [299] provided a solution

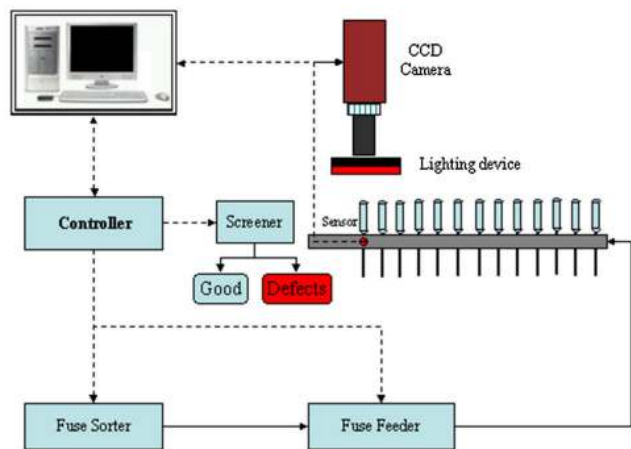


FIGURE 46. System configuration proposed by Sun *et al.* in [293].

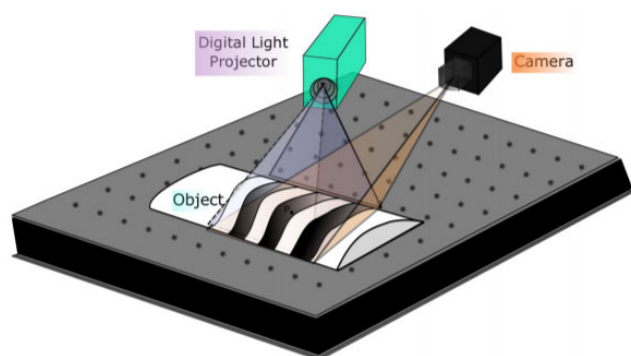


FIGURE 47. 3D acquisition system proposed in [415].

for this problem by implementing multiple image acquisition systems to acquire different views for the inspected film capacitors as shown in Figure 28. However, this solution is considered costly and needs special alignment. 3D optical inspection techniques proposed by Madrigal *et al.* in [415] can be considered an effective tool to mitigate these problems and to provide full description of the component 3D nature. Their proposed system uses structured light projection to help in acquiring the 3D nature of the object as shown in Figure 47. This system can be very useful in investigating PCB defects such as solder joints and IC components. Furthermore, authors in [416], [417] suggested robot arms for various industrial inspection and recognition tasks, which may provide more flexibility and mobility towards accessing different angle views of the inspected product. AOI systems are in general excellent tool in detecting external surface defects; however, it becomes cumbersome to investigate internal defects or any other defect that the system is not programmed to look for. Although X-ray and thermography can partially solve the problem of detecting internal defects; however, these systems are effective in inspecting certain electronic products such as PCBs and BGAs.

When integrating AOI techniques with machine learning, large number of samples are needed for the training process,

especially when implementing deep learning algorithm. This may force industries to rely on simulated data or mathematical models for providing enough training samples, which may not be sufficient in representing the defect features. Therefore, various electronic industries should consider building a relevant image database for their product defects to enhance their future optical inspection algorithm's performance.

VIII. CONCLUSION

Quality monitoring is essential step for minimizing product's defects in various industries. AOI is considered one of the simplest and commonly used quality monitoring approaches used for automatic industrial inspection. The field of AOI is vast as it involves a variety of subjects ranging from hardware setups for image acquisition to inspection and decision-making algorithms. For this reason, the research opportunities in this field are wide open and have the potential to improve in the near future.

Many electronics manufacturers are integrating AOI systems in their production steps to avoid human inspectors' extra cost and possible errors. The majority of these manufacturers are located in Asia. In this study, we reviewed and critiqued more than 300 articles that used AOI systems and algorithms to investigate various defects in electronics industry. During our searching process for relevant papers to be reviewed, we have found that AOI systems are widely used in four major applications: semiconductor wafers, FPDs, PCBs, and LEDs defect detection. Various types of defects were considered for each inspected component. Semiconductor wafer defects are usually inspected according to their distinguished defect patterns. Solder joints and IC component defects are commonly inspected defects in PCB industry. TFT-LCD defects are widely investigated using AOI among other types in FPD industry. Unlike previously mentioned electronic components, we observed that there are more variety of defects investigated using AOI in LED industry such as apertures, LED chips, SMD-LED and cosmetic defects. Other miscellaneous electronic components were also considered in this review such as camera modules, thermal fuses, and passive electronic components.

Hardware and software setups play vital role in the quality of the acquired image for inspection. We found in this paper that these setups can also affect the accuracy and false alarm rates of the final classification results. Environmental and variable illumination settings are avoided in AOI systems since they increase noise and false alarms. Customized illumination can be used in some applications for better defect description such as using tiered illumination for PCB solder joint inspection to capture the 3D nature of the inspected component. In this article, the advantages and limitations for different illumination settings used have been highlighted. Selecting the right image sensor and lens for inspection is also important. Many factors are considered in the selection process such as size of the inspected component, field of view, frame rate and resolution. While most of image samples are acquired using image sensors alone, auxiliary systems such

as OCT and SEM have been also used to aid the process. Thermography and X-ray can be also used to acquire sample images for certain applications such as in PCB and BGA inspection. Circuit probe inspection is widely used to investigate semiconductor wafer defects such that WM images can be generated for defect classification.

Inspection algorithms that process the acquired images were also introduced. Three main stages are used in applying the inspection algorithm: preprocessing, feature extraction & selection and classification. In preprocessing, several filtering, denoising and geometrical operations are applied to the acquired image. This is very useful in removing the unwanted noise that affects the classification decision. Denoising is essential step in removing random defects from WM patterns such that inspected samples can be classified according to the systematic defect. In the feature extraction & selection, the algorithm tries to isolate and locate the defective features in the image. Several statistical and geometrical measurements are also used to assess the features of defect. Segmentation and template matching are two well-used feature extraction algorithms according to the reviewed papers. Feature selection process can reduce the number of redundant extracted features such that the algorithm performs much faster. PCA is one of the mostly used algorithms for feature selection. Finally, classification is the decision-making stage of inspection algorithm. Rule-based and learning-based are two classification approaches used in the reviewed papers. In rule-based, a set of pre-programmed if-then rules are used to assess the features acquired from the previous step. In learning-based classification, supervised and unsupervised machine learning algorithms such as k -NN, Bayes, decision trees, SVM, clustering and ANNs are used for the classification process. Unsupervised machine learning algorithms are widely used in finding WM patterns to investigate semiconductor wafer defects, while supervised learning techniques are used in the rest of studies. In general, machine learning algorithms overcome rule-based learning by their ability to find anomalies in the input data (features) based on the training process and without any need of customized programming. However, overfitting and imbalanced data are two major drawbacks in using learning-based algorithm. These two problems can be solved by having sufficient data for each defect class considered or by applying several techniques such as regularization and bootstrapping.

Many recent articles have also used deep learning algorithms in investigating defects. The recent development of CNNs such as AlexNet opened the door for these models to be used in AOI tasks. Deep learning models can do preprocessing, feature extraction & selection and classification all at once within their hidden layers. In deep learning layers, many complex features can be captured that traditional feature extraction approaches may fail to recognize. The detection accuracy can be also improved using deep learning due to the large number of parameters used in training the models. Despite previously mentioned advantages, deep learning models are considered data hungry.

Furthermore, it requires large processing and GPU capabilities. The large data required for training are essential in providing high accuracy and to avoid overfitting. Several data augmentation approaches are used to address this issue such as using GAN. Transfer learning can be used to avoid large memory usage by implementing pretrained deep learning models.

AOI systems are still facing some limitations that require further improvements. For instance, they are most of the time limited for inspecting surface defects. Furthermore, the viewing angles for the inspected components are usually fixed to certain angles which may prevent the system to miss some parts. Robot arm and 3D inspection approaches can be used to mitigate these problems.

The current technologies and algorithms used in this review are currently being tested and some of them will be implemented in EU funded project called IQONIC that uses AOI technologies to investigate optoelectronics defects.

APPENDIX

SEARCHING CRITERIA & KEYWORDS SELECTION

The most logical choice of keywords that is relevant to the main scope of this research would be “Optical Inspection” AND “Electronic component”. However, researchers tend to use the specific electronic component that they are analyzing for the title and keyword indexing in their research articles instead of using general terms such as electronic parts. Therefore, it is not straightforward task to choose one keyword to follow in this research. In order to overcome this problem, more general keywords were used such as “Inspection” AND (“Machine Vision” OR “Computer Vision”). Even though the previous keyword will show many irrelevant results (the total is around 7000 results); however, it makes it possible to choose the relevant research articles manually. It has been found from the previous keyword search that a lot of researchers who studied electronics defects focused their attention to printed circuit boards PCBs, semiconductor wafers, light emitting diodes LEDs, flat panel displays FPDs, and other miscellaneous components such as passive electronics and camera modules. According to that, the keywords were adjusted to explore more about the most commonly investigated defects. The new keywords are:

- “Optical Inspection” AND “LED”
- “Optical Inspection” AND “Wafer”
- “Optical Inspection” AND “PCB”
- “Optical Inspection” AND “FPD”

Manual searching technique were also conducted by exploring the references used in the reviewed papers.

LIST OF ABBREVIATIONS

The acronyms and abbreviations used throughout the review and their definitions are listed below:

A-SVDD	Adaptive Support Vector Data Description	IFCM	Improved Fuzzy c-means Clustering
ACO	Ant Colony Optimization	INCC	Improved Normalized Cross Correlation
ADTree	Alternating Decision Tree	IR-CUT	Infrared Cut-off
AE	Autoencoder	k-NN	k-Nearest Neighbor
ANN	Artificial Neural Network	KPCA	Kernel Principle Component Analysis
ANOVA	Analysis of Variance	LBF	Local Binary Fitting
AOI	Automatic Optical Inspection	LBP	Local Binary Patterns
ART	Adaptive Resonance Theory	LCD	Liquid Crystal Display
AS-PSO	Accelerated Particle Swarm Optimization	LCL	Lower Control Limit
BDCT	Block Discrete Cosine Transform	LDIM	Localized Defects Image Model
BGA	Ball Grid Array	LED	Light Emitting Diode
BPNN	Back Propagation Neural Network	LVQ	Learning Vector Quantization
CART	Classification and Regression Tree	MCV	Markov Concurrent Vision
CCD	Charge-coupled Device	MDC	Minimum Distance Classifier
CCL	Connected Component Labelling	MKSVR	Multiple Kernel Support Vector Regression
CH	Contact Hole	MLP	Multi-layer Perceptron
CMOS	Complementary Metal-oxide Semiconductor	MS-FCAE	Fully Convolutional Autoencoder
CMP	Chemical Mechanical Process	MSCDAE	Multiscale Convolutional Denoising Autoencode
CNN	Convolutional Neural Network	MSE	Mean Square Error
COB	Chip-on-board	NCC	Normalized Cross Correlation
CR	Contour-based Registration	NDF	Neighboring Difference Filter
DAE	Denoising Autoencoder	NSCT	Non-subsampled Contourlet Transform
DBSCAN	Density-based Spatial Clustering of Applications with Noise	OCSVM	One-class Support Vector Machine
DCT	Direct Cosine Transform	OCT	Optical Coherence Tomography
DDPFinder	Dominant Defective Patterns Finder	OLED	Organic Light Emitting Diode
DFT	Discrete Fourier Transform	OPBC	Outlier prejudging-based Image Background Construction
DIP	Dual-in-line Package	OSC-TL	Online Sequential Classifier and Transfer Learning
DNN	Deep Neural Network	PC	Principle Component
DRAM	Dynamic-random Access Memory	PCA	Principle Component Analysis
DTSVM	Decision Tree Support Vector Machine	PCB	Printed Circuit Board
DTW	Dynamic Time Wrapping	PCC	Pearson's Correlation Coefficient
DWT	Direct Wavelet Transform	PE	Pixel Electrode
ECS	Example Contribution	PICC	Partial Information Correlation Coefficient
ESDAE	Enhanced Stacked Denoising Autoencoder	PLC	Programmable Logic Controller
EWMA	Exponentially Weighted Moving Average	PLED	Polymer Light Emitting diode
E-M	Expectation-maximization	PLS	Partial Least Squares
F-SVDD	Fast Support Vector Data Description	PR	Pixel Resolution
FCN	Fully Connected Network	PSO	Particle Swarm Optimization
FFT	Fast Fourier Transform	QK-SVDD	Quasiconformal Kernel Support Vector Data Description
FOV	Field of View	RBF	Radial-basis Function
FPD	Flat Panel Display	RGRN	Randomized General Regression Network
FR	Frame Rate	RMI	Rotational Moment Invariants
FVCP	Fuzzy Variable of Clustering Pattern	ROI	Region of Interest
GA	Genetic Algorithm	RPCA	Robust Principle Component Analysis
GAN	Generative Adversarial Network	SAE	Sparse Autoencoder
GB	Gradient Boosting	SD	Source and Drain
GE	Gate Electrode	SDAE	Stacked Denoising Autoencoder
gHMT	Growing Wavelet Hidden Markov Tree		
GLCM	Graylevel Co-occurrence Matrix		
GRN	General Regression Network		
HDR	High-dynamic-range		
HNN	Hopfield Neural Network		
HP	High Power		
IC	Integrated Circuit		
ICA	Independent Component Analysis		

SDC	Segmentation, Detection, and Cluster-Extraction
SE	Semiconductor Electrode
SEM	Scanning Electron Microscope
SMD	Surface-mounted Device
SMOTE	Synthetic Minority Over-sampling Technique
SMT	Surface Mount Technology
SOM	Self-organising Map
SPC	Statistical Process Control
SURF	Speeded Up Robust Feature Extraction
SVC	Support Vector Clustering
SVD	Singular Value Decomposition
SVDD	Support Vector Data Description
SVM	Support Vector Machine
SVR	Support Vector Regression
SZ	Sensor Size
TCS	Truncated Component Solution
TFT	Thin-film Transistor
THT	Through Hole Technology
UCL	Upper Control Limit
ViBe	Visual Background extraction
WBM	Wafer Bin Map
WD	Working Distance
WKDE	Weighted kernel density estimation
WM	Wafer Map
WMS	Wavelet-based Multivariate Statistical
WNN	Wavelet-based Neural Network
WTA	Winner Take All
WTMS	Wavelet Transform Modulus Sum

REFERENCES

- [1] J. A. C. Soto, F. Tavakolizadeh, and D. Gyulai, "An online machine learning framework for early detection of product failures in an industry 4.0 context," *Int. J. Comput. Integr. Manuf.*, vol. 32, nos. 4–5, pp. 452–465, May 2019.
- [2] Y. Liu, C. Jiang, and H. Zhao, "Using contextual features and multi-view ensemble learning in product defect identification from online discussion forums," *Decis. Support Syst.*, vol. 105, pp. 1–12, Jan. 2018.
- [3] T. Zimmermann, G. Ciuti, M. Milazzo, M. Chiurazzi, S. Roccella, C. M. Oddo, and P. Dario, "Visual-based defect detection and classification approaches for industrial applications—A survey," *Sensors*, vol. 20, no. 5, pp. 1–25, 2020.
- [4] T. D'Orazio, M. Leo, A. Distanto, C. Guaragnella, V. Pianese, and G. Cavaccini, "Automatic ultrasonic inspection for internal defect detection in composite materials," *NDT & E Int.*, vol. 41, no. 2, pp. 145–154, Mar. 2008.
- [5] S. Gholizadeh, "A review of non-destructive testing methods of composite materials," *Procedia Struct. Integrity*, vol. 1, pp. 50–57, Jan. 2016.
- [6] J. García-Martín, J. Gómez-Gil, and E. Vázquez-Sánchez, "Non-destructive techniques based on eddy current testing," *Sensors*, vol. 11, no. 3, pp. 2525–2565, Feb. 2011.
- [7] S. Mukhopadhyay, "Novel planar electromagnetic sensors: Modeling and performance evaluation," *Sensors*, vol. 5, no. 12, pp. 546–579, Dec. 2005.
- [8] K. Chomsuwan, S. Yamada, and M. Iwahara, "Bare PCB inspection system with SV-GMR sensor eddy-current testing probe," *IEEE Sensors J.*, vol. 7, no. 5, pp. 890–896, May 2007.
- [9] T. G. Santos, R. M. Miranda, and C. C. R. de Carvalho, "A new NDT technique based on bacterial cells to detect micro surface defects," *NDT & E Int.*, vol. 63, pp. 43–49, Apr. 2014.
- [10] P. Aryan, S. Sampath, and H. Sohn, "An overview of non-destructive testing methods for integrated circuit packaging inspection," *Sensors*, vol. 18, no. 7, p. 1981, Jun. 2018.
- [11] S.-C. Horng, F.-Y. Yang, and S.-S. Lin, "Applying PSO and OCBA to minimize the overkills and re-probes in wafer probe testing," *IEEE Trans. Semicond. Manuf.*, vol. 25, no. 3, pp. 531–540, Aug. 2012.
- [12] M.-J.-J. Wang and C.-L. Huang, "Evaluating the eye fatigue problem in wafer inspection," *IEEE Trans. Semicond. Manuf.*, vol. 17, no. 3, pp. 444–447, Aug. 2004.
- [13] R. T. Chin and C. A. Harlow, "Automated visual inspection: A survey," *IEEE Trans. Pattern Anal. Mach. Intell.*, vol. PAMI-4, no. 6, pp. 557–573, Nov. 1982.
- [14] M. H. Kim, T. Weyrich, and J. Kautz, "Modeling human color perception under extended luminance levels," *ACM Trans. Graph.*, vol. 28, no. 3, pp. 1–9, Jul. 2009.
- [15] G. Nam, H. Lee, S. Oh, and M. H. Kim, "Measuring color defects in flat panel displays using HDR imaging and appearance modeling," *IEEE Trans. Instrum. Meas.*, vol. 65, no. 2, pp. 297–304, Feb. 2016.
- [16] A. R. Rao, "Future directions in industrial machine vision: A case study of semiconductor manufacturing applications," *Image Vis. Comput.*, vol. 14, no. 1, pp. 3–19, 1996.
- [17] S.-H. Huang and Y.-C. Pan, "Automated visual inspection in the semiconductor industry: A survey," *Comput. Ind.*, vol. 66, pp. 1–10, Jan. 2015.
- [18] J. Chen and X. Ran, "Deep learning with edge computing: A review," *Proc. IEEE*, vol. 107, no. 8, pp. 1655–1674, Aug. 2019.
- [19] R. Huang, J. Gu, X. Sun, Y. Hou, and S. Uddin, "A rapid recognition method for electronic components based on the improved YOLO-V3 network," *Electronics*, vol. 8, no. 8, p. 825, 2019.
- [20] F. Timm and E. Barth, "Novelty detection for the inspection of light-emitting diodes," *Expert Syst. Appl.*, vol. 39, no. 3, pp. 3413–3422, 2012.
- [21] Y.-J. Cha, W. Choi, and O. Büyükoztürk, "Deep learning-based crack damage detection using convolutional neural networks," *Comput.-Aided Civil Infrastruct. Eng.*, vol. 32, no. 5, pp. 361–378, May 2017.
- [22] T. Brosnan and D.-W. Sun, "Improving quality inspection of food products by computer vision—A review," *J. Food Eng.*, vol. 61, no. 1, pp. 3–16, Jan. 2004.
- [23] A. Kumar, "Neural network based detection of local textile defects," *Pattern Recognit.*, vol. 36, no. 7, pp. 1645–1659, Jul. 2003.
- [24] Z. Xue-Wu, D. Yan-Qiong, L. Yan-Yun, S. Ai-Ye, and L. Rui-Yu, "A vision inspection system for the surface defects of strongly reflected metal based on multi-class SVM," *Expert Syst. Appl.*, vol. 38, no. 5, pp. 5930–5939, May 2011.
- [25] J. Ker, L. Wang, J. Rao, and T. Lim, "Deep learning applications in medical image analysis," *IEEE Access*, vol. 6, pp. 9375–9379, 2017.
- [26] S. Lv, H. Kim, B. Zheng, and H. Jin, "A review of data mining with big data towards its applications in the electronics industry," *Appl. Sci.*, vol. 8, no. 4, pp. 1–34, 2018.
- [27] *Global Consumer Electronics Manufacturing Industry—Market Research Report*, IBISWorld, Los Angeles, CA, USA, 2019.
- [28] M. Liukkonen, E. Havia, and Y. Hiltunen, "Computational intelligence in mass soldering of electronics—A survey," *Expert Syst. Appl.*, vol. 39, no. 10, pp. 9928–9937, Aug. 2012.
- [29] D.-M. Tsai and Y.-C. Hsieh, "Machine vision-based positioning and inspection using expectation-maximization technique," *IEEE Trans. Instrum. Meas.*, vol. 66, no. 11, pp. 2858–2868, Nov. 2017.
- [30] S. Gebus and K. Leiviskä, "Knowledge acquisition for decision support systems on an electronic assembly line," *Expert Syst. Appl.*, vol. 36, no. 1, pp. 93–101, Jan. 2009.
- [31] Y. Xie, Y. Ye, J. Zhang, L. Liu, and L. Liu, "A physics-based defects model and inspection algorithm for automatic visual inspection," *Opt. Lasers Eng.*, vol. 52, pp. 218–223, Jan. 2014.
- [32] R. Carnell, N. Mapa, I. Pang, and P. Sakpal, "Asia and the global tech slump: The chips are down," ING, Amsterdam, The Netherlands, Tech. Rep., 2019. [Online]. Available: <https://think.ing.com/reports/asia-and-the-global-tech-slump-the-chips-are-down>
- [33] D.-B. Perng, H.-W. Liu, and S.-H. Chen, "A vision-based LED defect auto-recognition system," *Nondestruct. Test. Eval.*, vol. 29, no. 4, pp. 315–331, Oct. 2014.
- [34] *Energy Savings Potential of Solid-State Lighting in General Illumination Applications*, U.S. Dept. Energy, Washington, DC, USA, 2012.

- [35] C.-C. Hsu and M.-S. Chen, "Intelligent maintenance prediction system for LED wafer testing machine," *J. Intell. Manuf.*, vol. 27, no. 2, pp. 335–342, Apr. 2016.
- [36] H.-D. Lin, "Automated defect inspection of light-emitting diode chips using neural network and statistical approaches," *Expert Syst. Appl.*, vol. 36, no. 1, pp. 219–226, Jan. 2009.
- [37] D.-B. Perng, H.-W. Liu, and C.-C. Chang, "Automated SMD LED inspection using machine vision," *Int. J. Adv. Manuf. Technol.*, vol. 57, nos. 9–12, pp. 1065–1077, Dec. 2011.
- [38] Y.-S. Chiu and H.-D. Lin, "An innovative blemish detection system for curved LED lenses," *Expert Syst. Appl.*, vol. 40, no. 2, pp. 471–479, Feb. 2013.
- [39] M. H. A. Fadzil and C. J. Weng, "LED cosmetic flaw vision inspection system," *Pattern Anal. Appl.*, vol. 1, no. 1, pp. 62–70, Mar. 1998.
- [40] H.-D. Lin and S. W. Chiu, "Flaw detection of domed surfaces in LED packages by machine vision system," *Expert Syst. Appl.*, vol. 38, no. 12, pp. 15208–15216, Nov. 2011.
- [41] Y. Yang, Y. Lou, M. Gao, and G. Ma, "An automatic aperture detection system for LED cup based on machine vision," *Multimedia Tools Appl.*, vol. 77, no. 18, pp. 23227–23244, Sep. 2018.
- [42] C.-F.-J. Kuo, T.-Y. Fang, C.-L. Lee, and H.-C. Wu, "Automated optical inspection system for surface mount device light emitting diodes," *J. Intell. Manuf.*, vol. 30, no. 2, pp. 641–655, Feb. 2019.
- [43] M. Bürmen, F. Pemuš, and B. Likar, "Automated optical quality inspection of light emitting diodes," *Meas. Sci. Technol.*, vol. 17, no. 6, pp. 1372–1378, Jun. 2006.
- [44] C.-Y. Chang, C.-H. Li, S.-Y. Lin, and M. Jeng, "Application of two hopfield neural networks for automatic four-element LED inspection," *IEEE Trans. Syst., Man, Cybern. C, Appl. Rev.*, vol. 39, no. 3, pp. 352–365, May 2009.
- [45] C.-F.-J. Kuo, C.-T.-M. Hsu, Z.-X. Liu, and H.-C. Wu, "Automatic inspection system of LED chip using two-stages back-propagation neural network," *J. Intell. Manuf.*, vol. 25, no. 6, pp. 1235–1243, Dec. 2014.
- [46] C.-F.-J. Kuo, C.-P. Tung, and W.-H. Weng, "Applying the support vector machine with optimal parameter design into an automatic inspection system for classifying micro-defects on surfaces of light-emitting diode chips," *J. Intell. Manuf.*, vol. 30, no. 2, pp. 727–741, Feb. 2019.
- [47] H. Lin, B. Li, X. Wang, Y. Shu, and S. Niu, "Automated defect inspection of LED chip using deep convolutional neural network," *J. Intell. Manuf.*, vol. 30, no. 6, pp. 2525–2534, Aug. 2019.
- [48] F. Zhong, S. He, and B. Li, "Blob analysis-based template matching algorithm for LED chip localization," *Int. J. Adv. Manuf. Technol.*, vol. 93, nos. 1–4, pp. 55–63, Oct. 2017.
- [49] R.-F. Fung, C.-Y. Yang, and C.-T. Lai, "Graphic supervisory control of an automatic optical inspection for LED properties," *Measurement*, vol. 44, no. 8, pp. 1349–1360, Oct. 2011.
- [50] C.-Y. Chang, C.-H. Li, Y.-C. Chang, and M. Jeng, "Wafer defect inspection by neural analysis of region features," *J. Intell. Manuf.*, vol. 22, no. 6, pp. 953–964, Dec. 2011.
- [51] H. D. Lin, G. C. Lin, C. Y. Chung, and W. T. Lin, "Wavelet-based neural network and statistical approaches applied to automated visual inspection of LED chips," *J. Sci. Ind. Res.*, vol. 67, no. 6, pp. 412–420, 2008.
- [52] D.-M. Tsai, I.-Y. Chiang, and Y.-H. Tsai, "A shift-tolerant dissimilarity measure for surface defect detection," *IEEE Trans. Ind. Informat.*, vol. 8, no. 1, pp. 128–137, Feb. 2012.
- [53] M. P.-L. Ooi, H. K. Sok, Y. C. Kuang, S. Demidenko, and C. Chan, "Defect cluster recognition system for fabricated semiconductor wafers," *Eng. Appl. Artif. Intell.*, vol. 26, no. 3, pp. 1029–1043, Mar. 2013.
- [54] V. Perminov, V. Putrolaynen, M. Belyaev, E. Pasko, and K. Balashkov, "Automated image analysis for evaluation of wafer backside chipping," *Int. J. Adv. Manuf. Technol.*, vol. 99, nos. 5–8, pp. 2015–2023, Nov. 2018.
- [55] J. Kim, Y. Lee, and H. Kim, "Detection and clustering of mixed-type defect patterns in wafer bin maps," *IIEE Trans.*, vol. 50, no. 2, pp. 99–111, Feb. 2018.
- [56] C. H. Jin, H. J. Na, M. Piao, G. Pok, and K. H. Ryu, "A novel DBSCAN-based defect pattern detection and classification framework for wafer bin map," *IEEE Trans. Semicond. Manuf.*, vol. 32, no. 3, pp. 286–292, Aug. 2019.
- [57] F. Adly, P. D. Yoo, S. Muhaidat, Y. Al-Hammadi, U. Lee, and M. Ismail, "Randomized general regression network for identification of defect patterns in semiconductor wafer maps," *IEEE Trans. Semicond. Manuf.*, vol. 28, no. 2, pp. 145–152, May 2015.
- [58] S.-C. Hsu and C.-F. Chien, "Hybrid data mining approach for pattern extraction from wafer bin map to improve yield in semiconductor manufacturing," *Int. J. Prod. Econ.*, vol. 107, no. 1, pp. 88–103, May 2007.
- [59] C.-W. Chang, T.-M. Chao, J.-T. Horng, C.-F. Lu, and R.-H. Yeh, "Development pattern recognition model for the classification of circuit probe wafer maps on semiconductors," *IEEE Trans. Compon., Packag., Manuf. Technol.*, vol. 2, no. 12, pp. 2089–2097, Dec. 2012.
- [60] M. Saqlain, B. Jargalsaikhan, and J. Y. Lee, "A voting ensemble classifier for wafer map defect patterns identification in semiconductor manufacturing," *IEEE Trans. Semicond. Manuf.*, vol. 32, no. 2, pp. 171–182, May 2019.
- [61] M. P.-L. Ooi, E. K. J. Joo, Y. C. Kuang, S. Demidenko, L. Kleeman, and C. W. K. Chan, "Getting more from the semiconductor test: Data mining with defect-cluster extraction," *IEEE Trans. Instrum. Meas.*, vol. 60, no. 10, pp. 3300–3317, Oct. 2011.
- [62] J. Yu and X. Lu, "Wafer map defect detection and recognition using joint local and nonlocal linear discriminant analysis," *IEEE Trans. Semicond. Manuf.*, vol. 29, no. 1, pp. 33–43, Feb. 2016.
- [63] H.-W. Hsieh and F.-L. Chen, "Recognition of defect spatial patterns in semiconductor fabrication," *Int. J. Prod. Res.*, vol. 42, no. 19, pp. 4153–4172, Oct. 2004.
- [64] F.-L. Chen and S.-F. Liu, "A neural-network approach to recognize defect spatial pattern in semiconductor fabrication," *IEEE Trans. Semicond. Manuf.*, vol. 13, no. 3, pp. 366–373, Aug. 2000.
- [65] S. F. Liu, F. L. Chen, and W. B. Lu, "Wafer bin map recognition using a neural network approach," *Int. J. Prod. Res.*, vol. 40, no. 10, pp. 2207–2223, Jan. 2002.
- [66] F. D. Palma, G. D. Nicolao, G. Miraglia, E. Pasquinetti, and F. Piccinini, "Unsupervised spatial pattern classification of electrical-wafer-sorting maps in semiconductor manufacturing," *Pattern Recognit. Lett.*, vol. 26, no. 12, pp. 1857–1865, Sep. 2005.
- [67] C.-H. Wang, S.-J. Wang, and W.-D. Lee, "Automatic identification of spatial defect patterns for semiconductor manufacturing," *Int. J. Prod. Res.*, vol. 44, no. 23, pp. 5169–5185, Dec. 2006.
- [68] C.-H. Wang, "Recognition of semiconductor defect patterns using spatial filtering and spectral clustering," *Expert Syst. Appl.*, vol. 34, no. 3, pp. 1914–1923, Apr. 2008.
- [69] C.-H. Wang, W. Kuo, and H. Bensmail, "Detection and classification of defect patterns on semiconductor wafers," *IIE Trans.*, vol. 38, no. 12, pp. 1059–1068, Dec. 2006.
- [70] C.-H. Wang, "Separation of composite defect patterns on wafer bin map using support vector clustering," *Expert Syst. Appl.*, vol. 36, no. 2, pp. 2554–2561, Mar. 2009.
- [71] C.-J. Huang, "Clustered defect detection of high quality chips using self-supervised multilayer perceptron," *Expert Syst. Appl.*, vol. 33, no. 4, pp. 996–1003, Nov. 2007.
- [72] C.-J. Huang, Y.-J. Chen, C.-F. Wu, and Y.-A. Huang, "Application of neural networks and genetic algorithms to the screening for high quality chips," *Appl. Soft Comput.*, vol. 9, no. 2, pp. 824–832, Mar. 2009.
- [73] Y.-S. Jeong, S.-J. Kim, and M. K. Jeong, "Automatic identification of defect patterns in semiconductor wafer maps using spatial correlogram and dynamic time warping," *IEEE Trans. Semicond. Manuf.*, vol. 21, no. 4, pp. 625–637, Nov. 2008.
- [74] K. P. White, B. Kundu, and C. M. Mastrangelo, "Classification of defect clusters on semiconductor wafers via the Hough transformation," *IEEE Trans. Semicond. Manuf.*, vol. 21, no. 2, pp. 272–277, May 2008.
- [75] T.-S. Li and C.-L. Huang, "Defect spatial pattern recognition using a hybrid SOM-SVM approach in semiconductor manufacturing," *Expert Syst. Appl.*, vol. 36, no. 1, pp. 374–385, Jan. 2009.
- [76] J. Chen, C.-J. Hsu, and C.-C. Chen, "A self-growing hidden Markov tree for wafer map inspection," *J. Process Control*, vol. 19, no. 2, pp. 261–271, Feb. 2009.
- [77] J. Y. Hwang and W. Kuo, "Model-based clustering for integrated circuit yield enhancement," *Eur. J. Oper. Res.*, vol. 178, no. 1, pp. 143–153, Apr. 2007.
- [78] T. Yuan and W. Kuo, "A model-based clustering approach to the recognition of the spatial defect patterns produced during semiconductor fabrication," *IIE Trans.*, vol. 40, no. 2, pp. 93–101, Nov. 2007.
- [79] T. Yuan and W. Kuo, "Spatial defect pattern recognition on semiconductor wafers using model-based clustering and Bayesian inference," *Eur. J. Oper. Res.*, vol. 190, no. 1, pp. 228–240, Oct. 2008.
- [80] T. Yuan, S. J. Bae, and J. I. Park, "Bayesian spatial defect pattern recognition in semiconductor fabrication using support vector clustering," *Int. J. Adv. Manuf. Technol.*, vol. 51, nos. 5–8, pp. 671–683, Nov. 2010.

- [81] T. Yuan, W. Kuo, and S. J. Bae, "Detection of spatial defect patterns generated in semiconductor fabrication processes," *IEEE Trans. Semicond. Manuf.*, vol. 24, no. 3, pp. 392–403, Aug. 2011.
- [82] Q. Zhou, L. Zeng, and S. Zhou, "Statistical detection of defect patterns using Hough transform," *IEEE Trans. Semicond. Manuf.*, vol. 23, no. 3, pp. 370–380, Aug. 2010.
- [83] J.-S. Lin, "Constructing a yield model for integrated circuits based on a novel fuzzy variable of clustered defect pattern," *Expert Syst. Appl.*, vol. 39, no. 3, pp. 2856–2864, Feb. 2012.
- [84] L.-C. Chao and L.-I. Tong, "Wafer defect pattern recognition by multi-class support vector machines by using a novel defect cluster index," *Expert Syst. Appl.*, vol. 36, no. 6, pp. 10158–10167, Aug. 2009.
- [85] G. Choi, S.-H. Kim, C. Ha, and S. J. Bae, "Multi-step ART1 algorithm for recognition of defect patterns on semiconductor wafers," *Int. J. Prod. Res.*, vol. 50, no. 12, pp. 3274–3287, Jun. 2012.
- [86] C.-F. Chien, S.-C. Hsu, and Y.-J. Chen, "A system for online detection and classification of wafer bin map defect patterns for manufacturing intelligence," *Int. J. Prod. Res.*, vol. 51, no. 8, pp. 2324–2338, Apr. 2013.
- [87] C.-W. Liu and C.-F. Chien, "An intelligent system for wafer bin map defect diagnosis: An empirical study for semiconductor manufacturing," *Eng. Appl. Artif. Intell.*, vol. 26, nos. 5–6, pp. 1479–1486, May 2013.
- [88] F. Adly, O. Alhoussein, P. D. Yoo, Y. Al-Hammadi, K. Taha, S. Muhaidat, Y.-S. Jeong, U. Lee, and M. Ismail, "Simplified subspace regression network for identification of defect patterns in semiconductor wafer maps," *IEEE Trans. Ind. Informat.*, vol. 11, no. 6, pp. 1267–1276, Dec. 2015.
- [89] M.-J. Wu, J.-S.-R. Jang, and J.-L. Chen, "Wafer map failure pattern recognition and similarity ranking for large-scale data sets," *IEEE Trans. Semicond. Manuf.*, vol. 28, no. 1, pp. 1–12, Feb. 2015.
- [90] M. Piao, C. H. Jin, J. Y. Lee, and J.-Y. Byun, "Decision tree ensemble-based wafer map failure pattern recognition based on radon transform-based features," *IEEE Trans. Semicond. Manuf.*, vol. 31, no. 2, pp. 250–257, May 2018.
- [91] J. Yu, X. Zheng, and J. Liu, "Stacked convolutional sparse denoising auto-encoder for identification of defect patterns in semiconductor wafer map," *Comput. Ind.*, vol. 109, pp. 121–133, Aug. 2019.
- [92] N. Yu, Q. Xu, and H. Wang, "Wafer defect pattern recognition and analysis based on convolutional neural network," *IEEE Trans. Semicond. Manuf.*, vol. 32, no. 4, pp. 566–573, Nov. 2019.
- [93] J. Yu, "Enhanced stacked denoising autoencoder-based feature learning for recognition of wafer map defects," *IEEE Trans. Semicond. Manuf.*, vol. 32, no. 4, pp. 613–624, Nov. 2019.
- [94] J. Wang, Z. Yang, J. Zhang, Q. Zhang, and W.-T.-K. Chien, "Ada-BalGAN: An improved generative adversarial network with imbalanced learning for wafer defective pattern recognition," *IEEE Trans. Semicond. Manuf.*, vol. 32, no. 3, pp. 310–319, Aug. 2019.
- [95] C.-S. Liao, T.-J. Hsieh, Y.-S. Huang, and C.-F. Chien, "Similarity searching for defective wafer bin maps in semiconductor manufacturing," *IEEE Trans. Autom. Sci. Eng.*, vol. 11, no. 3, pp. 953–960, Jul. 2014.
- [96] L. Xie, R. Huang, N. Gu, and Z. Cao, "A novel defect detection and identification method in optical inspection," *Neural Comput. Appl.*, vol. 24, nos. 7–8, pp. 1953–1962, Jun. 2014.
- [97] S. Kang, S. Cho, D. An, and J. Rim, "Using wafer map features to better predict die-level failures in final test," *IEEE Trans. Semicond. Manuf.*, vol. 28, no. 3, pp. 431–437, Aug. 2015.
- [98] S. C. Tan, J. Watada, Z. Ibrahim, and M. Khalid, "Evolutionary fuzzy ARTMAP neural networks for classification of semiconductor defects," *IEEE Trans. Neural Netw. Learn. Syst.*, vol. 26, no. 5, pp. 933–950, May 2015.
- [99] B. Kim, Y.-S. Jeong, S. Hoon Tong, I.-K. Chang, and M.-K. Jeongyoung, "A regularized singular value decomposition-based approach for failure pattern classification on fail bit map in a DRAM wafer," *IEEE Trans. Semicond. Manuf.*, vol. 28, no. 1, pp. 41–49, Feb. 2015.
- [100] B. Kim, Y.-S. Jeong, S. H. Tong, I.-K. Chang, and M.-K. Jeong, "Step-down spatial randomness test for detecting abnormalities in DRAM wafers with multiple spatial maps," *IEEE Trans. Semicond. Manuf.*, vol. 29, no. 1, pp. 57–65, Feb. 2016.
- [101] B. Kim, Y.-S. Jeong, S. H. Tong, and M. K. Jeong, "A generalised uncertain decision tree for defect classification of multiple wafer maps," *Int. J. Prod. Res.*, vol. 58, no. 9, pp. 2805–2821, May 2020.
- [102] K. Nakata, R. Orihara, Y. Mizuoka, and K. Takagi, "A comprehensive big-data-based monitoring system for yield enhancement in semiconductor manufacturing," *IEEE Trans. Semicond. Manuf.*, vol. 30, no. 4, pp. 339–344, Nov. 2017.
- [103] K. Taha, K. Salah, and P. D. Yoo, "Clustering the dominant defective patterns in semiconductor wafer maps," *IEEE Trans. Semicond. Manuf.*, vol. 31, no. 1, pp. 156–165, Feb. 2018.
- [104] K. Kyeong and H. Kim, "Classification of mixed-type defect patterns in wafer bin maps using convolutional neural networks," *IEEE Trans. Semicond. Manuf.*, vol. 31, no. 3, pp. 395–402, Aug. 2018.
- [105] M. B. Alawieh, F. Wang, and X. Li, "Identifying wafer-level systematic failure patterns via unsupervised learning," *IEEE Trans. Comput.-Aided Design Integr. Circuits Syst.*, vol. 37, no. 4, pp. 832–844, Apr. 2018.
- [106] T. Nakazawa and D. V. Kulkarni, "Wafer map defect pattern classification and image retrieval using convolutional neural network," *IEEE Trans. Semicond. Manuf.*, vol. 31, no. 2, pp. 309–314, May 2018.
- [107] T. Nakazawa and D. V. Kulkarni, "Anomaly detection and segmentation for wafer defect patterns using deep convolutional Encoder–Decoder neural network architectures in semiconductor manufacturing," *IEEE Trans. Semicond. Manuf.*, vol. 32, no. 2, pp. 250–256, May 2019.
- [108] G. Tello, O. Y. Al-Jarrah, P. D. Yoo, Y. Al-Hammadi, S. Muhaidat, and U. Lee, "Deep-structured machine learning model for the recognition of mixed-defect patterns in semiconductor fabrication processes," *IEEE Trans. Semicond. Manuf.*, vol. 31, no. 2, pp. 315–322, May 2018.
- [109] R. Wang and N. Chen, "Wafer map defect pattern recognition using rotation-invariant features," *IEEE Trans. Semicond. Manuf.*, vol. 32, no. 4, pp. 596–604, Nov. 2019.
- [110] P. Xie and S.-U. Guan, "A golden-template self-generating method for patterned wafer inspection," *Mach. Vis. Appl.*, vol. 12, no. 3, pp. 149–156, Oct. 2000.
- [111] C.-T. Su, T. Yang, and C.-M. Ke, "A neural-network approach for semiconductor wafer post-sawing inspection," *IEEE Trans. Semicond. Manuf.*, vol. 15, no. 2, pp. 260–266, May 2002.
- [112] S.-U. Guan, P. Xie, and H. Li, "A golden-block-based self-refining scheme for repetitive patterned wafer inspections," *Mach. Vis. Appl.*, vol. 13, nos. 5–6, pp. 314–321, Mar. 2003.
- [113] C.-Y. Chang, C. Li, J.-W. Chang, and M. Jeng, "An unsupervised neural network approach for automatic semiconductor wafer defect inspection," *Expert Syst. Appl.*, vol. 36, no. 1, pp. 950–958, Jan. 2009.
- [114] H. Liu, W. Zhou, Q. Kuang, L. Cao, and B. Gao, "Defect detection of IC wafer based on two-dimension wavelet transform," *Microelectron. J.*, vol. 41, nos. 2–3, pp. 171–177, 2010.
- [115] H. Liu, W. Zhou, Q. Kuang, L. Cao, and B. Gao, "Defect detection of IC wafer based on spectral subtraction," *IEEE Trans. Semicond. Manuf.*, vol. 23, no. 1, pp. 141–147, Feb. 2010.
- [116] R. Baly and H. Hajj, "Wafer classification using support vector machines," *IEEE Trans. Semicond. Manuf.*, vol. 25, no. 3, pp. 373–383, Aug. 2012.
- [117] H. W. Kim and S. I. Yoo, "Defect detection using feature point matching for non-repetitive patterned images," *Pattern Anal. Appl.*, vol. 17, no. 2, pp. 415–429, May 2014.
- [118] P. Bourgeat, F. Meriaudeau, K. W. Tobin, and P. Gorria, "Gabor filtering for feature extraction on complex images: Application to defect detection on semiconductors," *Imag. Sci. J.*, vol. 54, no. 4, pp. 200–210, Dec. 2006.
- [119] R. A. Zoroofi, H. Taketani, S. Tamura, Y. Sato, and K. Sekiya, "Automated inspection of IC wafer contamination," *Pattern Recognit.*, vol. 34, no. 6, pp. 1307–1317, Jun. 2001.
- [120] T. Kubota, P. Talekar, X. Ma, and T. S. Sudarshan, "A nondestructive automated defect detection system for silicon carbide wafers," *Mach. Vis. Appl.*, vol. 16, no. 3, pp. 170–176, May 2005.
- [121] N. G. Shankar and Z. W. Zhong, "Defect detection on semiconductor wafer surfaces," *Microelectron. Eng.*, vol. 77, nos. 3–4, pp. 337–346, Apr. 2005.
- [122] N. G. Shankar and Z. W. Zhong, "A rule-based computing approach for the segmentation of semiconductor defects," *Microelectron. J.*, vol. 37, no. 6, pp. 500–509, Jun. 2006.
- [123] N. G. Shankar and Z. W. Zhong, "Improved segmentation of semiconductor defects using area sieves," *Mach. Vis. Appl.*, vol. 17, no. 1, pp. 1–7, Apr. 2006.
- [124] C.-H. Yeh, C.-H. Chen, F.-C. Wu, and K.-Y. Chen, "Validation and evaluation for defect-kill-rate and yield estimation models in semiconductor manufacturing," *Int. J. Prod. Res.*, vol. 45, no. 4, pp. 829–844, Feb. 2007.
- [125] H.-D. Lin and D.-C. Ho, "Detection of pinhole defects on chips and wafers using DCT enhancement in computer vision systems," *Int. J. Adv. Manuf. Technol.*, vol. 34, nos. 5–6, pp. 567–583, Aug. 2007.

- [126] R. Nakagaki, T. Honda, and K. Nakamae, "Automatic recognition of defect areas on a semiconductor wafer using multiple scanning electron microscope images," *Meas. Sci. Technol.*, vol. 20, no. 7, Jul. 2009, Art. no. 075503.
- [127] R. Nakagaki, Y. Takagi, and K. Nakamae, "Automatic recognition of circuit patterns on semiconductor wafers from multiple scanning electron microscope images," *Meas. Sci. Technol.*, vol. 21, no. 8, Aug. 2010, Art. no. 085501.
- [128] C.-H. Yeh, F.-C. Wu, W.-L. Ji, and C.-Y. Huang, "A wavelet-based approach in detecting visual defects on semiconductor wafer dies," *IEEE Trans. Semicond. Manuf.*, vol. 23, no. 2, pp. 284–292, May 2010.
- [129] S. Usuki, H. Nishioka, S. Takahashi, and K. Takamasu, "Experimental verification of super-resolution optical inspection for semiconductor defect by using standing wave illumination shift," *Int. J. Adv. Manuf. Technol.*, vol. 46, nos. 9–12, pp. 863–875, Feb. 2010.
- [130] Z. Pan, L. Chen, W. Li, G. Zhang, and P. Wu, "A novel defect inspection method for semiconductor wafer based on magneto-optic imaging," *J. Low Temp. Phys.*, vol. 170, nos. 5–6, pp. 436–441, Mar. 2013.
- [131] C.-S. Chen, C.-L. Huang, and C.-W. Yeh, "A hybrid defect detection for in-tray semiconductor chip," *Int. J. Adv. Manuf. Technol.*, vol. 65, nos. 1–4, pp. 43–56, Mar. 2013.
- [132] C.-L. Tien, Q.-H. Lai, and C.-S. Lin, "Development of optical automatic positioning and wafer defect detection system," *Meas. Sci. Technol.*, vol. 27, no. 2, 2016, Art. no. 025205.
- [133] S. N. D. Chua, S. Mohamaddan, S. J. Tanjong, A. Yassin, and S. F. Lim, "Detection of bond pad discolorations at outgoing wafer inspections," *IEEE Trans. Semicond. Manuf.*, vol. 31, no. 1, pp. 144–148, Feb. 2018.
- [134] S. Cheon, H. Lee, C. O. Kim, and S. H. Lee, "Convolutional neural network for wafer surface defect classification and the detection of unknown defect class," *IEEE Trans. Semicond. Manuf.*, vol. 32, no. 2, pp. 163–170, May 2019.
- [135] M. Harada, Y. Minekawa, and K. Nakamae, "Defect detection techniques robust to process variation in semiconductor inspection," *Meas. Sci. Technol.*, vol. 30, no. 3, Mar. 2019, Art. no. 035402.
- [136] H. Gao, W. Jin, X. Yang, and O. Kaynak, "A line-based-clustering approach for ball grid array component inspection in surface-mount technology," *IEEE Trans. Ind. Electron.*, vol. 64, no. 4, pp. 3030–3038, Apr. 2017.
- [137] M. H. Annaby, Y. M. Fouda, and M. A. Rushdi, "Improved normalized cross-correlation for defect detection in printed-circuit boards," *IEEE Trans. Semicond. Manuf.*, vol. 32, no. 2, pp. 199–211, May 2019.
- [138] W. Dai, A. Mujeeb, M. Erdt, and A. Sourin, "Soldering defect detection in automatic optical inspection," *Adv. Eng. Informat.*, vol. 43, Jan. 2020, Art. no. 101004.
- [139] J.-D. Song, Y.-G. Kim, and T.-H. Park, "SMT defect classification by feature extraction region optimization and machine learning," *Int. J. Adv. Manuf. Technol.*, vol. 101, nos. 5–8, pp. 1303–1313, Apr. 2019.
- [140] D. W. Capson and S.-K. Eng, "A tiered-color illumination approach for machine inspection of solder joints," *IEEE Trans. Pattern Anal. Mach. Intell.*, vol. PAMI-10, no. 3, pp. 387–393, May 1988.
- [141] S. S. Zakaria, A. Amir, N. Yaakob, and S. Nazemi, "Automated detection of printed circuit boards (PCB) defects by using machine learning in electronic manufacturing: Current approaches," *IOP Conf. Ser., Mater. Sci. Eng.*, vol. 767, Mar. 2020, Art. no. 012064.
- [142] C. Benedek, O. Krammer, M. Janoczki, and L. Jakab, "Solder paste scooping detection by multilevel visual inspection of printed circuit boards," *IEEE Trans. Ind. Electron.*, vol. 60, no. 6, pp. 2318–2331, Jun. 2013.
- [143] G. Acciani, G. Brunetti, and G. Fornarelli, "Application of neural networks in optical inspection and classification of solder joints in surface mount technology," *IEEE Trans. Ind. Informat.*, vol. 2, no. 3, pp. 200–209, Aug. 2006.
- [144] R. T. Chin, C. A. Harlow, and S. J. Dwyer, III, "Automatic visual inspection of printed circuit boards," *Proc. SPIE*, vol. 155, pp. 199–213, Jan. 1979.
- [145] B. C. Jiang, S.-L. Tasi, and C.-C. Wang, "Machine vision-based gray relational theory applied to IC marking inspection," *IEEE Trans. Semicond. Manuf.*, vol. 15, no. 4, pp. 531–539, Nov. 2002.
- [146] R. Nagarajan, S. Yaacob, P. Pandian, M. Karthigayan, S. H. Amin, and M. Khalid, "A real time marking inspection scheme for semiconductor industries," *Int. J. Adv. Manuf. Technol.*, vol. 34, nos. 9–10, pp. 926–932, Sep. 2007.
- [147] F.-H. Hsu and C.-A. Shen, "The design and implementation of an embedded real-time automated IC marking inspection system," *IEEE Trans. Semicond. Manuf.*, vol. 32, no. 1, pp. 112–120, Feb. 2019.
- [148] C. L. S. C. Fonseka and J. A. K. S. Jayasinghe, "Implementation of an automatic optical inspection system for solder quality classification of THT solder joints," *IEEE Trans. Compon., Packag., Manuf. Technol.*, vol. 9, no. 2, pp. 353–366, Feb. 2019.
- [149] J. Richter and J. Schambach, "Three-dimensional THT solder joint reconstruction for inline inspection systems," *Proc. SPIE*, Sep. 2019, p. 25, Sep. 2019.
- [150] C. L. S. C. Fonseka and J. A. K. S. Jayasinghe, "Color model analysis for solder pad segmentation on printed circuit boards," *Int. J. Sci. Res. Publications*, vol. 6, no. 11, pp. 212–225, 2016.
- [151] C. L. S. C. Fonseka and J. A. K. S. Jayasinghe, "Localization of component lead inside a THT solder joint for solder defects classification," *J. Achievements Mater. Manuf. Eng.*, vol. 2, no. 83, pp. 57–66, Aug. 2017.
- [152] S. Fonseka and J. A. K. S. Jayasinghe, "Feature extraction and template matching algorithms classification for PCB fiducial verification," *J. Achievements Mater. Manuf. Eng.*, vol. 1, no. 86, pp. 14–32, Jan. 2018.
- [153] B. C. Jiang, C. C. Wang, and P. L. Chen, "Logistic regression tree applied to classify PCB golden finger defects," *Int. J. Adv. Manuf. Technol.*, vol. 24, nos. 7–8, pp. 496–502, Oct. 2004.
- [154] B. C. Jiang and Y. M. W. C. C. Wang, "Bootstrap sampling technique applied to the PCB golden fingers defect classification study," *Int. J. Prod. Res.*, vol. 39, no. 10, pp. 2215–2230, Jan. 2001.
- [155] D.-M. Tsai and B.-T. Lin, "Defect detection of gold-plated surfaces on PCBs using entropy measures," *Int. J. Adv. Manuf. Technol.*, vol. 20, no. 6, pp. 420–428, Sep. 2002.
- [156] Z. Ibrahim and S. A. Rahman Al-Attas, "Wavelet-based printed circuit board inspection algorithm," *Integr. Comput.-Aided Eng.*, vol. 12, no. 2, pp. 201–213, Apr. 2005.
- [157] L. Bai, X. Yang, and H. Gao, "A novel coarse-fine method for ball grid array component positioning and defect inspection," *IEEE Trans. Ind. Electron.*, vol. 65, no. 6, pp. 5023–5031, Jun. 2018.
- [158] B. C. Jiang, C. C. Wang, and Y. N. Hsu, "Machine vision and background remover-based approach for PCB solder joints inspection," *Int. J. Prod. Res.*, vol. 45, no. 2, pp. 451–464, Jan. 2007.
- [159] X. Hongwei, Z. Xianmin, K. Yongcong, and O. Gaofei, "Solder joint inspection method for chip component using improved AdaBoost and decision tree," *IEEE Trans. Compon., Packag., Manuf. Technol.*, vol. 1, no. 12, pp. 2018–2027, Dec. 2011.
- [160] F. Wu and X. Zhang, "Feature-extraction-based inspection algorithm for IC solder joints," *IEEE Trans. Compon., Packag., Manuf. Technol.*, vol. 1, no. 5, pp. 689–694, May 2011.
- [161] N. S. S. Mar, P. K. D. V. Yarlagaadda, and C. Fookes, "Design and development of automatic visual inspection system for PCB manufacturing," *Robot. Comput.-Integr. Manuf.*, vol. 27, no. 5, pp. 949–962, Oct. 2011.
- [162] W.-Y. Wu, C.-W. Hung, and W.-B. Yu, "The development of automated solder bump inspection using machine vision techniques," *Int. J. Adv. Manuf. Technol.*, vol. 69, nos. 1–4, pp. 509–523, Oct. 2013.
- [163] F. Wu and X. Zhang, "An inspection and classification method for chip solder joints using color grads and Boolean rules," *Robot. Comput.-Integr. Manuf.*, vol. 30, no. 5, pp. 517–526, Oct. 2014.
- [164] K. W. Ko and H. S. Cho, "Solder joints inspection using a neural network and fuzzy rule-based classification method," *IEEE Trans. Electron. Packag. Manuf.*, vol. 23, no. 2, pp. 93–103, Apr. 2000.
- [165] G. Acciani, G. Brunetti, and G. Fornarelli, "A multiple neural network system to classify solder joints on integrated circuits," *Int. J. Comput. Intell. Res.*, vol. 2, no. 4, pp. 337–348, 2006.
- [166] A. Giaquinto, G. Fornarelli, G. Brunetti, and G. Acciani, "A neurofuzzy method for the evaluation of soldering global quality index," *IEEE Trans. Ind. Informat.*, vol. 5, no. 1, pp. 56–66, Feb. 2009.
- [167] G. Acciani, G. Fornarelli, and A. Giaquinto, "A fuzzy method for global quality index evaluation of solder joints in surface mount technology," *IEEE Trans. Ind. Informat.*, vol. 7, no. 1, pp. 115–124, Feb. 2011.
- [168] S.-N. Chiu and M.-H. Perng, "Reflection-area-based feature descriptor for solder joint inspection," *Mach. Vis. Appl.*, vol. 18, no. 2, pp. 95–106, Mar. 2007.
- [169] T. Y. Ong, Z. Samad, and M. M. Ratnam, "Solder joint inspection with multi-angle imaging and an artificial neural network," *Int. J. Adv. Manuf. Technol.*, vol. 38, nos. 5–6, pp. 455–462, Aug. 2008.
- [170] N. S. S. Mar, C. Fookes, and P. K. Yarlagaadda, "Design of automatic vision-based inspection system for solder joint segmentation," *J. Achievements Mater. Manuf. Eng.*, vol. 34, no. 2, pp. 145–151, 2009.

- [171] H. Wu, X. Zhang, H. Xie, Y. Kuang, and G. Ouyang, "Classification of solder joint using feature selection based on Bayes and support vector machine," *IEEE Trans. Compon., Packag., Manuf. Technol.*, vol. 3, no. 3, pp. 516–522, Mar. 2013.
- [172] W. Hao, Z. Xianmin, K. Yongcong, O. Gaofei, and X. Hongwei, "Solder joint inspection based on neural network combined with genetic algorithm," *Optik*, vol. 124, no. 20, pp. 4110–4116, Oct. 2013.
- [173] N. Cai, J. Lin, Q. Ye, H. Wang, S. Weng, and B. W.-K. Ling, "A new IC solder joint inspection method for an automatic optical inspection system based on an improved visual background extraction algorithm," *IEEE Trans. Compon., Packag., Manuf. Technol.*, vol. 6, no. 1, pp. 161–172, Jan. 2016.
- [174] N. Cai, Y. Zhou, Q. Ye, G. Liu, H. Wang, and X. Chen, "IC solder joint inspection via robust principle component analysis," *IEEE Trans. Compon., Packag., Manuf. Technol.*, vol. 7, no. 2, pp. 300–309, Feb. 2017.
- [175] N. Cai, G. Cen, J. Wu, F. Li, H. Wang, and X. Chen, "SMT solder joint inspection via a novel cascaded convolutional neural network," *IEEE Trans. Compon., Packag., Manuf. Technol.*, vol. 8, no. 4, pp. 670–677, Apr. 2018.
- [176] Q. Ye, N. Cai, J. Li, F. Li, H. Wang, and X. Chen, "IC solder joint inspection based on an adaptive-template method," *IEEE Trans. Compon., Packag., Manuf. Technol.*, vol. 8, no. 6, pp. 1121–1127, Jun. 2018.
- [177] T.-W. Hui and G. K.-H. Pang, "Solder paste inspection using region-based defect detection," *Int. J. Adv. Manuf. Technol.*, vol. 42, nos. 7–8, pp. 725–734, Jun. 2009.
- [178] J. Jiang, J. Cheng, and D. Tao, "Color biological features-based solder paste defects detection and classification on printed circuit boards," *IEEE Trans. Compon., Packag., Manuf. Technol.*, vol. 2, no. 9, pp. 1536–1544, Sep. 2012.
- [179] A. J. Crispin and V. Rankov, "Automated inspection of PCB components using a genetic algorithm template-matching approach," *Int. J. Adv. Manuf. Technol.*, vol. 35, nos. 3–4, pp. 293–300, Dec. 2007.
- [180] H.-J. Cho and T.-H. Park, "Wavelet transform based image template matching for automatic component inspection," *Int. J. Adv. Manuf. Technol.*, vol. 50, nos. 9–12, pp. 1033–1039, Oct. 2010.
- [181] A.-A.-I. M. Hassanin, F. E. A. El-Samie, and G. M. El Banby, "A real-time approach for automatic defect detection from PCBs based on SURF features and morphological operations," *Multimedia Tools Appl.*, vol. 78, no. 24, pp. 34437–34457, Dec. 2019.
- [182] M. E. Zervakis, S. K. Goumas, and G. A. Rovithakis, "A Bayesian framework for multilead SMD post-placement quality inspection," *IEEE Trans. Syst. Man, Cybern. B, Cybern.*, vol. 34, no. 1, pp. 440–453, Feb. 2004.
- [183] S. K. Goumas, I. N. Dimou, and M. E. Zervakis, "Combination of multiple classifiers for post-placement quality inspection of components: A comparative study," *Inf. Fusion*, vol. 11, no. 2, pp. 149–162, Apr. 2010.
- [184] C.-H. Wu, D.-Z. Wang, A. Ip, D.-W. Wang, C.-Y. Chan, and H.-F. Wang, "A particle swarm optimization approach for components placement inspection on printed circuit boards," *J. Intell. Manuf.*, vol. 20, no. 5, pp. 535–549, Oct. 2009.
- [185] N. Dong, C.-H. Wu, W.-H. Ip, Z.-Q. Chen, and K.-L. Yung, "Chaotic species based particle swarm optimization algorithms and its application in PCB components detection," *Expert Syst. Appl.*, vol. 39, no. 16, pp. 12501–12511, Nov. 2012.
- [186] L. Bai, X. Yang, and H. Gao, "Corner point-based coarse-fine method for surface-mount component positioning," *IEEE Trans. Ind. Informat.*, vol. 14, no. 3, pp. 877–886, Mar. 2018.
- [187] S.-H. Chen and D.-B. Perng, "Automatic optical inspection system for IC molding surface," *J. Intell. Manuf.*, vol. 27, no. 5, pp. 915–926, Oct. 2016.
- [188] C.-C. Wang, B. C. Jiang, J.-Y. Lin, and C.-C. Chu, "Machine vision-based defect detection in IC images using the partial information correlation coefficient," *IEEE Trans. Semicond. Manuf.*, vol. 26, no. 3, pp. 378–384, Aug. 2013.
- [189] W.-C. Wang, S.-L. Chen, L.-B. Chen, and W.-J. Chang, "A machine vision based automatic optical inspection system for measuring drilling quality of printed circuit boards," *IEEE Access*, vol. 5, pp. 10817–10833, 2017.
- [190] G. Duan, H. Wang, Z. Liu, and Y.-W. Chen, "A machine learning-based framework for automatic visual inspection of microdrill bits in PCB production," *IEEE Trans. Syst., Man, Cybern. C, Appl. Rev.*, vol. 42, no. 6, pp. 1679–1689, Nov. 2012.
- [191] G. Duan, H. Wang, Z. Liu, J. Tan, and Y.-W. Chen, "Automatic optical phase identification of micro-drill bits based on improved ASM and bag of shape segment in PCB production," *Mach. Vis. Appl.*, vol. 25, no. 6, pp. 1411–1422, Aug. 2014.
- [192] H. Rau and C.-H. Wu, "Automatic optical inspection for detecting defects on printed circuit board inner layers," *Int. J. Adv. Manuf. Technol.*, vol. 25, nos. 9–10, pp. 940–946, May 2005.
- [193] P.-C. Chang, L.-Y. Chen, and C.-Y. Fan, "A case-based evolutionary model for defect classification of printed circuit board images," *J. Intell. Manuf.*, vol. 19, no. 2, pp. 203–214, Apr. 2008.
- [194] C.-T. Liao, W.-H. Lee, and S.-H. Lai, "A flexible PCB inspection system based on statistical learning," *J. Signal Process. Syst.*, vol. 67, no. 3, pp. 279–290, Jun. 2012.
- [195] E. Yuk, S. Park, C.-S. Park, and J.-G. Baek, "Feature-learning-based printed circuit board inspection via speeded-up robust features and random forest," *Appl. Sci.*, vol. 8, no. 6, p. 932, Jun. 2018.
- [196] T. Vafeiadis, N. Dimitriou, D. Ioannidis, T. Wotherspoon, G. Tinker, and D. Tzovaras, "A framework for inspection of dies attachment on PCB utilizing machine learning techniques," *J. Manage. Anal.*, vol. 5, no. 2, pp. 81–94, Apr. 2018.
- [197] S.-F. Chuang, W.-T. Chang, C.-C. Lin, and Y.-S. Tarng, "Misalignment inspection of multilayer PCBs with an automated X-ray machine vision system," *Int. J. Adv. Manuf. Technol.*, vol. 51, nos. 9–12, pp. 995–1008, Dec. 2010.
- [198] D.-M. Tsai and R.-H. Yang, "An eigenvalue-based similarity measure and its application in defect detection," *Image Vis. Comput.*, vol. 23, no. 12, pp. 1094–1101, Nov. 2005.
- [199] V. H. Gaidhane, Y. V. Hote, and V. Singh, "An efficient similarity measure approach for PCB surface defect detection," *Pattern Anal. Appl.*, vol. 21, no. 1, pp. 277–289, Feb. 2018.
- [200] D.-M. Tsai and C.-K. Huang, "Defect detection in electronic surfaces using template-based Fourier image reconstruction," *IEEE Trans. Compon., Packag., Manuf. Technol.*, vol. 9, no. 1, pp. 163–172, Jan. 2019.
- [201] C.-S. Lin and L. W. Lue, "An image system for fast positioning and accuracy inspection of ball grid array boards," *Microelectron. Rel.*, vol. 41, no. 1, pp. 119–128, Jan. 2001.
- [202] C.-C. Chu, B. C. Jiang, and C.-C. Wang, "Modified gamma correction method to enhance ball grid array image for surface defect inspection," *Int. J. Prod. Res.*, vol. 46, no. 8, pp. 2165–2178, Apr. 2008.
- [203] Y.-C. Chiou, C.-S. Lin, and B.-C. Chiou, "The feature extraction and analysis of flaw detection and classification in BGA gold-plating areas," *Expert Syst. Appl.*, vol. 35, no. 4, pp. 1771–1779, Nov. 2008.
- [204] A. F. Said, B. L. Bennett, L. J. Karam, and J. S. Pettinato, "Automated detection and classification of non-wet solder joints," *IEEE Trans. Autom. Sci. Eng.*, vol. 8, no. 1, pp. 67–80, Jan. 2011.
- [205] A. F. Said, B. L. Bennett, L. J. Karam, A. Siah, K. Goodman, and J. S. Pettinato, "Automated void detection in solder balls in the presence of vias and other artifacts," *IEEE Trans. Compon., Packag., Manuf. Technol.*, vol. 2, no. 11, pp. 1890–1901, Nov. 2012.
- [206] J. Li, B. L. Bennett, L. J. Karam, and J. S. Pettinato, "Stereo vision based automated solder ball height and substrate coplanarity inspection," *IEEE Trans. Autom. Sci. Eng.*, vol. 13, no. 2, pp. 757–771, Apr. 2016.
- [207] W. Jin, W. Lin, X. Yang, and H. Gao, "Reference-free path-walking method for ball grid array inspection in surface mounting machines," *IEEE Trans. Ind. Electron.*, vol. 64, no. 8, pp. 6310–6318, Aug. 2017.
- [208] M. van Veenhuizen, "Void detection in solder bumps with deep learning," *Microelectron. Rel.*, pp. 88–90, pp. 315–320, Sep. 2018.
- [209] X. Lu, Z. He, L. Su, M. Fan, F. Liu, G. Liao, and T. Shi, "Detection of micro solder balls using active thermography technology and K-means algorithm," *IEEE Trans. Ind. Informat.*, vol. 14, no. 12, pp. 5620–5628, Dec. 2018.
- [210] C. Hilsun, "Flat-panel electronic displays: A triumph of physics, chemistry and engineering," *Phil. Trans. Roy. Soc. A, Math., Phys. Eng. Sci.*, vol. 368, no. 1914, pp. 1027–1082, Mar. 2010.
- [211] H.-W. Chen, J.-H. Lee, B.-Y. Lin, S. Chen, and S.-T. Wu, "Liquid crystal display and organic light-emitting diode display: Present status and future perspectives," *Light, Sci. Appl.*, vol. 7, no. 3, p. 17168, Mar. 2018.
- [212] Y.-H. Liu, S.-H. Lin, Y.-L. Hsueh, and M.-J. Lee, "Automatic target defect identification for TFT-LCD array process inspection using kernel FCM-based fuzzy SVDD ensemble," *Expert Syst. Appl.*, vol. 36, no. 2, pp. 1978–1998, Mar. 2009.
- [213] Y.-H. Liu and Y.-J. Chen, "Automatic defect detection for TFT-LCD array process using quasiconformal kernel support vector data description," *Int. J. Mol. Sci.*, vol. 12, no. 9, pp. 5762–5781, Sep. 2011.
- [214] S.-W. Yang, C.-S. Lin, S.-K. Lin, and H.-T. Chiang, "Automatic defect recognition of TFT array process using gray level co-occurrence matrix," *Optik*, vol. 125, no. 11, pp. 2671–2676, Jun. 2014.

- [215] S. Mei, H. Yang, and Z. Yin, "Unsupervised-learning-based feature-level fusion method for mura defect recognition," *IEEE Trans. Semicond. Manuf.*, vol. 30, no. 1, pp. 105–113, Feb. 2017.
- [216] N. K. Park and S. I. Yoo, "Evaluation of TFT-LCD defects based on human visual perception," *Displays*, vol. 30, no. 1, pp. 1–16, Jan. 2009.
- [217] F. P. Ferreira, P. M. F. Forte, P. E. R. Felgueiras, B. P. J. Bret, M. S. Belsley, and E. J. Nunes-Pereira, "Evaluating sub-pixel functional defects of a display using an arbitrary resolution camera," *Displays*, vol. 49, pp. 40–50, Sep. 2017.
- [218] A. Wu, J. Zhu, Z. Tao, and C. Mao, "Automatic inspection and classification for thin-film transistor liquid crystal display surface defects based on particle swarm optimization and one-class support vector machine," *Adv. Mech. Eng.*, vol. 8, no. 11, pp. 1–11, 2016.
- [219] Y. Gan and Q. Zhao, "An effective defect inspection method for LCD using active contour model," *IEEE Trans. Instrum. Meas.*, vol. 62, no. 9, pp. 2438–2445, Sep. 2013.
- [220] C. Ngo, Y. J. Park, J. Jung, R. U. Hassan, and J. Seok, "A new algorithm on the automatic TFT-LCD mura defects inspection based on an effective background reconstruction," *J. Soc. Inf. Display*, vol. 25, no. 12, pp. 737–752, Dec. 2017.
- [221] T.-Y. Li, J.-Z. Tsai, R.-S. Chang, L.-W. Ho, and C.-F. Yang, "Pretest gap mura on TFT LCDs using the optical interference pattern sensing method and neural network classification," *IEEE Trans. Ind. Electron.*, vol. 60, no. 9, pp. 3976–3982, Sep. 2013.
- [222] J. Z. Tsai, R.-S. Chang, and T.-Y. Li, "Detection of gap mura in TFT LCDs by the interference pattern and image sensing method," *IEEE Trans. Instrum. Meas.*, vol. 62, no. 11, pp. 3087–3092, Nov. 2013.
- [223] Y.-G. Yoon, S.-L. Lee, C.-W. Chung, and S.-H. Kim, "An effective defect inspection system for polarized film images using image segmentation and template matching techniques," *Comput. Ind. Eng.*, vol. 55, no. 3, pp. 567–583, Oct. 2008.
- [224] W.-W. Lai, X.-X. Zeng, J. He, and Y.-L. Deng, "Aesthetic defect characterization of a polymeric polarizer via structured light illumination," *Polym. Test.*, vol. 53, pp. 51–57, Aug. 2016.
- [225] Y.-L. Deng, S.-P. Xu, and W.-W. Lai, "A novel imaging-enhancement-based inspection method for transparent aesthetic defects in a polymeric polarizer," *Polym. Test.*, vol. 61, pp. 333–340, Aug. 2017.
- [226] Y.-L. Deng, S.-P. Xu, H.-Q. Chen, Z.-H. Liang, and C.-L. Yu, "Inspection of extremely slight aesthetic defects in a polymeric polarizer using the edge of light between black and white stripes," *Polym. Test.*, vol. 65, pp. 169–175, Feb. 2018.
- [227] Y. Deng, X. Pan, X. Wang, and X. Zhong, "Vision-based 3D shape measurement system for transparent microdefect characterization," *IEEE Access*, vol. 7, pp. 105721–105733, 2019.
- [228] C.-F.-J. Kuo, C.-Y. Lai, C.-H. Kao, and C.-H. Chiu, "Integrating image processing and classification technology into automated polarizing film defect inspection," *Opt. Lasers Eng.*, vol. 104, pp. 204–219, May 2018.
- [229] C. Yu, P. Chen, X. Zhong, X. Pan, and Y. Deng, "Saturated imaging for inspecting transparent aesthetic defects in a polymeric polarizer with black and white stripes," *Materials*, vol. 11, no. 5, p. 736, May 2018.
- [230] R. E. Wijesinghe, K. Park, Y. Jung, P. Kim, M. Jeon, and J. Kim, "Industrial resin inspection for display production using automated fluid-inspection based on multimodal optical detection techniques," *Opt. Lasers Eng.*, vol. 96, pp. 75–82, Sep. 2017.
- [231] C.-S. Lin, W.-Z. Wu, Y.-L. Lay, and M.-W. Chang, "A digital image-based measurement system for a LCD backlight module," *Opt. Laser Technol.*, vol. 33, no. 7, pp. 499–505, Oct. 2001.
- [232] W.-J. Lin and S.-S. Jhuo, "A fast luminance inspector for backlight modules based on multiple kernel support vector regression," *IEEE Trans. Compon., Packag., Manuf. Technol.*, vol. 4, no. 8, pp. 1391–1401, Aug. 2014.
- [233] J. Kwak, K. B. Lee, J. Jang, K. S. Chang, and C. O. Kim, "Automatic inspection of salt-and-pepper defects in OLED panels using image processing and control chart techniques," *J. Intell. Manuf.*, vol. 30, no. 3, pp. 1047–1055, Mar. 2019.
- [234] Y. Park and I. S. Kweon, "Ambiguous surface defect image classification of AMOLED displays in smartphones," *IEEE Trans. Ind. Informat.*, vol. 12, no. 2, pp. 597–607, Apr. 2016.
- [235] S.-H. Chen and D.-B. Perng, "Directional textures auto-inspection using principal component analysis," *Int. J. Adv. Manuf. Technol.*, vol. 55, nos. 9–12, pp. 1099–1110, Aug. 2011.
- [236] D.-B. Perng and S.-H. Chen, "Directional textures auto-inspection using discrete cosine transform," *Int. J. Prod. Res.*, vol. 49, no. 23, pp. 7171–7187, Dec. 2011.
- [237] J. Y. Lee and S. I. Yoo, "Automatic detection of region-mura defect in TFT-LCD," *IEICE Trans. Inf. Syst.*, vol. E87-D, no. 10, pp. 2371–2378, 2004.
- [238] B. C. Jiang, C.-C. Wang, and H.-C. Liu, "Liquid crystal display surface uniformity defect inspection using analysis of variance and exponentially weighted moving average techniques," *Int. J. Prod. Res.*, vol. 43, no. 1, pp. 67–80, 2005.
- [239] S. L. Chen and J. H. Chang, "TFT-LCD mura defects automatic inspection system using linear regression diagnostic model," *Proc. Inst. Mech. Eng., B, J. Eng. Manuf.*, vol. 222, no. 11, pp. 1489–1501, Nov. 2008.
- [240] L.-C. Chen and C.-C. Kuo, "Automatic TFT-LCD mura defect inspection using discrete cosine transform-based background filtering and 'just noticeable difference' quantification strategies," *Meas. Sci. Technol.*, vol. 19, no. 1, 2008, Art. no. 015507.
- [241] S.-L. Chen and S.-T. Chou, "TFT-LCD mura defect detection using wavelet and cosine transforms," *J. Adv. Mech. Des., Syst., Manuf.*, vol. 2, no. 3, pp. 441–453, 2008.
- [242] X. Bi, C. Zhuang, and H. Ding, "A new mura defect inspection way for TFT-LCD using level set method," *IEEE Signal Process. Lett.*, vol. 16, no. 4, pp. 311–314, Apr. 2009.
- [243] H. Yang, K. Song, S. Mei, and Z. Yin, "An accurate mura defect vision inspection method using outlier-prejudging-based image background construction and region-gradient-based level set," *IEEE Trans. Autom. Sci. Eng.*, vol. 15, no. 4, pp. 1704–1721, Oct. 2018.
- [244] H. Yang, S. Mei, K. Song, B. Tao, and Z. Yin, "Transfer-learning-based online mura defect classification," *IEEE Trans. Semicond. Manuf.*, vol. 31, no. 1, pp. 116–123, Feb. 2018.
- [245] Y.-S.-P. Chiu and H.-D. Lin, "A hybrid approach based on hotelling statistics for automated visual inspection of display blemishes in LCD panels," *Expert Syst. Appl.*, vol. 36, no. 10, pp. 12332–12339, Dec. 2009.
- [246] Y.-H. Tseng and D.-M. Tsai, "Defect detection of uneven brightness in low-contrast images using basis image representation," *Pattern Recognit.*, vol. 43, no. 3, pp. 1129–1141, Mar. 2010.
- [247] S.-K.-S. Fan and Y.-C. Chuang, "Automatic detection of mura defect in TFT-LCD based on regression diagnostics," *Pattern Recognit. Lett.*, vol. 31, no. 15, pp. 2397–2404, Nov. 2010.
- [248] W.-C. Li and D.-M. Tsai, "Defect inspection in low-contrast LCD images using Hough transform-based nonstationary line detection," *IEEE Trans. Ind. Informat.*, vol. 7, no. 1, pp. 136–147, Feb. 2011.
- [249] D.-M. Tsai and H.-Y. Tsai, "Low-contrast surface inspection of mura defects in liquid crystal displays using optical flow-based motion analysis," *Mach. Vis. Appl.*, vol. 22, no. 4, pp. 629–649, Jul. 2011.
- [250] S. Mei, H. Yang, and Z. Yin, "An unsupervised-learning-based approach for automated defect inspection on textured surfaces," *IEEE Trans. Instrum. Meas.*, vol. 67, no. 6, pp. 1266–1277, Jun. 2018.
- [251] D.-M. Tsai and C.-Y. Hung, "Automatic defect inspection of patterned thin film transistor-liquid crystal display (TFT-LCD) panels using one-dimensional Fourier reconstruction and wavelet decomposition," *Int. J. Prod. Res.*, vol. 43, no. 21, pp. 4589–4607, Nov. 2005.
- [252] D.-M. Tsai, S.-T. Chuang, and Y.-H. Tseng, "One-dimensional-based automatic defect inspection of multiple patterned TFT-LCD panels using Fourier image reconstruction," *Int. J. Prod. Res.*, vol. 45, no. 6, pp. 1297–1321, Mar. 2007.
- [253] D.-M. Tsai and S.-T. Chuang, "1D-based defect detection in patterned TFT-LCD panels using characteristic fractal dimension and correlations," *Mach. Vis. Appl.*, vol. 20, no. 6, pp. 423–434, Oct. 2009.
- [254] Y.-G. Cen, R.-Z. Zhao, L.-H. Cen, L.-H. Cui, Z.-J. Miao, and Z. Wei, "Defect inspection for TFT-LCD images based on the low-rank matrix reconstruction," *Neurocomputing*, vol. 149, pp. 1206–1215, Feb. 2015.
- [255] M. Kim, M. Lee, M. An, and H. Lee, "Effective automatic defect classification process based on CNN with stacking ensemble model for TFT-LCD panel," *J. Intell. Manuf.*, vol. 31, no. 5, pp. 1165–1174, Oct. 2019.
- [256] H. Yang, Y. Chen, K. Song, and Z. Yin, "Multiscale feature-clustering-based fully convolutional autoencoder for fast accurate visual inspection of texture surface defects," *IEEE Trans. Autom. Sci. Eng.*, vol. 16, no. 3, pp. 1450–1467, Jul. 2019.
- [257] C.-J. Lu and D.-M. Tsai, "Defect inspection of patterned thin film transistor-liquid crystal display panels using a fast sub-image-based singular value decomposition," *Int. J. Prod. Res.*, vol. 42, no. 20, pp. 4331–4351, Oct. 2004.
- [258] C.-J. Lu and D.-M. Tsai, "Automatic defect inspection for LCDs using singular value decomposition," *Int. J. Adv. Manuf. Technol.*, vol. 25, nos. 1–2, pp. 53–61, Jan. 2005.

- [259] C.-F.-J. Kuo, C.-H. Chiu, and Y.-C. Chou, "Research and development of intelligent on-line real-time defect inspection system for polymer polarizer," *Polymer-Plastics Technol. Eng.*, vol. 48, no. 2, pp. 185–192, Feb. 2009.
- [260] C.-H. Noh, S.-L. Lee, D.-H. Kim, C.-W. Chung, and S.-H. Kim, "An effective and efficient defect inspection system for TFT-LCD polarised films using adaptive thresholds and shape-based image analyses," *Int. J. Prod. Res.*, vol. 48, no. 17, pp. 5115–5135, Sep. 2010.
- [261] D. Lim and D.-H. Jeong, "Zone-based inspection and defect classification for LCD manufacturing: Trivial defect free procedure for TFT glass inspection," *Int. J. Optomechtron.*, vol. 1, no. 3, pp. 312–330, Sep. 2007.
- [262] S.-M. Chao and D.-M. Tsai, "An anisotropic diffusion-based defect detection for low-contrast glass substrates," *Image Vis. Comput.*, vol. 26, no. 2, pp. 187–200, Feb. 2008.
- [263] A. Yousefian-Jazi, J.-H. Ryu, S. Yoon, and J. J. Liu, "Decision support in machine vision system for monitoring of TFT-LCD glass substrates manufacturing," *J. Process Control*, vol. 24, no. 6, pp. 1015–1023, Jun. 2014.
- [264] L.-F. Chen, C.-T. Su, and M.-H. Chen, "A neural-network approach for defect recognition in TFT-LCD photolithography process," *IEEE Trans. Electron. Packag. Manuf.*, vol. 32, no. 1, pp. 1–8, Jan. 2009.
- [265] D.-M. Tsai, P.-C. Lin, and C.-J. Lu, "An independent component analysis-based filter design for defect detection in low-contrast surface images," *Pattern Recognit.*, vol. 39, no. 9, pp. 1679–1694, Sep. 2006.
- [266] S.-M. Chao and D.-M. Tsai, "Anisotropic diffusion with generalized diffusion coefficient function for defect detection in low-contrast surface images," *Pattern Recognit.*, vol. 43, no. 5, pp. 1917–1931, May 2010.
- [267] D.-M. Tsai, M.-C. Chen, W.-C. Li, and W.-Y. Chiu, "A fast regularity measure for surface defect detection," *Mach. Vis. Appl.*, vol. 23, no. 5, pp. 869–886, Sep. 2012.
- [268] Y.-H. Liu, Y.-K. Huang, and M.-J. Lee, "Automatic inline defect detection for a thin film transistor-liquid crystal display array process using locally linear embedding and support vector data description," *Meas. Sci. Technol.*, vol. 19, no. 9, Sep. 2008, Art. no. 095501.
- [269] Y.-H. Liu, C.-K. Wang, Y. Ting, W.-Z. Lin, Z.-H. Kang, C.-S. Chen, and J.-S. Hwang, "In-TFT-array-process micro defect inspection using nonlinear principal component analysis," *Int. J. Mol. Sci.*, vol. 10, no. 10, pp. 4498–4514, Oct. 2009.
- [270] Y.-H. Liu, Y.-C. Liu, and Y.-J. Chen, "Fast support vector data descriptions for novelty detection," *IEEE Trans. Neural Netw.*, vol. 21, no. 8, pp. 1296–1313, Aug. 2010.
- [271] Y.-H. Liu, Y.-C. Liu, and Y.-Z. Chen, "High-speed inline defect detection for TFT-LCD array process using a novel support vector data description," *Expert Syst. Appl.*, vol. 38, no. 5, pp. 6222–6231, May 2011.
- [272] C.-F. Kuo, C.-T.-M. Hsu, C.-H. Fang, S.-M. Chao, and Y.-D. Lin, "Automatic defect inspection system of colour filters using taguchi-based neural network," *Int. J. Prod. Res.*, vol. 51, no. 5, pp. 1464–1476, Mar. 2013.
- [273] C.-F. J. Kuo, K.-C. Peng, H.-C. Wu, and C.-C. Wang, "Automated inspection of micro-defect recognition system for color filter," *Opt. Lasers Eng.*, vol. 70, pp. 6–17, Jul. 2015.
- [274] C.-S. Lin, K.-H. Huang, Y.-L. Lay, K.-C. Wu, Y.-C. Wu, and J.-M. Lin, "An improved pattern match method with flexible mask for automatic inspection in the LCD manufacturing process," *Expert Syst. Appl.*, vol. 36, no. 2, pp. 3234–3239, Mar. 2009.
- [275] C.-S. Lin, K.-H. Huang, T.-C. Lin, H.-J. Shei, and C.-L. Tien, "An automatic inspection method for the fracture conditions of anisotropic conductive film in the TFT-LCD assembly process," *Int. J. Optomechtron.*, vol. 5, no. 3, pp. 286–298, Jul. 2011.
- [276] X. Sheng, L. Jia, Z. Xiong, Z. Wang, and H. Ding, "ACF-COG interconnection conductivity inspection system using conductive area," *Microelectron. Rel.*, vol. 53, no. 4, pp. 622–628, Apr. 2013.
- [277] G. Ni, L. Liu, X. Du, J. Zhang, J. Liu, and Y. Liu, "Accurate AOI inspection of resistance in LCD anisotropic conductive film bonding using differential interference contrast," *Optik*, vol. 130, pp. 786–796, Feb. 2017.
- [278] M. F. Shirazi, K. Park, R. E. Wijesinghe, H. Jeong, S. Han, P. Kim, M. Jeon, and J. Kim, "Fast industrial inspection of optical thin film using optical coherence tomography," *Sensors*, vol. 16, no. 10, pp. 1–13, 2016.
- [279] J.-Y. Lee, T.-W. Kim, and H. J. Pakh, "Robust defect detection method for a non-periodic TFT-LCD pad area," *Int. J. Precis. Eng. Manuf.*, vol. 18, no. 8, pp. 1093–1102, Aug. 2017.
- [280] Q. Lu, Q. Fu, L. Luo, Q. Yuan, W. Hua, and Y. Yunguang, "Measurement method of LCD surface deformation for smartphone based on optical vision sensing system," *Optik*, vol. 172, pp. 1079–1088, Nov. 2018.
- [281] V. A. Sindagi and S. Srivastava, "Domain adaptation for automatic OLED panel defect detection using adaptive support vector data description," *Int. J. Comput. Vis.*, vol. 122, no. 2, pp. 193–211, Apr. 2017.
- [282] D. Li, L.-Q. Liang, and W.-J. Zhang, "Defect inspection and extraction of the mobile phone cover glass based on the principal components analysis," *Int. J. Adv. Manuf. Technol.*, vol. 73, nos. 9–12, pp. 1605–1614, Aug. 2014.
- [283] C. Jian, J. Gao, and Y. Ao, "Imbalanced defect classification for mobile phone screen glass using multifractal features and a new sampling method," *Multimedia Tools Appl.*, vol. 76, no. 22, pp. 24413–24434, Nov. 2017.
- [284] C. Jian, J. Gao, and Y. Ao, "Automatic surface defect detection for mobile phone screen glass based on machine vision," *Appl. Soft Comput.*, vol. 52, pp. 348–358, Mar. 2017.
- [285] Z.-C. Yuan, Z.-T. Zhang, H. Su, L. Zhang, F. Shen, and F. Zhang, "Vision-based defect detection for mobile phone cover glass using deep neural networks," *Int. J. Precis. Eng. Manuf.*, vol. 19, no. 6, pp. 801–810, Jun. 2018.
- [286] H. Jo and J. Kim, "Regularized auto-encoder-based separation of defects from backgrounds for inspecting display devices," *Electronics*, vol. 8, no. 5, p. 533, May 2019.
- [287] L.-Q. Liang, D. Li, X. Fu, and W.-J. Zhang, "Touch screen defect inspection based on sparse representation in low resolution images," *Multimedia Tools Appl.*, vol. 75, no. 5, pp. 2655–2666, Mar. 2016.
- [288] M. Chang, B.-C. Chen, J. L. Gabayno, and M.-F. Chen, "Development of an optical inspection platform for surface defect detection in touch panel glass," *Int. J. Optomechtron.*, vol. 10, no. 2, pp. 63–72, Apr. 2016.
- [289] K. W. Ko, D. H. Kim, M. Y. Kim, and J. H. Kim, "An automatic optical inspection system for inspection of CMOS compact camera module assembly," *Int. J. Precis. Eng. Manuf.*, vol. 10, no. 5, pp. 67–72, Dec. 2009.
- [290] Y. Liu and F. Yu, "Automatic inspection system of surface defects on optical IR-CUT filter based on machine vision," *Opt. Lasers Eng.*, vol. 55, pp. 243–257, Apr. 2014.
- [291] H.-D. Lin, "Computer-aided visual inspection of surface defects in ceramic capacitor chips," *J. Mater. Process. Technol.*, vol. 189, nos. 1–3, pp. 19–25, Jul. 2007.
- [292] H.-D. Lin, "Automated visual inspection of ripple defects using wavelet characteristic based multivariate statistical approach," *Image Vis. Comput.*, vol. 25, no. 11, pp. 1785–1801, Nov. 2007.
- [293] T.-H. Sun, F.-C. Tien, F.-C. Tien, and R.-J. Kuo, "Automated thermal fuse inspection using machine vision and artificial neural networks," *J. Intell. Manuf.*, vol. 27, no. 3, pp. 639–651, Jun. 2016.
- [294] Y.-J. Chen, T.-H. Lin, K.-H. Chang, and C.-F. Chien, "Feature extraction for defect classification and yield enhancement in color filter and micro-lens manufacturing: An empirical study," *J. Ind. Prod. Eng.*, vol. 30, no. 8, pp. 510–517, Dec. 2013.
- [295] Y.-J. Chen, C.-Y. Fan, and K.-H. Chang, "Manufacturing intelligence for reducing false alarm of defect classification by integrating similarity matching approach in CMOS image sensor manufacturing," *Comput. Ind. Eng.*, vol. 99, pp. 465–473, Sep. 2016.
- [296] C.-F. J. Kuo, W.-C. Lo, Y.-R. Huang, H.-Y. Tsai, C.-L. Lee, and H.-C. Wu, "Automated defect inspection system for CMOS image sensor with micro multi-layer non-spherical lens module," *J. Manuf. Syst.*, vol. 45, pp. 248–259, Oct. 2017.
- [297] C. F. Chang, J. L. Wu, K. J. Chen, and M. C. Hsu, "A hybrid defect detection method for compact camera lens," *Adv. Mech. Eng.*, vol. 9, no. 8, pp. 1–19, 2017.
- [298] H.-D. Lin, "Tiny surface defect inspection of electronic passive components using discrete cosine transform decomposition and cumulative sum techniques," *Image Vis. Comput.*, vol. 26, no. 5, pp. 603–621, May 2008.
- [299] Y. Yang, Z.-J. Zha, M. Gao, and Z. He, "A robust vision inspection system for detecting surface defects of film capacitors," *Signal Process.*, vol. 124, pp. 54–62, Jul. 2016.
- [300] E. N. Malamas, E. G. M. Petrakis, M. Zervakis, L. Petit, and J.-D. Legat, "A survey on industrial vision systems, applications and tools," *Image Vis. Comput.*, vol. 21, no. 2, pp. 171–188, Feb. 2003.
- [301] M. Teena, A. Manickavasagan, A. Mothershaw, S. El Hadi, and D. S. Jayas, "Potential of machine vision techniques for detecting fecal and microbial contamination of food products: A review," *Food Bioprocess Technol.*, vol. 6, no. 7, pp. 1621–1634, Jul. 2013.
- [302] V. Chauhan and B. Surgenor, "Fault detection and classification in automated assembly machines using machine vision," *Int. J. Adv. Manuf. Technol.*, vol. 90, nos. 9–12, pp. 2491–2512, Jun. 2017.

- [303] C. Vedang, F. Heshan, and S. Brian, "Effect of illumination techniques on machine vision inspection for automated assembly machines," in *Proc. Can. Soc. Mech. Eng. Int. Congr.*, Toronto, ON, Canada, Jun. 2014, pp. 1–6.
- [304] S. L. Bartlett, P. J. Besl, C. L. Cole, R. Jain, D. Mukherjee, and K. D. Skifstad, "Automatic solder joint inspection," *IEEE Trans. Pattern Anal. Mach. Intell.*, vol. PAMI-10, no. 1, pp. 31–43, Jan. 1988.
- [305] Z. Zeng, L. Z. Ma, and Z. Y. Zheng, "Automated extraction of PCB components based on specularly using layered illumination," *J. Intell. Manuf.*, vol. 22, no. 6, pp. 919–932, Dec. 2011.
- [306] Z. Zeng, L. Ma, and M. Suwa, "Algorithm of locating PCB components based on colour distribution of solder joints," *Int. J. Adv. Manuf. Technol.*, vol. 53, nos. 5–8, pp. 601–614, Mar. 2011.
- [307] N. Nourani-Vatani, P. V. K. Borges, and J. M. Roberts, "A study of feature extraction algorithms for optical flow tracking," in *Proc. Australas. Conf. Robot. Automat. (ACRA)*, 2012, pp. 3–5.
- [308] F. Wu, S. Li, X. Zhang, and W. Ye, "A design method for LEDs arrays structure illumination," *J. Display Technol.*, vol. 12, no. 10, pp. 1177–1184, Oct. 2016.
- [309] *IMAQ Vision Concepts Manual Number 322916A-01*, Nat. Instrum., Austin, TX, USA, 2000.
- [310] S. Shirmohammadi and A. Ferrero, "Camera as the instrument: The rising trend of vision based measurement," *IEEE Instrum. Meas. Mag.*, vol. 17, no. 3, pp. 41–47, Jun. 2014.
- [311] G. Rosati, G. Boschetti, A. Biondi, and A. Rossi, "Real-time defect detection on highly reflective curved surfaces," *Opt. Lasers Eng.*, vol. 47, nos. 3–4, pp. 379–384, Mar. 2009.
- [312] D. Zhao, F. Kong, and F. Du, "Vision-based adaptive stereo measurement of pins on multi-type electrical connectors," *Meas. Sci. Technol.*, vol. 30, no. 10, Oct. 2019, Art. no. 105002.
- [313] S.-H. Kim, J.-H. Kim, and S.-W. Kang, "Nondestructive defect inspection for LCDs using optical coherence tomography," *Displays*, vol. 32, no. 5, pp. 325–329, Dec. 2011.
- [314] N. H. Cho, K. Park, J.-Y. Kim, Y. Jung, and J. Kim, "Quantitative assessment of touch-screen panel by nondestructive inspection with three-dimensional real-time display optical coherence tomography," *Opt. Lasers Eng.*, vol. 68, pp. 50–57, May 2015.
- [315] T.-K. Lin, "Automatic inspection of an LCD light-guide plate based on weighted central moments combined with neural networks," *J. Chin. Inst. Eng.*, vol. 36, no. 7, pp. 890–901, Oct. 2013.
- [316] J. Zhang, "China needs 'five to 10 years' to catch up in semiconductors, peking university professor Zhou Zhiping says," *South China Morning Post*, Sep. 2019. Accessed: Jul. 2020. [Online]. Available: <https://www.scmp.com/tech/tech-leaders-and-founders/article/3024315/china-needs-five-10-years-catch-semiconductors>
- [317] Utechzone Co. Ltd. (2018). *Semiconductor Wafer Inspection*. Accessed: Jul. 2020. [Online]. Available: <https://www.utechzone.com.tw/en/html/product/index.php?cid=67>
- [318] S. Purandare, J. Zhu, R. Zhou, G. Popescu, A. Schwing, and L. L. Goddard, "Optical inspection of nanoscale structures using a novel machine learning based synthetic image generation algorithm," *Opt. Express*, vol. 27, no. 13, p. 17743, 2019.
- [319] X. Lu, G. Liao, Z. Zha, Q. Xia, and T. Shi, "A novel approach for flip chip solder joint inspection based on pulsed phase thermography," *NDT & E Int.*, vol. 44, no. 6, pp. 484–489, Oct. 2011.
- [320] Y. J. Roh, W. S. Park, and H. Cho, "Correcting image distortion in the X-ray digital tomosynthesis system for PCB solder joint inspection," *Image Vis. Comput.*, vol. 21, no. 12, pp. 1063–1075, Nov. 2003.
- [321] Y. Wang, M. Wang, and Z. Zhang, "Microfocus X-ray printed circuit board inspection system," *Optik*, vol. 125, no. 17, pp. 4929–4931, Sep. 2014.
- [322] K. Zhang, W. Zuo, Y. Chen, D. Meng, and L. Zhang, "Beyond a Gaussian denoiser: Residual learning of deep CNN for image denoising," *IEEE Trans. Image Process.*, vol. 26, no. 7, pp. 3142–3155, Jul. 2017.
- [323] D.-G. Kim and Z. H. Shamsi, "Enhanced residual noise estimation of low rank approximation for image denoising," *Neurocomputing*, vol. 293, pp. 1–11, Jun. 2018.
- [324] S. Gu, L. Zhang, W. Zuo, and X. Feng, "Weighted nuclear norm minimization with application to image denoising," in *Proc. IEEE Conf. Comput. Vis. Pattern Recognit.*, Jun. 2014, pp. 2862–2869.
- [325] S. U. Lee, S. Y. Chung, and R. H. Park, "A comparative performance study of several global thresholding techniques for segmentation," *Comput. Vis., Graph., Image Process.*, vol. 52, no. 2, pp. 171–190, Nov. 1990.
- [326] K. S. Fu and J. K. Mui, "A survey on image segmentation," *Pattern Recognit.*, vol. 13, no. 1, pp. 3–16, 1981.
- [327] H.-F. Ng, "Automatic thresholding for defect detection," *Pattern Recognit. Lett.*, vol. 27, no. 14, pp. 1644–1649, Oct. 2006.
- [328] F. Yan, H. Zhang, and C. R. Kube, "A multistage adaptive thresholding method," *Pattern Recognit. Lett.*, vol. 26, no. 8, pp. 1183–1191, Jun. 2005.
- [329] N. Otsu, "A threshold selection method from gray-level histograms," *IEEE Trans. Syst., Man, Cybern.*, vol. SMC-9, no. 1, pp. 62–66, Jan. 1979.
- [330] S. Nuanprasert, S. Baba, and T. Suzuki, "An efficient method of occluded solder ball segmentation for automated BGA void defect inspection using X-ray images," in *Proc. 41st Annu. Conf. IEEE Ind. Electron. Soc. (IECON)*, Nov. 2015, pp. 003308–003313.
- [331] P. Perona and J. Malik, "Scale-space and edge detection using anisotropic diffusion," *IEEE Trans. Pattern Anal. Mach. Intell.*, vol. 12, no. 7, pp. 629–639, Jul. 1990.
- [332] A. K. Jain, R. P. W. Duin, and J. C. Mao, "Statistical pattern recognition: A review," *IEEE Trans. Pattern Anal. Mach. Intell.*, vol. 22, no. 1, pp. 4–37, Jan. 2000.
- [333] N. Dong, C.-H. Wu, W.-H. Ip, Z.-Q. Chen, C.-Y. Chan, and K.-L. Yung, "An improved species based genetic algorithm and its application in multiple template matching for embroidered pattern inspection," *Expert Syst. Appl.*, vol. 38, no. 12, pp. 15172–15182, Nov. 2011.
- [334] E. M. Taha, E. Emary, and K. Moustafa, "Automatic optical inspection for PCB manufacturing: A survey," *Int. J. Sci. Eng. Res.*, vol. 5, no. 7, pp. 1095–1102, 2014.
- [335] D.-M. Tsai and Y.-H. Chou, "Fast and precise positioning in PCBs using deep neural network regression," *IEEE Trans. Instrum. Meas.*, vol. 69, no. 7, pp. 4692–4701, Jul. 2020.
- [336] M. Arebey, M. A. Hannan, R. A. Begum, and H. Basri, "Solid waste bin level detection using gray level co-occurrence matrix feature extraction approach," *J. Environ. Manage.*, vol. 104, pp. 9–18, Aug. 2012.
- [337] C. E. Honeycutt and R. Plotnick, "Image analysis techniques and gray-level co-occurrence matrices (GLCM) for calculating bioturbation indices and characterizing biogenic sedimentary structures," *Comput. Geosci.*, vol. 34, no. 11, pp. 1461–1472, Nov. 2008.
- [338] X. Xie, "A review of recent advances in surface defect detection using texture analysis techniques," *ELCVIA Electron. Lett. Comput. Vis. Image Anal.*, vol. 7, no. 3, p. 1, Jun. 2008.
- [339] M. Tuceryan and A. K. Jain, "Texture analysis," in *Handbook of Pattern Recognition and Computer Vision*. Singapore: World Scientific, Aug. 1993, pp. 235–276.
- [340] W. Du, S. Addepalli, and Y. Zhao, "The spatial resolution enhancement for a thermogram enabled by controlled subpixel movements," *IEEE Trans. Instrum. Meas.*, vol. 69, no. 6, pp. 3566–3575, Jun. 2020.
- [341] Y. Peng, F. Liu, and S. Liu, "A normalized local binary fitting model for image segmentation," in *Proc. 4th Int. Conf. Intell. Netw. Collaborative Syst.*, Sep. 2012, pp. 77–80.
- [342] T. F. Chan and L. A. Vese, "Active contours without edges," *IEEE Trans. Image Process.*, vol. 10, no. 2, pp. 266–277, Feb. 2001.
- [343] E. Liu, K. Chen, Z. Xiang, and J. Zhang, "Conductive particle detection via deep learning for ACF bonding in TFT-LCD manufacturing," *J. Intell. Manuf.*, vol. 31, no. 4, pp. 1037–1049, Apr. 2020.
- [344] C. Xu, X. Yang, Z. He, J. Qiu, and H. Gao, "Precise positioning of circular mark points and transistor components in SMT applications," *IEEE Trans. Ind. Inform.*, early access, Jun. 1, 2020, doi: 10.1109/TII.2020.2999023.
- [345] H. Uğuz, "A two-stage feature selection method for text categorization by using information gain, principal component analysis and genetic algorithm," *Knowl.-Based Syst.*, vol. 24, no. 7, pp. 1024–1032, Oct. 2011.
- [346] W. Li, T. Shi, G. Liao, and S. Yang, "Feature extraction and classification of gear faults using principal component analysis," *J. Qual. Maintenance Eng.*, vol. 9, no. 2, pp. 132–143, Jun. 2003.
- [347] M. S. Bartlett, J. R. Movellan, and T. J. Sejnowski, "Face recognition by independent component analysis," *IEEE Trans. Neural Netw.*, vol. 13, no. 6, pp. 1450–1464, Nov. 2002.
- [348] H.-W. Liu, S.-H. Chen, and D.-B. Perng, "Defect inspection of patterned thin-film ceramic light-emitting diode substrate using a fast randomized principal component analysis," *IEEE Trans. Semicond. Manuf.*, vol. 29, no. 3, pp. 248–256, Aug. 2016.
- [349] J. Lu, K. N. Plataniotis, and A. N. Venetsanopoulos, "Face recognition using kernel direct discriminant analysis algorithms," *IEEE Trans. Neural Netw.*, vol. 14, no. 1, pp. 117–126, Jan. 2003.

- [350] F. De la Torre and M. J. Black, "Robust principal component analysis for computer vision," in *Proc. 8th IEEE Int. Conf. Comput. Vis. (ICCV)*, vol. 1, Jul. 2001, pp. 362–369.
- [351] X. Wang, R. Dong, and B. Li, "TFT-LCD mura defect detection based on ICA and multi-channels fusion," in *Proc. 3rd Int. Conf. Inf. Sci. Control Eng. (ICISCE)*, Jul. 2016, pp. 687–691.
- [352] Q. Huangpeng, H. Zhang, X. Zeng, and W. Huang, "Automatic visual defect detection using texture prior and low-rank representation," *IEEE Access*, vol. 6, pp. 37965–37976, 2018.
- [353] C. Bugli and P. Lambert, "Comparison between principal component analysis and independent component analysis in electroencephalograms modelling," *Biometrical J.*, vol. 49, no. 2, pp. 312–327, Apr. 2007.
- [354] D.-M. Tsai and S.-C. Lai, "Defect detection in periodically patterned surfaces using independent component analysis," *Pattern Recognit.*, vol. 41, no. 9, pp. 2812–2832, Sep. 2008.
- [355] C.-J. Lu and D.-M. Tsai, "Independent component analysis-based defect detection in patterned liquid crystal display surfaces," *Image Vis. Comput.*, vol. 26, no. 7, pp. 955–970, Jul. 2008.
- [356] F. M. Megahed, W. H. Woodall, and J. A. Camelio, "A review and perspective on control charting with image data," *J. Qual. Technol.*, vol. 43, no. 2, pp. 83–98, Apr. 2011.
- [357] K. Assaleh and Y. Al-Assaf, "Features extraction and analysis for classifying causable patterns in control charts," *Comput. Ind. Eng.*, vol. 49, no. 1, pp. 168–181, Aug. 2005.
- [358] T. Zan, Z. Liu, Z. Su, M. Wang, X. Gao, and D. Chen, "Statistical process control with intelligence based on the deep learning model," *Appl. Sci.*, vol. 10, no. 1, p. 308, Dec. 2019.
- [359] T. Wuest, D. Weimer, C. Irgens, and K.-D. Thoben, "Machine learning in manufacturing: Advantages, challenges, and applications," *Prod. Manuf. Res.*, vol. 4, no. 1, pp. 23–45, Jan. 2016.
- [360] D.-H. Kim, T. J. Y. Kim, X. Wang, M. Kim, Y.-J. Quan, J. W. Oh, S.-H. Min, H. Kim, B. Bhandari, I. Yang, and S.-H. Ahn, "Smart machining process using machine learning: A review and perspective on machining industry," *Int. J. Precis. Eng. Manuf.-Green Technol.*, vol. 5, no. 4, pp. 555–568, Aug. 2018.
- [361] Z. Ge, Z. Song, S. X. Ding, and B. Huang, "Data mining and analytics in the process industry: The role of machine learning," *IEEE Access*, vol. 5, pp. 20590–20616, 2017.
- [362] D. T. Pham and A. A. Afify, "Machine-learning techniques and their applications in manufacturing," *Proc. Inst. Mech. Eng., B, J. Eng. Manuf.*, vol. 219, no. 5, pp. 395–412, 2005.
- [363] M.-A. Amal and B.-A. Ahmed, "Survey of nearest neighbor condensing techniques," *Int. J. Adv. Comput. Sci. Appl.*, vol. 2, no. 11, pp. 302–305, 2011.
- [364] Y. Freund and M. Llew, "The alternating decision tree learning algorithm," in *Proc. 16th Int. Conf. Mach. Learn.* San Mateo, CA, USA: Morgan Kaufmann, 1999, pp. 124–133.
- [365] E. Osuna, R. Freund, and F. Girosit, "Training support vector machines: An application to face detection," in *Proc. IEEE Comput. Soc. Conf. Comput. Vis. Pattern Recognit.*, Jun. 1997, pp. 130–136.
- [366] C.-W. Hsu and C.-J. Lin, "A comparison of methods for multiclass support vector machines," *IEEE Trans. Neural Netw.*, vol. 13, no. 2, pp. 415–425, Mar. 2002.
- [367] Y.-J. Cha, K. You, and W. Choi, "Vision-based detection of loosened bolts using the Hough transform and support vector machines," *Autom. Construct.*, vol. 71, pp. 181–188, Nov. 2016.
- [368] G. Cavallaro, M. Riedel, M. Richerzhagen, J. A. Benediktsson, and A. Plaza, "On understanding big data impacts in remotely sensed image classification using support vector machine methods," *IEEE J. Sel. Topics Appl. Earth Observ. Remote Sens.*, vol. 8, no. 10, pp. 4634–4646, Oct. 2015.
- [369] H. Dong, N. Chen, and K. Wang, "Wafer yield prediction using derived spatial variables," *Qual. Rel. Eng. Int.*, vol. 33, no. 8, pp. 2327–2342, Dec. 2017.
- [370] C. Jian, J. Gao, and Y. Ao, "A new sampling method for classifying imbalanced data based on support vector machine ensemble," *Neurocomputing*, vol. 193, pp. 115–122, Jun. 2016.
- [371] X. Zhu, Y. Zhang, and Y. Zhu, "Bearing performance degradation assessment based on the rough support vector data description," *Mech. Syst. Signal Process.*, vol. 34, nos. 1–2, pp. 203–217, Jan. 2013.
- [372] M. A. Selver, O. Akay, F. Alim, S. Bardakçı, and M. Ölmez, "An automated industrial conveyor belt system using image processing and hierarchical clustering for classifying marble slabs," *Robot. Comput.-Integr. Manuf.*, vol. 27, no. 1, pp. 164–176, Feb. 2011.
- [373] J. Leskovec, A. Rajaraman, and J. D. Ullman, *Mining of Massive Datasets*. Cambridge, U.K.: Cambridge Univ. Press, Jan. 2020.
- [374] G. Gan, C. Ma, and J. Wu, *Data Clustering: Theory, Algorithms, and Applications*. Philadelphia, PA, USA: Society for Industrial and Applied Mathematics, 2007.
- [375] M.-S. Chen, P. S. Yu, and B. Liu, Eds., *Advances in Knowledge Discovery and Data Mining (Lecture Notes in Computer Science)*, vol. 2336. Berlin, Germany: Springer, 2002.
- [376] F. Petitjean, A. Ketterlin, and P. Gançarski, "A global averaging method for dynamic time warping, with applications to clustering," *Pattern Recognit.*, vol. 44, no. 3, pp. 678–693, Mar. 2011.
- [377] Y. Liu and S. Zhou, "Detecting point pattern of multiple line segments using Hough transformation," *IEEE Trans. Semicond. Manuf.*, vol. 28, no. 1, pp. 13–24, Feb. 2015.
- [378] D. Birant and A. Kut, "ST-DBSCAN: An algorithm for clustering spatial-temporal data," *Data Knowl. Eng.*, vol. 60, no. 1, pp. 208–221, Jan. 2007.
- [379] M. R. G. Meireles, P. E. M. Almeida, and M. G. Simoes, "A comprehensive review for industrial applicability of artificial neural networks," *IEEE Trans. Ind. Electron.*, vol. 50, no. 3, pp. 585–601, Jun. 2003.
- [380] T. Kohonen, "Improved versions of learning vector quantization," in *Proc. Int. Joint Conf. Neural Netw. (IJCNN)*, 1990, pp. 545–550.
- [381] A. J. Al-Mahasneh, S. G. Anavatti, and M. A. Garratt, "Review of applications of generalized regression neural networks in identification and control of dynamic systems," May 2018, *arXiv:1805.11236*. [Online]. Available: <https://arxiv.org/abs/1805.11236>
- [382] A. K. Jain, J. Mao, and K. M. Mohiuddin, "Artificial neural networks: A tutorial," *Computer*, vol. 29, no. 3, pp. 31–44, Mar. 1996.
- [383] L. Xu, S. Lv, Y. Deng, and X. Li, "A weakly supervised surface defect detection based on convolutional neural network," *IEEE Access*, vol. 8, pp. 42285–42296, 2020.
- [384] A. Shrestha and A. Mahmood, "Review of deep learning algorithms and architectures," *IEEE Access*, vol. 7, pp. 53040–53065, 2019.
- [385] Y. Guo, Y. Liu, A. Oerlemans, S. Lao, S. Wu, and M. S. Lew, "Deep learning for visual understanding: A review," *Neurocomputing*, vol. 187, pp. 27–48, Apr. 2016.
- [386] W. Sun, S. Shao, R. Zhao, R. Yan, X. Zhang, and X. Chen, "A sparse auto-encoder-based deep neural network approach for induction motor faults classification," *Measurement, J. Int. Meas. Confederation*, vol. 89, pp. 171–178, Jul. 2016.
- [387] C. Zhang, X. Cheng, J. Liu, J. He, and G. Liu, "Deep sparse autoencoder for feature extraction and diagnosis of locomotive adhesion status," *J. Control Sci. Eng.*, vol. 2018, pp. 1–9, Jul. 2018.
- [388] X. Liu, X. Zhang, W. Zhang, W. Wei, Y. Zhao, Y. Xi, and S. Cao, "Data mining from haier air-conditioner equipment running data for fault prediction," in *Proc. IEEE SmartWorld, Ubiquitous Intell. Comput., Adv. Trusted Comput., Scalable Comput. Commun., Cloud Big Data Comput., Internet People Smart City Innov. (SmartWorld/SCALCOM/UIC/ATC/CBDCCom/IOP/SCI)*, Oct. 2018, pp. 1829–1836.
- [389] H. Lee, Y. Kim, and C. O. Kim, "A deep learning model for robust wafer fault monitoring with sensor measurement noise," *IEEE Trans. Semicond. Manuf.*, vol. 30, no. 1, pp. 23–31, Feb. 2017.
- [390] I. J. Goodfellow, J. Pouget-Abadie, M. Mirza, B. Xu, D. Warde-Farley, S. Ozair, A. Courville, and Y. Bengio, "Generative adversarial nets," in *Proc. Adv. Neural Inf. Process. Syst.*, 2014, pp. 2672–2680.
- [391] Q. Wang, X. Zhou, C. Wang, Z. Liu, J. Huang, Y. Zhou, C. Li, H. Zhuang, and J.-Z. Cheng, "WGAN-based synthetic minority over-sampling technique: Improving semantic fine-grained classification for lung nodules in CT images," *IEEE Access*, vol. 7, pp. 18450–18463, 2019.
- [392] S. Shao, P. Wang, and R. Yan, "Generative adversarial networks for data augmentation in machine fault diagnosis," *Comput. Ind.*, vol. 106, pp. 85–93, Apr. 2019.
- [393] Y. Lecun, L. Bottou, Y. Bengio, and P. Haffner, "Gradient-based learning applied to document recognition," *Proc. IEEE*, vol. 86, no. 11, pp. 2278–2324, Nov. 1998.
- [394] A. Krizhevsky, I. Sutskever, and G. E. Hinton, "ImageNet classification with deep convolutional neural networks," in *Proc. Adv. Neural Inf. Process. Syst.*, 2012, pp. 1097–1105.
- [395] K. Simonyan and A. Zisserman, "Very deep convolutional networks for large-scale image recognition," 2014, *arXiv:1409.1556*. [Online]. Available: <http://arxiv.org/abs/1409.1556>
- [396] K. He, X. Zhang, S. Ren, and J. Sun, "Deep residual learning for image recognition," 2015, *arXiv:1512.03385*. [Online]. Available: <http://arxiv.org/abs/1512.03385>

- [397] G. Huang, Z. Liu, L. van der Maaten, and K. Q. Weinberger, "Densely connected convolutional networks," 2016, *arXiv:1608.06993*. [Online]. Available: <http://arxiv.org/abs/1608.06993>
- [398] J.-K. Park, B.-K. Kwon, J.-H. Park, and D.-J. Kang, "Machine learning-based imaging system for surface defect inspection," *Int. J. Precis. Eng. Manuf.-Green Technol.*, vol. 3, no. 3, pp. 303–310, Jul. 2016.
- [399] J. Wang, P. Fu, and R. X. Gao, "Machine vision intelligence for product defect inspection based on deep learning and Hough transform," *J. Manuf. Syst.*, vol. 51, pp. 52–60, Apr. 2019.
- [400] B. Devika and N. George, "Convolutional neural network for semiconductor wafer defect detection," in *Proc. 10th Int. Conf. Comput., Commun. Netw. Technol. (ICCCNT)*, Jul. 2019, pp. 1–6.
- [401] M. Saqlain, Q. Abbas, and J. Y. Lee, "A deep convolutional neural network for wafer defect identification on an imbalanced dataset in semiconductor manufacturing processes," *IEEE Trans. Semicond. Manuf.*, vol. 33, no. 3, pp. 436–444, Aug. 2020.
- [402] J. Long, E. Shelhamer, and T. Darrell, "Fully convolutional networks for semantic segmentation," 2014, *arXiv:1411.4038*. [Online]. Available: <http://arxiv.org/abs/1411.4038>
- [403] V. Badrinarayanan, A. Kendall, and R. Cipolla, "SegNet: A deep convolutional encoder-decoder architecture for image segmentation," *IEEE Trans. Pattern Anal. Mach. Intell.*, vol. 39, no. 12, pp. 2481–2495, Dec. 2017.
- [404] O. Ronneberger, P. Fischer, and T. Brox, "U-Net: Convolutional networks for biomedical image segmentation," 2015, *arXiv:1505.04597*. [Online]. Available: <http://arxiv.org/abs/1505.04597>
- [405] T.-H. Kim, T.-H. Cho, Y. S. Moon, and S. H. Park, "Visual inspection system for the classification of solder joints," *Pattern Recognit.*, vol. 32, no. 4, pp. 565–575, Apr. 1999.
- [406] H.-H. Loh and M.-S. Lu, "Printed circuit board inspection using image analysis," *IEEE Trans. Ind. Appl.*, vol. 35, no. 2, pp. 426–432, Mar./Apr. 1999.
- [407] M. Li and B. Yuan, "2D-LDA: A statistical linear discriminant analysis for image matrix," *Pattern Recognit. Lett.*, vol. 26, no. 5, pp. 527–532, Apr. 2005.
- [408] X. Chen, N. Liu, B. You, and B. Xiao, "A novel method for surface defect inspection of optic cable with short-wave infrared illuminance," *Infr. Phys. Technol.*, vol. 77, pp. 456–463, Jul. 2016.
- [409] W.-C. Lee and C.-H. Chen, "A fast template matching method with rotation invariance by combining the circular projection transform process and bounded partial correlation," *IEEE Signal Process. Lett.*, vol. 19, no. 11, pp. 737–740, Nov. 2012.
- [410] B. Zhang, H. Yang, and Z. Yin, "A region-based normalized cross correlation algorithm for the vision-based positioning of elongated IC chips," *IEEE Trans. Semicond. Manuf.*, vol. 28, no. 3, pp. 345–352, Aug. 2015.
- [411] J. Choi and C. Kim, "Unsupervised detection of surface defects: A two-step approach," in *Proc. 19th IEEE Int. Conf. Image Process.*, Sep. 2012, pp. 1037–1040.
- [412] V. A. Sindagi and S. Srivastava, "OLED panel defect detection using local inlier-outlier ratios and modified LBP," in *Proc. 14th IAPR Int. Conf. Mach. Vis. Appl. (MVA)*, May 2015, pp. 214–217.
- [413] F. Tajeripour, E. Kabir, and A. Sheikhi, "Fabric defect detection using modified local binary patterns," *EURASIP J. Adv. Signal Process.*, vol. 2008, no. 1, pp. 1–12, Dec. 2007.
- [414] P. Vithu and J. A. Moses, "Machine vision system for food grain quality evaluation: A review," *Trends Food Sci. Technol.*, vol. 56, pp. 13–20, Oct. 2016.
- [415] C. Madrigal, J. Branch, A. Restrepo, and D. Mery, "A method for automatic surface inspection using a model-based 3D descriptor," *Sensors*, vol. 17, no. 10, p. 2262, Oct. 2017.
- [416] L. Pérez, Í. Rodríguez, N. Rodríguez, R. Usamentiaga, and D. García, "Robot guidance using machine vision techniques in industrial environments: A comparative review," *Sensors*, vol. 16, no. 3, p. 335, Mar. 2016.
- [417] J.-G. Juang, Y.-J. Tsai, and Y.-W. Fan, "Visual recognition and its application to robot arm control," *Appl. Sci.*, vol. 5, no. 4, pp. 851–880, Oct. 2015.



ABD AL RAHMAN M. ABU EBAYYEH was born in Amman, Jordan, in 1990. He received the B.Sc. degree in mechatronics engineering from the University of Jordan, Amman, in 2013, and the M.Sc. degree in aerospace engineering from the Queen Mary University of London, London, U.K., in 2015. He is currently pursuing the PhD. degree in computer and electronics engineering with Brunel University London, London, U.K.

He is working on the EU Horizon 2020 IQONIC project which focuses on offering zero defects in optoelectronics manufacturing systems. From 2016 to 2019, he was a Research and Teaching Assistant with the Higher Colleges of Technology (HCT) and the Institute of Applied Technology (IAT) in UAE. His research interests include industrial automation, machine vision, machine learning, and robotics and process control.

Mr. Abu Ebayyeh was a recipient of the International Science and Engineering Excellence Award from the Queen Mary University of London, in 2014.



ALIREZA MOUSAVI (Senior Member, IEEE) received the B.Sc. degree in industrial engineering and the Ph.D. degree in system engineering from Brunel University London, London, U.K., in 1998.

He is currently a Reader of systems engineering and computing with Brunel University London. His current research interests include smart supervisory control and data acquisition systems applied to real-time systems modeling and optimization. The key areas of application are in stochastic modeling, ontology alignment, and sensor networks.

• • •